A comparison of buried andesites at Ngatamariki and Rotokawa geothermal fields, Taupo

A thesis

submitted in partial fulfilment

of the requirements for the degree

of

Master of Science in Earth Sciences

at

The University of Waikato

by

Linda Christina Vestman Andersen

THE UNIVERSITY OF
WAIKATO
Te Whare Wānanga o Waikato

2011

"Geology, perhaps more than any other department of natural philosophy, is a science of contemplation. It requires no experience or complicated apparatus, no minute processes upon the unknown processes of matter. It demands only an enquiring mind and senses alive to the facts almost everywhere presented in nature. And as it may be acquired without much difficulty, so it may be improved without much painful exertion."[1]

Humphry Davy

Sir Humphry Davy, 1st Baronet (1778–1829)[2]

1. 'Lectures on Geology, 1805 Lecture', in R. Siegfried and R. H. Dott (eds.), Humphry Davy on Geology (1980).
2. Courtesy of Les Nouvelles Conquêtes de la Science, Vol 1, Louis Figuier, Paris, 1883.

Abstract

The Rotokawa and Ngatamariki geothermal systems are hosted by hydrothermally altered Quaternary andesitic, dacitic and rhyolitic volcanics resting on Mesozoic Torlesse greywacke basement, and covered by lacustrine sediments and surficial deposits. Andesitic lava and breccia (> 2 km thick) below 1 km depth at Rotokawa is an important production aquifer for geothermal power due to its interconnected fracture permeability. Exploration drilling at Ngatamariki has revealed andesite at several depth intervals, with an approximate age of 1.2 Ma for the shallow andesite lavas, interlayered with ~1 km of ignimbrite.

Rotokawa andesite is a massive to flow-banded, fine-medium grained porphyritic lava with primary plagioclase (An_{51-82}), clino- and orthopyroxene in an aphanitic groundmass. Accessory minerals are biotite and Fe-Ti oxides. The Ngatamariki andesite has primary plagioclase (An_{54-82}) and clinopyroxene phenocrysts. Intercalated breccia contains andesite, minor rhyolite and greywacke lithics in a fine grained matrix. Hydrothermal alteration is propylitic, albeit with minor potassic or argillic mineralogy resulting from variable conditions within the thermally-evolving reservoirs. The andesite is commonly veined and/or has a vuggy texture.

XRF analysis, particularly plots of immobile element data, e.g. Ti vs. Zr, Y vs. Zr, has been used to fingerprint the hydrothermally altered volcanics, and infer the intensity of fluid-rock interaction. The TiO_2/Zr ratio in Rotokawa andesite is 27-63 whereas in the Ngatamariki andesite it is 13-48. Chemical data, combined with inferred stratigraphic relationships suggest that Rotokawa andesites derive from an older, basaltic andesite composite cone volcano, compared to a younger dacite/andesite volcanic centre at Ngatamariki.

Acknowledgements

This thesis would not have been possible without the generous support of some special people and organizations. I would like to express my sincere appreciation to Mighty River Power Ltd. for providing me with this project and for their financial and logistical support along the way, in particular Tom Powell for giving me the idea to study geothermal geology in the first place, Joe Gamman, Deborah Bowyer, Catherine Boseley and Linda Price for their helpful comments and assistance with getting access to core sheds and well reports. I would also like to thank GNS Science for much needed help with the geology and alteration mineralogy of Ngatamariki and Rotokawa fields, especially Greg Bignall, Andrew Rae, Michael Rosenberg and Briony Jones.

A very special thanks goes to my supervisors Associate Professor Roger Briggs and Dr. Adrian Pittari for taking the time to answer all my questions about the physical and geochemical aspects of volcanology, reviewing conference abstracts and presentations, and especially for showing great patience while I tried to get my research down on paper. The thesis was also completed with valuable assistance of the University of Waikato staff Steve Hood, Annette Rodgers, Jacinta Parenzee, Xu Ganqing, Indar Singh, Chris McKinnon and above all Renat Radosinsky, for outstanding technical help in the rocklab and all interesting discussions which reminded me that there is a life outside the university. I would like to express my sincere gratitude to Sydney Wright, Professor Cam Nelson, Professor David Lowe, Talia Heslop and Cheryl Ward for getting me through the finishing of my thesis. I would also like to thank the University of Waikato for granting me a Master Fees Award.

There are also some people who were not directly involved in this thesis that I would like to thank; April, Jared and Michele for being the best possible office mates, Ritchie Sims at the University of Auckland for turning microprobe analysis

into something fun☺, Anders Hallberg at SGU for helping me out with rock classification and mass change calculations, and also Jackson Browne and John Fogerty for keeping me company all those long nights while I was writing up my thesis…

Last but not least a huge thank you to my friends and family; in particular Mum and Dad for their support from "back home" in Sweden, Annette who persuaded me to swap the cold north for New Zealand and Paula and Tillmann for many shared bottles of bubbles! My dear, dear husband Tobbe; thank you for being a source of encouragement and inspiration throughout five years of studies! I could never have done it without you.

Table of Contents

List of Figures

Chapter 2 – Geological background

Chapter 3 – Primary mineralogy

List of Tables

Chapter 1
Introduction

1.1 Background

The name "geothermal" comes from two Greek words: "geo" means "Earth" and "thermal" means "heat". We have utilized surface manifestations of geothermal systems such as hot springs for cooking and bathing since antiquity. It is only recently that we have learned to harness the energy for industrial purposes such as electricity production and direct heating by drilling for high pressured steam. New Zealand commissioned the world's second large-scale geothermal power plant at Wairakei in 1958, initially to act as a base load energy source during years of drought as geothermal energy is the only renewable energy which is not dependent on weather. With an increasing demand for "clean" energy as the cost of reducing CO_2 emissions is being added to electricity bills, several new and technically improved power plants have been built over the years and geothermal energy currently provides about 10% of New Zealand's electricity demand. Recent estimates by Lawless (2002) conclude that only a fraction of this country's geothermal resources are being utilized, and the large development potential hence justifies substantial research within the area. For example, valuable information can be obtained by studying fluid-rock interactions in different geological units as this gives us a better understanding of hydrological pathways and controls on the deep hydrology within a geothermal system. The findings will be taken into account when determining if a site will provide adequate quantities of hot fluids to sustain the production of a power plant.

The Rotokawa and Ngatamariki geothermal fields have been the subject of exploration in recent years to determine their energy production potentials. Several

consultancy reports regarding the local geology and stages of hydrothermal alteration have been created as a result of this activity (Rae, 2007; Kilgour & Ramirez, 2008; Ramirez et al., 2008a, b; Bignall, 2009; Rae et al., 2009a, b, c, d; Ramirez & Rae, 2009a, b) although only one previous study has focused on comparing the two adjacent fields (Browne et al., 1992), more specifically the andesitic lavas and breccias found at ~1-3 km depth. A geochronological study of the Ngatamariki and Rotokawa geothermal fields was performed by Arehart et al. (2002), giving new insight to the onset of andesitic volcanism in the east-central Taupo Volcanic Zone (TVZ). The Rotokawa Andesite has proved to be an excellent aquifer during the production history of Rotokawa power station, which is located at approximately the same depth as another andesitic unit which has been encountered during exploration drilling at Ngatamariki. This thesis discusses the primary and secondary petrological properties of the Ngatamariki and Rotokawa andesites and their lateral extent.

1.2 Research objectives

The aim of this thesis is to correlate buried andesites at Ngatamariki and Rotokawa geothermal fields in order to see if there is a connection between the two, as this may be an important consideration for the regional deep hydrology and future development of both fields. This will involve:

- ✧ petrological examination of drill core and cuttings of andesite lava and breccia, focussing on the primary textural and mineralogical characteristics;
- ✧ geochemical work including whole-rock XRF analysis to establish chemical fingerprints of the andesites and also any petrogenetic relationships which may exist within flow units and/or between the two fields;
- ✧ petrogenetic characterisation of intensely hydrothermally altered rocks by the use of immobile trace elements, which enables to “see-through” the effects of hydrothermal alteration; and

- ✧ whole-rock chemistry will be complemented, where appropriate, by electron microprobe analysis of preserved primary igneous minerals, particularly primary plagioclase, pyroxene and magnetite. This should help establish the evolutionary development of the Ngatamariki and Rotokawa andesites and compare andesites in adjacent wells, and possibly across geothermal fields.

1.3 Thesis outline

The remaining chapters of this thesis will delineate the geological background in addition to petrological and geochemical characteristics of the Ngatamariki and Rotokawa geothermal fields. In Chapter 2, previous work regarding the regional and local geology of the Ngatamariki and Rotokawa geothermal fields are reviewed to provide a background. The principal topics covered include the tectonic setting and structure of the study area in addition to its geology and geothermal systems. Chapter 3 presents the petrological and mineralogical work on the Rotokawa and Ngatamariki andesites, while Chapter 4 is an overview of the hydrothermal alteration. Chapter 5 presents geochemical analyses of the two fields. The petrogenesis and volcanic evolution of the Ngatamariki and Rotokawa is discussed in Chapter 6, while Chapter 7 provides a summary and conclusion of the thesis.

Chapter 2
Geological background

2.1 Introduction

The Rotokawa and Ngatamariki geothermal fields are high-temperature (>200°C), liquid-dominated geothermal fields located within the Taupo Volcanic Zone (TVZ). These areas contain a series of hydrothermally altered Quaternary andesitic to rhyolitic volcanics, covered by lacustrine sediments. The intensity of hydrothermal alteration increases with depth, and is commonly expressed as acid alteration zones produced by localised steam heated waters in shallow stratigraphy followed by a deeper zone of mainly propylitic alteration with minor occurrences of potassic or argillic alterations as a result of changed conditions within the reservoir. The 34 MW Rotokawa power station has been in use since 1997 and was supplemented by the 140 MW Nga Awa Purua power station in May 2010, which features the largest single shaft geothermal turbine in the world. Resource consent for the construction and operation of a 110 MW power station at Ngatamariki was approved in May 2010 and it is scheduled to commence production in 2013.

This chapter will provide the reader with background information of the Ngatamariki and Rotokawa geothermal fields. The mechanisms for heat and water transport will be described, and it will also include both the regional and local setting of the two fields in addition to their surface- and subsurface geology.

2.2 Location and physiography

The Ngatamariki geothermal field is situated in the central part of the TVZ, about 17 km north-east of Taupo Township and 7 km north of the Nga Awa Purua and Rotokawa power stations (Fig. 2.1).

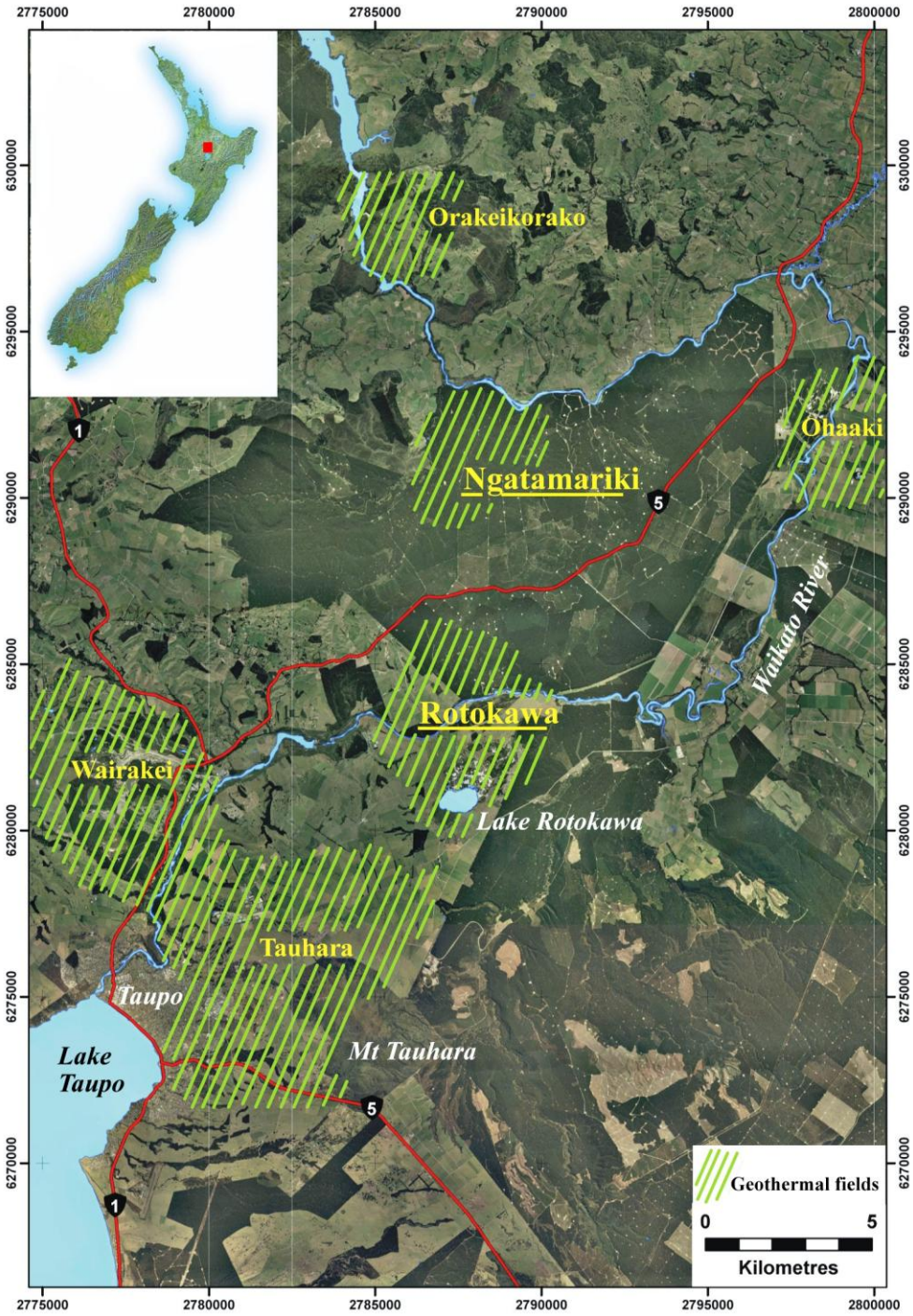

Figure 2.1: Map of field area located NE of Taupo, with surrounding geothermal fields (after Risk et al., 2003).

Electrical resistivity surveys conducted by Bennie (1983), Risk (1986), Stagpoole & Bibby (1998a; 1998b) have estimated the field to cover an area of 7-12 km^2 in the Tahorakuri Forest, between the Waikato River and State Highway 5 (SH5). The lightly rolling topography is covered in vegetation consisting of a central pine

forest surrounded by dairy pasture. There are few thermal features at Ngatamariki, with hot springs and pools on the banks of Waikato River and the Orakonui Stream discharging dilute chloride-bicarbonate waters of near neutral pH. The southern area of Orakonui Stream is dominated by a ~ 50 x 40 m crater rimmed with breccia deposits formed during the most recent hydrothermal eruption in 2005 when rock material was ejected up to 200 m in the air. The hot thermal water occupying the crater feeds several springs and mud pools at its margin (Fig. 2.2a-b). The hydrothermal eruption history of Ngatamariki has been described by Brotheridge (1995) and the 2005 eruption was reported by Environment Waikato (2005). Studies of surface manifestations and their chemistry have been carried out by Grange (1937), Gregg & Laing (1951), Healy (1974), Bennie (1983) and Hedenquist (1986). A summary can be found in Milicich & Reeves (2007).

The Rotokawa geothermal field 7 km south of Ngatamariki is located between State Highway 5 (SH5) and Broadlands Road, and covers an area of ~ 17-28 km^2. The boundary of the field has been established by resistivity surveys by Hatherton et al. (1966), Geophysics Division DSIR (1985) and Hunt & Harms (1990). Risk et al. (2003) reviewed previous works to refine the field's boundary. According to the current model, the field is divided by the Waikato River with ~ 40% on the north bank and the remainder on the south side. The vegetation in the northern field area is mainly pine forest while the southern area is dairy pasture with some new pine plantings. The dominant surface manifestation is Lake Rotokawa, a hydrothermal eruption crater of 1.5 km in diameter filled with hot, acid waters located at the southern end of the field (Fig. 2.2c-d). The lake receives significant amounts of geothermal fluid from the field, and drains through the Parariki Stream to the Waikato River. It contains considerable bedded sulphur deposits which formed in an earlier crater lake at the same location. The area around the lake has been considerably modified by sulphur mining, but still contains a number of important geothermal ecosystems. There have been at least 8 hydrothermal eruptions at Rotokawa during the last 22,700 years. Lake Rotokawa was formed 9,000-9,700 years ago, but its shape was

modified during one of the largest hydrothermal eruptions in New Zealand 6,000 years ago, where ejected material formed a deposit that covers an area of 4 km in diameter with a maximum thickness of 11 m. Smaller craters are located along a north-easterly, 1.5 km structural feature extending from within Lake Rotokawa and are filled with young tephra. Studies of the hydrothermal eruptions at Rotokawa have been published by Collar & Browne (1985) and Browne & Lawless (2001). Localized hot springs, thermal ground and a fumarole can also be found in the field. Early studies of the thermal features at Rotokawa include Grange (1937), Gregg & Laing (1951), Mahon (1960) and Khabar et al. (1986). During the exploration drilling, DSIR compiled analytical data from the geothermal wells and natural features in the area and the results were published by Hedenquist et al. (1988). Bromley et al. (2002) made a post-commissioning evaluation where he studied the changes in geochemistry at Rotokawa.

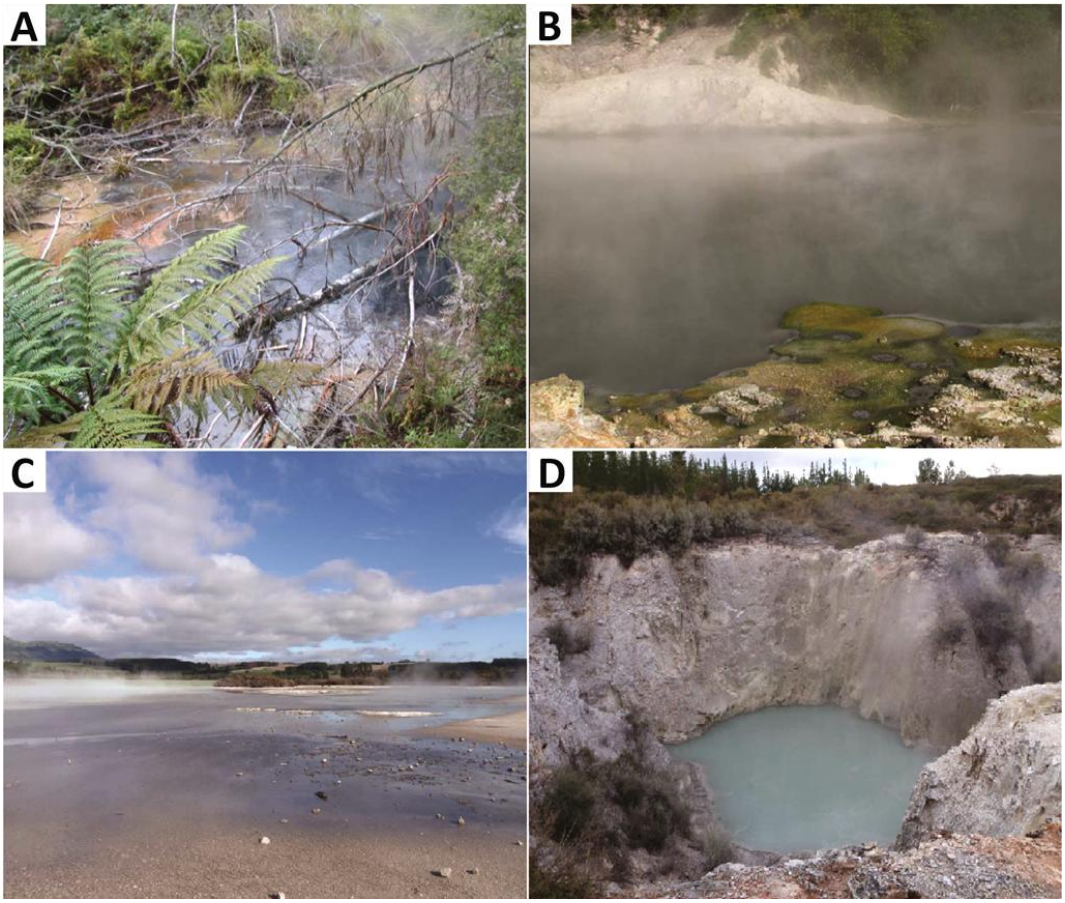

Figure 2.2: Thermal features of the study area. Image a) and b) are of the Orakonui Stream (source: Milicich & Reeves, 2009); c) is of Lake Rotokawa and d) an explosion crater at Lake Rotokawa (source: C. Bardsley, MRP).

A summary of the thermal features was produced by Milicich & Hunt (2007). Significant landmarks are visible from these geothermal fields, including the volcanic domes of Oruhineawa and Kaimanawa to the north and northeast, as well as the volcanic landforms of Tahorakuri, Tauhara and the Tongariro National Park to the south. To the southwest, Lake Taupo dominates the district as a natural landform, although is not visible from the fields (Isthmus Group Ltd, 2007).

2.3 Geothermal system

Since Maoris had no written language themselves, Dieffenbach (1843) was the first person to formally record some of the geothermal surface features in the TVZ during his journey from Taupo to Rotoroa in 1840 where he followed the east bank of the Waikato River, passing Wairakei and Rotokawa or Rotu-kaua (bitter lake) as he called it. As the geothermal features like hot springs and geysers became a booming tourist attraction and most recently a source of renewable energy, there have been plenty of scientific studies about geothermal systems and their origin. According to Maori folklore, the origin of volcanic geothermal systems is attributed to Ngatoroirangi, the priest who navigated the Arawa canoe to New Zealand. While exploring the central part of North Island he climbed the slopes of Mt Tongariro to gain a better view of the land and was benumbed with the cold on the snowy mountain. Fearing he would die, he called out for his sisters to bring him fire from Hawaiki where they had been left behind. His sisters heard his cry for help and set out immediately, travelling beneath sea and land in form of fire. Wherever they stopped and rose to the surface to look for Ngatoroirangi the heat burst out as thermal activity, the route leading through the Taupo Volcanic Zone from Whakaari (White Island), Tarawera, Taupo and Tokaanu to Tongariro. Ngatoroirangi was saved and the chain of thermal activity has been of great value to the people of Aotearoa (New Zealand) ever since (Grace, 1959).

It has been known from antiquity that Earth's interior is a great heat reservoir. For humans to be able to extract and utilize the heat, it requires a carrier to

convey the heat to an accessible depth in the Earth's crust. This can happen in two ways, or a combination of both: conduction or by convection. The conduction between solids in a geothermal system works under the influence of the geothermal gradient as kinetic energy is transferred among molecules without the overall transfer of material. Conversely, convection allows heat to be transferred in liquid or gaseous form from one place to another, and since motion of material occurs, this will be a much more efficient way of transferring heat than conduction (Barbier, 2002). Despite being a recurrent topic in scientific literature over the centuries, it was not until 1882 that Lord Kelvin, also called the father of thermodynamics, managed to obtain the values for geothermal gradient and the thermal conductivity of rocks in Great Britain. He based most of his work on the chemist and fellow countryman Robert Boyle's discovery from 1671 that temperature increases with depth in mines (Pollack, 1982).

The convecting fluids within a geothermal system are mostly meteoric, which penetrates into the Earth's crust from recharge zones. The fluids can be heated up to ~300°C as they come into contact with the hot rocks, and accumulate in reservoirs where an impermeable rock layer keeps the fluids under high pressure. If the rock is fractured, hot water will be able to rise to the surface as geothermal features, such as steam vents or hot springs (Barbier, 2002). The geothermal gradient, as described by Lord Kelvin, is on average 30 °C/km. If the surface temperature is 20 °C, the temperature at 3 km should be around 110 °C. This will be sufficient for direct use, but not for electricity production which requires a minimum of 150 °C. Therefore an additional heat source is necessary closer to the surface, such as a magmatic intrusion. This is why the majority of the world's potential for geothermal energy is associated with areas of volcanism originating from subduction and crustal spreading, such as the Pacific Ring of Fire (Hammons, 2004).

The accepted model that convecting fluids create the geothermal fields within the Taupo Volcanic Zone (Fig. 2.3) has been developed since the 1950s.

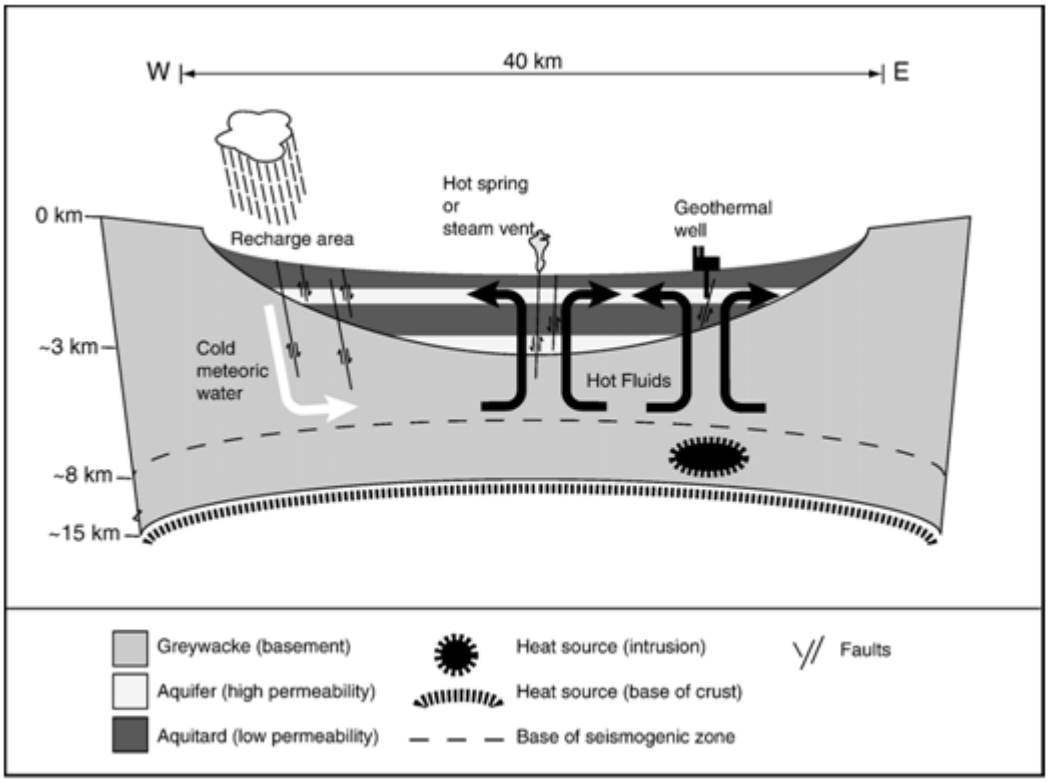

Figure 2.3: Schematic of the structure and hydrology of the TVZ showing the heat source at the base of the crust and possible intrusions (from Hole et al., 2007).

At that time, the government began to realize the potential of geothermal systems as a source of energy and subsequently laid pressure on the scientific community to conduct comprehensive research within the area. Fundamental works include Banwell et al. (1957), Donaldson (1962), Wooding (1963, 1964), McNabb (1965) and Elder (1965, 1966).

Geothermal fields in the TVZ are located within an area defined by calderas and the Taupo Fault Belt (TFB) (Fig. 2.4). Out of 23 mapped fields, 6 have small surface area and low (<20 MW) or unknown heat output, which might represent declining geothermal systems. The total heat output of the remaining 17 fields is 4200 ± 500 MW from an area of 6000 km^2. This means a heat flux of 700mW/m^3, a number which is only comparable to Yellowstone, USA (Bibby et al., 1995). Hochstein (1995) suggests that there is an association between high heat fluxes and volume of rhyolitic volcanism. At Yellowstone, the rate is on average 0.13 m^3/s, compared to 0.28 m^3/s at TVZ during the last 0.34 Ma.

The spacing of geothermal fields is 10-15 km, and between the fields the convective system is recharged by cold, meteoric water. The meteoric water is believed to circulate down to 7-9 km, an observation based on geophysical data which shows a sharp drop off in the number of earthquake swarm events at this depth (Bibby et al., 1995). This is interpreted to be a transition zone where rocks change from a brittle to ductile state, and fractures (and therefore permability) are reduced by thermally activated creep. A study by Villamor & Berryman (2001) supports this theory, as the maximum depth of major faults in the TVZ has been estimated to 6-10 km based on fault geometry and extension rates. This effectively determines how deep the meteoric water can descend, before being heated and returned to the surface as discrete plumes.

The heat source is not necessarily the same size as the permeable regions as some models predicts, where magma is intruded at the same volume as permeability is created by tectonic extension (e.g. Stern, 1987). A study of the deep structure below the Taupo Fault Belt by Bibby et al. (2000) using magnetotelluric data showed that there is a 'significant conductive structure' at 10 km depth, believed to be magma in the crust. A second conductive structure was identified below 20 km depth towards the eastern margin of TVZ, where majority of high temperature geothermal fields are located. This was believed to be an area of 'connected melt' in the upper mantle. Although the volcanic activity has changed in TVZ over time, the geothermal fields appear to have been spatially stable during the last 0.2 Ma (even though the heat output might have varied). Wairakei, for example, was estimated by Grindley (1965) to be >0.5 Ma, and Arehart et al. (2002) gave Ngatamariki an age of >0.5 Ma based on Ar-dating of a plutonic diorite. Ngatamariki is a good example of a long-lived geothermal activity. The diorite is overlain by Wairakei Ignimbrite (0.3 Ma), which is characterised by low hydrothermal alteration intensity. This indicates that there has been two different geothermal systems at this location; an old geothermal system which was extinct sometime before 0.3 Ma; and a new (and current) geothermal system is younger than 0.3 Ma.

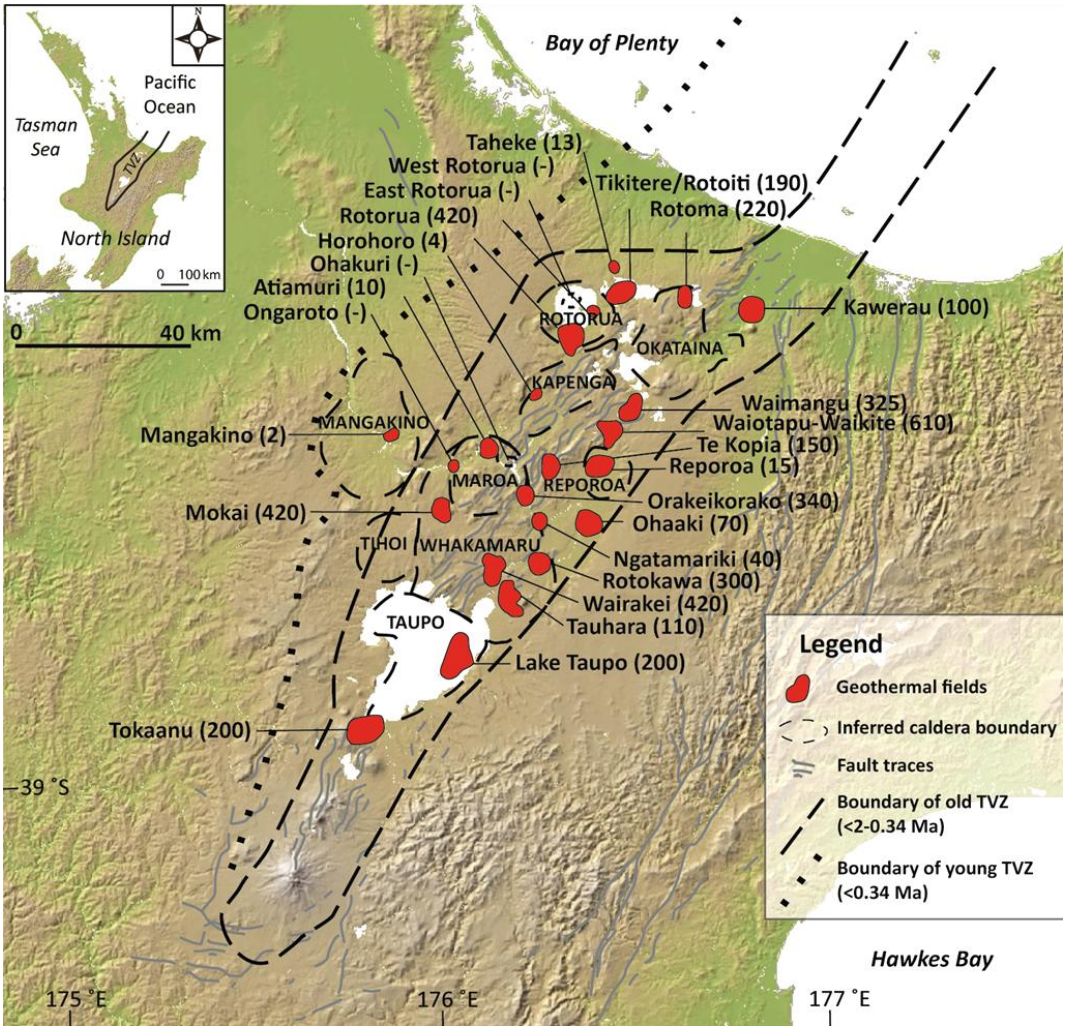

Figure 2.4: Geothermal fields within TVZ, natural heat output (MW) is in brackets, a dash means unknown heat output. Caldera boundaries and the Taupo Fault Belt indicate areas where hot geothermal fluids have easy access to the surface (modified from Kissling et al., 2009).

Areas of high resistivity between the fields prove that there has been no hydrothermal alteration outside present field boundaries, so there has been no change in location due to migrating, intrusive heat sources. The stability and longevity of each geothermal field may therefore be explained by being parts of a large-scale fluid-circulation system.

2.4 Geological setting and structure

2.4.1 Plate tectonics

The New Zealand micro-continent (termed Zealandia by Luyendyk, 1995) covers an area of more than 3 million square kilometers of which only one tenth is

emergent above sea level, such as the New Zealand mainland. The major submerged parts include Lord Howe Rise, Challenger Plateau, Chatham Rise and Campbell Plateau. Zealandia is made up of 2 nearly parallel ridges separated by a failed rift running in a northwest direction at 1-1.5 km depth. The basement geology consists of Cambrian to Cretaceous terranes and batholiths which are covered by Late Cretaceous to Neogene strata (Mortimer, 2004; Adams et al., 2008; Mortimer et al., 2009). Zealandia was separated from the eastern margin of Gondwanaland during the Late Cretaceous sea floor spreading. The separation led to rapid subsidence and the formation of rift basins. By the Eocene the Tasman Sea spreading had ceased. The area surrounding New Zealand experienced regional post-rift thermal subsidence which resulted in the deposition of fine-grained clastics and increasing amounts of carbonaceous sediments. During the Mid-Eocene there was a convergent margin was established with major reconfiguration of tectonic plates. A southward propagation of subduction along the Australian-Pacific plate margin concurs with deposition of sediments rich in carbonate, reflecting widespread submergence. In Early Miocene the Alpine Fault developed and hence formed a link between the northern subduction and the oblique extension in the south. The southern end of Zealandia (situated on the Pacific plate) began to move clockwise relative to the northern part (situated on the Australian plate) and this clockwise-movement has continued until present time (King, 2000; Uruski et al., 2002; Kamp & Furlong, 2006).

The northeast-southwest trending Taupo Volcanic Zone is the southernmost part of the Havre-Lau volcanic rift zone and a result of the westward subduction of the Pacific plate beneath the Australian plate (Fig. 2.5a). Seismic studies have revealed that the subducted plate dips initially at a shallow angle of 12-15° for 250 km before it steepens to 50° at a depth of 80 km, creating a Wadati-Benioff zone beneath the median axis of the TVZ (Fig. 2.5b). This increased dip of the Pacific plate corresponds at the surface with the lineation of the Taupo Volcanic Zone. The plane of the subducted plate strikes 045 and dips to the northwest (Kamp, 1984).

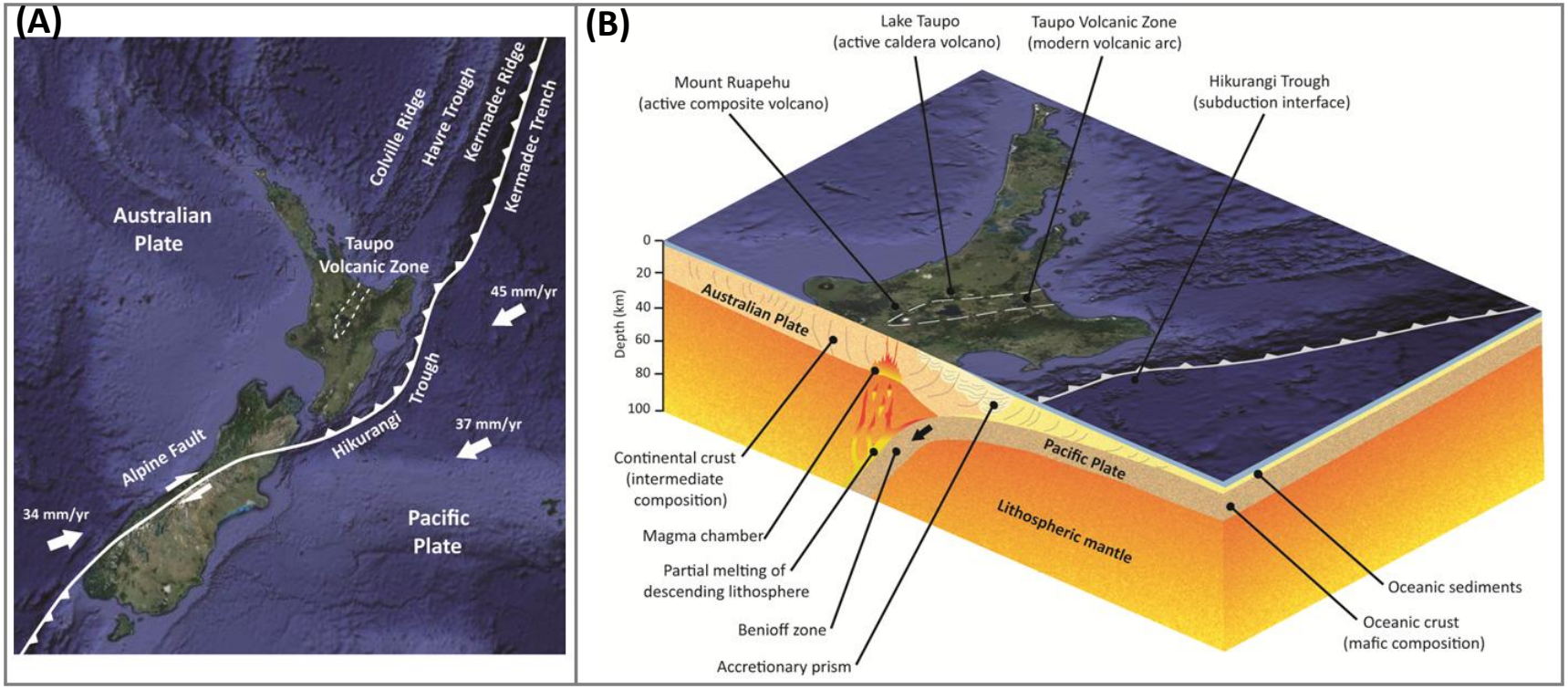

Figure 2.5: a) The regional setting of TVZ. b) A cut-away model of the modern subduction setting of North Island, involving subduction of the Pacific Plate beneath the Australian Plate (modified from Bland et al., 2008).

The TVZ itself is described as a volcanic arc and marginal basin of the Taupo-Hikurangi arc-trench system (Cole & Lewis, 1981; Cole, 1984, 1990), extending over 200 km from Mt. Ruapehu to the Bay of Plenty and continues some distance offshore, with a width of up to 60 km. The Hikurangi Trough is the present-day boundary marking the zone of convergence and strike-slip motion between the two tectonic plates, which passes into the Kermadec Trench to the north-northeast and the Alpine Fault to the southwest. The Alpine Fault itself is a significant dextral transform structure which links the westward-dipping subduction zone in the North Island, with the eastward-dipping subduction zone in the South Island (Furlong & Kamp, 2009).

2.4.2 Subduction-related volcanism

The subduction zone north of New Zealand is migrating eastward, and the Kermadec Trench is currently forming the active convergent margin. Associated volcanism is expressed at the Kermadec Ridge which has a similar tectonic setting as TVZ, being a back-arc zone of crustal thinning, rifting and subsidence. The volcanic chain comprises mainly seamounts with felsic magma composition, and some have had large caldera-forming eruptions. The Havre Trough is a result of back-arc extension, and remnant volcanic structures of Early Miocene age have been found further west, at the Colville Ridge (Ballance et al., 1999). In the TVZ, volcanic activity is spatially separated depending on magma composition. The northern and southern extremes are dominated by andesitic to dacitic composite cones, while a central area from Okataina to Taupo is dominated by rhyolite calderas (Fig. 2.6). Minor amounts of basalt (<2% of total erupted volume) are associated with rhyolitic volcanism and occur mainly where faults intersect caldera margins (Hiess et al., 2007).

Volcanic activity commenced in the TVZ about 2 Ma ago with an onset of calc-alkaline andesitic lava, joined by voluminous rhyolitic activity 1.6 Ma ago (Houghton

et al., 1995). The basin has subsequently been infilled with up to 2 km thickness of volcaniclastic material, most of it (>10,000 km^3) of rhyolitic composition and erupted within the last 0.6 Ma from the Maroa, Okataina, Kapenga, Whakamaru, Rotorua and Taupo Volcanic Centres (Wright, 1992). Several interpretations of the structure and evolution of the volcanism in TVZ have been suggested (Wilson et al., 1984, 1995; Houghton et al., 1995), but most apparently there seems to be an association between the volume and style of eruption and the amount of extension in each of these segments. The segments with the most dextral transtension correspond to less active (by volume) andesitic composite volcanoes whereas the segments with the most extension correspond with the highly active Taupo and Okataina caldera complexes (Spinks et al., 2005). The complex plate re-arrangements north of New Zealand have caused a southward migration of eruptive activity during Late Cenozoic (Smith, 1990).

Airborne magnetic data has revealed normally (<0.73 Ma) magnetized volcanic deposits in the eastern parts of TVZ, and reversed (0.73-2 Ma) in the western parts of TVZ (Soengkono et al., 1992). This suggests that the volcanic activity has not only migrated southwards but also from west to east where the volcanoes are active at the present, supporting the theory that the TVZ might act as a hinge contact for an intraplate rotation (Hochstein & Regenauer-Lieb, 1989). A large volume of magma is still trapped at depth mainly concentrated within the central TVZ, feeding heat, volatiles and chemicals through 23 geothermal fields with a total of ~4200 MW thermal energy release, an amount which is unparalleled on this planet (Bibby et al., 1995; Hochstein, 1995).

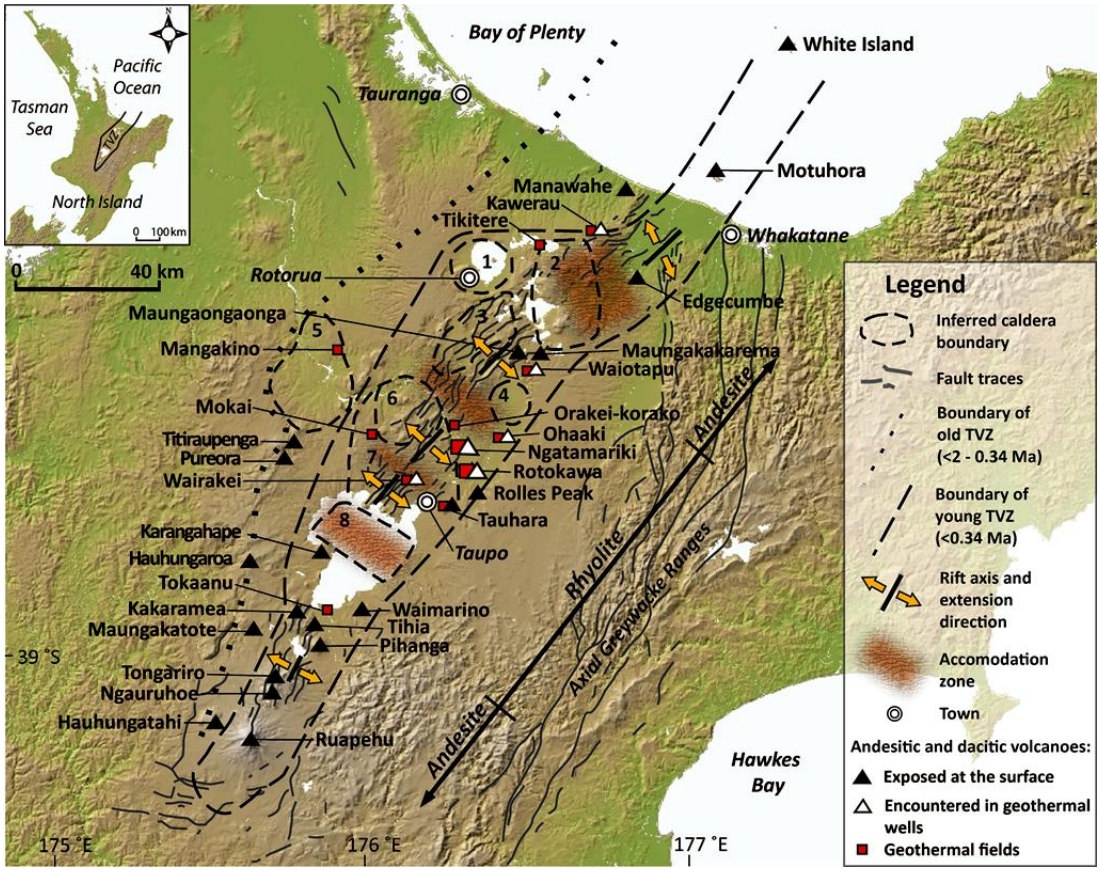

Figure 2.6: Volcanic- and fault structure within the TVZ. The central part is dominated by rhyolitic activity while extremities are mainly andesitic. Calderas: (1) Rotorua; (2) Okataina; (3) Kapenga; (4) Reporoa; (5) Mangakino; (6) Maroa; (7) Whakamaru; (8) Taupo. Data regarding andesitic/dacitic composite volcanoes is from Wilson et al. (1995), rift structure from Rowland & Sibson (2001) and caldera volcanoes Spinks et al. (2005). Fault traces are from the GNS Faults Database.

2.4.2.1 Subsurface andesites in the TVZ

Modern andesitic volcanism in TVZ occurs at the southern and northern ends of the rift zone; Tongariro Volcanic Complex (TgVC), Rolles Peak, Edgecumbe and White Island. However, buried andesite lavas and breccias have been encountered in geothermal wells at various depths in the centre of TVZ similar to Ngatamariki and Rotokawa, at; Kawerau, Waiotapu, Ohaaki-Broadlands and Wairakei-Tauhara (Fig. 2.6). It is difficult to correlate the Kawerau Andesite with andesitic units to the south, as neither the Wairakei Ignimbrite nor Tahorakuri Formation has been encountered in these wells. Andesite at Waiotapu is overlain by the Akatarewa Ignimbrite, which belongs to the Tahorakuri Formation, while shallow and deep

andesitic units at Wairakei and Ohaaki are separated by the Wairakei Ignimbrite. This suggests that there have been several instances of andesitic volcanism in the TVZ, separated by an onset of felsic and voluminous volcanism, which deposited the thick units of Whakamaru group ignimbrites.

Kawerau Andesite

The Kawerau Andesite is located in the western and northern parts of the field and is an important production aquifer due to its fracture permeability (Allis et al., 1995). The andesite occurs between 500-1100 mRSL, where it rests upon Te Teko Ignimbrite and is overlain by Caxton Rhyolite. The andesite is thickest (~400 m) at KA17 in the west, and thins out towards east at KA21 (~50 m), suggesting an andesitic volcanic centre in the NW part of the field. In the eastern parts, the andesite is intercalated with other units which indicate prolonged periods of quiescence between eruptions. In the southern part of the field, andesitic tuff has been found at the same stratigraphic level as the Kawerau Andesite (Bignall and Harvey, 2005).

Waiotapu

Ngakoro Andesite occurs at ~500 mRSL, resting upon Ignimbrite C and is overlain by Akatarewa Ignimbrite (A and B). The andesite is a two-pyroxene, medium-K calc-alkaline lava. It is thickest at WT7 in the south (114 m), and thins out in wells located towards north; WT6 (53 m) and WT4 (<10 m) (Steiner, 1963; Grindley, 1994). The vent location has been proposed to be within the Reporoa Caldera, ~500 m to the south of the Waiotapu geothermal field, as a buried andesitic volcano was disrupted during the Kaingaroa Ignimbrite eruption (Nairn et al., 1994).

Ohaaki-Broadlands

There are two main andesitic units at Broadlands-Ohaaki, Andesite C and Andesite A, which are separated by the Rangitaiki Ignimbrite (Browne, 1973). Rangitaiki

Ignimbrite belongs to the 330 ka Whakamaru-type ignimbrites (Brown et al., 1998). A thin unit (~2 m) of Andesite C was encountered at the very end of well BR17 at ~1100 mCHF. The mineralogy comprised altered plagioclase in a matrix of small feldspar crystals. The andesite was directly overlain by lithic crystal lapilli tuff and rhyolite at shallow depths.

Andesite A occurs in well BR15 at ~1100 mCHF. The andesite is ~50 m thick and described as pale-green and hard, containing phenocrysts of andesine (Browne, 1973). It is overlain by varying units of argillite and greywacke conglomerate, tuffaceous sandstone and tuffs. A ~200 m unit of argillite and greywacke conglomerate and crystal-vitric tuff separates the andesite from greywacke basement.

Wairakei-Tauhara

Shallow layers of Waiora Valley Andesite lava are present in 13 wells at the Wairakei geothermal field, overlying the Wairakei Ignimbrite (Rosenberg et al., 2005). The Waiora Valley Andesite is on average 50 m thick and has a moderate permeability, but is not a drilling target due to its sporadic occurrence in the field. Andesite lava and breccia at deeper levels have been encountered in wells WK121, WK247 and WK301, and belong to the Tahorakuri Formation. The separation of the andesite occurrences suggests that there have been at least two separate episodes of volcanism, originating from the general Western Borefield – Te Mihi area. Browne et al. (1992) and Arehart et al. (1997) rejected any petrogenetic relationship between the Waiora Valley Andesite and Rotokawa Andesites based on petrographical and chronological observations.

2.4.3 Regional faulting

A northwest-southeast extensional fault-belt, known as the Taupo Fault Belt (TFB) after Grindley (1960), intermittently follows the length of the TVZ (Fig. 2.6).

Extension fractures run both along and across faults, and normal faults have an average dip of 75° (Villamor & Berryman, 2001). Extension rate is ~8 mm/yr (Darby & Meertens, 1995), and is partly accommodated by northeast-southwest trending normal faults. The length of individual faults ranges between a few hundred meters to 40 km, spaced up to 3 km apart. Faults near Ruapehu and Rotorua form graben structures in the central part of the zone, while faults at Taupo are characterised by a series of high- and low-standing blocks.

Similar to volcanism in TVZ, faulting has a spatial separation depending on activity. Faults that have been active within the last 20 ka are grouped under the name of modern TFB. The area is 20 km wide and stretches between Rotorua and the Waikato River in the central part of TVZ, manifested as the Ngakuru-Waikite depression. The concentration of extension coincides with rhyolitic volcanism, and Spinks et al. (2005) theorises that it is caused by thinning of the crust, reduced pressure and partial melting of the asthenosphere. This creates a very high heat flow which provides partial melting of suitable crustal material in addition to large rates of mafic magma below the crust, which is subsequently transformed by fractionation into the large volumes of rhyolitic volcanism typical for TVZ. There is no sign of displacement of the surficial Hinuera Formation (<20 ka) along the margins of central TVZ, which suggests that any faults in these areas are relict extension zones. The northern and southern extremes commonly associated with andesitic volcanism are undergoing dextral shearing at ~2.6 mm/yr, and signs of faulting are scarce (Acocella et al., 2003).

Tectonic extension in the TVZ also coincides with geothermal activity. Faults, fractures and dikes cut through the convective system and they may either provide pathways through zones of low permeability, or create a barrier where intense alteration has replaced primary rock composition with clay minerals. The majority (~80%) of the geothermal fields are located within the TFB, and ~60% of those in

accommodation zones. A study by Rowland & Sibson (2004) suggests that rift segments have an increased axial flow, while accommodation zones typically have vertical flow patterns (Fig. 2.7). This could explain the larger presence of geothermal fields at accommodations zones, compared to densely faulted rift segments which are likely to act as drawdown regions.

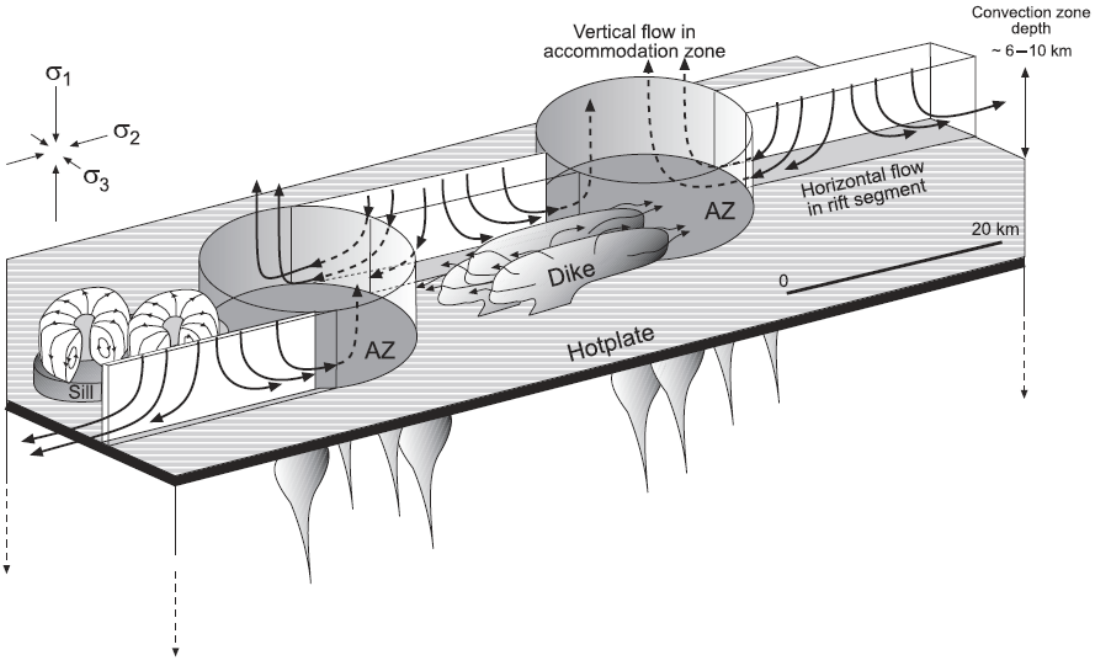

Figure 2.7: Conceptual model for fluid flow in a segmented rift system. Heat transfer may be via sill, dike or small pluton emplacement which is affected by rift kinematics; or a large-scale hot plate which is less affected by rifting. In rift segments, fluid flow is toward accommodation zones except where sills form localized hot plates. Accommodation zones have an enhanced vertical permeability which promotes development of geothermal plumes (from Rowland & Sibson, 2004).

2.4.4 Local faulting

Normal faults form a NE-SW trend through the geothermal fields, creating small horst and graben structures (Fig. 2.8). Most are covered by young volcanic deposits, but lineaments suggesting structural control are visible from the air and correlates with topographical features, such as streams at Ngatamariki (Brotheridge, 1995) and several hydrothermal eruption craters at Rotokawa (Collar & Browne, 1985). Drilling has revealed significant elevation differences of greywacke basement between the fields, ~1100 m between RK4 and NM6. It appears as block faulting by NE-SW

trending normal faults has caused the surface of greywacke basement to dip to the NE (Rae, 2007; Bignall, 2009).

The Ngangiho Fault is part of the larger Orakonui Fault Zone. It cuts the Waikato River north of Tutukau Bridge at Ngatamariki and dips toward northwest (Grindley, 1961). It has been interpreted as bounding a major slump zone caused by caldera collapse of the Taupo Volcano (Rowland & Sibson, 2001). The fault is located far away from existing wells, and has not been encountered during drilling. The Aratiatia Fault Zone stretches between the Tauhara geothermal field and ~2 km north of Rotokawa, consisting of more than 20 segments (GNS Science, 2011). It marks the eastern boundary of the young Taupo Fault Belt (Villamor & Berryman, 2001). The fault, which cuts through both fields, was originally mapped as the Wairakei Fault Zone by Grindley (1961), but is part of the Aratiatia Fault Zone (M. Rosenberg, personal communication, Feb. 2011).

A fault was intersected during drilling of well RK17 at Rotokawa, which might be part of the Aratiatia Fault Zone. The Rotokawa Andesite appears massive (<2100 m), except in the western part of the field. Drilling at RK17 deviated to E-SE intersected shallow levels of andesite between 864-1387 mCHF, followed by layers of Waikora Formation conglomerate and Tahorakuri Formation before returning to Rotokawa Andesite at 1558 mCHF (Rosenberg et al., 2005). The same divergence in stratigraphic succession was repeated in wells RK26, RK27 and RK28 (also deviated towards east) and the most probable explanation to this is the presence of a major normal fault just eastwards of these wells (Fig. 2.8). Wells RK16 and RK18 (share the same pad as RK17 and RK27) were drilled vertically and SW respectively, and show no sign of faulting. At RK28, sampled andesite just above the fault at 1246 mCHF is described as broken and fragmented with slickenside striations, which indeed indicate slip movement associated with faulting.

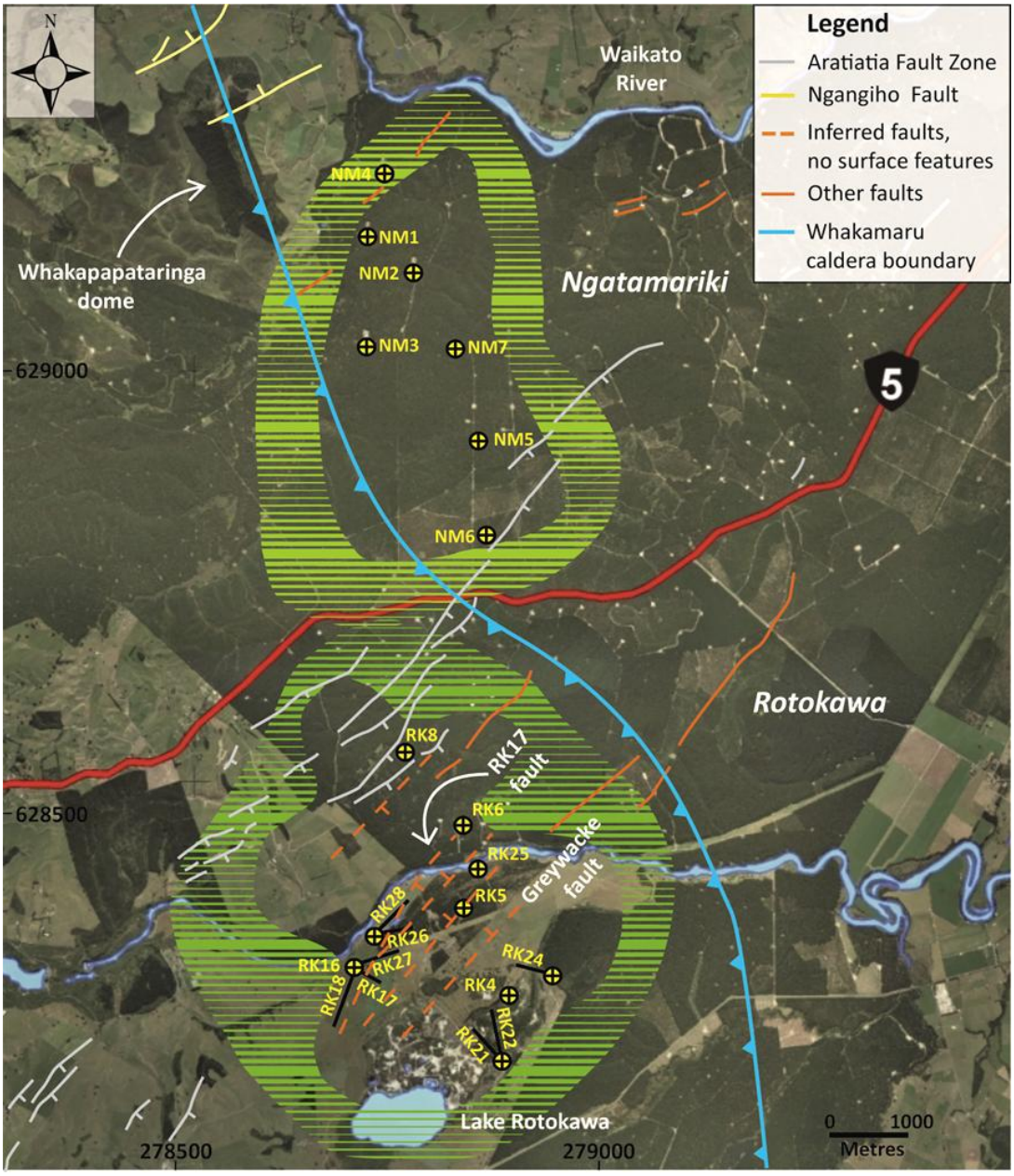

Figure 2.8: Active faults and proposed fault structure of Ngatamariki and Rotokawa fields. Except for the Aratiatia Fault Zone (a surface feature) and greywacke basement fault, inferred faults such as the one encountered in well RK17 are shown in approximate position at the upper layer of Rotokawa Andesite. Modified from Rosenberg et al. (2005) and references therein. Whakamaru Caldera boundary is from Wilson (1986) and faults from GNS Science (2011).

A 75-80° dip angle was estimated based on comparison of formation boundary depths by Rosenberg et al. (2005), which corresponds with the dip angle of most other faults in TVZ (Villamor & Berryman, 2001). Also, by comparing the depth of andesitic units between wells it becomes apparent that the fault has downthrown

strata in the east to northeastern part where the depth of the topmost andesite ranges from about 1200-1800 mCHF, compared to 800-900 mCHF in the western part (Table 2.3).

Rosenberg et al. (2005) sketched a model of historical geology and structure at Rotokawa based on the findings at RK17 (Fig. 2.9). Phase 1 include ponding of andesite lava flows against greywacke fault scarp, followed by reactivation of basement fault system in phase 2 which either created or deepened existing graben structure in which Rotokawa Andesite, Tahorakuri (former Ohakuri Group) tuff and Waikora conglomerate were deposited during phase 3. In phase 4, the graben had been completely infilled by volcaniclastic/pyroclastic material and then covered by Wairakei Ignimbrite. This formation has very slight elevation differences through Rotokawa (<50 m), so any fault movement after ~320 ka is therefore believed to be minor. Another fault structure is the eastern boundary of Whakamaru Caldera. Calderas are a collapse structure caused by an explosive eruption which empties the magma chamber to a point where it is unable to support the weight of the volcanic structure above it, effectively creating a ring fault. The caldera boundary runs through the Ngatamariki field in a NNW-SSE trend, marked by volcanic structures such as the Whakapapataringa dome, and curves around the outside of the Rotokawa field (Wilson et al., 1986). The caldera has no clear topographic margin, so it is defined by the thickness and distribution of the Whakamaru Group ignimbrites (Wairakei Ignimbrite). Thick units intersected in drillholes places Wairakei, Mokai, Tauhara and Rotokawa within the structure, while thin outflow sheets at Broadlands and Waiotapu places them outside the structure.

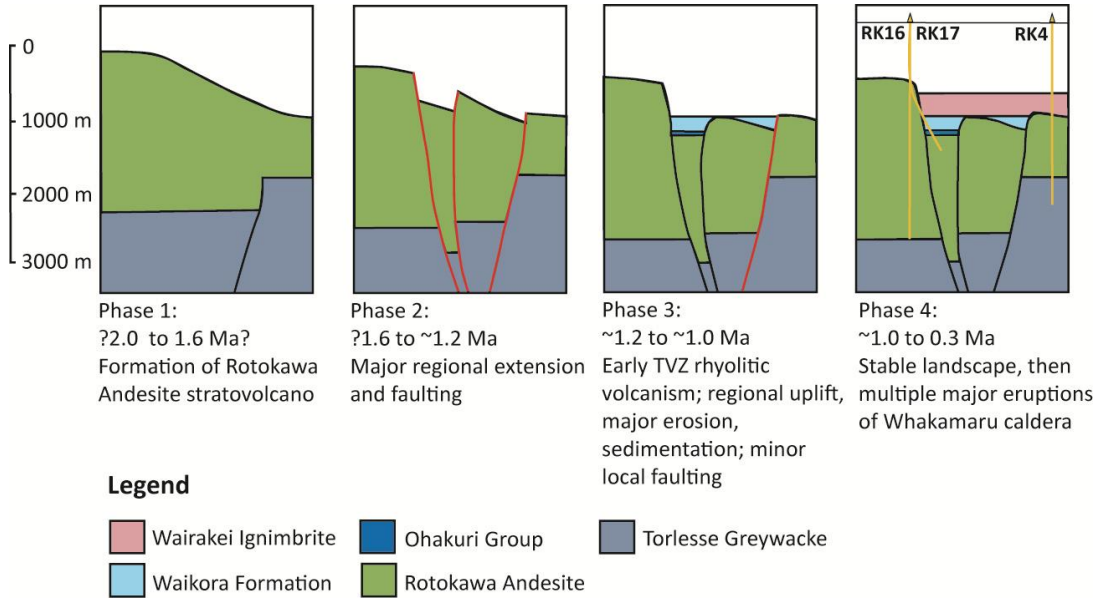

Figure 2.9: Schematic model of Rotokawas geological history and structure before the deposition of Wairakei Ignimbrite (~320 ka) to explain stratigraphic deviation and major fault intersected at RK17 (modified from Rosenberg et al., 2005).

2.5 Stratigraphy

2.5.1 Geological surveys and new stratigraphic nomenclature

Hochstetter observed the graben-like structure of the TVZ (which he named), and related the distribution of hot springs to fault lines as he traveled through the Taupo District in 1859. He carried out the first scientific survey of the area by using systematic geological mapping (Hochstetter & Petermann, 1864). Grange (1937) published the first detailed study of Taupo Volcanic Zone. It included further geological mapping, the relationship of the geology and a comprehensive account of the 18 main hot spring groups in the Rotorua-Taupo Subdivision. Grindley (1959, 1961) continued this work by creating stratigraphic sequences in and around geothermal fields in the TVZ, in addition to the first series of 1:250 000 geological maps of the central North Island (Grindley, 1960). The regional geology of TVZ is commonly described as a volcanic-tectonic depression that has been infilled with almost 3 km of Quaternary volcaniclastic and sedimentary deposits on top of the Mesozoic Torlesse greywacke basement. Surficial deposits are known to comprise

lacustrine sediments, alluvium, hydrothermal eruption breccias and pyroclastics from recent eruptions such as Ruapehu (Gamble et al., 1999). The stratigraphic names have been altered during the years, most lately by Gravley et al. (2006) (Fig. 2.10). The name "Ohakuri" was introduced by Grindley (1959) as a formation name for old pumiceous volcanics in the TVZ and was later replaced by Grindley (1960) with Ohakuri Group to be used for aggradational outwash from old ignimbrites. "Ohakuri" was subsequently used for both surface- and deeply buried deposits, and Gravley et al. (2006) therefore proposed changes to clarify the use of stratigraphic names. The Ohakuri Formation should now only be used for surface deposits composed mainly of primary pyroclastic deposits that postdate the Whakamaru Group ignimbrites (0.32-0.34 Ma).

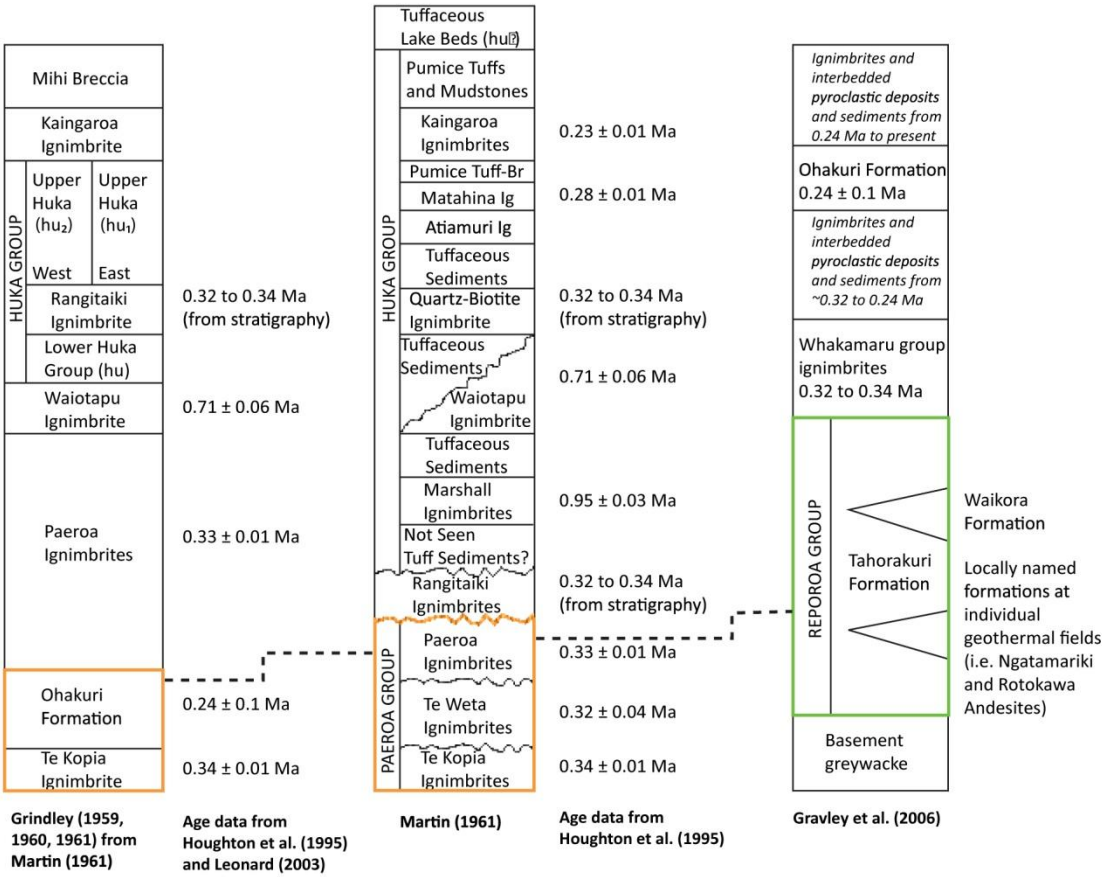

Figure 2.10: Early interpretations of stratigraphic columns in the central TVZ. The left and middle column is accompanied with later obtained radiometric data; the right column is the new stratigraphical names (modified from Gravley et al., 2006).

The Ohakuri Group has been replaced by Reporoa Group as an overall term for deposits predating the Whakamaru Group ignimbrites. This will include the Waikora Formation (sedimentary units with abundant greywacke clasts), Tahorakuri Formation (other volcaniclastic and sedimentary units) and other locally named formations of ignimbrites and lava flows. This thesis will adopt the stratigraphic nomenclature as proposed by Gravley et al. (2006).

Knowledge of the sequence, nature and architecture of the stratigraphy is fundamental in understanding the Ngatamariki and Rotokawa geothermal systems. Exploration drilling began in the 1970-80s when the Government recognized the potentials of Ngatamariki and Rotokawa as geothermal resources (Hunt, 1998). A number of production and injection wells have since been drilled at the Ngatamariki and Rotokawa geothermal fields (Fig. 2.11). Well reports containing stratigraphy, hydrothermal alteration and measurements of porosity and density have been produced by Department of Scientific and Industrial Research (DSIR) and since 1992 by GNS Science, one of the eight Crown Research Institutes formed after the re-structuring of DSIR. Some of well reports (where samples have been collected from or they are mentioned in Browne, 1992) will be summarized in this section (Table 2.1). A cross-section of the subsurface stratigraphy has been created based on these well reports (Fig. 2.12).

Table 2.1: A list of well reports which have been used in this study. MWD = Ministry of Works and Development, DSIR = Department of Scientific and Industrial Research, GNS = Institute of Geological and Nuclear Sciences Ltd.

Well	Author(s)	Year/Report no.	Title	Organisation
Ngatamariki:				
NM1	Berry	1985/37/33/1	Ngatamariki geothermal investigations well NM1	MWD
NM2	Wood	1986a/Unpubl.	Stratigraphy and petrology of NM2: Ngatamariki geothermal field	DSIR
NM3	Wood	1986b/Unpubl.	Stratigraphy and petrology of NM3: Ngatamariki geothermal field	DSIR
NM4	Wood	1986c/Unpubl.	Stratigraphy and petrology of NM4: Ngatamariki geothermal field	DSIR
NM5	Ramirez & Rae	2009a/253	Geology of injection well NM5/5A, Ngatamariki geothermal field	GNS
NM6	Rae, Ramirez & Bardsley	2009a/130	Geology of exploration well NM6, Ngatamariki geothermal field.	GNS
NM7	Rae, Ramirez & Boseley	2009b/289	Geology of exploration well NM7, Ngatamariki geothermal field	GNS
NM1-7	Bignall	2009/94	Ngatamariki geothermal field: Geoscience overview.	GNS
Rotokawa:				
RK4	No well report available, information based on Browne et al. (1992).			
RK5				
RK6	Browne	1985/Unpubl.	Stratigraphy of RK6: Preliminary report	DSIR
RK8	Nairn	1986/Unpubl.	Rotokawa RK8 stratigraphy	DSIR
RK16-18	Rosenberg, Kilgour & Fraser	2005/144	Geology of RK16, RK17 and RK18	GNS
RK21	Ramirez, Kilgour, Rae & Bignall	2008/90	Geology of injection well RK21	GNS
RK22	Kilgour & Ramirez	2008/272	Geology of injection well RK22, Rotokawa geothermal field.	GNS
RK24	Ramirez & Rae	2009b/90	Geology of injection well RK24/RK24 ST1, Rotokawa geothermal field	GNS
RK25	Ramirez, Milicich, Rae & Bignall	2008/332	Geology of injection well RK25.	GNS
RK26-27	Rae, McCoy-West & Ramirez	2009c/202	Geology of production wells RK26 and RK27, Rotokawa geothermal field	GNS
RK28	Rae, McCoy-West , Ramirez & Alcaraz	2009d/253	Geology of production well RK28, Rotokawa geothermal field	GNS
RK1-18	Rae	2007/83	Rotokawa geology and geophysics	GNS

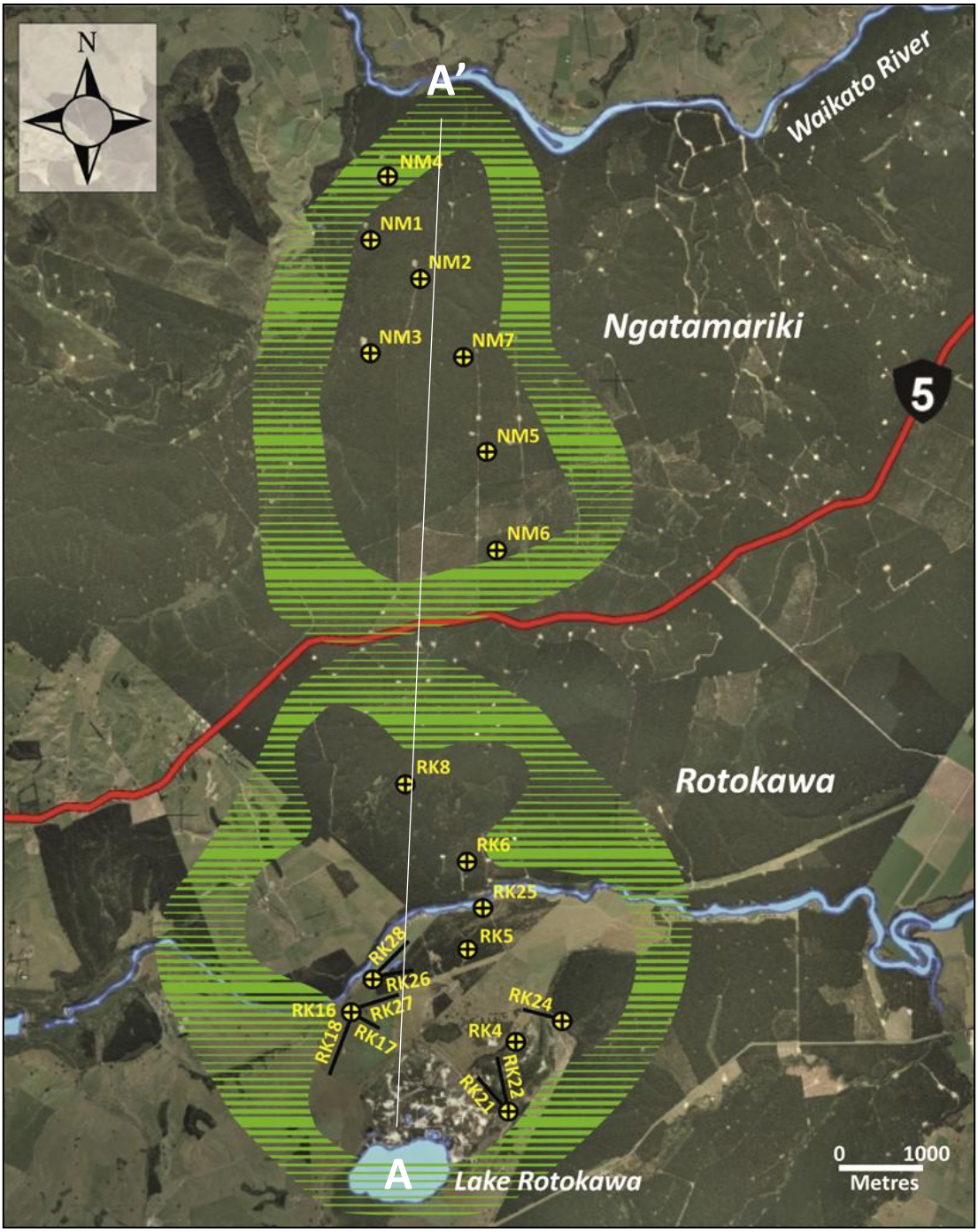

Figure 2.11: Map of wells at the Ngatamariki and Rotokawa fields. Cross-section (Fig. 2.12) is based on the line A to A' (modified from MRP Ltd.).

South

Rotokawa

Ngatamariki

North

A

A’

Lake Rotokawa

RK21

RK4

RK24

RK18

RK27

RK5

RK25

Waikato River

RK6

RK8

NM6

NM5

NM7

NM3

NM2

NM1

NM4

Depth (mRL)

500

0

-500

-1000

-1500

-2000

-2500

3000

?

?

?

?

?

Stratigraphy

- Oruanui Formation
- Taupo Pumice Alluvium
- Pararíki Breccia
- Huka Falls Formation
- Waiora Formation
- Rhyolite-dacite lava and breccia
- Tuffaceous siltstone
- Wairakei Ignimbrite
- Volcanic breccia
- Waikora Formation
- Tahorakuri Formation (Finely lam, pum, tuff sed.)
- Tahorakuri Formation (Akatarewa Ign and similar)
- Andesite lava and breccia
- Diorite
- Micro diorite
- Torlesse greywacke

Faults

0 1000

Metres

Figure 2.12: A north to south cross-section of the subsurface geology at the Ngatamariki and Rotokawa geothermal fields (a summary of all well reports).

2.5.2 Holocene to Pleistocene alluvium and hydrothermal eruption deposits

Lloyd (1972) mapped the surface geology of Ngatamariki in conjunction with his study of nearby Orakeikorako, and a more detailed study of surface features and the geophysical properties of the area by Bennie (1983). The deposits that cover the surface of Ngatamariki were described by Brotheridge (1995), while Rotokawa surface geology has been summarised by Grindley et al. (1985).

2.5.2.1 Orakonui Formation

This is a surficial deposit occurring at Ngatamariki, comprising of (~10 m) pumice breccias with common volcanic lithics, quartz and minor feldspar. It originates from the most recent hydrothermal eruptions in 1948 and 2005, from a large crater in the southern area of Orakonui Stream. The formation was named by Beck & Robertson (1955), and adopted by Lloyd (1972). It has been divided into five members:

- ✧ a lowermost layer of gritty pumice tuff, grey in colour with glass and rhyolite inclusions (>12 m);
- ✧ a buff to pink/orange coloured pumice breccia with quartz and rhyolite inclusions (<30 m);
- ✧ pumice breccias with large, quartz-rich pumice inclusions (>30 m);
- ✧ a grey-coloured ignimbrite with minor quartz-rich pumice and rhyolite inclusions (~20 m); and
- ✧ an uppermost ignimbrite, buff in colour with rhyolite lapilli and abundant pumice inclusions (~15 m).

2.5.2.2 Parariki Breccia

This deposit comprises hydrothermal breccias which partially covers up to 15 km^2 on the southern side of Waikato River, originating from multiple eruptions during the last 20 ka.

2.5.2.3 Taupo pumice alluvium

The pumice alluvium originates from the 232 AD Taupo eruption which was one of the largest caldera-forming eruptions occurring from a vent located at Horomatangi Reefs, the total eruption volume is estimated to have been ~100 km^3. The deposit is visible in outcrops and road cuts at Ngatamariki and also forms a low terrace near the Taupo River at Rotokawa.

2.5.2.4 Oruanui Formation

This is an extensive surficial deposit occurring at both fields, comprising (<70 m) vitric-lithic tuff, cream to pink in colour with volcanic lithics, quartz and rare biotite and pyroxene crystals. The formation originates from the 27 ka Oruanui eruption, and was mapped by Vucetich & Pullar (1969). They correlated it provisionally with the Wairakei Breccia, occurring at the Wairakei geothermal field. It was previously divided into two members; Oruanui Breccia and Oruanui Ash, but any internal formal stratigraphic subdivisions were proposed by Wilson (1988) to be replaced with simply:

- *Oruanui Ignimbrite* – all ignimbrite flow units generated during this eruption (previously named Oruanui Breccia) defined as the uppermost layer of fine-grained, massive breccia pale brownish grey in colour containing pumice and rhyolite lapilli with rare chalazoidites (~2.5 m); and
- *Oruanui Fall deposit* – all the fall units (previously named Oruanui Ash) defined as fine, massive ash with minor lapilli, brownish to pinkish grey containing chalazoidites and a showerbedded fine to coarse ash at the base (~3 m).

One of the reasons for this was due to existing confusion regarding definition and lateral correlations in previous work (e.g. Vucetich & Howorth, 1976; Froggatt, 1981; Self & Healy, 1987). Another reason was the widespread dispersal and large volume

of the eruption, as fall deposits have been replaced by ignimbrite at distal locations; hence there is no single locality with a representative Oruanui eruption deposit and identification of members may be difficult.

2.5.2.5 Hinuera Formation

This is a fluvial deposit which forms low angle river terraces at Ngatamariki. It consists of interbedded silt, sand and pumiceous gravels believed to be mainly eroded volcanic detritus from the Oruanui Formation transported by the Waikato River when it shifted direction northwards after the 27 ka Oruanui eruption (Vucetich & Pullar, 1969).

2.5.3 Pleistocene lake sediments: Huka Group

Lake sediments, interbedded vitric tuff and volcanic rocks were given the name Huka Formation by Steiner (1953). Grindley (1959) later renamed it the Huka Group, and subdivided the deposits into a Waiora Formation and Huka Formation (now Huka Falls Formation). The sediments, consisting of pyroclastic eruptives and normal stream and mudflow erosion, were deposited during Middle to Late Pleistocene into the Huka lake basin which was formed by a volcanic-tectonic collapse of the Taupo Volcanic Zone. The Huka Group occurs at both fields.

2.5.3.1 Huka Falls Formation

The Huka Falls Formation includes mainly laminated lacustrine sediments. Sandy gravels in the uppermost layer grades into fine sandstone and siltstone with rare pumice-rich layers in lower layers (<215 m). An interesting find is the Parekauau andesite dyke which is exposed at the Tutukau Road at Ngatamariki, intruding into Haparangi Rhyolite and the overlying Huka Falls Formation.

2.5.3.2 Waiora Formation

This formation was defined by Grindley (1965) at Wairakei geothermal field to comprise all strata between the Wairakei Ignimbrite and Huka Falls Formation, subdivided into five members. It is mainly of volcanic origin, with intercalated layers of mudstones and sandstones. However, any rhyolite lavas were assigned to the Haparangi Rhyolite Group and andesite lavas to the Waiora Valley Andesite, the latter is not used at Ngatamariki and Rotokawa. At Ngatamariki it comprises of up to 240 m thick pumice-rich vitric tuff with intercalated crystal tuff (quartz, feldspar and rare pyroxene). At Rotokawa, the deposits comprise of up to 460 m thick, crystal-rich (hornblende) vitric tuff.

2.5.4 Quaternary igneous rocks and associated breccias: Whakamaru and Reporoa Group

2.5.4.1 Rhyolite lava and breccia

Rhyolite lava and breccia occur below the Waiora Formation and the Tahorakuri Formation at the Ngatamariki field, and between Waiora Formation and the Wairakei Ignimbrite at the Rotokawa field. Pleistocene rhyolite domes and flows were named Haparangi Rhyolites by Grange (1937), while Grindley (1959) named all Huka or post-Huka rhyolite domes and associated pyroclastic rocks as Haparangi Rhyolite Group. One of the sources is the Whakapapataringa rhyolite dome, located to the west of the Orakonui springs where it has extruded along NNW-trending fractures. At the Ngatamariki field, the petrographic descriptions differ between a shallow layer and a deeper layer:

- ✧ glassy with perlitic texture, phenocrysts are quartz, feldspar, pyroxene and magnetite with a thickness of up to 200 m, and
- ✧ hard, porphyritic quartz-rich with phenocrysts of quartz, minor feldspar and ferromagnesian minerals with a thickness of up to 285 m.

At the Rotokawa field, the rhyolite is described as slightly banded, porphyritic although crystal-poor with phenocrysts of quartz, plagioclase and minor hydrothermally altered ferromagnesian minerals set in a perlitic or spherulitic groundmass, with a thickness of up to 550 m.

2.5.4.2 Wairakei Ignimbrite

The Wairakei Ignimbrite was described by Grindley (1965) when found in bore holes at Wairakei geothermal field. It belongs to the Whakamaru Group, which was named by Wilson et al. (1986) to include the Whakamaru, Manunui, Rangitaiki, Te Whaiti, Wairakei and the Paeroa Range Group ignimbrites as they have similar age (330-340 ka) and petrographic properties. The ignimbrites erupted from the central TVZ after a ~350 ka hiatus in caldera-forming activity and deposits with a total volume of >1000 km^3 occur on the eastern and western margins of the TVZ.

At the Ngatamariki field, the Wairakei Ignimbrite is described as a crystal-lithic tuff or breccia, with abundant quartz, minor feldspar, rare biotite and pyroxene, minor volcanic lithics and pumice in a fine ash (<100 m). At the Rotokawa field, the ignimbrite (<190 m thick) can be non-welded to densely welded, typically white in colour and crystal-rich with heavily embayed, large quartz crystals.

2.5.4.3 Waikora Formation

The Waikora Formation is one of the members of the Reporoa Group, and is defined to cover pre-Whakamaru sedimentary deposits which comprise abundant greywacke pebble conglomerates, probably derived from old river gravels (Grindley & Browne, 1968). This formation only occurs at the Rotokawa field, up to 240 m in thickness, and is described as rounded to sub-rounded gravels of greywacke and argillite.

2.5.4.4 Tahorakuri Formation

Whereas the Waikora Formation is used for greywacke conglomerate, Gravley et al. (2006) proposed the new formation name Tahorakuri to cover other volcaniclastic and sedimentary deposits within the Reporoa Group, located between the Whakamaru Group ignimbrites and the greywacke basement. The Tahorakuri Formation occurs at both geothermal fields, although it is divided into three members at the Ngatamariki field:

- *tuffs and sediments* – a lithic tuff/breccia white to pale grey in colour, intercalated with fine sediments (<240 m);
- *Akatarewa ignimbrite* – a pale grey lithic tuff/breccia with heterolithic clasts of grey to brown lava, rhyolite, pumice, greywacke-argillite and sandstone in a silty matrix (<640 m), and
- *andesite lava, breccia* – a grey porphyritic andesite lava and associated breccias (>830 m), with abundant feldspar, common pyroxene and minor amphibole (i.e. Ngatamariki Andesite).

The Tahorakuri Formation at Rotokawa is described as a white, crystal-vitric-lithic tuff up to 230 m thick.

2.5.4.5 Ngatamariki and Rotokawa andesites

The andesites at Ngatamariki and Rotokawa were named by Browne et al. (1992) as part of their work with describing and interpreting the andesite flows encountered during exploration drilling at the geothermal fields. However, the andesites at Ngatamariki have traditionally been categorized under the Tahorakuri Formation (see above), while the andesites at Rotokawa have been named as a separate formation. The andesites are described as a dark grey to green, massive to slightly flow banded porphyritic lava and associated breccia with phenocrysts of feldspar, pyroxene and minor amphibole set in a microcrystalline groundmass. They are in the

same stratigraphic position, as both are overlain by the 330 ka Wairakei Ignimbrite, and Mesozoic Torlesse greywacke basement has been encountered directly below the andesites in wells RK4, RK21, RK24 and NM6. However, there are occasional layers of other formations within the andesitic units at both Ngatamariki and Rotokawa fields.

At Ngatamariki, there are thin, shallow units of andesitic to dacitic compositions with an upper formation boundary at ~700-1300 mCHF overlying thick, deeper units with an upper boundary at 1600-2200 mCHF, separated by layers of Tahorakuri Formation (Table 2.2). The same formation has also been intersected within the deeper andesitic units in wells NM2 and NM5, which suggests periods of quiescence between eruptions which allowed ignimbrites from a nearby volcano to accumulate on top of the andesite lava/breccia. The andesitic units are thickest at in the southern part of the field, NM6 and NM7. Circulation loss caused only fragments of andesite to be recovered in NM5, making it impossible to estimate the thickness of the andesite at this location, and with the small amount of wells in this field it is difficult to give even an approximate position of the vent system.

The Rotokawa Andesite appears massive, but drilling of deviated wells RK17, RK26, RK27 and RK28 intersected layers of Waikora and Tahorakuri Formation before returning to andesite. The unexpected stratigraphic succession in this area of the field was caused by a normal fault located to the east of the wells. At Rotokawa, the andesitic unit is thickest in the western part of the field with 2190 m at RK16 and 1521 m at RK18 while thinning out towards E-NE to ~800 m (Table 2.3). Even though the volcano has been significantly reduced by erosion during the period it was exposed at the surface, it is likely that the centre of the volcano once was located towards west based on the lateral variation in thickness.

Table 2.2: Overview of andesite occurrences at Ngatamariki (based on references in Table 2.1).

Well	Depth (mCHF)	Thickness (m)	Lithology
NM2	920 to 960	40	Intensely altered andesite breccia.
	1678 to 2100	422	Intensely altered andesite breccia.
NM3	777 to 987	210	Intensely altered dacite lava.
	1942 to 2192	250	Andesite breccia (feldspar-pyroxene-amphibole), similar to NM2 but less altered.
NM4	892 to 1082	190	Intensely altered dacite lava and tuffs. Petrographically different to the dacite in NM3.
	1140 to 2092	952	Intensely altered andesite lava/breccia representing the phyllic zone of the diorite.
	2092 to 2642	550	Micro-quartz diorite, representing the quartz diorite transition.
	2642 to 2741	99	Quartz-diorite, comprising altered porphyry with a groundmass texture that suggests plutonic crystallisation.
NM5	2457 to 2987	530	Circulation loss, but core fragment of moderately altered andesite at 2575-76.5 mRF was recovered, and also intensely altered lava or breccia from 2903-5.5 mRF.
NM6	1270 to 1350	80	Andesite lava, top 15 m is brecciated.
	1450 to 1630	180	Andesite/dacite lava. The bottom ~100 m is a brecciated.
	2210 to 3150	940	Andesite lava.
NM7	1380 to 1650	270	Volcanic breccia
	1650 to 2174	524	Andesite breccia
	2174 to 2953	779	Circulation loss, although core of andesite breccia was recovered from 2179-84 mRF.

Table 2.3: Overview of andesite occurrences at Rotokawa (based on references in Table 2.1).

Well	Depth (mCHF)	Thickness (m)	Lithology
RK4	1350 to 2200	850	Andesite
RK5	1500 to 2500	1000	Andesite
RK6	1697 to 2437	740	Andesite lava (feldspar-pyroxene), interlayered with tuffs and greywacke.
RK8	1892 to 2719	827	Andesite lava (feldspar-pyroxene), breccia is present at 1953-55 mRF.
RK16	860 to 3050	2190	Moderately to strongly altered andesite lava.
RK17	864 to 1387	523	Moderately to strongly altered andesite lava.
	1558 to 1837	279	Moderately to strongly altered andesite lava.
RK18	917 to 2438	1521	Moderately to strongly altered andesite lava.
RK21	1243 to 2253	1010	Andesite lava (feldspar-hornblende-pyroxene).
RK22	1398 to 2453	1055	Andesite lava (feldspar-hornblende-pyroxene).
RK24	1413 to 2178	765	Andesite lava (feldspar-pyroxene-amphibole), rare intercalated andesitic tuff and breccia.
RK25	1810 to 2697	887	Andesite lava (feldspar-pyroxene-amphibole). Andesitic tuff and breccia are intercalated below ~2150 mRF.
RK26	812 to 1267	455	Andesite lava (feldspar-pyroxene).
	1566 to 2110	544	Circulation loss, but assume that andesite unit continues down to greywacke basement
RK27	850 to 1395	545	Andesite lava (feldspar-pyroxene).
	1810 to 2000	190	Andesite breccia (feldspar-pyroxene), core #1.
	2000 to 2143	143	Andesite breccia (feldspar-pyroxene) core #2.
	2143 to 2550	407	Circulation loss, but assume that andesite unit continues down to greywacke basement
RK28	806 to 1250	444	Moderately altered andesite lava (feldspar-pyroxene).
	2307 to 2491	184	Circulation losses, but sidetrack core# 2 recovered andesite lava (feldspar-pyroxene).

Based on the thickness of the andesite (<2100 m at Rotokawa, <900 m at Ngatamariki), this represents an accumulation of several lava flows, which have been erupted over an extended period of time. Age-dating by Arehart et al. (2002) of samples from Ngatamariki returned an age of 1.2 Ma for shallow andesitic units (~1000 m) and 550 ka for the diorite (~2208 m), by using sericite and hornblende separates respectively. However, hydrothermal alteration makes it difficult to determine an age of the andesites, especially when using Ar-dating as the minerals are contaminated by atmoshperic Ar from circulating geothermal fluids, and the age might therefore reflect the latest thermal event instead of primary crystallisation ages. Zircon U-Pb dating has proved to be a reliable method for altered volcanic rocks (Wilson et al., 2010), but it is a very rare accessory mineral in TVZ andesites which makes sampling of sufficient material for analysis unfeasible.

2.5.5 Basement geology

The basement geology of New Zealand consists of the mobile Eastern Province and foreland Western provinces, separated by a Median Tectonic Zone (Sutherland, 1999) (Fig. 2.13). The early Paleozoic Western Province covers an area west and southeast of the Alpine Fault, extending some distance offshore. It contains the Buller terrane which is largely composed of quartz-rich clastics and black shales, and the Takaka terrane which is composed of a diverse range of rock types such as volcaniclastics, silt, limestone and turbidites (Cooper & Tulloch, 1992). The Median Tectonic Zone (also called Median Batholith) is continuous through the South Island except for a 480 km offset across the Alpine Fault, and is composed of mid Triassic to early Cretaceous plutonic rocks related to a subduction zone-setting (Mortimer et al., 1999). The Permian to early Cretaceous Eastern Province forms the basement for the rest of New Zealand and is composed of eastern terranes (Torlesse, Waipapa and Caples) created in an accretionary prism environment and western terranes (Dun Mountain-Maitai, Murihiku and Brook Street) created in either back- or forearc environments, and they consist mainly of deformed metamorphosed sandstone-

mudstone sequences with minor occurrences of lava, chert and limestone (Bishop et al., 1985; in Mortimer et al., 1999).

The boundary between the Torlesse and Waipapa terranes runs along the length of the Taupo Volcanic Zone (TVZ) in a northeast-southwest direction. The only surface outcrops in the TVZ are north of Rotorua and Okataina Volcanic Centres in the Bay of Plenty. Torlesse greywacke has been encountered during drilling at several geothermal fields located along the eastern margin of the TVZ (Graham et al., 1992). Geochemical analysis by Browne (1992) of rock samples from Rotokawa revealed isochron- and Sr^{87}/Sr^{86}-values (123 Ma and 0.70778) close to those of the Kaimanawa Ranges (139 Ma and 0.70735) to the east suggesting that the basement rock belongs to Torlesse terrane rather than the less radiogenic Waipapa terrane (<0.7055) to the west. At Ngatamariki geothermal well NM6, a massive meta-sandstone with veins filled with quartz and calcite has been intersected at -3016 mRL (Bignall, 2009).

At Rotokawa geothermal wells RK4 and RK16 at -1850 mRL and -2720 mRL respectively, drilling has intersected a weakly metamorphosed argillite and fine silty sandstone (Rae, 2007). The low matrix porosity (<5%) of the greywacke in both geothermal fields and decreasing hydrothermal alteration below 1.2 km depth at Rotokawa indicates that fluid flow through the basement is largely controlled by secondary permeability related to brittle faulting and fractures. The difference in depth of ~1100 m between RK4 and NM6 and the absence of greywacke in other deep wells suggests that the basement surface dips to the northwest as a result of block faulting by northeast-southwest striking normal faults.

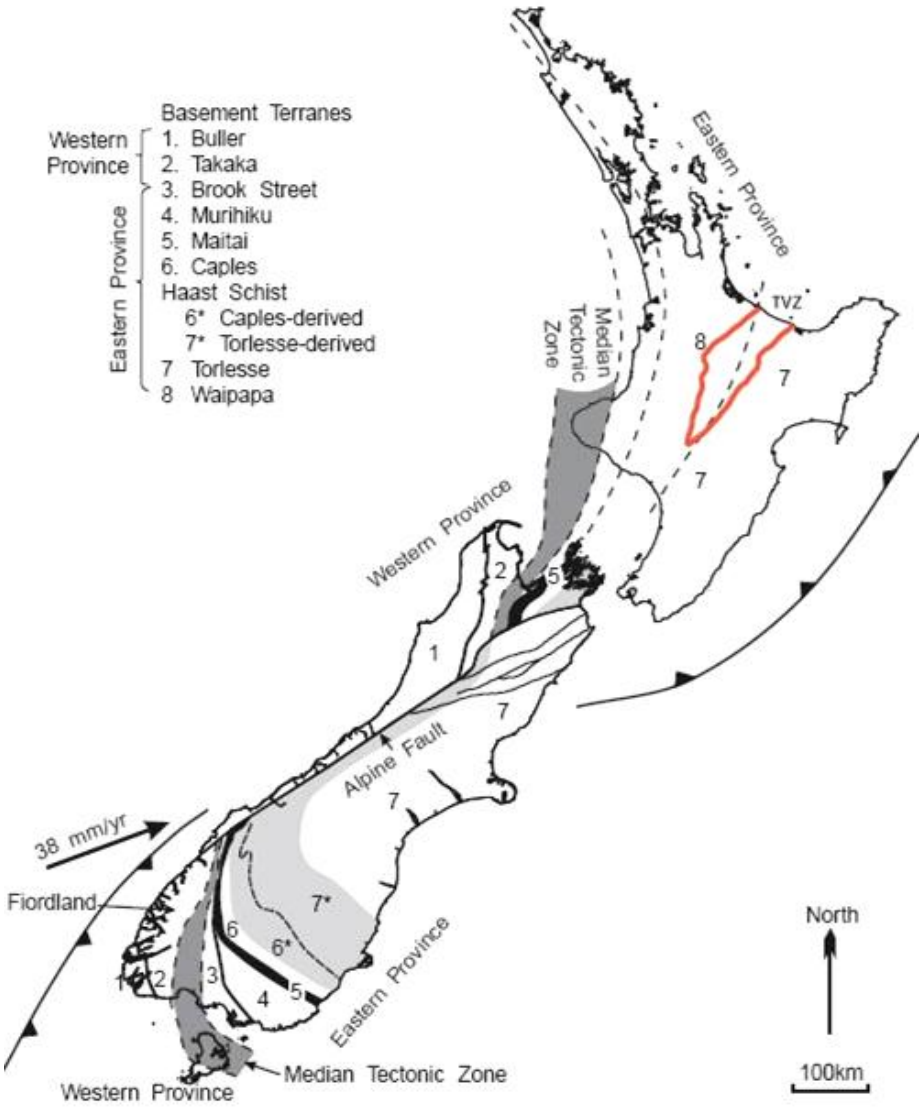

Figure 2.13: Basement terranes of New Zealand (modified from Sutherland, 1999).

Chapter 3
Primary mineralogy

3.1 Introduction

The andesites at the Ngatamariki and Rotokawa geothermal fields are dark grey to green in colour, massive to slightly flowbanded or vuggy porphyritic lava with associated hydrothermally altered breccia. The andesites have primary phenocrysts of plagioclase, augite, orthopyroxene and occasional hornblende, biotite, quartz, Fe-Ti oxides. The crystalline groundmass consists of plagioclase laths, interstitial pyroxenes, disseminated Fe-Ti oxides and volcanic glass. Breccia clasts are commonly andesitic, with minor rhyolitic or sedimentary occurrences. Browne et al. (1992) recognised different petrographic types at the two fields based on the presence of major phenocrysts:

- *hornblende andesite* – a composition of plagioclase > clinopyroxene > hornblende found at the Ngatamariki field (although only rare outlines of primary hornblende are visible due to alteration); and
- *pyroxene andesite* – a composition of plagioclase > clinopyroxene > orthopyroxene found at the Rotokawa field.

Two more petrographic types have been recognised in this thesis:

- *felsophyric quartz andesite (e.g. dacite)* – where the primary phenocrysts are quartz > plagioclase set in a groundmass of microcrystalline quartz, plagioclase, glass and rare Fe-Ti oxides, found in shallow units (<2000 mRF) at Ngatamariki; and
- *biotite andesite* - where the primary phenocrysts are plagioclase > biotite > augite > orthopyroxene set in a groundmass of plagioclase laths, interstitial pyroxenes, disseminated Fe-Ti oxides and volcanic glass, found in well RK18 at 2219-2221 mRF.

Petrographic investigations are made difficult by extensive hydrothermal alteration in these units, as secondary mineral assemblages replace and obscure primary phenocrysts and groundmass textures. This chapter will therefore discuss the mineral chemistry and modal analyses of a small selection of subtle to weakly altered samples from both geothermal fields.

3.2 Methodology

A total of 123 samples were collected from wells NM5, NM6 and NM7 at Ngatamariki (1080-3035 mRF) and wells RK18, RK21, RK24, RK25 and RK27 at Rotokawa (1250-2705mRF), which represents a widely spaced cross-section of the two fields (Table 3.1). 17 of the samples were discarded, as they belonged either from the overlying Tahorakuri Formation (LA.60-65, 79-80, 85), rhyolite lava (LA.74-76), or the greywacke basement (LA.100-104).

The availability of cores were sparse, commonly ~3 m of andesite per well, but cuttings had been collected every 5 m by the drilling companies. Due to the time constraint of a MSc thesis, it was impossible to do continuous downhole profiles as the andesite is up to 2 km thick in some areas so this would result in several hundred samples per well. Therefore, samples were taken from cores where a change in alteration could be seen, and cuttings were obtained at regular intervals in order to provide an overview of rock compositions existing within the fields. A few representative samples were selected for reflected light microscopy, electron microprobe analysis and modal analysis (Table 3.2).

Table 3.1: Overview of collected samples from Ngatamariki and Rotokawa fields

Well	Rock type	Sample type	Depth (mRF)	Sample no.	Interval (m)
NM5A	Deep Nm andesite	Core	2575-2905	2	
	Deep Nm andesite/Tahorakuri FM	Cuttings	2440-2465	6	5
NM6	Deep Nm andesite	Core	2686-3035	3	
	Shallow Nm andesite	Cuttings	1080-1675	12	50
	Deep Nm andesite	Cuttings	2210-2550	8	50
NM7 core #1	Deep Nm andesite	Core	2179-2184	3	
	Shallow Nm andesite/Volc breccia	Cuttings	1390-1460	8	10
RK18	Rk andesite	Core	2219-2221	3	
RK21	Rk andesite	Core	1876	3	
	Rk andesite	Cuttings	1250-2300	22	50
RK24ST1	Rk andesite	Core	1820-1823	2	
	Rk andesite	Cuttings	1505-2400	19	50
RK25 core #1	Rk andesite	Core	2000-2003	3	
	Rk andesite	Cuttings	1835-2705	19	50
RK27 core# 2	Rk andesite	Core	1850-2152	10	

3.2.1 Thin section petrography

Core samples were cut to blocks which fit standard size petrographic glass slides (27x46x1.2 mm) and the surface was grinded to remove any unevenness, first by a horizontal brass grinder and then by 600 grit aluminium oxide (Al_2O_3) powder on a glass surface. The petrographic glass slides were frosted on one side to remove any unevenness from production, and placed on a hot plate prior to mounting. The core blocks and a mixture of 2-component Hillquist resin were heated up to 60 °C before the blocks were mounted on glass slides as this lowers the viscosity of the resin and lets air bubbles escape freely, and left for 3 hours on a hot plate set at 60°C. Cuttings had to be mixed with resin in foil containers, to create a similar shape as the core blocks. The cuttings along with a 2-component Araldite resin were heated up to 60 °C on a hot plate before placing into foil containers. Due to the thermal behaviour of resin, the foil containers were left to set in room temperature to avoid deformation of the glass slide. The main part of core and cutting blocks was cut off with a Struers Discoplan-TS, and the remaining rock was grinded down to a thickness of ~30 microns. The correct thickness was determined by the interference colours under cross-polarized light, where plagioclase should have a light straw-yellow to white colour.

Table 3.2: Location and alteration intensity of the selected samples. Subtle = plg is almost intact, Weak = plg is partly replaced, Moderate = plg is partly to completely replaced, Strong = plg is completely replaced, Intense = no primary minerals left.

Sample	Field	Well	Depth (mRF)	Alteration intensity
LA.4	Ngatamariki	NM5A	2575-2578	Weak
LA.5	Ngatamariki	NM6	2686-2689	Weak
LA.12	Rotokawa	RK18	2219.1	Weak
LA.14	Rotokawa	RK18	2221	Weak
LA.15	Ngatamariki	NM6	2210	Weak
LA.22	Ngatamariki	NM6	2550	Weak
LA.23	Rotokawa	RK21	1250	Weak
LA.67	Ngatamariki	NM7	1400	Weak
LA.75	Ngatamariki	NM6	1130	Weak
LA.1	Rotokawa	RK21	1876.8	Moderate
LA.9	Rotokawa	RK27 core #2	2153	Moderate
LA.11	Rotokawa	RK27 core #2	1851	Moderate
LA.48	Rotokawa	RK25	2000	Moderate
LA.44	Rotokawa	RK21	2300	Strong
LA.47	Ngatamariki	NM7	2179	Strong
LA.51	Rotokawa	RK24 ST1	1820	Strong
LA.53	Rotokawa	RK27 core #2	2147	Strong
LA.3	Rotokawa	RK21	1876.2	Subtle
LA.58	Rotokawa	RK27 core #2	2152	Subtle
LA.7	Ngatamariki	NM6	3032-3035	Intense

A cover slip was placed on top of the thin section with the aid of Petropoxy 154 mixed with a curing agent (both heated up to 60 °C) to protect the surface from scratches and improve visibility under the microscope. Those samples selected for reflected light microscopy and electron microprobe analysis were polished on a Bueler twin polish grinder with a 0.3 micron grit silica carbon (SiC) powder to achieve as smooth surface as possible and left uncovered.

3.2.2 Modal analysis

Phenocryst and groundmass modal data were collected by standard point-counting, with 300 counts per thin section. Secondary minerals were included due to lack of completely unaltered samples, and thin sections made from both cores and cuttings have been used due to the scarce amount of cores collected by the drilling companies (Table 3.3).

3.2.3 Electron Microprobe Analysis (EMA)

A map of the polished thin section and microphotographs of each analysis point was created to assist with identification while using the microprobe. The EMA was carried out at the University of Auckland using a JEOL JXA-840A EMPA with an eumeX EDS detector supported by Moran Scientific. The beam current was 800 pA with an analysis live-time of 100 seconds and an analytical spot of ~2 microns, whereas calibration was done by using a suite of Astimex mineral standards. EMA obtains the geochemical composition of plagioclase, orthopyroxene and clinopyroxene phenocrysts in addition to Fe-Ti oxides and secondary minerals such as calcite, chlorite, epidote and hydrothermal biotite, although the data does not always add up to 100% due to the hydrous nature of some minerals, e.g. chlorite and biotite. Analysis points were mainly focused on the rims of phenocrysts where the composition reflects the conditions present during the final stage of crystallisation, although a combination of core and rim analysis was also used to detect zoning. A selection of the EMA data is given in Table 3.4.

3.2.4 Cathodoluminescence (CL)

A few, selected polished thin sections were photographed with a cathodoluminescence microscope. When subjected to a high energy electron beam, the colouration of alteration minerals becomes distinctively orange to red and they are easier to spot in the rock matrix with regards to mineral boundaries and distribution. The instrument used was a CITL (Cambridge Image Technology Limited) Mk5-1, combined with a Nikon D5-5Mc camera and Nikon NIS Elements software. The conditions for the electron gun current were 350 uA and 16-20kV.

3.3 Petrography and mineralogy

Analysis of modal components obtained from the andesites show a slightly higher abundance of groundmass at Ngatamariki (54-61%) compared to Rotokawa (32-51%) (Table 3.3, Fig. 3.1). The amount of plagioclase (23-30% vs. 32-37%) and pyroxene (0-3% vs. 6-11%) is however lower at Ngatamariki.

Table 3.3: Modal data analysis of least altered samples from Ngatamariki and Rotokawa fields. Sample marked with * is a thin section made from cuttings instead of cores.

Sample	**LA.3**	**LA.4**	**LA.5**	**LA.14**	**LA.58**	**LA.67***
Well/mRF	**RK21/1876**	**NM5A/2575-78**	**NM6/2686-89**	**RK18/2221**	**RK27#2 /2152**	**NM7/1400**
Alteration	**Subtle**	**Weak**	**Weak**	**Weak**	**Subtle**	**Weak**
Groundmass	50.33	61	54.33	32.33	51	79.23
Primary minerals:						
Plagioclase	32.33	23.33	30.67	37.67	32.33	4.23
Augite	5.33	3.33	0	6	5.33	0
Orthopyroxene	1.67	0.67	0	2.67	5.67	0
Quartz	0	0	0	0.33	0	8.5
Fe-Ti oxides	3.67	1	3.33	9.67	3.67	5.93
Secondary minerals:						
Calcite	1.33	1	1	1.33	0	2.11
Chlorite	0	5.67	2.33	1.33	0	0
Epidote	0	0.33	0.33	0	0.33	0
Secondary biotite	5.33	0.33	0	8.33	1.67	0
Secondary hornblende	0	3.33	8	0.33	0	0
Total (%)	100	100	100	100	100	100

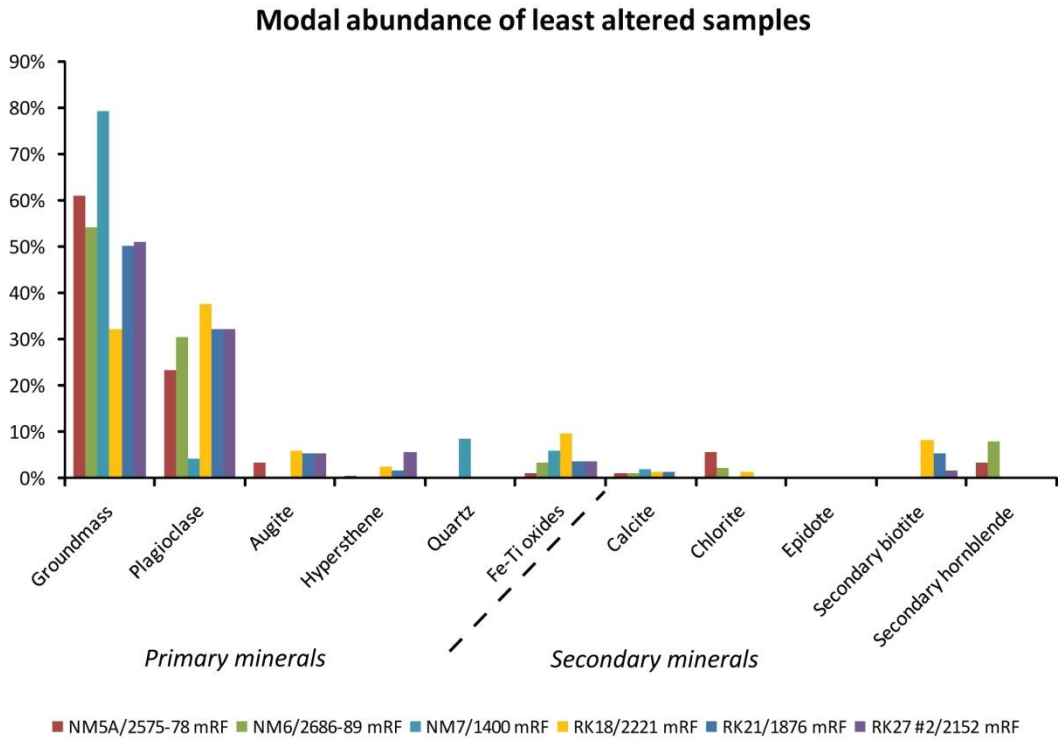

Figure 3.1: Modal abundance of primary and secondary minerals in least altered samples from Ngatamariki and Rotokawa andesites, determined from 300 counts per thin section.

Table 3.4: Mineral chemistry of selected samples from Ngatamariki and Rotokawa fields (wt. %). Plg = plagioclase, opq = opaque, c = core and r = rim. More microprobe data can be found in Appendix 1.

Geothermal field Sample no/ID	Mineral	SiO_2	TiO_2	Al_2O_3	FeO	MnO	MgO	CaO	Na_2O	K_2O	P_2O_5	SO_3	Cl	Cr_2O_3	NiO	TOTAL
Ngatamariki																
LA4 3 /5244	Plg (c) labradorite	54.05	0.09	27.87	0.53	-	-	11.56	5.01	0.37	0.12	0.07	0.03	0.02	-	**99.72**
LA4 3/5245	Plg (r) labradorite	52.72	0.10	28.75	0.56	0.03	-	12.22	4.56	0.37	0.13	0.14	0.07	0.06	0.10	**99.81**
LA4 8/5251	Opq titanomagnetite	2.16	13.23	0.17	77.53	0.15	0.02	0.25	-	0.09	-	0.02	-	0.55	0.15	**94.32**
LA5 7/5350	Plg (c) bytownite	47.07	0.09	33.08	0.59	0.08	-	16.74	1.90	0.19	-	-	-	0.03	0.11	**99.88**
LA5 7/5351	Plg (r) labradorite	52.42	0.09	29.01	0.57	0.06	0.05	12.90	3.94	0.29	0.18		0.00	0.02	-	**99.53**
LA5 1/5342	Opx (c) augite	51.84	0.51	1.42	11.07	0.32	14.23	19.89	0.25	0.12	0.08	-	0.01	0.00	-	**99.74**
LA5 1/5343	Opx (r) augite	51.20	0.60	2.45	11.73	0.41	13.74	19.72	0.34	0.10	0.18	0.16	0.04	0.12	-	**100.79**
LA15 11/5318	Plg (c) albite	67.39	0.05	19.60	0.05	0.19	0.04	0.54	11.55	0.18	0.08	0.17	0.02	-	0.01	**99.87**
LA15 11/5319	Plg (r) albite	67.12	-	19.30	0.05	0.01	-	0.22	11.60	0.12	0.19	-	0.00	0.00	-	**98.61**
LA15 5/5313	Quartz	96.93	-	-	-	-	0.05	0.13	-	0.05	0.28	0.01	0.03	-	0.04	**97.52**
Rotokawa																
LA3 1/5320	Plg (c) labradorite	52.90	0.09	28.38	0.57	-	-	12.02	4.43	0.25	0.01	0.09	0.06	0.07	-	**98.87**
LA3 1/5322	Plg (r) labradorite	51.72	-	29.77	0.56	0.03	-	13.36	3.89	0.27	-	0.00	0.03	0.09	0.02	**99.74**
LA3 5/5326	Opq. titanomagnetite	3.70	10.47	1.87	76.91	0.10	0.01	0.32	0.38	0.25	0.01	0.10	-	0.12	-	**94.24**
LA3 8/5329	Orthopyroxene(c)	52.15	0.39	2.10	9.37	0.33	14.70	20.26	0.35	0.08	0.40	0.06	0.04	0.17	0.00	**100.40**
LA3 8/5330	Orthopyroxene(r)	51.46	0.57	2.55	9.58	0.32	14.54	20.37	0.22	0.12	-	0.11	-	0.20	0.06	**100.10**
LA3 10/5332	Plg (c) bytownite	47.83	0.09	32.15	0.63	0.06	-	16.03	2.43	0.24	-	0.19	0.03	0.03	-	**99.71**
LA3 10/5333	Plg (r) labradorite	54.81	0.05	27.84	0.55	0.08	0.01	10.61	5.34	0.40	-	-	0.02	0.05	-	**99.76**
LA14 10/5269	Clinopyroxene	52.76	0.34	1.18	19.36	0.51	22.92	1.71	0.18	0.08	0.08	-0.03	0.07	-	0.14	**99.30**
LA48 3/5386	Quartz	97.72	-	-	-	0.04	0.08	0.10	0.04	0.08	0.27	0.04	0.03	0.16	-	**98.56**

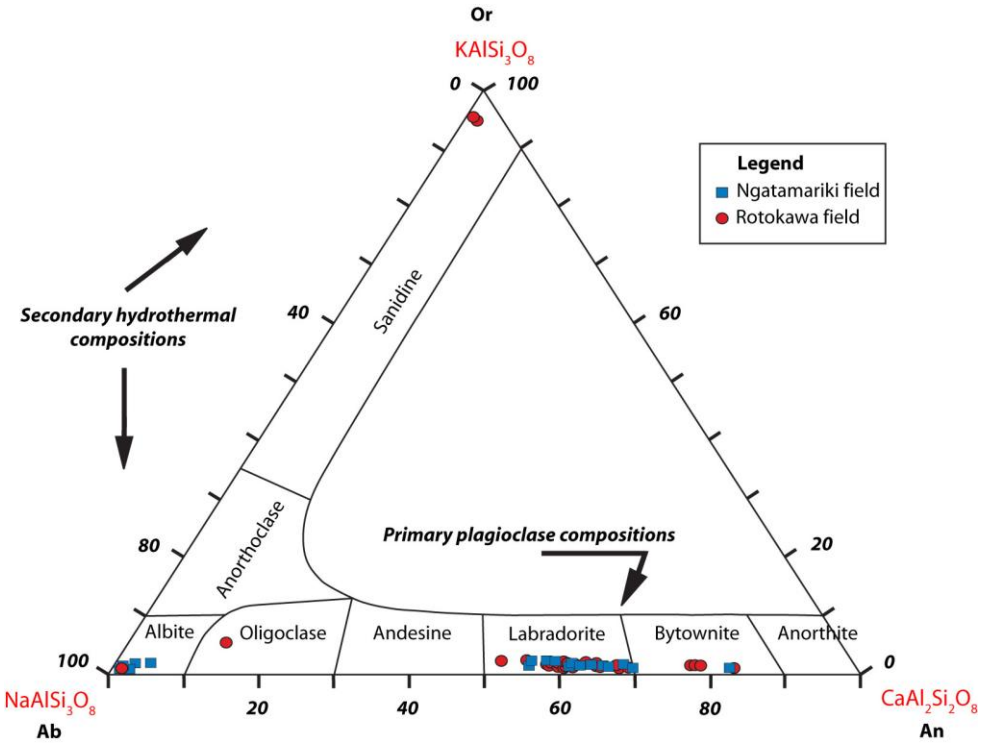

Figure 3.2: Feldspar compositions of Ngatamariki and Rotokawa andesites.

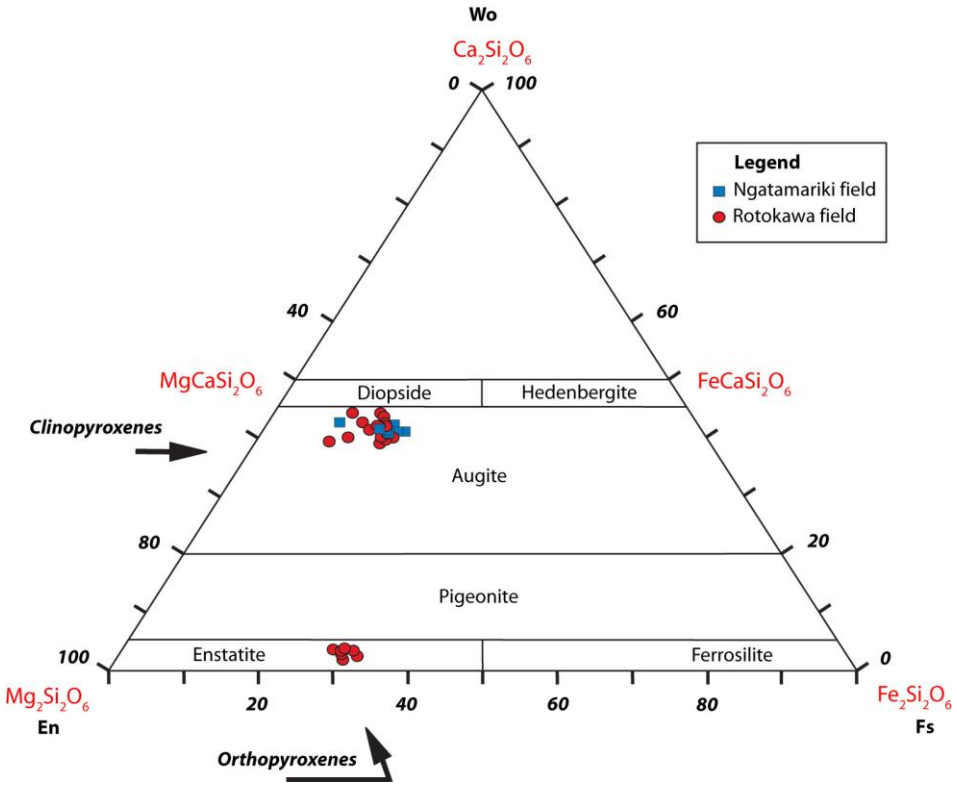

Figure 3.3: Pyroxene compositions of Ngatamariki and Rotokawa andesites.

Primary and secondary biotite is mostly associated with the pyroxene andesite at Rotokawa (1-8%), while secondary hornblende is common at Ngatamariki (3-8%).

Mineral chemistry (Table 3.4) of Ngatamariki and Rotokawa andesites is represented on standard ternary diagrams (Fig. 3.2, 3.3). Plagioclase compositions are plotted with orthoclase (Or), albite (Ab) and anorthite (An) as end members, where plots along the Ab to An-axis represents primary plagioclase compositions and plots along the Ab to Or-axis are hydrothermally altered plagioclases. This occurs when Ca has been removed from phenocrysts and instead they have been enriched in either Na or K., e.g. adularia, albite, oligoclase. The plagioclase phenocrysts at Ngatamariki range from An_{54-82} and An_{51-82} at Rotokawa (labradorite to bytownite), and they commonly exhibit zoning with a calcic core and sodic rim. Pyroxenes are plotted with wollastonite (Wo), enstatite (En) and ferrosilite (Fs) as end members. The ternary diagram for pyroxene compositions from Rotokawa shows plots of augite and orthopyroxene, but only plots of augite from Ngatamariki which is expected since it is a hornblende andesite rather than a two-pyroxene andesite. The augite at Ngatamariki has a range of Wo_{39-44}, Fs_{9-19}, En_{42-50} and at Rotokawa Wo_{41-42}, Fs_{9-17}, En_{39-47}. The orthopyroxene at Rotokawa has a range of Wo_{2-3}, Fs_{28-31}, En_{65-67}.

3.3.1 Ngatamariki Andesite

Both andesite lava and hydrothermal breccias have been sampled from wells NM5A, NM6 and NM7 at the Ngatamariki field. Breccias are present in NM6 at 2686-89 mRF depth and NM7 at 2179-84 mRF. The samples range from subtle to intense alteration intensity, making the identification of pyroxene and amphibole difficult due to secondary mineral replacement.

3.3.1.1 Andesite lava flows

Handspecimen description: Pieces of broken core (<10 cm) were retrieved from NM5A and NM6 (Fig. 3.4). Most pieces are angular and fragmented during core

recovery, although some pieces are subangular and were possibly broken along naturally occurring joints. Andesite lava at Ngatamariki is dark grey to greenish grey in color, depending on the intensity of alteration. The lava is porphyritic, with primary phenocrysts of plagioclase and clinopyroxene set in a groundmass of fine, volcanic glass. The least (subtle) altered cores are dark grey with patches of green minerals such as chlorite and secondary hornblende where they have replaced primary phenocrysts in the lava, with no visible pyrite or veins (Fig. 3.4a). Cores with weak alteration are grey in color, with green chlorite and secondary hornblende replacing primary phenocrysts (Fig. 3.4b).

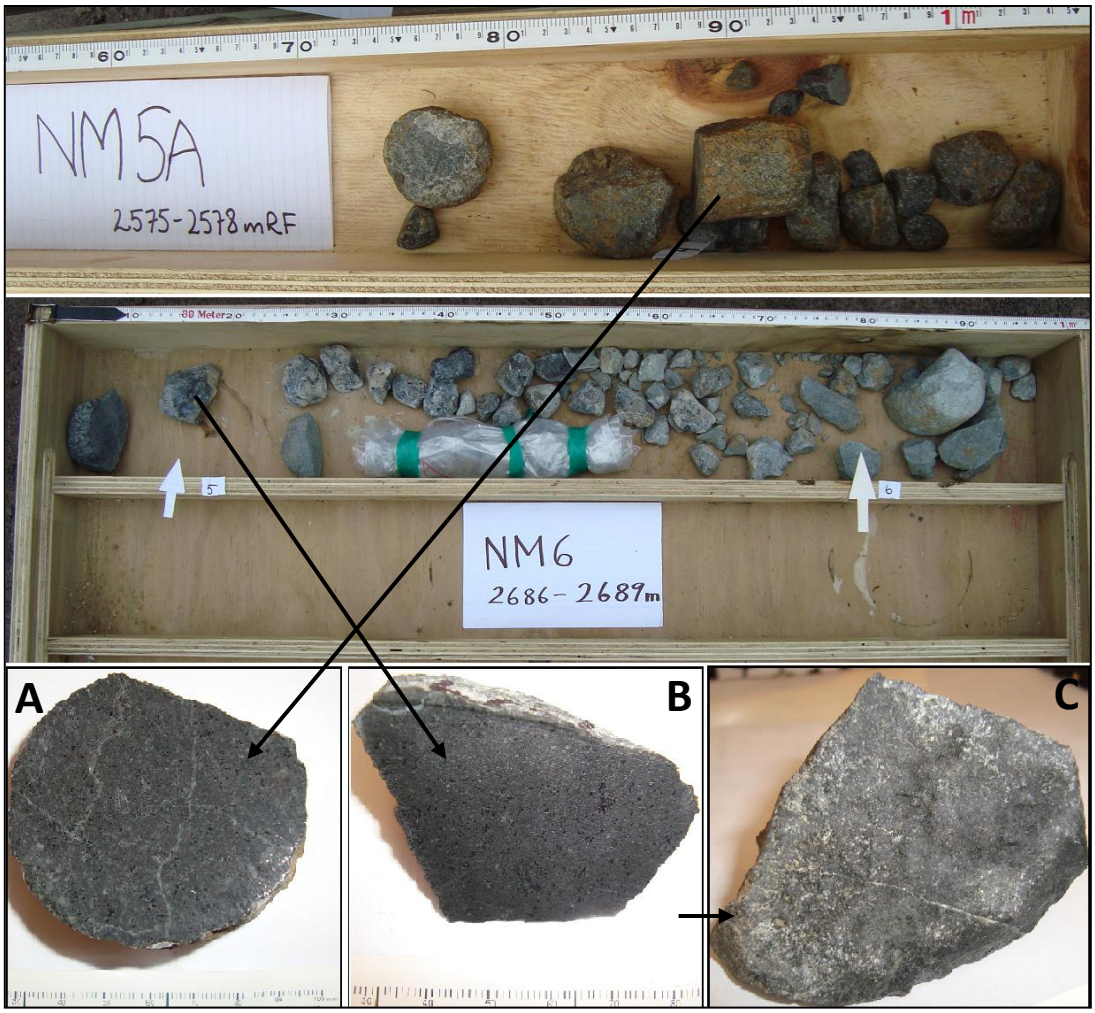

Figure 3.4: Box containing cores of andesite lava from a) NM6/2686-89 mRF sample LA.4, and b) NM5A/2575-78 mRF sample LA.5. c) Core surface of LA.5, showing patches of green chlorite, flaky white calcite and a calcite vein.

Chlorite, in addition to calcite and pyrite, are also covering joint surfaces. Thin veinlits of calcite are visible (Fig. 3.4c).

Plagioclase

Plagioclase composition ranges from labradorite to bytownite (An_{54-82}) (Fig. 3.2) with a range of 4 to 30% in modal abundance (Table 3.3). Phenocrysts are typically tabular with an average length of 0.7 mm although some may be up to 3 mm in length. The plagioclase displays albite polysynthetic twinning although with lesser amounts of Carlsbad simple twinning. Plagioclase mainly appear as single phenocrysts, but may also be intergrown with each other, or joined along their broader face and thus creating secondary twinning (Fig. 3.5a-b).

Stress during crystallisation and/or eruption has created intragranular fractures in some instances. Indications of disequilibrium during crystallisation are sieve-texture, oscillatory zoning as well as normal zoning with a calcic bytownite core and sodic labradorite rim. Core and zonal texture is common, as they are readily replaced by calcite or epidote already at subtle alteration intensity (Fig. 3.5c-d). Cathodoluminescence (CL) has been employed to ease identification of zones with different An-compositions (Fig. 3.5e-f).

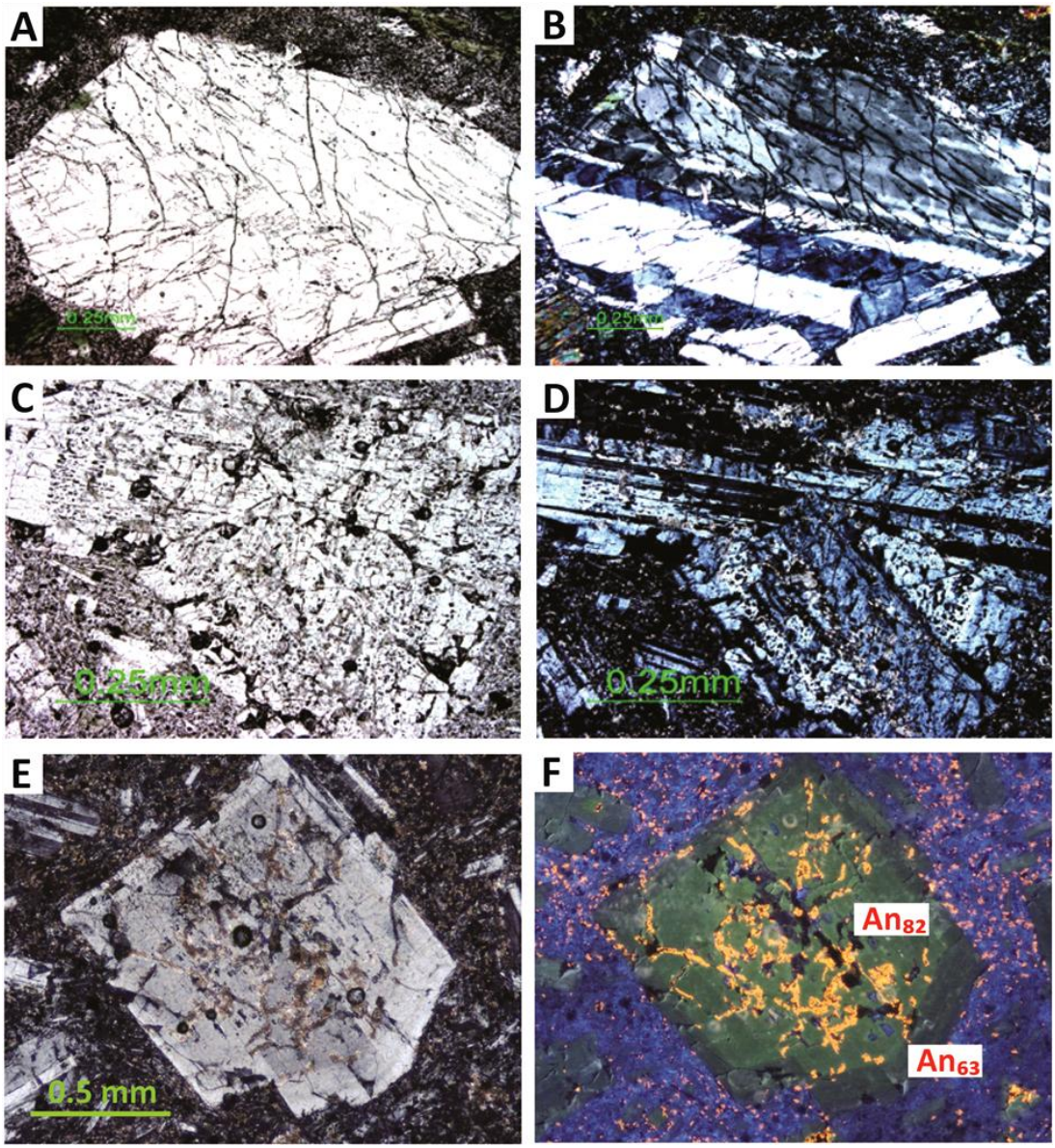

Figure 3.5: a-b) Plagioclase with synneusis twinning and stress fractures at Ngatamariki, note the different styles of twinning in the lower and upper phenocrysts, and a weak oscillatory zoning of the whole plagioclase (sample LA.4). c-d) Plagioclase with core and zonal texture (sample LA.5). e-f) Plagioclase with normal zoning where the core has the composition of bytownite (light green) and the rim labradorite (dark green) (sample LA.5). A, C = PPL; B, D, E = XPL; F = CL .

Clinopyroxene

Clinopyroxene has a modal abundance of 0-3% (Table 3.3), the low amount is partly caused by extensive hydrothermal alteration of the sampled cores where it has been replaced by secondary minerals such as chlorite and/or epidote. However, clinopyroxene is non-existent in shallow units of andesite (ca <2000 mRF). Phenocrysts are on average 0.6 mm long but can grow up to 2 mm, and they have a prismatic shape with a perfect cleavage at 90°. They are colourless to pale brown with an oblique extinction angle. Interference colours are up to low second order, usually in blue, purple and yellow.

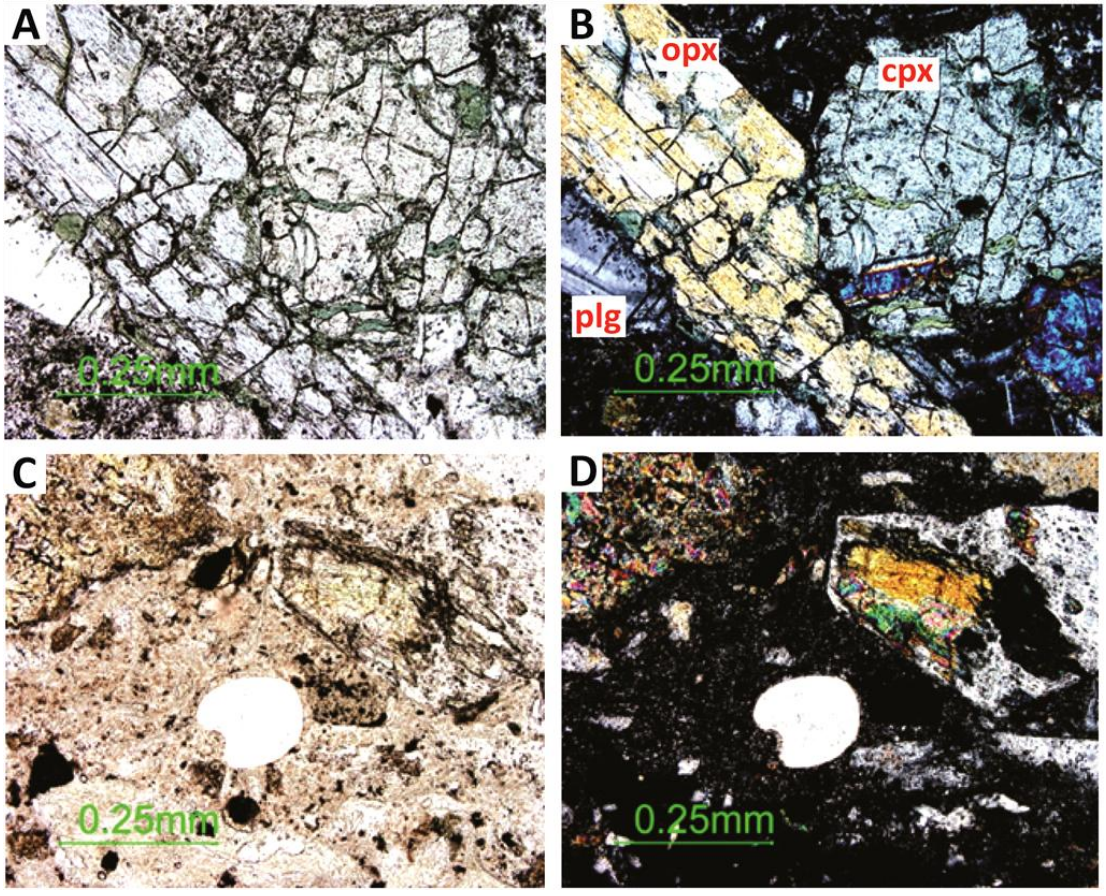

Figure 3.6: a-b) Glomerocryst of plagioclase (left), orthopyroxene (centre) and twinned clinopyroxene (right). Note minor alteration to green chlorite in pyroxene cleavages (sample LA.4). c-d) Primary quartz (sample LA.45). A, C = PPL; B, D = XPL.

Twinning is a common feature often a single lamellae band of different orientation runs through the phenocryst (Fig. 3.6a-b). Microprobe analysis of the clinopyroxenes from Ngatamariki showed a composition of Wo_{39-44}, Fs_{9-19}, En_{42-50}, which plots within the augite field on the pyroxene ternary diagram (Fig. 3.3).

Orthopyroxene

Andesite at Ngatamariki is commonly described as a hornblende andesite, so orthopyroxene is very rare. Orthopyroxene has only been identified in well NM5 at 2575-78 mRF (Fig. 3.6a-b). This is coincidently also the least altered sample from Ngatamariki, so orthopyroxene might therefore also be present in smaller amounts among pseudomorphs of pyroxenes in more altered samples. However, orthopyroxenes are non-existent in shallow units of andesite (ca <2000 mRF). This unaltered phenocryst is tabular with perfect cleavage at 90°, ~0.7 mm in length with a weak pleochroism from very pale pink to green and straight extinction. The interference colour is of upper first order, bright yellow. It has been intergrown with plagioclase and augite. There is a subtle alteration to chlorite along cleavages. No orthopyroxene has been identified by microprobe analysis, and the chemical composition is therefore unknown.

Hornblende

No primary hornblende has been identified in samples collected at Ngatamariki, only outlines are present in weakly altered samples. The hydrous nature of hornblende makes them susceptible to hydrothermal alteration and is therefore among the first primary phenocrysts to be replaced by secondary minerals such as calcite or chlorite.

Quartz

Quartz with an average SiO_2 composition of 97% (Table 3.4), is common in shallow units of andesites (<2000 mRF) with a modal count of <8% (Table 3.3). As a primary

mineral, quartz occurs as single grains (monocrystalline) with an average size of 0.25 mm (Fig. 3.9c-d), while in deeper units quartz is often present as a secondary mineral, lining vugs, veins and filling voids in the groundmass.

Opaque minerals

Fine, disseminated grains of Fe-Ti oxides are abundant in the groundmass of deeper andesites, although in lesser amonts in shallow andesites (ca <2000 mRF) at Ngatamariki. Titanomagnetite is the dominant opaque mineral, followed by ilmenite. A cluster of titanomagnetite crystals were observed in sample LA.67 from well NM7 at 1400 mRF (Fig. 3.7a-b). The crystals are <0.1 mm in length and have a cubic shape.

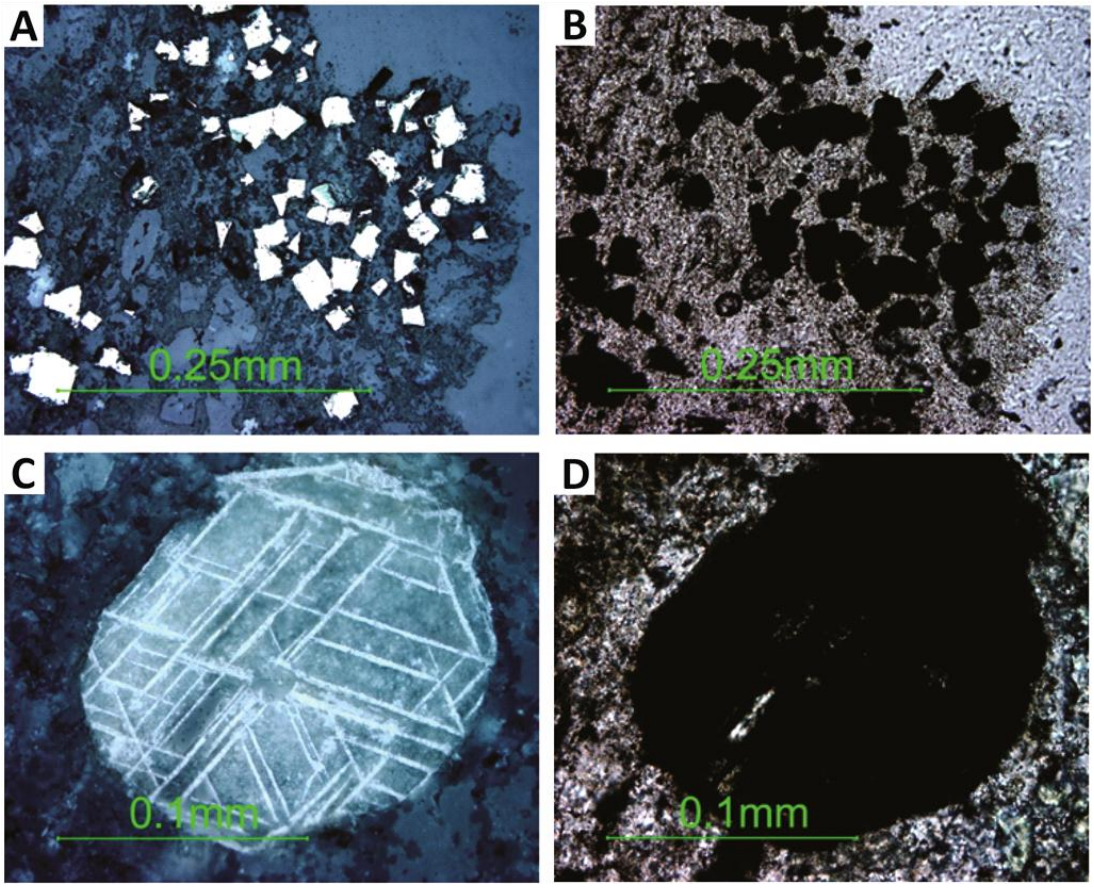

Figure 3.7: a-b) White titanomagnetite with a cubic habit clustered in rhyolitic groundmass (sample LA.67). c-d) Ilmenite lamellae in titanomagnetite (sample LA.59). A, C = RL; B, D = PPL.

The colour is pinkish white in reflected light and isotropic in transmitted light. Dull, white ilmenite is also found in sample LA.59 (Fig. 3.7c-d). It is <0.2 mm in size. Ilmenite also occurs as lamellae parallel to (111) octahedral directions in titanomagnetite. Altered ilmenite forms fine, granular leucoxene which is abundant at Ngatamariki.

Groundmass

The groundmass is typically intersertal or rarely trachytic. The groundmass consists of microcrystalline plagioclase laths, granular pyroxenes, quartz and Fe-Ti oxides (<0.05 mm), set in volcanic glass. Depending on the level of devitrification, the glass can be in various shades of brown. Two groundmass varieties have been recognised based on modal abundance and composition:

- ✧ *andesitic* – unaltered groundmass is grey in hand specimen, consisting of microcrystalline plagioclase, pyroxenes, Fe-Ti oxides and glass (Fig. 3.8a-b) with a modal abundance of 51-54 % (Table 3.3), and
- ✧ *dacitic/rhyolitic* – unaltered groundmass is greyish white in hand specimen consisting of microcrystalline quartz, feldspar, glass, Fe-Ti oxides (Fig. 3.8c-d) with a modal abundance of ~79 % (Table 3.3).

Groundmass crystals have often been replaced in varying intensity by secondary minerals such as chlorite, calcite and leucoxene.

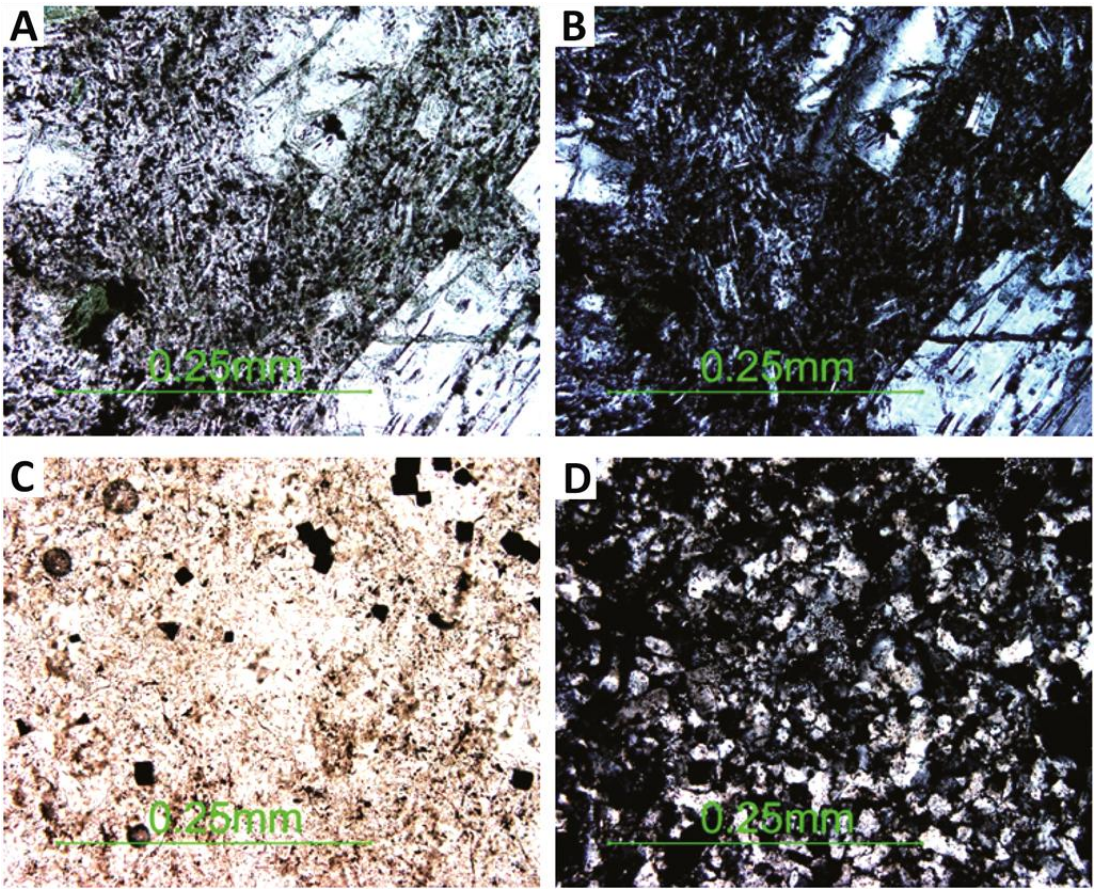

Figure 3.8: Andesitic groundmass with slight flow alignment (sample LA.4). c-d) Dacitic/rhyolitic groundmass of mainly quartz (sample LA.67). A, C = PPL; B, D = XPL.

3.3.1.2 Andesite breccia

Hand specimen description: Pieces of broken core (<40 cm) were retrieved from NM7, consisting of andesite breccia. The breccia includes green to grey subangular to rounded polylithic clasts set in a light grey matrix. Clasts of porphyritic volcanics plus greywacke are easily identified, plus some small, compacted green clasts which might be altered pumice. Some of the primary phenocrysts have been replaced by dark green chlorite or light green epidote. There are three main textures in this core.

The first texture is a crumbly, very pale grey andesite breccia with moderate alteration intensity. Disseminated pyrite is visible, plus ~0.5-2 cm angular to

subangular clasts which have been altered to epidote and chlorite. There are also occasional soft, white areas of non-acid clay or silica (Fig. 3.9a).

The second texture is a light to dark grey breccia which is denser than the previous one, with weak alteration intensity. Primary phenocrysts in subrounded clasts have again been altered to chlorite and epidote, with only a small amount of pyrite visible. There are some large (~3 mm) white crystals and larger patches (~1 cm) scattered throughout the rock, of possibly feldspar. Thin veins cut across the length of the core and are infilled with small white and green crystals, possibly calcite and epidote. Smaller veins filled with white crystals (quartz?) occur throughout the rock (Fig. 3.9b).

The third texture is a more pronounced breccia or conglomerate with large (~2-8 cm) subrounded clasts of greywacke and porphyritic volcanics in a grey matrix. Large (~2 mm) white crystals of feldspar and blue-green grains (~1 cm) of chlorite are scattered throughout the rock. Patches of epidote (~2-15 mm) are common where it has replaced primary minerals in matrix and volcanic clasts, around which it occasionally also appears as a rim. Thin, white veins of calcite cut across the core axis (Fig. 3.9c).

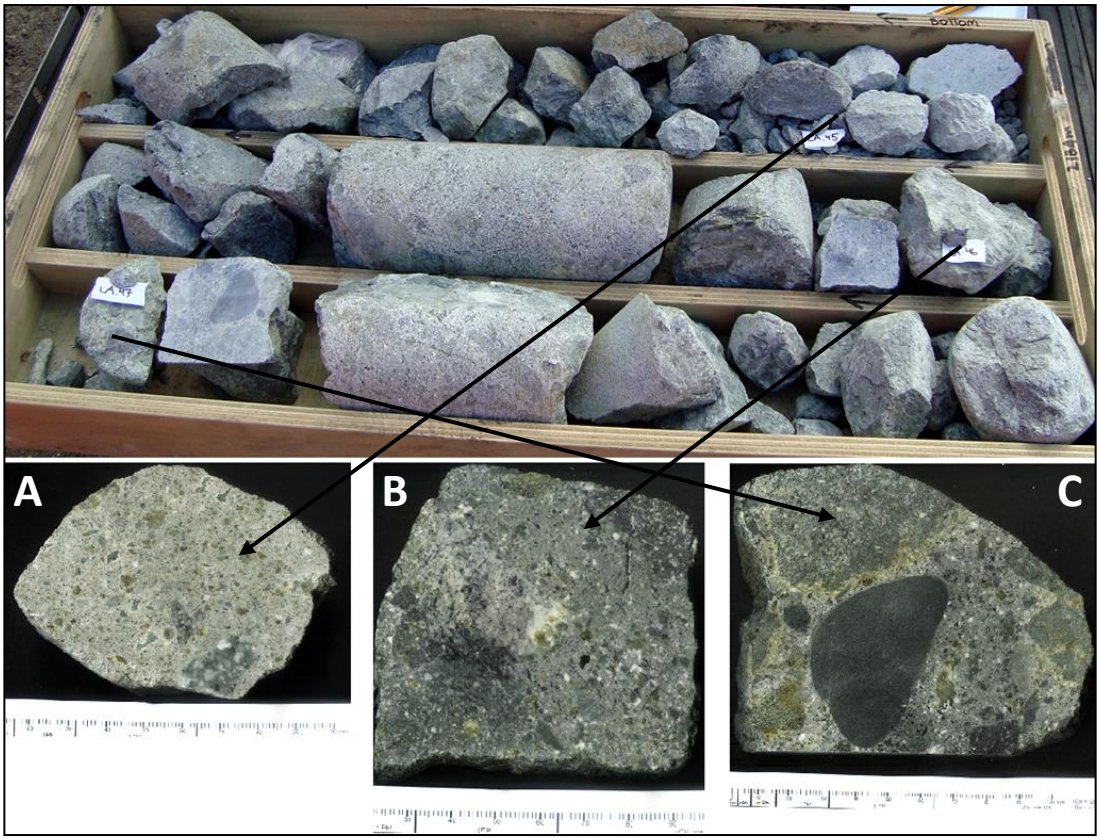

Figure 3.9: Box containing cores of andesite breccia from NM7/2179-84 mRF (above). Image a-c shows different breccia textures. A=LA.45, B=LA.46, C=LA.47.

Breccia mineralogy

The first breccia type is strongly altered. In the andesite matrix, primary minerals have been replaced by dirty-looking alkali feldspar with weak twinning, chlorite, calcite, epidote, large secondary quartz crystals and Fe-Ti oxides. Some of the Fe-Ti oxides have been replaced by dusty leucoxene. The breccia clasts include rhyolite/dacite and plagioclase-phyric pumice which occasionally has been compacted to fiamme, where the glass has been completely altered to chlorite and dissolution vugs in the feldspar have been infilled with epidote (Fig. 3.10a-d). This type of alteration has been caused by a sequence of hydration and dissolution reactions common for glass-bearing rocks, where elements leached from the glass are consumed by the formation of new minerals (Fisher & Schmincke, 1984).

The second breccia type has a weakly altered matrix where plagioclase and groundmass have patchy chlorite and calcite, whereas ferromagnesian minerals have been replaced by chlorite and green amphibole. Volcanic clasts are moderately altered, where primary phenocrysts often have been replaced by chlorite, epidote and leucoxene (Fig. 3.10d-e, 3.11a-b). Greywacke clasts consist of granular quartz and silt/mudstone, giving it a brownish dirty-looking appearance. A thin vein (<0.1 mm) is identified as quartz.

The third breccia type has a weakly altered matrix with plagioclase only partly altered although most ferromagnesian minerals have been replaced by chlorite and epidote. Plagioclase in volcanic clasts has been altered to dusty brown alkali feldspar with a wavy extinction, and dissolution vugs in cores are filled with epidote. Ferromagnesian minerals are completely replaced by chlorite, calcite and epidote, whereas Fe-Ti oxides have been replaced by leucoxene. A few rhyolitic clasts have spherical aggregates. Greywacke clasts consist mainly of granular quartz with minor silt/mudstone. There are thin (<0.1 mm) veins of epidote and calcite (Fig. 3.11c-f). The presence of volcanic plus sedimentary clasts in this heterolithic breccias/conglomerate in addition to pumice, suggests formation due to a pyroclastic event (hydrothermal eruption through greywacke gravels?), rather than autobrecciation.

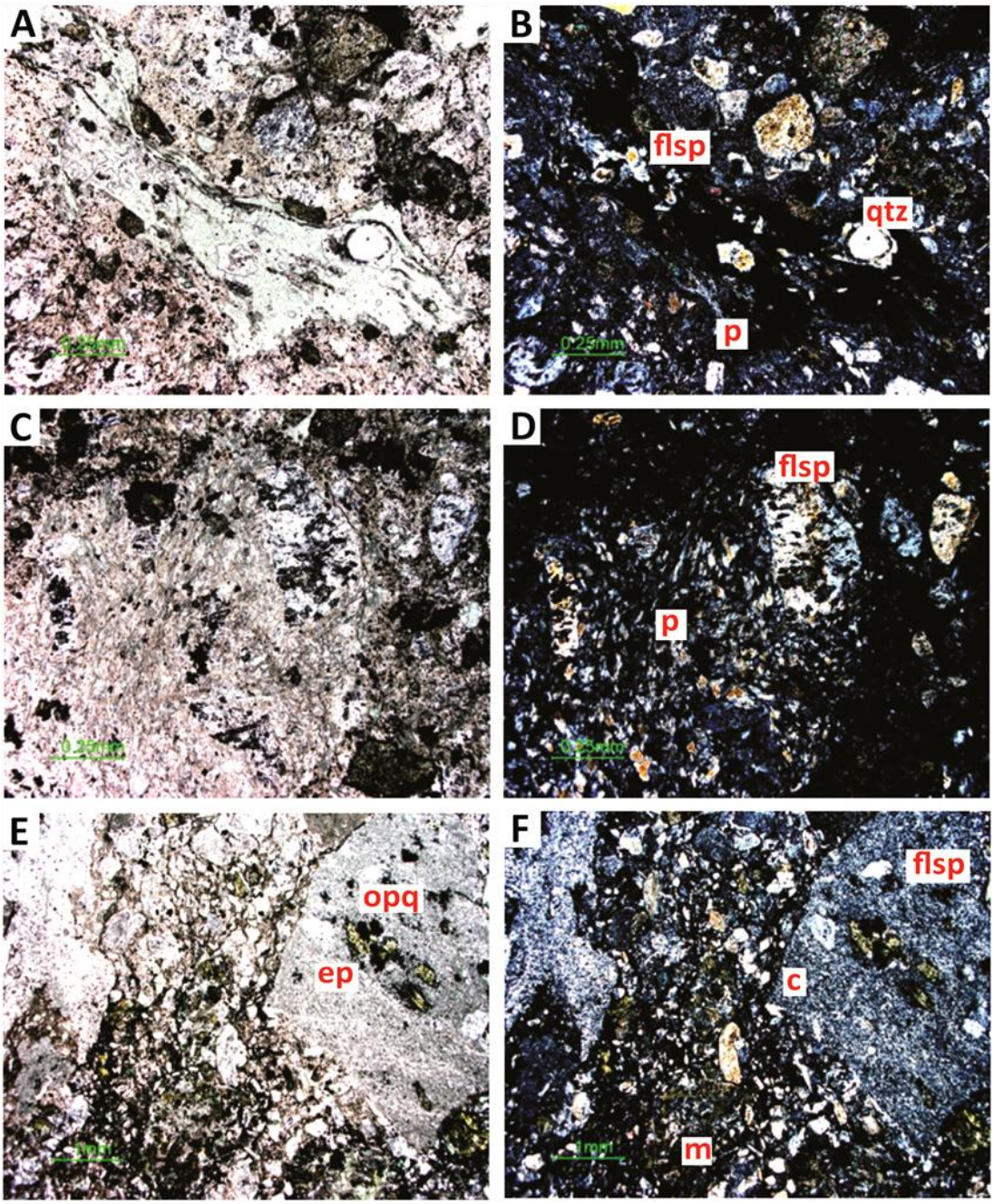

Figure 3.10: a-b) Early stage alteration of compacted pumice clast (p), or fiamme, with inclusions of feldspar (flsp) and quartz (qtz) in an altered andesitic matrix (sample LA.45). c-d) More intense alteration of pumice clast (p) where dissolution vugs in feldspar (flsp) are filled with epidote; altered andesite matrix consists of plagioclase and secondary mineral assemblage (sample LA.45). e-f) Overview of breccia. Weakly altered andesite matrix (m) with plagioclase and pyroxene; dacite/rhyolite clast (c) with feldspar (flsp), minor calcite and granular epidote (ep) and Fe-Ti oxides (opq) (sample LA.46). A, C, E = PPL; B, D, F = XPL.

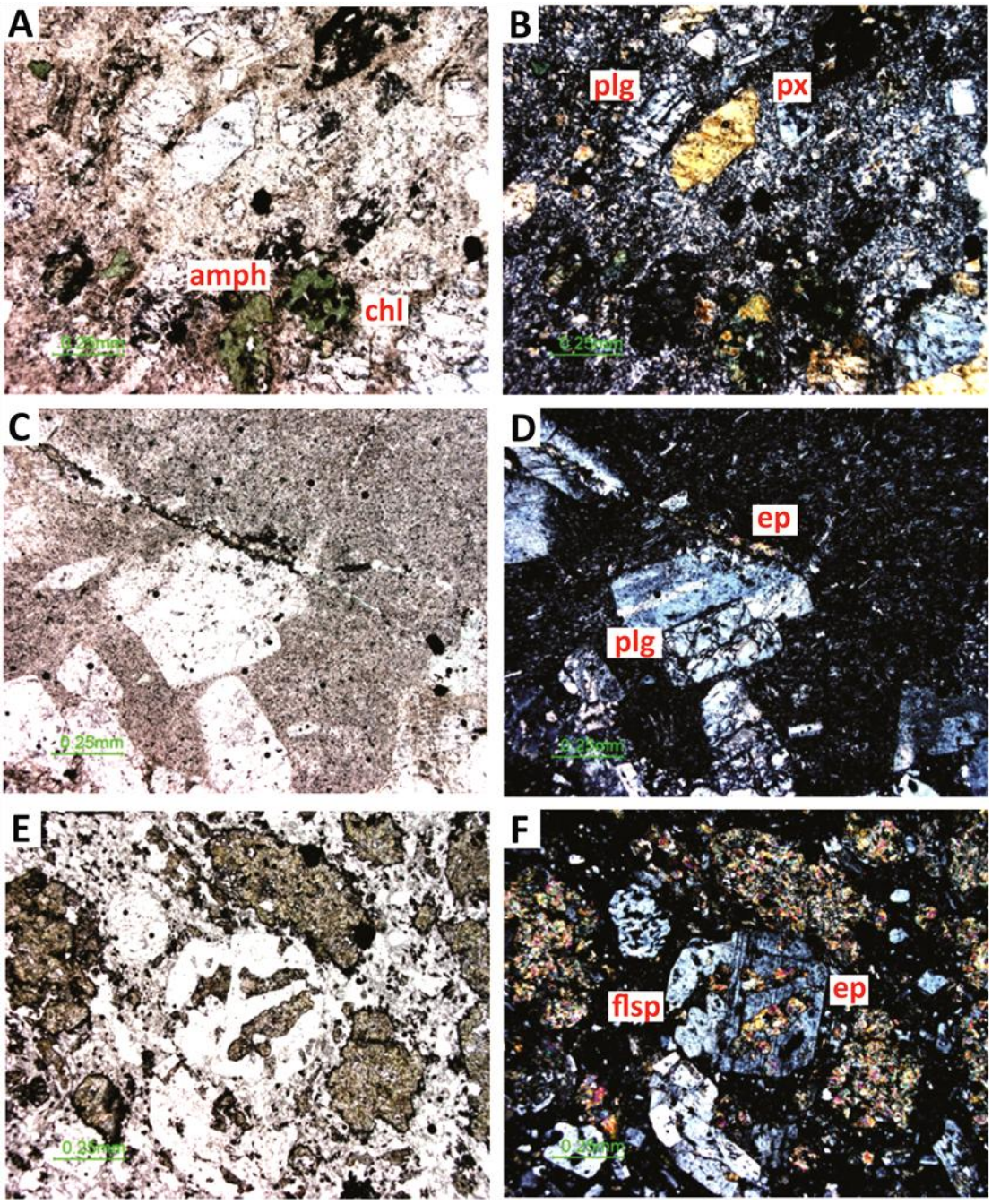

Figure 3.11: a-b) Andesite matrix with unaltered plagioclase (plg), pyroxene (px) and pseudomorphs of Fe-Ti oxides and part chlorite (chl), part green amphibole (amph) (sample LA.46). c-d) Dacite/rhyolite clast with unaltered plagioclase (plg) and a thin epidote (ep) vein running through the clast but stops at the edge, so it has been hydrothermally altered before brecciation. Groundmass is weakly trachytic (sample LA.47). e-f) Andesite clast which has been strongly altered, epidote (ep) has replaced any ferromagnesian minerals and dissolution vugs in feldspar (flsp) (sample LA.47). A, C, E = PPL, B, D, E = XPL.

3.3.2 Rotokawa Andesite

Cores and cuttings of andesite lava and breccias have been recovered from wells RK18, RK21, RK24, RK25 and RK27 at the Rotokawa field. Breccia was encountered at RK27/1853-56 mRF and 2147-53 mRF, RK25/2000-3 mRF, RK24/1820-23 mRF. The samples have subtle to moderate alteration intensity, sometimes making the identification of ferromagnesian minerals difficult due to secondary mineral replacement.

3.3.2.1 Andesite lava flows

Hand specimen description: Pieces of core (<15 cm) have been used to study the mineralogy of andesite lava from RK21. The pieces are angular and have probably fragmented during recovery of the core. The colour ranges from greenish grey to dark grey, depending on the intensity of alteration. The lava is porphyritic, with primary phenocrysts of plagioclase and pyroxene set in a groundmass of fine, volcanic glass. The most altered sample (Fig. 3.12a) of moderate intensity is greenish grey with a relict porphyritic texture. Dark green chlorite and white plagioclase are visible, but there is no calcite, pyrite or veins. Joint planes are smooth and with almost a soapy feeling, which might indicate shearing. Andesite lava with weak alteration intensity appears to represent a gradational transition zone of ~5 cm, were the colour ranges from pale greyish green to dark greenish grey. There is no stratigraphic contact. The relict porphyritic texture continues here, with phenocrysts of dark green chlorite and white plagioclase but no visible pyrite. Shear planes are smooth and have traces of pinkish to red hematite on the surface (Fig. 3.12b). The least altered sample of subtle intensity is dark grey in colour, although with small amounts of red hematite in the groundmass. Green chlorite and cubic pyrite with reddish green reflection surfaces cover shear planes, which are sub-parallel to the core (Fig. 3.12c).

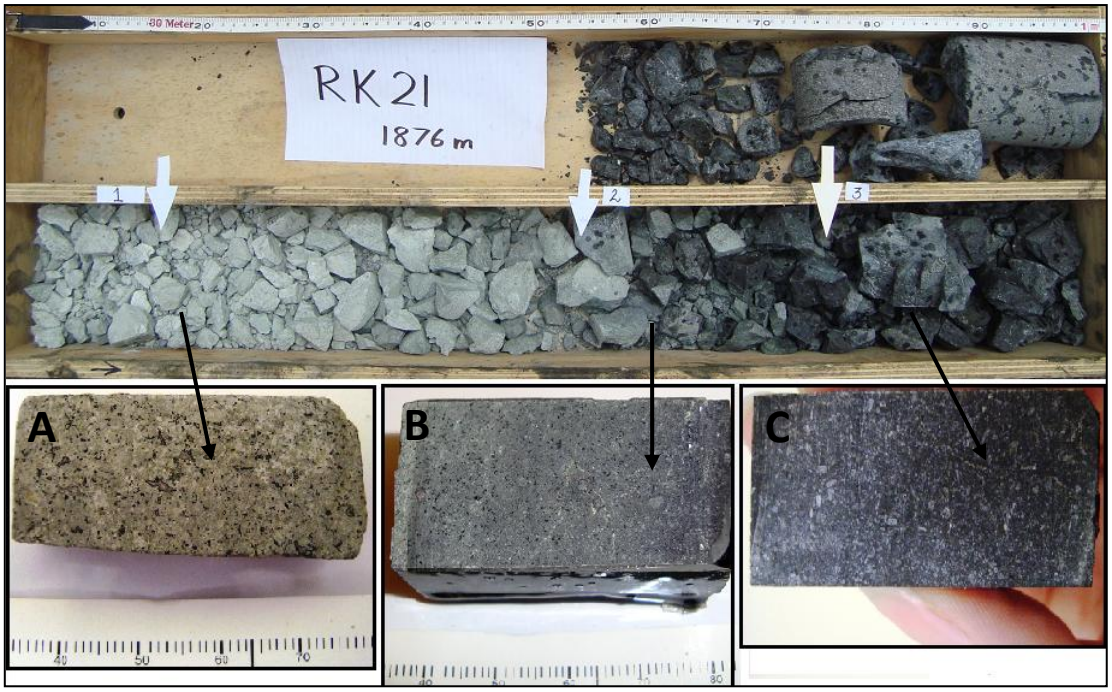

Figure 3.12: Box with core of andesite lava from well RK21 at 1876 mRF, changing from moderate to subtle alteration intensity with increasing depth (A=LA.1, B=LA.2, C=LA.3).

Plagioclase

Plagioclase is the dominant mineral at Rotokawa with an average range of 32-37 % in modal abundance (Table 3.3). The composition ranges from calcic labradorite to sodic bytownite (An_{51-82}) (Fig. 3.2). Phenocrysts are typically tabular with an average length of 0.6 mm although some may be up to 2 mm in length. Plagioclase commonly displays Albite polysynthetic twinning, with lesser amounts of Carlsbad simple twinning. Phenocrysts subjected to moderate alteration intensity may lack twinning altogether, indicating potassic composition in the Or-range of the ternary diagram. Plagioclase mainly appears as single phenocrysts, but may also be intergrown with each other, or joined along their broader face and thus creating secondary twinning. Stress during crystallisation and/or eruption has created intragranular fractures in some instances. There is evidence that the plagioclases have experienced disequilibrium during crystallisation.

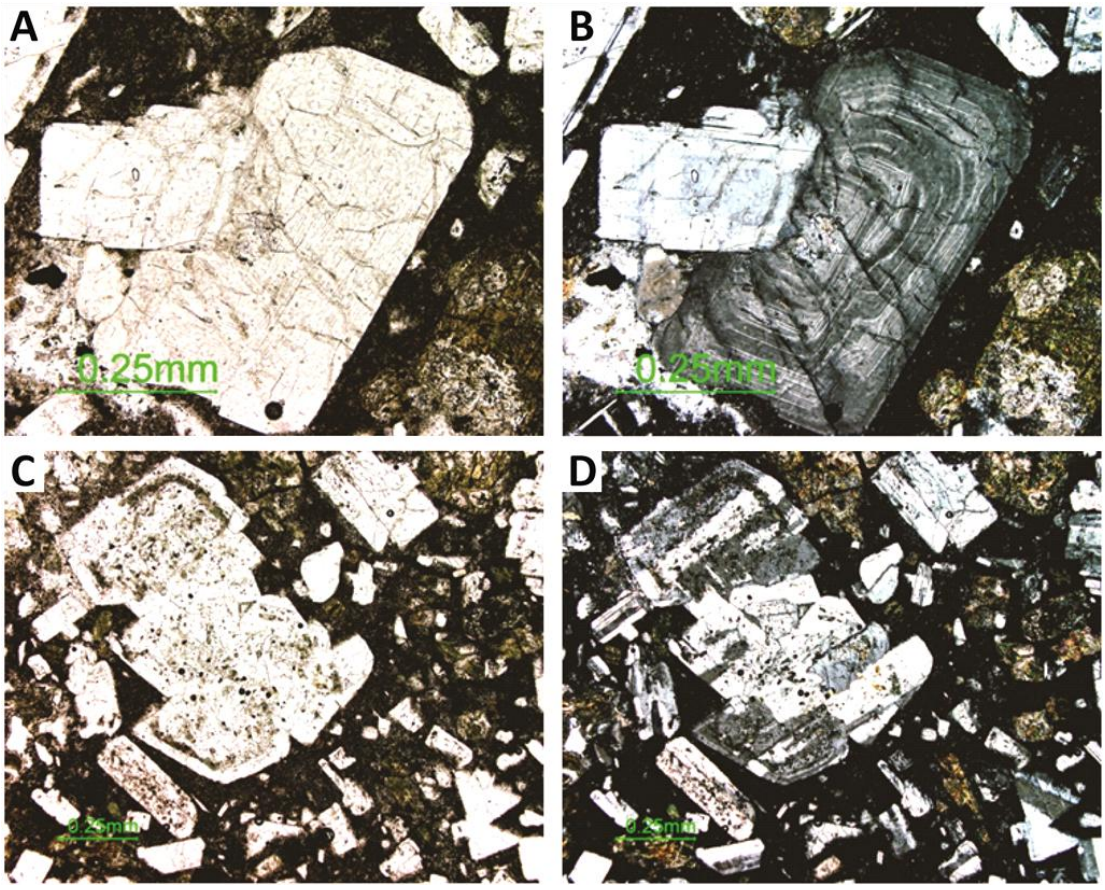

Figure 3.13: a-b) Oscillatory zoning in plagioclase (sample LA.2). c-d) Plagioclase with sieve texture (sample LA.2). A, C = PPL; B, D = XPL.

Examples are normal zoning with a calcic bytownite core and sodic labradorite rim, reversed zoning with labradorite core and bytownite rim, sequences of oscillatory zoning (Fig. 3.13a-b) and sieve-texture (Fig. 3.13c-d). Core and zonal texture is common as they are readily replaced by secondary minerals such as calcite or epidote even at weak alteration intensity.

Clinopyroxene

Clinopyroxene is the second most common mineral after plagioclase at Rotokawa, and has a modal abundance of 5-6% (Table 3.3). Phenocrysts have an average length of 0.4 mm but can grow up to 2 mm, and they have a prismatic shape with a perfect cleavage at 90°. They are colourless to pale brown with an oblique extinction angle. Interference colours are of low second order, usually in blue, purple and yellow.

Twinning is a common feature, often with a single, colourful lamellae band running through the phenocryst, or hour-glass twinning (Fig. 3.14a-b). Microprobe analysis of the clinopyroxenes showed a composition of Wo_{41-42}, Fs_{9-17}, En_{39-47}, which plots within the augite field on the pyroxene ternary diagram (Fig. 3.3).

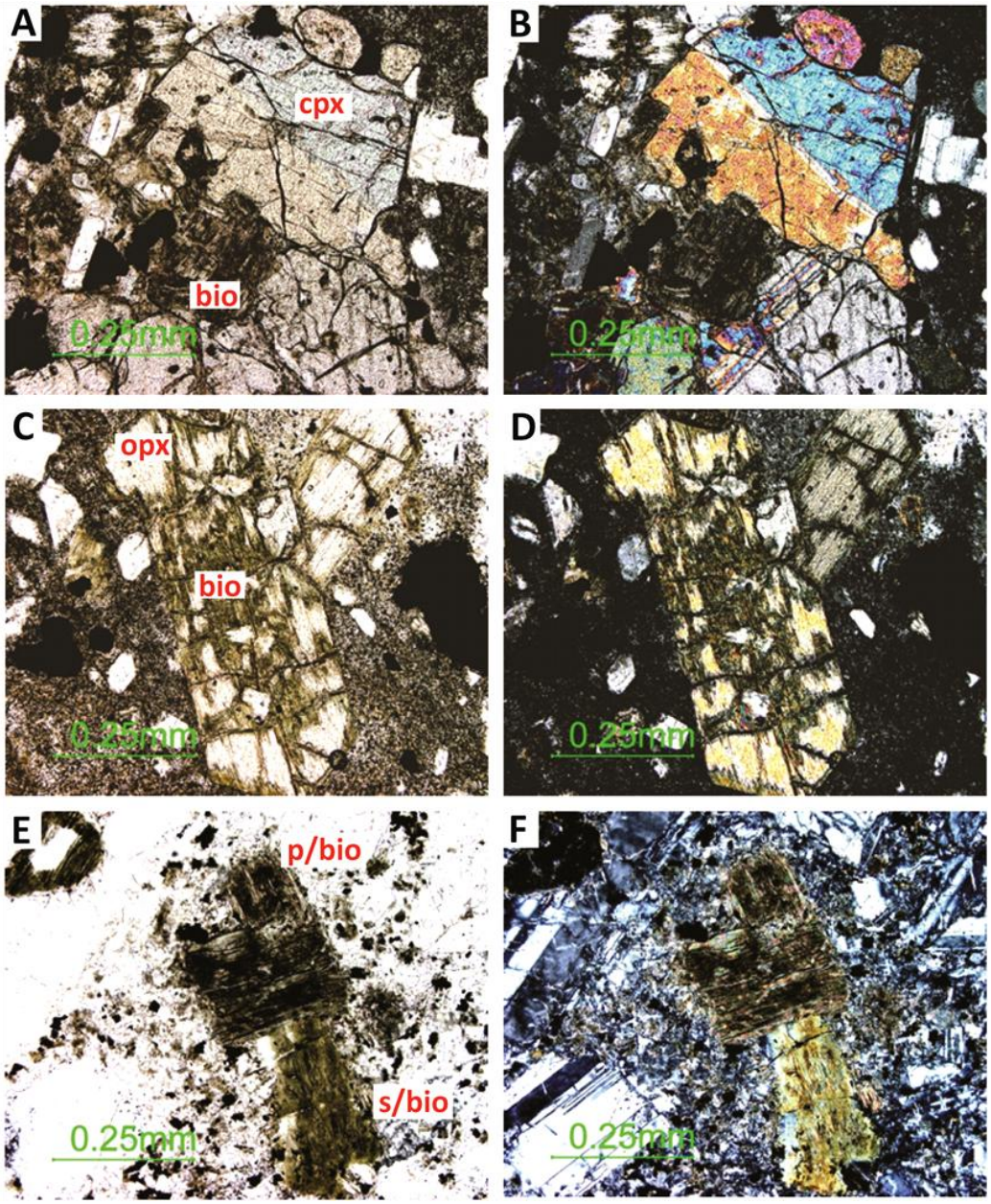

Figure 3.14: a-b) Twinned augites (cpx) in a glomerocryst with hydrothermal biotite (bio) (sample LA.3). c-d) Aggregated orthopyroxene (opx) in an oblique angle, note hydrothermal biotite (bio) along cleavages (sample LA.3). e-f) Brown, primary biotite (p/bio) together with green, secondary biotite (s/bio) (sample LA. 13). A, C, E = PPL; B, D, F = XPL.

Orthopyroxene

Orthopyroxene at Rotokawa has a modal abundance of 1-5 % (Table 3.3). Orthopyroxene is the first of the phenocrysts to be replaced by secondary minerals. Phenocrysts are tabular with perfect cleavage at 90°, ~0.6 mm in length with a maximum of ~0.8 mm. Orthopyroxene has a weak pleochroism from very pale pink to green and straight extinction. The interference colour is of upper first order, bright yellow. They commonly form glomerocrysts either with other pyroxenes or plagioclase. There is often a subtle alteration to hydrothermal biotite along cleavages (Fig. 3.14c-d). Microprobe analyse of orthopyroxene all plot in a tight cluster in the field of enstatite on the pyroxene ternary diagram, with a composition of Wo_{2-3}, Fs_{28-31}, En_{65-67} (Fig. 3.2).

Biotite

Biotite is a common accessory mineral at Rotokawa, although most have a hydrothermal origin. Primary biotite is abundant in well RK18 at 2219-21 mRF, and at 2221 mRF the modal abundance of biotite is even greater than for augite, 8.3 % vs. 6 % (Table 3.3). Primary biotite is tabular or flaky and pleochroic in shades of streaky brown, with an average length of ~0.4 mm although some can grow up to 1 mm. It has straight extinction, excellent cleavage and is easily recognised by its undulating, mottled extinction. The interference colours are of high second order but are masked by the colour of the mineral. Hydrothermal biotite is pleochroic in shades of green, often replacing pyroxene, and occurs together with primary biotite (Fig. 3.14e-f).

Opaque minerals

At Rotokawa, titanomagnetite is the most common opaque mineral followed by ilmenite. Fine, disseminated grains (<0.01 mm) of Fe-Ti oxides are abundant in the groundmass, in addition to lesser amounts of larger (~0.1 mm), cubic titanomagnetite.

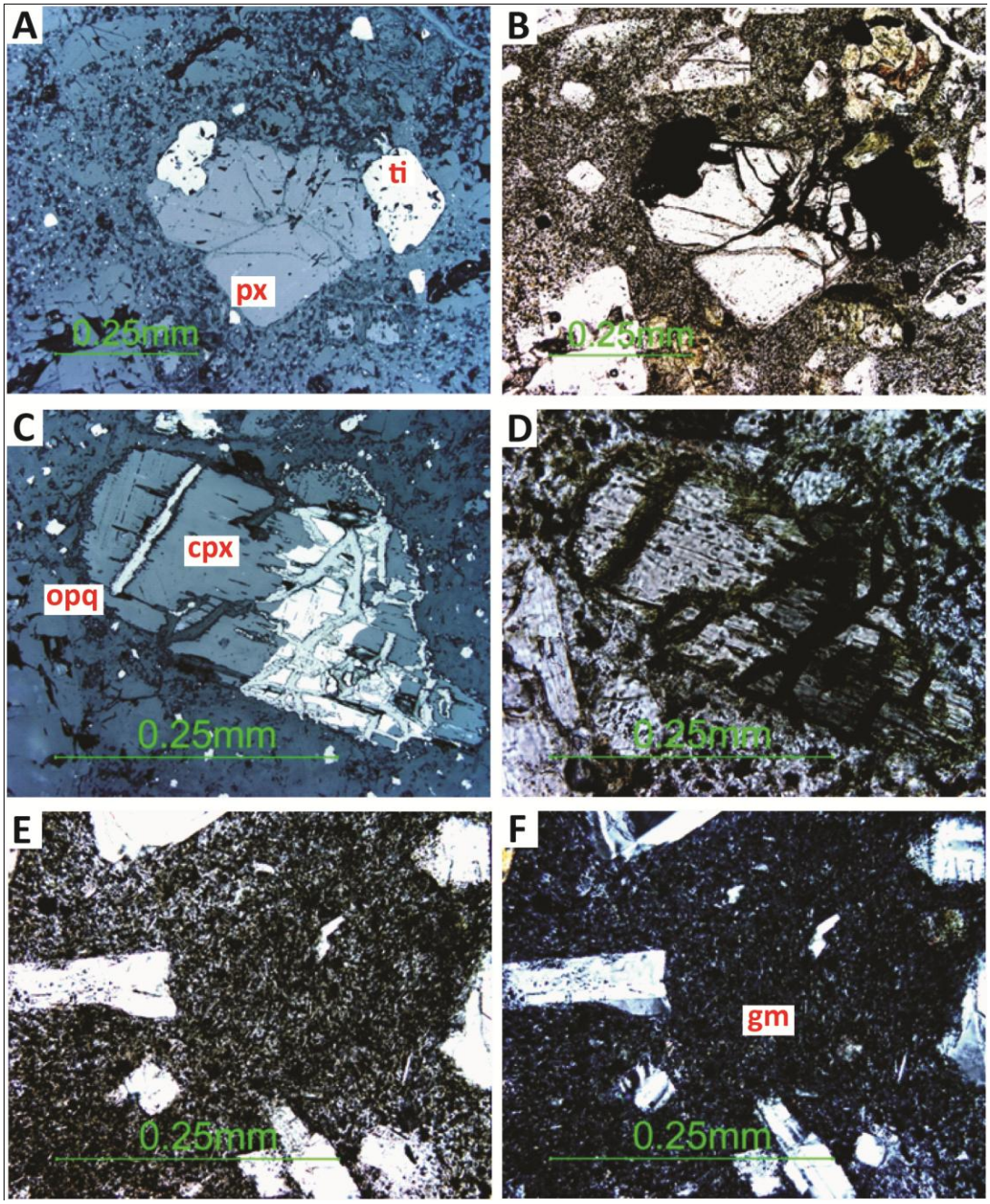

Figure 3.15: a-b) Fine, disseminated Fe-Ti oxides plus large, cubic titanomagnetite (ti) intergrown with pyroxene (px) (sample LA.2). c-d) Fe-Ti oxide (opq) in cleavage of clinopyroxene (cpx) (sample LA.58). e-f) Intersertal, subtly altered groundmass (gm) (sample LA.3). A, C = RL; B, D, E = PPL; F = XPL.

The colour is pinkish white in reflected light and isotropic in transmitted light. Titanomagnetite often occurs as inclusions in pyroxenes (Fig. 3.15a-d).

Groundmass

Unaltered groundmass is dark grey in hand specimen, changing to pale green by secondary mineral assemblages during alteration. The groundmass is typically intersertal, consisting of microcrystalline plagioclase laths, granular pyroxene and Fe-Ti oxides (<0.05 mm), set in volcanic glass. Depending on the level of devitrification, the glass can be in various shades of brown. The modal abundance ranges from 32-51 % (Table 3.3). Groundmass crystals have often been replaced in varying intensity by secondary minerals such as chlorite, calcite and leucoxene (Fig. 3.15e-f).

3.3.2.2 Andesite breccia

Hand specimen description: Pieces of broken core (<50 cm) were retrieved from well RK27 at 1850-1856 mRF, consisting of andesite breccia. The breccia includes greyish purple to purple or creamy white subrounded porphyritic volcanic clasts set in a pale greenish grey matrix. They are either pebble or cobble sized, with a slight jigsaw pattern. The green colour is probably caused by primary minerals being replaced by chlorite, while oxidation of ferromagnesian minerals to hematite gives a purple discolouration. The bottom core (1853-1856 mRF) seems to have been subjected to two types of alteration, as clasts in the upper part are mainly purple while the lower part has creamy white clasts with a green rim (Fig. 3.16a). This could be interpreted as a heterolithic composition (hence not an autobreccia), or different intensities in alteration due to proximity to hot hydrothermal fluids. The top core (1850-1853 mRF) has a coherent interval of almost 2 m with purple banding and some shear planes, surrounded by breccias with purple clasts in a pale green matrix (Fig. 3.16b). This might be interpreted as a lava flow with an upper and lower autobreccia.

Figure 3.16: Box of core with andesite breccia from well RK27 at 1850-56 mRF (A=LA.10, B=LA.11). The top (a) and lower (b) samples show different colouration due to the presence of alteration minerals.

Breccia mineralogy

In the bottom part of the core (sample LA.10), the primary minerals of the matrix are plagioclase, pyroxene and Fe-Ti oxides set in a microcrystalline groundmass. The alteration intensity is strong, with plagioclase altered to a dusty brown albite with patches of calcite, quartz and chlorite, and pyroxenes completely altered to chlorite with occasional epidote and leucoxene.

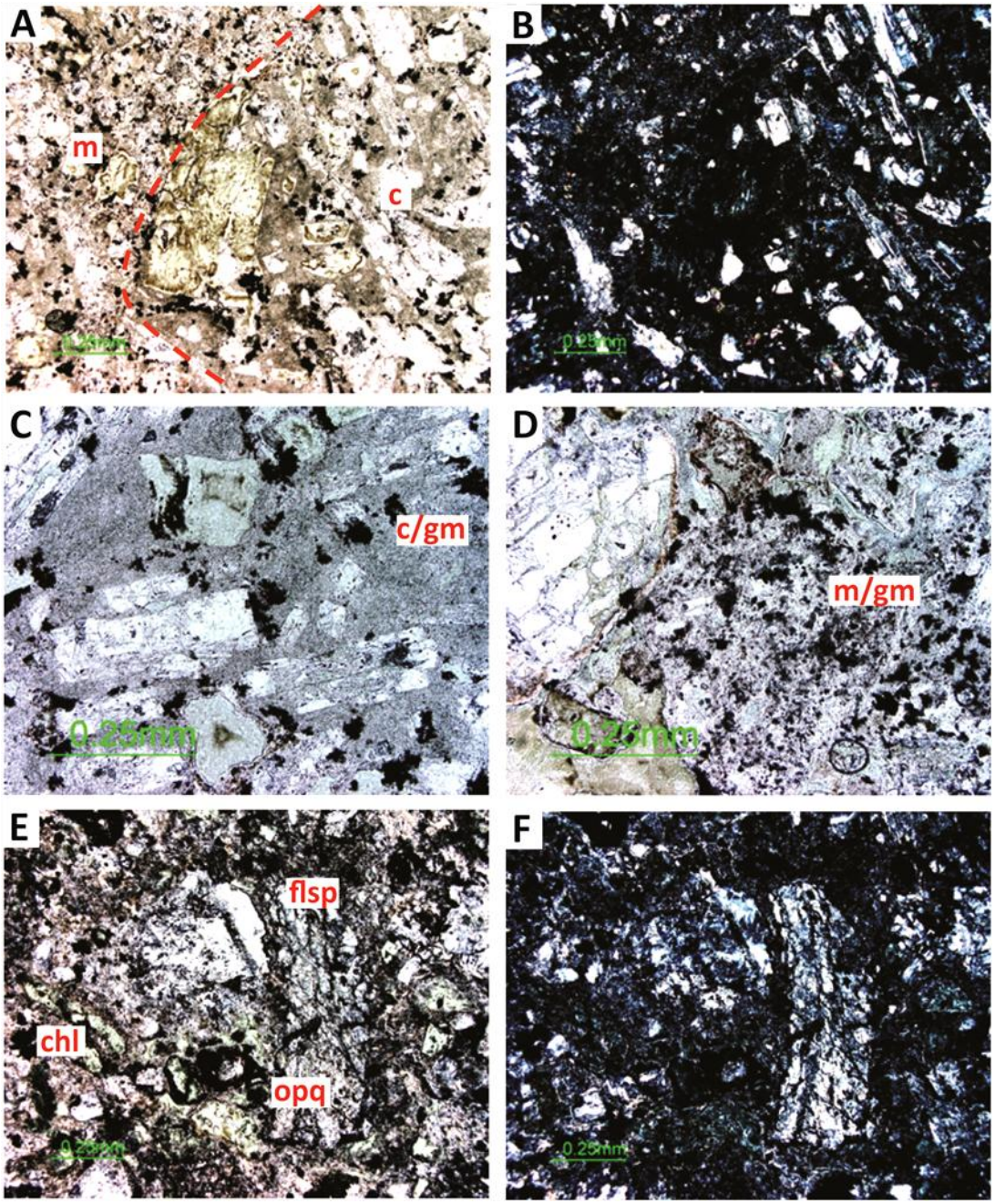

Figure 3.17: Overview of andesite breccia. Primary minerals are the same in clast and breccia, with plagioclase, pyroxene and scattered Fe-Ti oxides. Clast (c) is distinguished from matrix (m) by less altered primary minerals and a very fine grained groundmass with strong alteration intensity (sample LA.10). c) darker, fine grained groundmass of clast (c/gm) (sample LA.10). d) lighter, microcrystalline groundmass of matrix (m/gm) (sample LA.10). e-f) Strongly altered andesite clast, with partly dissolved alkali feldspar (flsp) in a groundmass with abundant chlorite (chl) and Fe-Ti oxides (opq) (sample LA.11). A, C, D, E = PPL, B, F = XPL.

Breccia clasts have primary minerals of plagioclase, pyroxene and Fe-Ti oxide, set in a very fine grained (cryptocrystalline?) groundmass. The alteration intensity is moderate, with plagioclase partially altered to albite, calcite, quartz and epidote. The groundmass is completely replaced by secondary minerals, and is of the same alteration intensity as the matrix. There are more light-coloured minerals such as calcite and quartz in the matrix compared with the clasts (Fig. 3.17). The mineralogy is similar in the top part of the core (sample LA.11), although with more abundant chlorite and Fe-Ti oxides which gives it a more strongly coloured appearance in hand specimen (Fig. 3.17). The weak boundary (if existent) between clasts and matrix makes the breccia resemble a false polymictic texture where multi-phase alteration along fractures of alkali feldspar, hematite and epidote alteration overprints the normal, coherent texture of andesite. Colour differences between the degrees of alteration thereby give the cores a heterogeneous appearance.

3.4 Summary

Pyroxene andesite is the most common petrological type at the Ngatamariki and Rotokawa fields, with minor occurrences of hornblende, biotite and quartz andesite. The different mineralogical compositions reflect a changing magmatic evolution over the life of the andesitic composite cone. The changes in composition are noticeable as minerals such as quartz, hornblende and biotite appear progressively in shallow, more evolved units, with a concurrent decrease in Fe/Ti oxide modal content.

The Ngatamariki Andesite has a more evolved composition compared to Rotokawa, with a phenocryst assemblage of plagioclase, clinopyroxene, quartz, hornblende and Fe-Ti oxides. The lava becomes more felsic at shallow depths, with an increase in modal abundance of quartz. The key characteristics are:

- ✧ plagioclase often displays normal or oscillatory zoning and sieve-texture, indicating disequilibrium during crystallisation;
- ✧ plagioclase modal abundance of 4-30% with a composition of An_{54-82};
- ✧ quartz modal abundance of 0-8%;
- ✧ augite modal abundance of 0-3% and a composition of Wo_{39-44}, Fs_{9-19}, En_{42-50};
- ✧ localised, abundant hornblende (0-8% abundance) implies hydrous magmas;
- ✧ Fe-Ti oxide modal abundance of 1-5%;
- ✧ intersertal, microcrystalline groundmass with a modal abundance of 54-79%; and
- ✧ recovered core of pumice-lithic breccia suggests a late event of hydrothermal eruption.

The Rotokawa Andesite has a more basic composition compared to Ngatamariki, with a phenocryst assemblage of plagioclase, clino-and orthopyroxene, biotite and Fe-Ti oxides. The key characteristics are:

- ✧ disequilibrium during crystallisation is evident from normal or oscillatory zoning and sieve-textured plagioclase;
- ✧ plagioclase modal abundance of 32-37% with a composition of An_{51-82};
- ✧ presence of biotite (5-8% abundance), which is useful for identification of separate lavaflows;
- ✧ augite modal abundance of 5-6% and a composition of Wo_{41-42}, Fs_{9-17}, En_{39-47};
- ✧ orthopyroxene modal abundance of 1-5% and a composition of Wo_{2-3}, Fs_{28-31}, En_{65-67};
- ✧ Fe-Ti oxide modal abundance of 3-9%;
- ✧ intersertal, microcrystalline groundmass with a modal abundance of 32-51%; and
- ✧ andesite breccia with weak boundaries between clast and matrix suggests autobrecciation or multiphase alteration of fractured lava.

Chapter 4
Secondary mineralogy

4.1 Introduction

Hydrothermal alteration is defined as the alteration of rocks or minerals by the reaction of hydrothermal fluid with pre-existing solid phases (Henley & Ellis, 1983). The formation of alteration mineral assemblages may have a significant impact on geothermal production. Propylitic and zeolitic mineral assemblages can reduce primary porosity and infill fractures, thereby restricting the fluid flow within a reservoir. Retrograde and overprinting by argillic mineral assemblages may on the other hand enhance porosity and permeability which may increase the fluid flow. There is also an economic importance of certain alteration mineral assemblages, in the sense that they are used for localising associated ore deposits or hot, permeable production zones at geothermal fields. In the case of geothermal production, it is important to distinguish between mineral assemblages of an active versus a fossil geothermal system where a high-temperature mineral (i.e. adularia) has been overprinted by a low-temperature mineral (sericite).

This chapter seeks to describe common alteration minerals and their occurrence at the Ngatamariki and Rotokawa fields. Overprinting and layered alteration textures such as veins and vugs provide information about the order of deposition of these minerals. By considering what kind of conditions they preferable form in (e.g. temperature, pH-level, permeability), it is possible to identify changes to the geothermal system over time.

4.1.1 Formation of secondary minerals

Browne (1978) and Reyes (2000) discussed several factors that may affect the formation of secondary minerals. The alteration process and resulting type of

minerals depends on primary mineral assemblage, fluid chemistry and temperature, while the intensity of alteration is also dependent on duration and the texture of host rock. The main factors which will be discussed in this section are:

- ✧ temperature;
- ✧ pressure;
- ✧ rock type;
- ✧ permeability;
- ✧ fluid composition; and
- ✧ duration of activity.

4.1.1.1 Temperature

There are several high-temperature geothermal fields in the TVZ, with a typical temperature of 265°C along the western boundary and 310°C along the eastern boundary (Kissling & Weir, 2005). One of the highest temperatures was measured at Rotokawa well RK4 below -2200 mRL at 330°C (Ellis & Mahon, 1977), while the average reservoir temperature at Ngatamariki is ~270°C (Fig. 4.1). By extrapolating the low geothermal gradients observed in some of the deeper wells (e.g. ~20°C/km at Wairakei) to the brittle-ductile transition zone at 8 km depth, maximum temperature of the large-scale fluid circulation system below TVZ should range between 350 and 400°C (Kissling & Weir, 2005).

When the host rock of a geothermal system is heated to the upper limit of a particular mineral stability range, a reaction will take place where the unstable mineral is consumed and a new mineral is formed which is stable under the new condition. One of the most common reactions is dehydration of volatile-bearing minerals, such as gypsum which will alter to anhydrite. A narrow range in temperature stability of certain minerals may be used as a geothermometer during geothermal exploration (Browne, 1993).

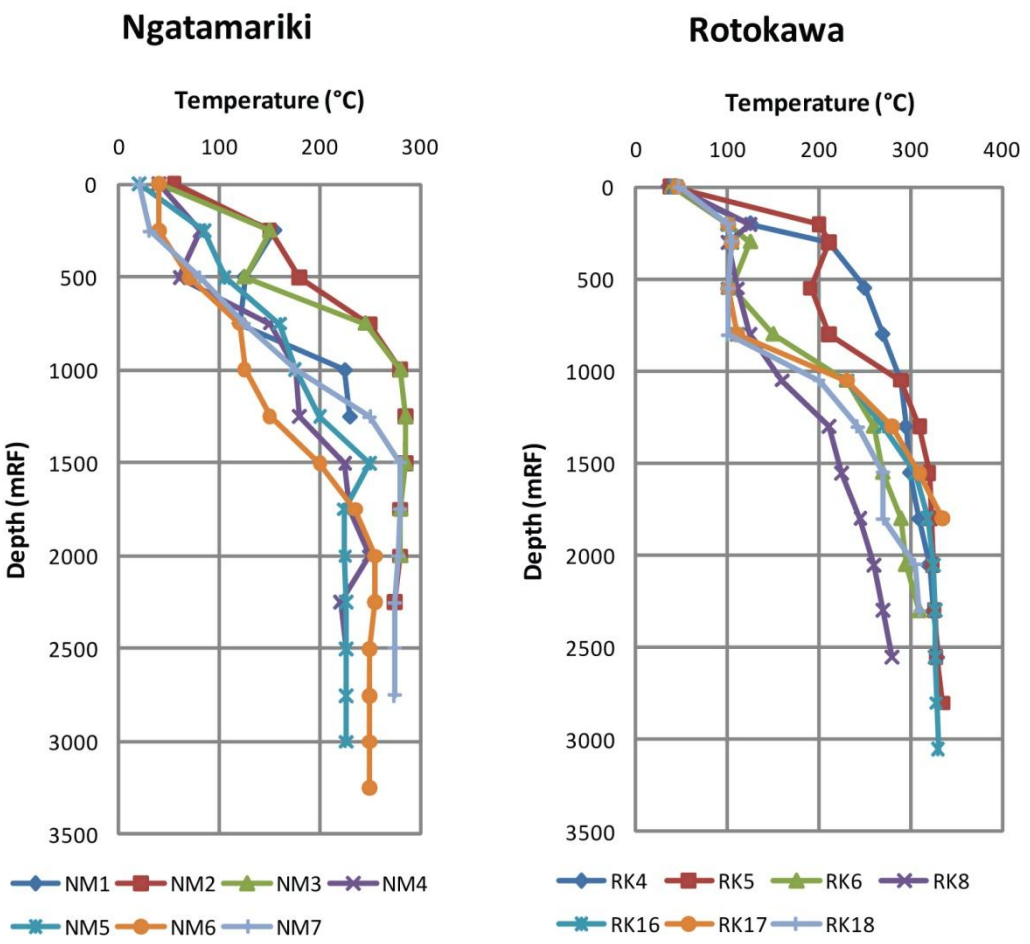

Figure 4.1: Approximate well temperatures in selected Ngatamariki and Rotokawa wells (modified from Rotokawa Joint Venture, 2007; Rae, 2007; Bignall, 2009).

The thermal regime is easily disturbed by drilling and it can take months before equilibrium in fluid flow is restored. In addition, extraction from a well will also cause permanent temperature changes between the ground surface and the well's feed zone. The measured temperature in a well obtained by a sensor is therefore not necessarily the same as prior to drilling so estimates based on key minerals can be very useful, such as smectite, illite, epidote or hydrothermal biotite by gas analysis of fluid inclusions and thin section examination. Microscopic gas and liquid bubbles from geothermal fluids are commonly trapped and preserved during crystallisation, so the temperature, pressure and composition of the original fluid can be obtained by heating up gas bubbles to the point of resorption (Hedenquist et al., 1992). Identifying secondary minerals in thin sections is a simple method but mineral stability can vary between

geothermal fields due to changing host rock and fluid conditions so temperature ranges need to be calibrated for each locality (Browne, 1993).

Three main types of minerals are commonly used as geothermometers:

- ✧ *clays* – with increasing depth and to a temperature of <210 C° smectite becomes more interlayered with illite, whereas assemblages of chlorite and illite exist in zones >210 C° (Harvey & Browne, 1991);
- ✧ *zeolites* – typical zones at higher temperatures are characterised by mordenite at ~50 C°, laumontite and lastly wairakite at >215 C° (Steiner, 1968; Browne & Ellis, 1970); and
- ✧ *calc-silicates* – minerals rich in Ca and Mg, cristobalite is a known low-temperature mineral (<50 C°) while epidote and hydrothermal biotite + amphibole indicate high-temperature zones (>240 C°) (Cathelineau et al, 1983).

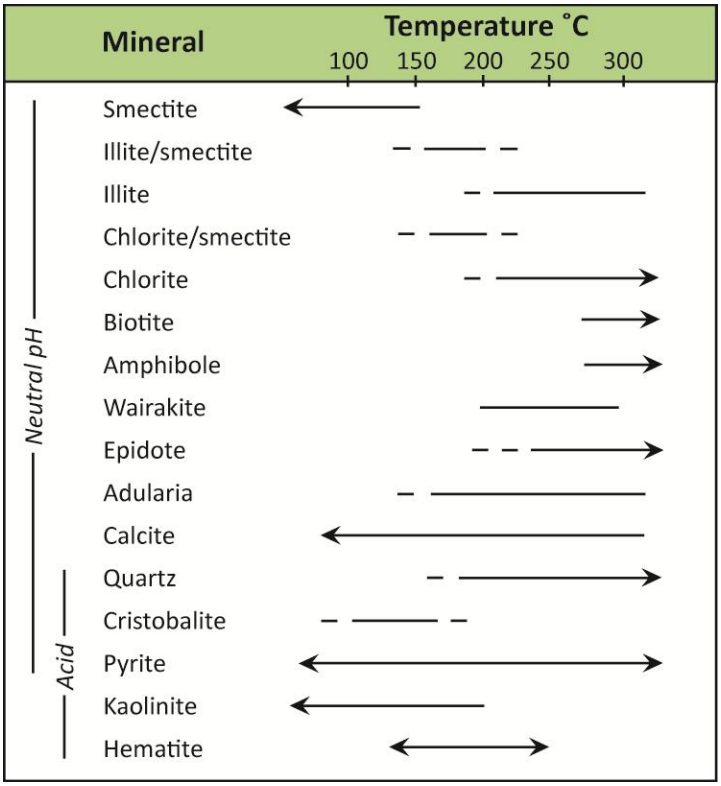

Figure 4.2: Generalised temperature stability of secondary minerals (modified from White & Hedenquist, 1995; Rae et al., 2009). Minerals can exist outside their temperature stability range depending on host-rock, fluid chemistry and mineral metastability.

Some minerals can be found in a range of temperature zones, such as calcite, chlorite and pyrite so they are hence not reliable as geothermometers (Fig. 4.2).

4.1.1.2 Permeability

Low permeability prevents equilibrium between host rock and geothermal fluids, so primary minerals can stay unaltered up to very high temperatures (Browne & Ellis, 1970; Keith et al., 1978). Hence, fluid access through the host rock is a key factor for alteration processes to take place and is often provided in the form of dykes, faults or fractures where fluid infiltration and hence element mobility are significantly greater than for the surrounding host rock. This structural control is easily observed by alteration zones radiating out from these structures, or the layered infill of secondary minerals in fractures and veins. The highest permeability is often in vertically aligned structures (Arnorsson, 1995), although horizontal contact zones between lithological units or intrusion boundaries also provide fluid access through the host rocks (Franzon et al., 1986; Bödvarsson et al., 1990).

However, overprinting by low-temperature minerals in well NM4 at Ngatamariki is believed to be caused by cooling fluids and lowered permeability in the host rock surrounding the diorite due to contact metamorphism. The diorite may even define the northern boundary of the geothermal system in this field (Bignall, 2009). At both Ngatamariki and Rotokawa, the lack of intense alteration style at most depth intervals indicates low permeability and that hydrothermal alteration, and thus permeability, is fault controlled (Rae, 2007; Bignall, 2009). At Broadlands, Browne (1970) observed that increasing levels of permeability are associated with different types of feldspars, starting with primary plagioclase → albite → albite plus adularia → only adularia at high permeability. The presence of adularia will increase K_2O-values of the host rock by three to four times the normal, making it easy to identify zones with high permeability. Kendall (1976) also found a connection between depletion of O^{18} in calcite and high permeability.

4.1.1.3 Rock type

The host rock mainly affects the formation of secondary minerals through its permeability. The primary mineralogy appears to have a greater influence on low-temperature alteration minerals than high-temperature assemblages. Si-rich zeolites (e.g. mordenite) are associated with rhyolites whereas Si-depleted zeolites (e.g. thomsonite) are found in basalts and andesites (Steiner, 1968; Browne & Ellis, 1970; Honda & Muffler, 1970; Naboko, 1970; Kristmanndottir & Tomasson, 1978). Assemblages of high-temperature alteration minerals (e.g. K-feldspar, chlorite, epidote, calcite, quartz, illite, pyrite) are indiscriminately formed in sandstone, basalt, andesite and rhyolite (Browne, 1978). The porosity of rock types at Ngatamariki and Rotokawa fields correspond with the median of other host rocks in the TVZ, which is ~10% for volcaniclastic and sedimentary rocks and <5% for the greywacke basement (Table 4.1). The shallow and deep aquifers of tuffs and breccia at Rotokawa have the highest porosity of ~25%, while deep tuff/breccia and ignimbrites (>1700 mRF) have the highest porosity at Ngatamariki.

Table 4.1: Average porosity (%) of rock types at Ngatamariki and Rotokawa fields (Rae, 2007; Bignall, 2009).

Rock type	Ngatamariki	Rotokawa
Tuffs and breccia (Waiora Fm)	6	25
Ignimbrite, rhyolite and sediments	9-13	10
Andesite lava	1.3-5.9	10
Deep andesite tuffs and breccia	-	25
Greywacke	2.5-3.2	<5

4.1.1.4 Fluid composition

There is a chemical equilibrium between fluids and secondary minerals in most volcanic-hosted hydrothermal systems (Giggenbach, 1980, 1981; Reed, 1982, 1997, 1998; Arnorsson, 1983; Arnorsson et al., 1983; Reed et al., 1984). This means that analysis of fluid chemistry may reveal mineral assemblages present at depth, and this information can subsequently be used for geothermometry. If equilibrium is in place, there are several elements which are commonly used for estimating reservoir temperatures, such as Si for quartz (Mahon, 1966) and Na-K

or Na-K-Ca for albite and K-feldspar (Ellis & Mahon, 1967). Giggenbach (1988) devised a ternary diagram comprising Na-K-Mg, which is a common analytical tool for geothermometry. Giggenbach (1988) assumed that as K-Mg has a faster rate of equilibrium than Na-K in addition to the inherent high Mg-content of immature waters, the improved diagram would therefore reflect conditions at shallower levels and also allow for identification of unsuitable sample fluids.

Some conditions can disturb the equilibrium such as low temperatures causing slow rates of chemical reaction, different fluid flow rates between lithological units or the presence of minerals containing reduction-oxidation elements (Fe, S) which require higher temperatures than others. Equilibrium between geothermal fluids and primary minerals is commonly lacking.

Geothermal fluids can be classified as primary or secondary. Primary fluids are found at the bottom of a convection cell and have two or more origins; seawater, meteoric and magmatic volatiles. Secondary fluids are created from primary fluids by two main processes during their ascent to the surface (Nicholson, 1993):

- *physical* – boiling, mixing and conductive cooling, and
- *chemical* – mineral/fluid interaction such as dissolution and precipitation of minerals as they reach saturation due to homogeneous equilibration in the fluid.

Boiling, or adiabatic cooling, occurs when geothermal fluids experience a reduction in hydrostatic pressure. This will create a two-phase system as vapour is separated from the liquid, and as a result chemical elements which are dissolved in the liquid will become concentrated. The loss of CO_2, for example, can raise the pH-level which has a reducing effect on calcite solubility and an increase in silica solubility. The benefit of boiling is that there is less time for fluid-mineral interaction and the discharged fluid has a similar composition as to the primary fluid. Mixing of primary fluids with shallow groundwater may lead to

changes in the concentration of chemical elements, typically an increase in Ca and Mg contents while Na/K ratios have been decreased. Slow ascent will allow a cool host rock to reduce the temperature of geothermal fluids by conduction. This will preserve the concentration of chloride as no steam is produced, but there will be plenty of time for fluid-mineral interaction which will result in changes of other chemical elements in the fluid.

At Ngatamariki, water samples collected from most springs plot within the area of partial equilibrium, which indicates dilution or mixing with shallow groundwater, with an estimated temperature of 160 to 180°C (Fig. 4.3). Exceptions are samples from Devils Mouth and Southern Pool, which plot above the equilibrium line. Samples collected from wells NM2, NM3, NM5 and NM6 plots along the equilibrium line, with estimated temperatures between 280°C and 320°C (O'Brien, 2010).

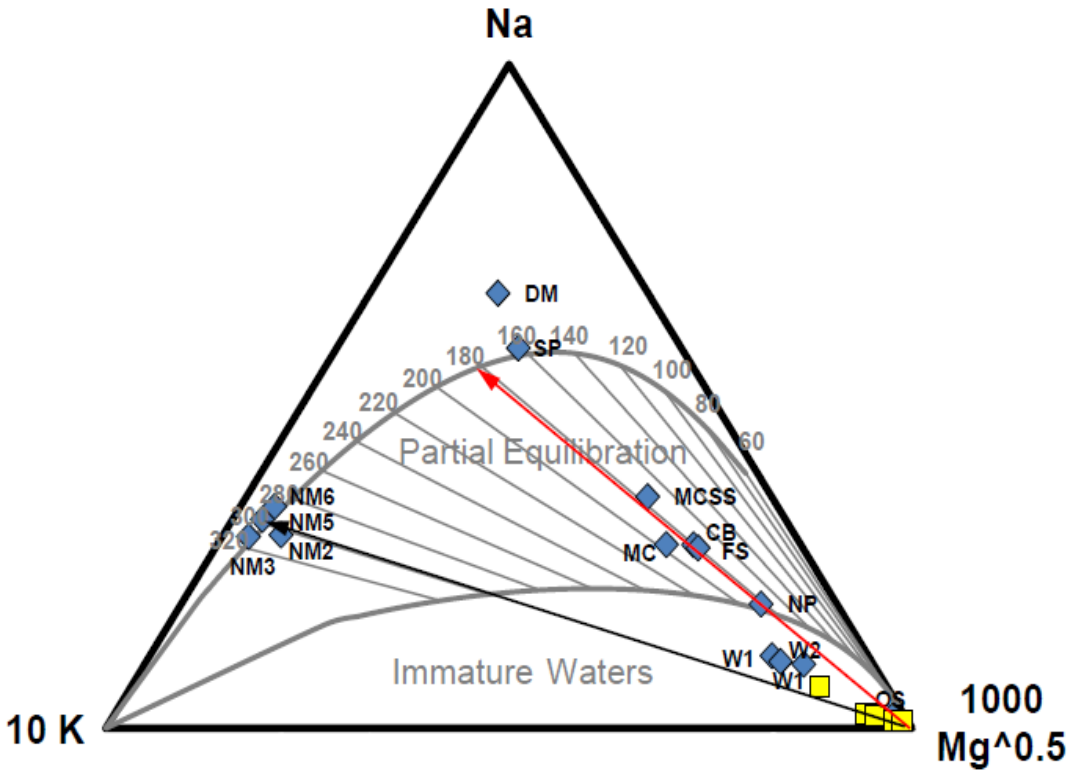

Figure 4.3: Na/K/Mg geothermometer for fluids at Ngatamariki, based on the ternary plot by Giggenbach (1988). Yellow square represents monitor wells while blue diamond represents all other waters, DM = Devils Mouth, OS = Orakonui South, SP = Orakonui South, Southern Pool, FS = Father and Son, CB = Clear Black, NP = North Pool, MC = Main Crater, MCSS = Main Crater Side Spring, W1-2 = Waikato River Springs (from O'Brien, 2010).

Measured temperatures and a propylitic mineral assemblage at Rotokawa indicate low permeability at depth or a young system where fluids and minerals are still in disequilibrium (Rae, 2007).

The type of reaction caused by fluid-mineral interaction depends on changes in pressure, temperature, salinity and host rock. A solubility reaction determines the amount of chemical elements that enters and remains in solution prior to precipitation, with three different behaviours;

- ✧ increased solubility with increasing temperature, i.e. alkali metal chlorides (Li, Na, K, Rb);
- ✧ increased solubility to a certain point after which it decreases with increased temperature, i.e. silica, (Si); and
- ✧ decreased solubility with decreased temperature, also called retrograde solubility, e.g. gypsum, anhydrite, calcite ($CaSO_4$, $CaCO_3$).

A reaction which involves the transfer of ions between aluminosilicate minerals controls the ratio of cations in solution, and pH-levels may increase by the presence of a silicate mineral assemblage. Examples of alteration mineral assemblages are: albite → K-feldspar, K-feldspar → K-mica + quartz, wairakite → Ca-montmorillonite + quartz and pyrite → pyrrhotite.

Table 4.2: Properties of geothermal fluids in New Zealand (from Hedenquist, 1986).

Description	NaCl (wt. %)	Source	pH	Temperature (°C)	Alteration
Chloride	0.1-0.2	Deep meteoric circulation	5.5-6.5	250-350+	Argillic-propylitic silicification
Acid sulphate	0	Surficial	2-3	100-130+	Advanced argillic
Mixed acid sulphate-chloride	Intermediate	Near surface mixture of chloride and acid sulphate	2-5	100-180	Argillic to advanced argillic
CO_2-rich condensate	0	Condensed steam and gas into non-oxygenated groundwater	5-6	120-180	Argillic-silicification

Propylitic and zeolitic mineral assemblages which may reduce porosity and infill fractures in the host rock, are often associated with Na-Cl, slightly alkaline fluids (Table 4.2). Argillic mineral assemblages known to enhance permeability and porosity of host rocks are associated with acidic thermal waters with complex ion composition (Kralj et al., 2010).

4.1.1.5 Pressure

Fluid pressures in geothermal areas are normally below 200 bars, and in liquid-dominated fields such as Ngatamariki and Rotokawa they are often close to hot hydrostatic. According to Browne (1978), pressure has mostly got an *indirect* effect on the formation of secondary minerals, through changes in fluid composition. As mentioned previously, a drop in pressure may incur boiling and the result is a loss of CO_2. This creates a more alkaline fluid which subsequently increases the solubility of Si and decreases the solubility of Ca. These zones of subsurface boiling are often characterised by the presence of hydrothermal quartz, K-feldspar and bladed calcite (Browne & Ellis, 1970; Ellis & McFadden, 1972; Keith & Muffler, 1978; Keith et al., 1978).

4.1.1.6 Duration of activity

Geothermal systems are very sensitive to any changes in their groundwater supply caused by natural events such as earthquakes and landslides, and their intensity and location will most likely vary during their lifetimes. Geysers geothermal field in the USA is believed to be around 1.8 Ma old based on age dating of a granite intrusion beneath the field, and the system has experienced changes in temperature every ~0.3 Ma, in addition to a conversion to vapour-phase system 0.26 Ma ago (Dalrymple et al., 1999). Geothermal fields in the TVZ are younger than Geysers but have also had variation in heat output over time. Wairakei (Grindley, 1965), Kawerau (Browne, 1979) and Ngatamariki (Arehart et al., 2002) are all estimated to be >0.3 Ma old.

Ngatamariki is a good example of long-lived geothermal activity. The age estimation was based on Ar/Ar-dating of a plutonic diorite encountered in NM4, which is overlain by 0.3 Ma Wairakei Ignimbrite (Arehart et al., 2002). The ignimbrite is characterised by low hydrothermal alteration intensity, and this indicates that there has been two different geothermal systems at this location; an old geothermal system which was extinct sometime before 0.3 Ma; and a new (active) geothermal system younger than 0.3 Ma. There are signs that the system is contracting, with overprinting by low-temperature minerals occurring in NM4, and the presence of relict hydrothermal amphibole (occurring >300°) in NM5 and NM7 (Bignall, 2009).

Fossil geothermal systems have become accessible through mining or erosion in the Coromandel district in addition to the Ohakuri field, which has been thoroughly studied by Henneberger (1982, 1983, 1986) and Henneberger & Browne (1988). Ohakuri is located ~20 km northwest of Rotokawa and is believed to have been active between 0.7 and 0.16 Ma ago. Causes that might shorten the duration of geothermal activity do not necessarily need to be related to the thermal activity itself. Geothermal exploitation may cause a range of negative impacts on geothermal systems. For example, fifty years of exploitation at Wairakei has resulted in extinction of surface features, change in fluid chemistry, lowered reservoir pressure and temperature in addition to the highest rate of ground subsidence in the world (Bixley, 1986; Allis, 1990; Barrick, 2007; Glover & Mroczek, 2009). Lowered temperature of geothermal fluids at Orakeikorako – Te Kopia caused deposition of silica at the top and margin of the fields, which subsequently clogged up fluid pathways and resulted in self-sealing of the host rock itself (Sheppard & Lyon, 1984).

Areas of high resistivity between geothermal fields in the TVZ prove that there has been no hydrothermal alteration outside present field boundaries during the last 0.2 Ma (Bibby, 2000). The spatial stability and longevity of each geothermal field despite changing volcanism implies that they are parts of a large-scale fluid-circulation system.

4.1.2 Alteration styles

The alteration process will create different secondary mineral assemblages, depending on chemical and physical conditions in a geothermal system and its host rocks, as discussed in previous section. The resulting changes in the rocks mineralogy, texture and composition may be used to determine alteration intensity and also style of alteration. When describing altered rocks, Gifkins et al. (2005) recognized that there are four variables to consider:

- ✧ intensity;
- ✧ distribution;
- ✧ texture; and
- ✧ mineral assemblage.

At least two of the factors are recommended to be used (e.g. mineral assemblage plus one more) in order to provide a satisfying description of altered rocks. For example: strong (intensity) chlorite + epidote (mineral assemblage) alteration facies, or: local (distribution) layered infill (texture) of chlorite + calcite (mineral assemblage) alteration facies.

4.1.2.1 Intensity

The intensity is a measurement of how much of the rock has been altered, and the abundance of secondary minerals, with a scale ranging from subtle to intense alteration (Gifkins et al., 2005):

- ✧ *subtle alteration* - secondary minerals coat fractures and vugs or the surface of existing phenocrysts, e.g. plagioclase has been dusted with sericite, carbonate or hematite and glass is devitrified while textural changes are insignificant;
- ✧ *weak alteration* - plagioclase is partly replaced by albite, sericite, carbonate, hematite and/or epidote while ferromagnesian minerals are replaced by chlorite, epidote and Fe-oxides;

- ✧ *moderate alteration* - plagioclase is partly to completely replaced by feldspar, sericite, carbonate, epidote, quartz and/or magnetite, although outlines are still visible while ferromagnesian minerals are completely replaced and there may be recrystallisation or replacement of quartz, most textures are modified or destroyed by alteration whereas vugs and clasts are completely recrystallised but still detectable;
- ✧ *strong alteration* - there is a complete replacement of plagioclase by chlorite, sericite, carbonate and/or opaques although outlines may still be partly visible, but textures are almost completely destroyed; and
- ✧ *intense alteration* - there are no primary minerals left, only occasional outlines may still be visible. Alteration distribution is pervasive, homogenous and there can be a transgression to other rock units.

4.1.2.2 Distribution

Alteration zones are commonly stratigraphically or spatially related with host rock, veins or other structures. Although easy to recognize under a microscope, the zones may be difficult to establish in the field due to lack of exposure and structural deformation of host rock. Also, there may be overprinting of low- or high temperature mineral assemblages as the geothermal system changes over time. Distribution and zonational patterns may be used to study fluid flow patterns, alteration systems and changes to physical and chemical conditions in the geothermal system. Distribution is commonly divided into regional vs. local alteration zones, where a *regional zonation* is used to describe a kilometer-large area while *local zonation* is used for a scale of centimeters and upwards (Gifkins et al., 2005).

4.1.2.3 Texture

Hydrothermal alteration often modifies both texture and mineralogy of a rock. The texture can be affected by changes in shape form, orientation and size of grains within a rock. These changes are able to destroy, preserve or even enhance primary textures. Alteration textures may be used to identify alteration

mineral assemblages which are in equilibrium with geothermal fluids, overprinting relationships and alteration intensities. There are five common types of alteration textures in volcanic rocks (Gifkins et al., 2005):

- ✧ *replacement* – primary glass or minerals are replaced by secondary minerals;
- ✧ *infill* – secondary minerals are precipitated from solution into vugs and other open spaces;
- ✧ *dissolution* – primary minerals are dissolved and removed by solution, sometimes followed by replacement;
- ✧ *static or dynamic recrystallisation* – a change in morphology and/or recrystallisation of primary minerals to secondary minerals, dynamic recrystallisation include a change in orientation of the mineral; and
- ✧ *deformation* – primary minerals may be rotated, broken, compressed, or modified.

Pseudotextures are less common, but they can make identification of primary composition tricky. This type of alteration texture may cause rocks to be mistaken as brecciated, pyroclastic, eutaxitic, polymictic, coherent or thin-bedded volcaniclastic. Of these, pseudobreccia is one of the most common types. False breccias textures are often formed by overprinting of secondary minerals in coherent lavas (Allen, 1988). This is caused by a two-phase alteration, where a pseudomatrix contains a different alteration assemblage compared to the pseudoclasts. The alteration assemblages have been formed during different alteration stages, causing different proportions and types of alteration minerals (hence varying colours and textures). This is then followed by extensive and preferential replacement of volcanic glass, fracture and/or matrix-controlled pervasive alteration (McPhie, 1993). As alteration progresses along fractures and matrix towards unaltered margins, more advance alteration is created in isolated areas (pseudoclasts) which are enclosed in an interconnected area with a different alteration assemblage (pseudomatrix). Pseudobreccia may also appear

polymictic due to patchy or mottled alteration distribution which varies in colour or preservation of primary minerals (Gifkins et al., 2005).

4.1.2.4 Mineral assemblage

It is difficult to identify the original host rock in ancient geothermal fields where there has been extensive alteration. However, if the alterations have occurred at low to moderate temperatures, the secondary mineral assemblage may reflect if the host rock had a mafic or felsic composition. Below 200°C and up to moderate alteration intensity, typical mafic alteration minerals are epidote, calcite, albite and actinolite-tremolite plus clays whereas examples of felsic alteration minerals are quartz, micas, cristobalite and clays (Table 4.3). Above 200°C, alteration minerals are more influenced by fluid composition, permeability, pressure and temperature rather than primary mineralogy (Gifkins et al., 2005). Geochemical techniques may be required in order to identify the original host rock at this stage. Mineral assemblages may be either in equilibrium or disequilibrium with the geothermal fluids, as discussed in Chapter 4.1.1. Rocks consisting of primary minerals are rarely in equilibrium, it is more common among intensely altered rocks. It is important to recognize disequilibrium assemblages when mapping altered rocks, and also the processes which form alteration minerals. Scenarios which may complicate disequilibrium assemblages with the addition of other mineral assemblages are disrupted alteration processes or overprinting.

Table 4.3: Common replacement of alteration minerals (from Gifkins et al., 2005, and references therein).

Original component	Alteration minerals
Silicic volcanic glass	Zeolites, cristobalite, opaline silica, quartz, calcite, smectite, mixed layer clays
Mafic volcanic glass	Smectite, nontronic clays, calcite, chlorite, epidote, Ca-rich zeolites, Fe/Ti/Mn-oxides
Magnetite, ilmenite and titanomagnetite	Pyrite, leucoxene, titanite, pyrrhotite, hematite
Pyroxene, amphibole, olivine and biotite	Chlorite, illite, quartz, calcite, pyrite, anhydrite
Plagioclase	Calcite, albite, adularia, wairakite, quartz, anhydrite, chlorite, illite, kaolinite, smectite, epidote, sericite
Anorthoclase, sanidine and orthoclase	Adularia, albite, sericite
Quartz	Microcrystalline quartz

4.1.3 Alteration minerals

This section provides background information about common alteration minerals at Ngatamariki and Rotokawa. Their chemical formula and d-spacing intensity is summarized in Table 4.4.

Table 4.4: Summary of chemical formulas and d-spacing intensities for common alteration minerals at Ngatamariki and Rotokawa (from Brown, 1961; Deer et al., 1992, Nelson, 2008).

Secondary mineral	Chemical formula	d-spacing (Å)
Illite	$K_{1.5\text{-}1.0}Al_4(Si_{6.5\text{-}7.0}, Al_{1.5\text{-}1.0})O_{20}(OH)_4$	9.9-10.1 (100), 3.3 or 4.4-4.5 (90)
Smectite	$(_{1/2}\ Ca,Na)_{0.7}(Al,Mg,Fe)_4[(Si,Al)_8O_{20}](OH).nHO$	air dry: 14-15 (10), ethylene glycol: 17 (100) and furnace: 9.5-10 (100)
Anhydrite	$CaSO_4$	3.5 (100), 2.8 (33)
Hematite	Fe_2O_3	2.69 (100), 1.69 (45)
Limonite	$FeO.OH.nH_2O$	4.205 (vs), 2.414 (s), 2.719 (ms), 1.758 (ms)
Kaolinite	$Al_4[Si_4O_{10}](OH)_8$	7.2-7.5 or 3.5 (100), 2.4-2.5 (90), furnace: no peak
Quartz	SiO_2	3.34 (100), 4.26 (35)
Biotite	$K(Mg, Fe)_3AlSi_3O_{10}(OH,F)_2$	10.1 or 3.37 (100), 2.66 or 2.45 (80)
Adularia	$KAlSi_3O_8$	3.33 (100), 3.22 (90)
Albite	$NaAlSi_3O_8$	3.2 (100), 3.78 (25)
Calcite	$CaCO_3$	3.03 (100), 2.28 or 1.87 (20)
Chlorite	$(Mg, Fe^{2+}, Fe^{3+}, Mn, Al)_{12}[(Si, Al)_8O_{20}](OH)_{16}$	7.12 or 3.56 (100), 14.2 or 4.75 (80), furnace: 14.2 only
Epidote	$Ca_2Al_2O.(Al, Fe3^+)OH[Si_2O_7][SiO_4]$	2.92 (100), 2.58 (49)
Amphibole (actinolite)	$Ca_2(Mg, Fe^{2+})_5[Si_8O_{22}](OH, F)_2$	2.719 or 2.543 (100), 3.401 (80)
Chalcopyrite	CuFeS2	3.038 (100), 1.8570 (35), 1.5927(27)
Sphalerite	ZnS	3.123 (100), 1.912 (51), 1.633 (30)
Galena	PbS	2.969 (100), 3429 (84), 2.099 (57)

Clays

Clay minerals are hydrous silicates containing mainly aluminium or magnesium. The occurrence of smectite, illite-smectite or illite is commonly used as a temperature indicator since smectite forms <140˚C and illite >210˚C (Harvey & Browne, 1991). They are often difficult to distinguish from each other by microscopy as they do not form visible crystals, so the preferred method to identify clay types is by XRD analysis (e.g. d-spacings). The peaks are easily recognisable in XRD graphs as they react differently to ethylene glycol or heating in furnace. Conversion of smectite to illite involves incorporation of K and substitution of Al for Si, while more acid conditions causes smectite to convert to kaolinite instead.

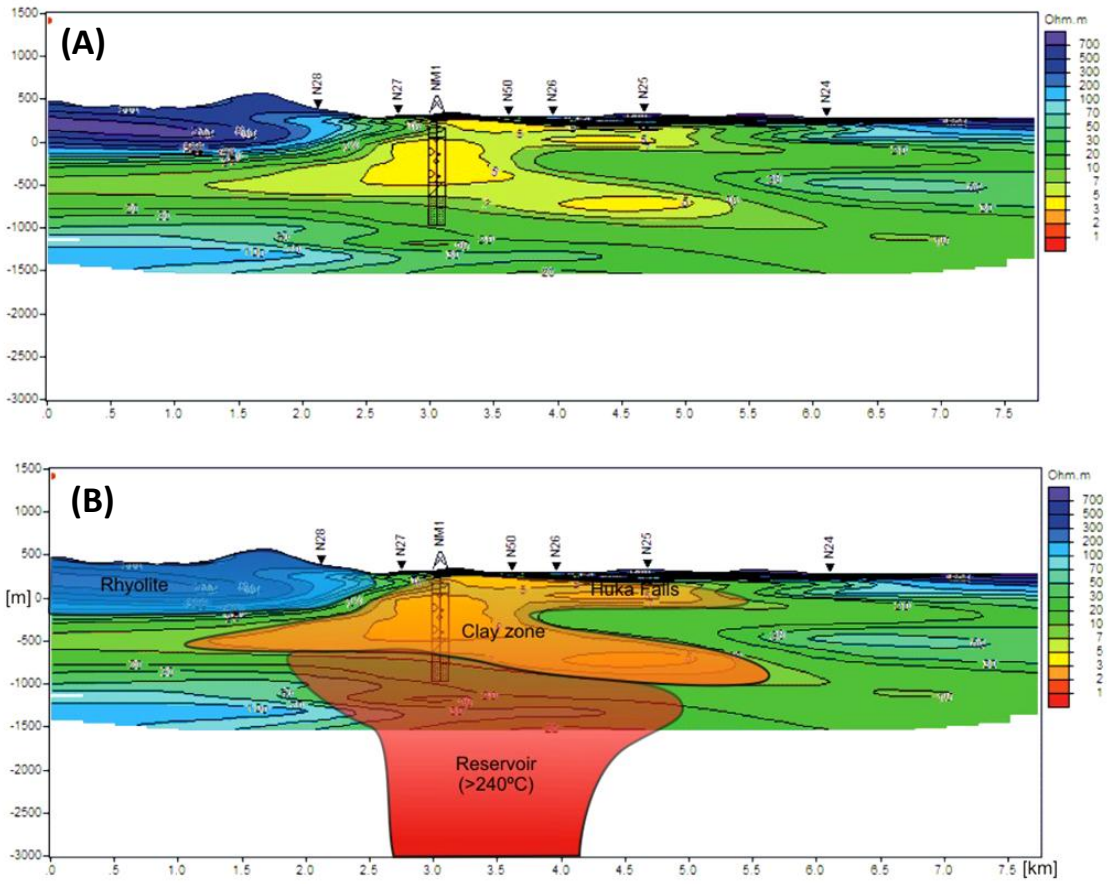

Figure 4.4: a) Example of a cross-section of Ngatamariki at well NM1 created by an MT-image. b) Interpretation of clay occurrence where ohm-m <10 (from Urzua, 2008).

Clays often create an impermeable cap on top of a geothermal reservoir, which can be identified by using geophysical exploration methods such as resistivity imaging (Gunderson et al., 2000). The aim of using this type of method is to map the structure and conductance of smectite zones with characteristically low temperatures (<140°C) and low resistivity, in addition to the underlying propylitic reservoir with high temperatures (>240°C) and high resistivity. Together with geological and geochemical data, it is possible to estimate resource capacity and target wells for high temperature permeability. MT-TDEM surveys at Ngatamariki between 2004 and 2005 detected a low resistivity zone below the Huka Falls Formation which corresponds with the distribution of smectite or illite-smectite (Fig. 4.4). By identifying the top boundary of the reservoir, it was then possible to estimate the extension of the field (Urzua, 2008). A conservative number was

given for the outer boundary at 5 km^2 (>280°C) while a less conservative number was 12 km^2 (>240°C).

Anhydrite

Anhydrite exhibits retrograde solubility and is deposited directly from a SO-rich geothermal liquid, when mixed with cooler groundwater at temperatures above >150°C (Bischoff & Seyfried, 1978). Anhydrite has been identified in El Chichón trachyandesite and Pinatubo andesite-dacite, where both magmas have been characterised as water-rich and highly oxidized with fugacity-levels well above normal. The properties of these intermediate magmas most likely created H_2O-dominated vapour bubbles containing SO_2-gases, which promoted the precipitation of anhydrite (Luhr, 2008). Sulfate-saturated environments like this can be used to identify potential hydrothermal ores, such as epithermal gold deposits (Chambefort et al., 2008).

Hematite

Hematite is a form of iron oxide and crystallises in the rhombohedral system, similar to ilmenite. It is a replacement product of titanomagnetite or ilmenite crystals during reducing conditions, but may also form by oxidation of silicates (Beske-Diehl & Li (1993). Progressed alteration in reducing conditions where there are abundant S and Fe, ilmenite may be replaced by leucoxene while the hematite lamellae are replaced by pyrite (Mange & Wright, 2007).

Kaolinite

Kaolinite is a low-temperature alteration of volcanic glass or Al-rich minerals such as feldspar under acid conditions, and may be represented by the reaction (Deer et al., 1992):

$$2KAlSi_3O_8 + 3H_2O$$
$$= Al2Si_2O_5(OH)_4 + 4SiO_2 + 2K(OH)$$

If potassium is not leached away during alteration, illite may form instead of kaolinite. Kaolinite may also occur as infill of vugs and veins.

Limonite

Limonite is an alteration product of Fe-bearing minerals and often consists of a mixture of hydrated Fe-oxides, mainly cryptocrystalline goethite (Deer et al., 1992). It is known to replace pyrite, and is often associated with hematite. Limonite is normally isotropic, and is recognised by a semi-transparent, brownish yellow colour in plain polarised light.

Quartz

Primary quartz is known to be unaffected by hydrothermal alteration (Browne, 1970), and is mostly an accessory mineral in intermediate volcanic rocks. Secondary quartz is however common in a geothermal setting. Silica is the most abundant element of crustal rocks, and has a high solubility in high-temperature hydrothermal fluids. Silica dissolves from host rocks in the lower levels of a geothermal system and is carried by hydrothermal fluid towards the ground surface. As the fluid cool at shallower levels, it may become supersaturated with silica which causes the silica to precipitate out of solution. According to Fournier & Rowe (1966), there will be little silica deposition if the fluid ascends rapidly at temperatures <250°C. Conversely, at high temperatures and slow ascent rates, quartz, chalcedony or amorphous silica will precipitate as a result of conductive cooling. Precipitation can clog fluid pathways (self sealing) and therefore poses a threat to the dynamics of a geothermal system, but on a positive note the presence (or absence) of silica deposition may also be useful as a geothermometer (Lowell & Martin, 2000).

Cristobalite

It has been described by Honda & Muffler (1970) as a high-temperature devitrification mineral at Yellowstone, while Deer et al. (1992) suggested that it as a late-stage crystallisation product. Browne (1970) found that cristobalite occurs at low temperatures (<176°C) at Broadlands, and theorised that it may be

a first alteration mineral of volcanic glass which then alters to quartz at higher temperatures.

Hydrothermal biotite

A study by Parry & Downey (1982) found that breakdown of igneous biotite to chlorite begin at ~200°C, as F, Cl, Fe^{2+} and K is removed from the interlayer of biotite and lost to solution. Meanwhile, Mg, Fe^{3+} and Mn are added from solution to form chlorite. This process is most likely accompanied by a conservation of Al and redistribution of other elements including oxygen isotopes in both tetrahedral and octahedral sheets of the biotite (Fiebig & Hoefs, 2002). Further alteration caused by raised temperature (>280°C) and the presence of a K-rich fluid may then cause hydrothermal biotite to replace the chlorite pseudomorphs of igneous biotite (Sales and Meyer, 1948).

More recent studies by Nachit et al. (2005) and Zacharias (2008) recognized that biotite with different compositions may exist within a single facies. They were classified as primary magmatic, re-equilibrated and neoformed biotites, and attributed the alteration to circulating late- to postmagmatic fluids. The Mg- and TiO_2-content of biotite may be used to determine how far the process has come, to either partial or complete alteration. Ti in biotite is thermo-dependent, and will decrease with rising temperature. Mg will on the other hand increase. Decreasing Ti will cause the brown colour typical for igneous biotite to change to the pale green colouring of hydrothermal biotite. Even though hydrothermal biotite may replace igneous biotite by a simple change of elements, it is more commonly an alteration product of pre-existing ferromagnesian minerals.

Adularia

Adularia is a high temperature potassium feldspar, which is generally distinguished from plagioclase by its K-content (<5-10%). Adularia is a replacement product of plagioclase, either alone or together with albite. Adularia, albite and quartz have traditionally been used in geothermal

exploration as an indicator for permeability, high if adularia occurs alone or with quartz, medium to low if mixed with albite (Browne, 1970).

A shift in alteration style of plagioclase to albitization or saussurization to replacement by adularia may be caused by increased ratio of a^{+}_{K}/a^{+}_{H} ratio and decreased temperature. Albite is dominant at high temperatures (~300°C), while K-feldspar is stabilized at ~250°C. Morad et al. (2010) suggested one internal source of K to be chloritization of biotite, whereas Browne (1970) proposed that it can also be derived from a mineral assemblage containing quartz and illite (another K-mica):

K-mica + Quartz = Adularia

$KAl_2AlSi_3O_{10}(OH)_2 + 2K^+ + 6SiO_2$

$= 3KAlSi_3O_8 + 2H^4$

This process results in the growth of adularia in order to remove excess K-ions and restore fluid equilibrium. There are several causes for the replacement of albite by adularia, for example enhanced ionic diffusion due to micropores in albite (Caussiux et al., 2006) or fluid mixing and release of CO_2 from the geothermal system (Parry, 1998).

Albite

Browne (1970) suggested that the contrast with a clear primary plagioclase is caused by the addition of tiny inclusions of Fe-oxides during the alteration process. This observation was confirmed by Morad et al. (2010), and they also described vacuolization (riddled with micro-pores) of pervasively albitized plagioclase crystals which is caused by dissolution.

Albite may be part of propylitic sub-alteration styles albitization or saussuritization. Saussuritization is a high-temperature process (250-400°C) where hydrothermal fluids reacts with Ca-rich plagioclase and creates a mineral assemblage of Na-rich albite, epidote, chlorite and amphibole and calcite.

Eliasson (1993) suggested there is a connection between this type of alteration and chloritization of biotite, as this may provide the required Fe and Mg to form epidote and amphibole while plagioclase will provide CaO for the formation of calcite, assuming Al is preserved among the solid phases (Ferry, 1979):

$$1.0 \text{ plagioclase} + 0.3 \text{ biotite} + 2.2H^{+}$$
$$= 0.6 \text{ albite} + 0.2 \text{ epidote} + 0.2 \text{ mica}$$
$$+ 0.7\ H_4SiO_4 + 0.3Fe^{2+} + 0.7\ Mg^{2+} + 0.2\ K^{+}$$

Morad et al. (2010) observed that albitization is most common where chloritized biotite is rare or absent, thereby restricting the formation of epidote and mica (Ferry, 1979):

$$1.0 \text{ plagioclase} + 1.2\ SiO_2 + 0.6\ Na^{+}$$
$$= 1.3 \text{ albite} + 0.3\ Ca^{2+}$$

They drew the conclusion that the alteration style of plagioclase is dependent on the geochemical environment. Albitization of plagioclase does not simply reflect addition of SiO_2 and Na. Fiebeg & Hoef (2002) studied the distribution patterns of oxygen isotopes within altered plagioclase, and concluded that albite is precipitated from dissolved plagioclase accompanying a restructuring of aluminosilicate tetrahedra within the plagioclase.

Calcite

The formation of calcite in geothermal systems is dependent on the movement of CO_2, and is therefore associated with zones of boiling, dilution and condensation (Simmons & Christenson, 1994). Platy calcite precipitates from boiling fluids through exsolution of CO_2 close to the two-phase upflow zone in a geothermal system. Replacement takes place in the surrounding one-phase zone, through hydrolysis reactions between near-boiling liquids containing CO_2 and Ca-/Al-silicates.

Chlorite

Chlorite occur in a wide range of temperatures, and is mainly an alteration product of ferromagnesian minerals such as pyroxene, hornblende or biotite, plagioclase or more rarely precipitated directly from solution (Bailey, 1988).

Epidote

Epidote is a commonly used indicator for high temperatures in geothermal wells. It is an alteration product of saussuritization, which is a process where hydrothermal fluids reacts with Ca-rich plagioclase and creates a mineral assemblage of Na-rich albite, epidote, chlorite and amphibole and carbonates (calcite).

Green amphibole

Hornblende is an alteration mineral in many igneous rocks, commonly replacing pyroxene (Deer et al., 1992). If alteration progresses it is in turn readily replaced by chlorite. Amphibole is a group name, and may be used if the chemical composition is unknown, as there is a large variety of sub-species which are difficult to distinguish from each other by thin section examination. Altered, green amphibole at Ngatamariki has previously been classified as actinolite or actinolite-tremolite in well reports (Bignall, 2009).

Opaques

Chalcopyrite is an important copper-bearing mineral. It may be formed either by exolution from a Cu-Fe-Ni-S solid solution in mafic rocks, or by precipitation from late-stage saline fluids in felsic rocks (Putnis & Mc Connell, 1976). In hydrothermal vein deposits, small crystals of chalcopyrite are often intergrown in sphalerite. Chalcopyrite appears to be little affected by reducing conditions, except in oxidizing conditions at low pH-levels. Pseudomorphs after chalcopyrite are for example pyrite, calcite and iron oxides.

Galena, sphalerite and chalcopyrite often occur together in a wide range of temperatures. Galena is easily recognised by the triangular pits on its crystal

surface, and is a major ore of lead while sphalerite is an important ore of zink. Both galena and sphalerite have a low solubility in pure water, and they are thought to be formed by precipitation of Zn- and Pb-enriched hydrothermal fluids (Vaughan & Ixer, 1980; Scott, 1983).

4.1.4 Alteration at Ngatamariki and Rotokawa

At Ngatamariki and Rotokawa, there are four common alteration styles with associated mineral assemblages (Rae, 2007; Bignall, 2009):

- *argillic* – a low temperature event sometimes occurring in atmospheric conditions, commonly forms clay minerals (smectite and illite) and is recognized by the bleaching out of feldspar;
- *advanced argillic* – a subcategory of argillic, common in low pH-environments and high temperatures (<220°C) where the alteration assemblage consist of kaolinite, alunite, anhydrite, quartz, hematite, limonite and sericite;
- *potassic* – a high temperature alteration type taking place deep in the geothermal system, characterized by K-enrichment which can form before the magma has completely crystallized (evident by sinuous vein patterns) where the alteration assemblage consists of biotite and adularia; and
- *propylitic* – also called saussuritization, the alteration assemblage typically consists of green minerals and this is another high temperature alteration type, with the presence of chlorite and epidote indicating temperatures between 220-340°C while green amphibole (actinolite-tremolite) occur at 280-350°C, and they usually form from the dissolution of ferromagnesian minerals such as biotite, amphibole or pyroxene or more rarely from feldspar.

The hydrothermal alteration at Ngatamariki and Rotokawa generally increases in intensity with depth (Fig. 4.5).

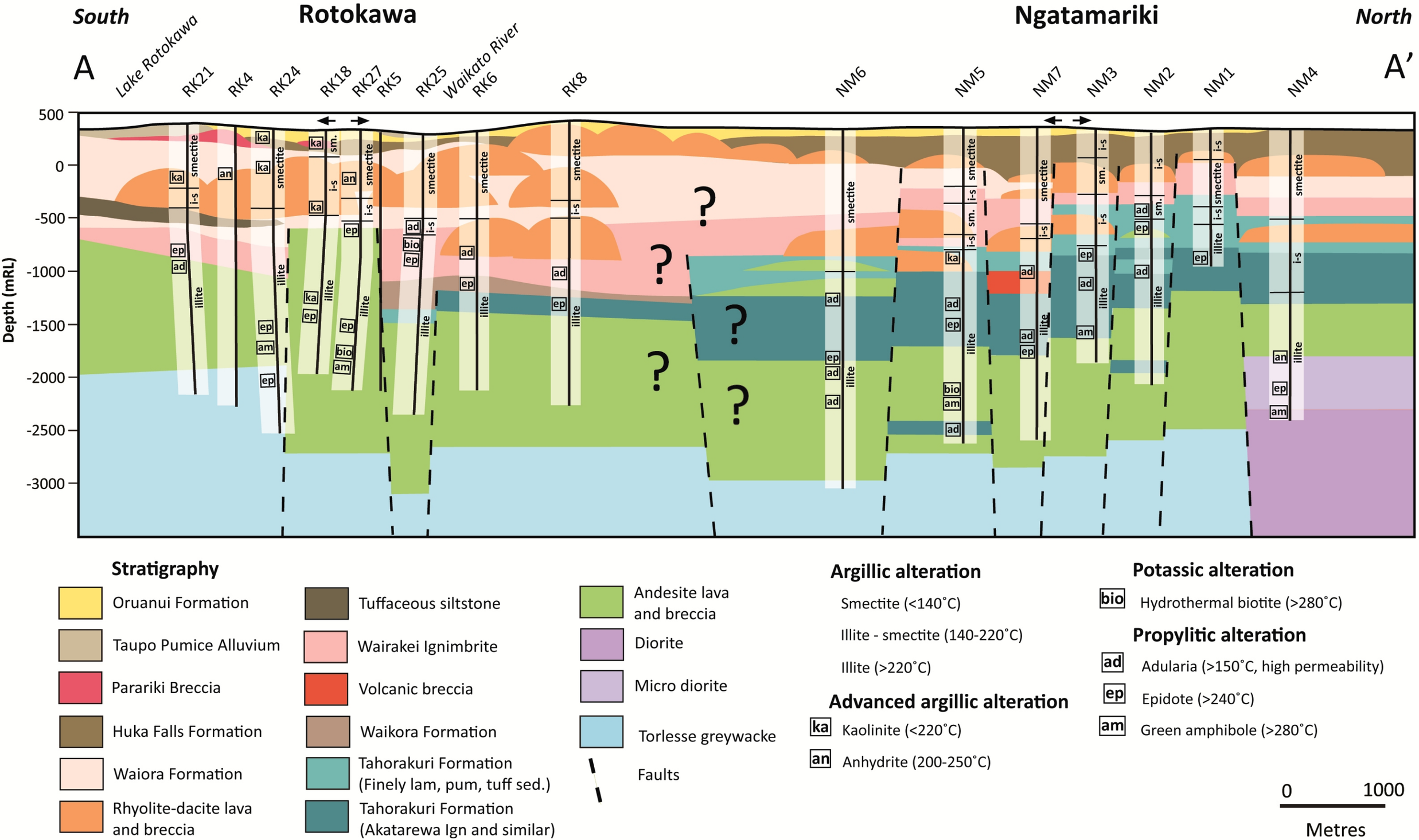

Figure 4.5: Cross-section of Ngatamariki and Rotokawa geothermal fields. Occurrence of smectite and illite in RK18 and RK24 is based on data nearby wells RK16 and RK20/23 respectively (a summary of all well reports).

Smectite occurs at shallow depths at both Ngatamariki and Rotokawa, before transgressing into illite-smectite or illite at ~800-1100 mRF. Illite occurs below ~800 mRF at Rotokawa whereas the first occurrence at Ngatamariki is ~1100 mRF. Clay minerals formed by argillic alteration style is present at shallow levels (<200 m depth) in areas close to surface manifestations, where there is localized steam heated waters with low pH-levels enriched in S and CO_2. At some places acid fluids have permeated to deeper levels, identified by the presence of anhydrite, kaolinite, hematite or a mix of illite plus kaolinite along faults or contact zones between rock units. The presence of advanced argillic alteration assemblage is indicative of corrosive CO_2-rich fluids which are known to cause casing failure (Rae, 2007).

Chloride fluids with near neutral pH-levels and additional Na and Ca occur at deeper levels at Ngatamariki and Rotokawa, creating a propylitic alteration style (Robb, 2005; Rae, 2007; Bignall, 2009). The alteration assemblage consists of quartz, illite, chlorite, wairakite, epidote, adularia, albite and calcite. Epidote is the most abundant high-temperature alteration mineral and indicates temperatures >240°C below 1000 mRF depth. In RK25 at ~1050 mRF, an andesitic dike-intrusion into the Wairakei Ignimbite has created a mixed potassic/propylitic alteration, indicated by the presence of both epidote and hydrothermal biotite (Ramirez et al., 2008). Common alteration textures in both fields are veins and cavities with layered infill of calcite, quartz and epidote.

4.2 Methodology

To identify secondary minerals from Ngatamariki and Rotokawa fields, the same techniques were used as for primary minerals described in Chapter 3: thin section petrography, modal analysis, electron microprobe analysis and cathodoluminescence (CL). 20 samples were selected for X-ray diffraction (XRD) analysis where six are from a 6 m continuous core and six are from a down-hole log in well RK21 at Rotokawa, while another eight samples are from a down-hole log in well NM6 of changing rock type at Ngatamariki (Table 4.5).

Table 4.5: Samples selected for XRD-analysis. Rock type is based on geochemical classification by TiO_2/Zr-ratio in Chapter 5.4.

Sample	Well	Depth (mRF)	Rock type	Alteration intensity
Ngatamariki				
LA.5	NM6	2686-2689	Andesite	Weak
LA.7	NM6	3032-3035	Basaltic andesite	Strong
LA.15	NM6	2210	Andesite	Weak
LA.17	NM6	2300	Andesite	Moderate
LA.19	NM6	2400	Andesite	Moderate
LA.22	NM6	2550	Andesite	Moderate
LA.78	NM6	1330	Dacite	Weak-Moderate
LA.82	NM6	1530	Rhyolite	Moderate-Strong
Rotokawa				
LA.23	RK21	1250	Basaltic andesite	Weak
LA.27	RK21	1450	Basaltic andesite	Weak
LA.31	RK21	1650	Basaltic andesite	Weak-Moderate
LA.35	RK21	1850	Andesite	Moderate
LA.39	RK21	2050	Andesite	Weak-Moderate
LA.44	RK21	2300	Basaltic andesite	Moderate
LA.53	RK27 #2	2147	Andesite	Strong
LA.54	RK27 #2	2148	Andesite	Moderate
LA.55	RK27 #2	2149	Andesite	Moderate
LA.56	RK27 #2	2150	Andesite	Weak
LA.57	RK27 #2	2151	Andesite	Weak
LA.58	RK27 #2	2152	Basaltic andesite	Subtle

A few samples were also analysed by cathodoluminescence (CL) as the distribution of alteration minerals becomes more visual in photographs due to their luminescence colour.

4.2.1 XRD analysis

To prepare the samples, rocks were crushed in a tungsten carbide mill to a fine powder. A few drops of distilled water was added to ~1 g of the powder on a petrographic glass slide and then stirred together with a metallic spatula. The added water allows potential, flaky clay minerals to settle horizontally, which is essential for a correct identification. Each sample was analysed three times, also to help with the identification as it will cause expansion or collapse of different clay minerals (Fig. 4.6);

- ✧ first as air-dried at 60° C overnight to remove moisture in general;
- ✧ a second time as soaked in ethylene glycol overnight as this causes smectite to expand (water molecules are substituted with larger radii glycol molecules) and consequently increases the peak height or move the Ångstrom position; and
- ✧ a third time after being heated up to 550°C in a furnace for 1 hour as this will decrease peak height or move the Angstrom position of smectite, chlorite, illite and mixed layers whereas kaolinite is completely destroyed.

Analysis was carried out on a Philips (X'PERT) XRD instrument at the University of Waikato. Powder diffraction analyses were run using two different configurations, low and high 2 theta angle (Table 4.6). Both low and high 2 theta angles identify clay minerals while the high 2 theta angle also identifies other minerals such as feldspar and ferromagnesians. The mineralogy of each sample was determined from primary and secondary peak positions on graphs produced by the software X'PERT Highscore.

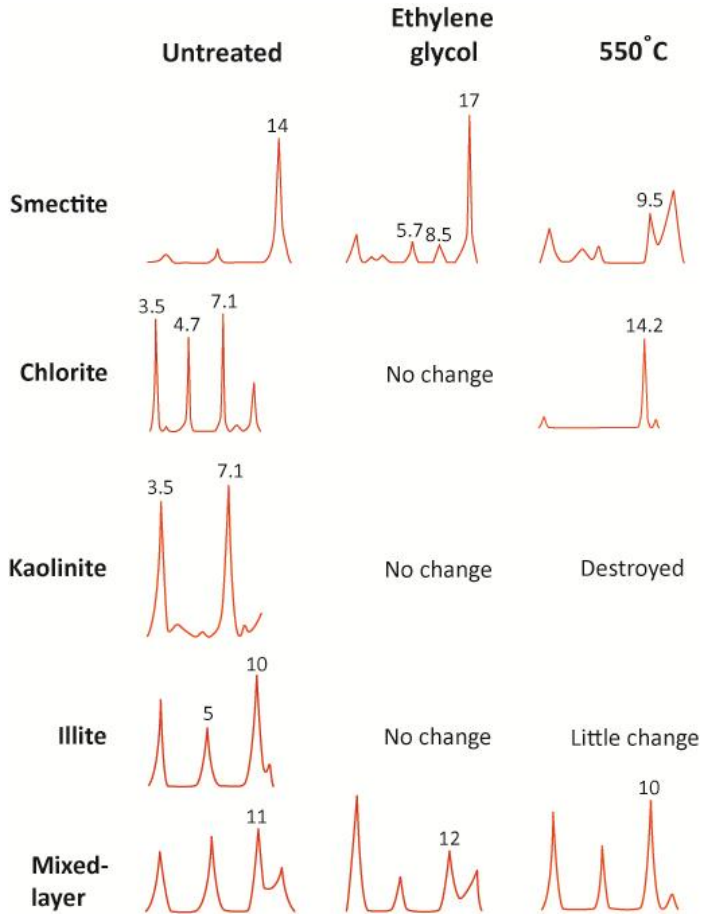

Figure 4.6: XRD patterns of typical Angstrom positions (Å) of five common clays as they react to the three different treatments; untreated, soaked in ethylene glycol and heated to 550°C (modified from Weaver, 1967).

Table 4.6: Settings for XRD configurations. Beam intensity was 40kV and 40 mA.

Configuration	2 Theta °		Step size	Time per step
	Start	End		
Low angle	2	12	0.02	1.5
High angle	12	44	0.02	1.5

4.3 Petrography and mineralogy

4.3.1 Mineral chemistry

The chemical composition of selected alteration minerals (Table 4.7) from Ngatamariki and Rotokawa andesites is represented on standard ternary diagrams. Hydrothermally altered plagioclase compositions are plotted along the axis with orthoclase (Or) and albite (Ab) as end members (Fig. 4.7).

Table 4.7: Mineral chemistry of selected samples from Ngatamariki and Rotokawa fields (wt. %). K-flsp = K-feldspar, Opq = opaque, opx = orthopyroxene, cpx = clinopyroxene, c = core and r = rim. More data is available in Appendix 1.

Geothermal field Sample no/ID	Mineral	SiO_2	TiO_2	Al_2O_3	FeO	MnO	MgO	CaO	Na_2O	K_2O	P_2O_5	SO_3	Cl	Cr_2O_3	NiO	TOTAL
Ngatamariki																
LA4 13/5256	Chlorite on opx	30.55	-	15.86	21.46	0.33	19.04	0.37	0.01	0.09	-	-	-	0.09	0.05	**87.85**
LA15 11/5318	K-flsp (c) albite	67.39	0.05	19.60	0.05	0.19	0.04	0.54	11.55	0.18	0.08	0.17	0.02	-	0.01	**99.87**
LA15 11/5319	K-flsp (r) albite	67.12	-	19.30	0.05	0.01	-	0.22	11.60	0.12	0.19	-	0.00	0.00	-	**98.61**
LA15 5/5313	Quartz	96.93	-	-	-	-	0.05	0.13	-	0.05	0.28	0.01	0.03	-	0.04	**97.52**
LA15 4/5312	Opq rutile	0.20	97.62	0.13	0.51	0.00	0.03	0.12	0.09	0.00	-	-	0.07	0.03	0.12	**98.87**
Rotokawa																
LA14 10/5271	Hydroth. biotite on opx	45.83	0.45	10.65	17.64	0.14	17.49	0.84	0.25	4.22	0.04	-	0.04	-	0.24	**97.83**
LA48 3/5385	Epidote	38.09	0.04	23.62	11.24	0.14	0.05	23.12	0.00	0.08	0.16	-	-	0.12	-	**96.66**
LA48 3/5386	Quartz	97.72	-	-	-	0.04	0.08	0.10	0.04	0.08	0.27	0.04	0.03	0.16	-	**98.56**
LA48 8/5392	K-flsp adularia	64.52	-	18.07	0.27	0.00	-	0.10	0.45	16.01	-	-	0.00	0.04	-	**99.46**
LA48 3/5387	Calcite	-	-	0.05	0.15	1.25	0.12	51.94	0.01	0.09	-	-	0.06	-	0.10	**53.77**
LA53 3/5371	K-flsp (c) albite	68.37	0.03	19.39	0.06	0.07	-	0.22	11.92	0.15	0.01	-	0.00	0.01	-	**100.23**
LA53 3/5372	K-flsp (r) albite	63.72	-	21.94	0.29	0.04	0.09	2.75	9.43	0.93	0.13	0.10	0.01	0.02	0.05	**99.50**
LA53 6/5377	K-flsp adularia	63.17	0.23	18.60	0.26	-	0.04	-	0.45	15.69	0.21	-	-	0.12	0.09	**98.86**
LA58 1/5282	Chlorite on cpx	35.11	0.11	12.26	21.27	0.36	17.25	0.62	0.14	1.14	-	0.14	0.03	0.04	0.21	**88.68**
LA58 2/5285	Amph magnesio-hornblende	48.89	0.42	6.30	14.52	0.16	15.89	10.43	0.29	1.59	-	0.04	0.05	0.13	0.13	**98.84**

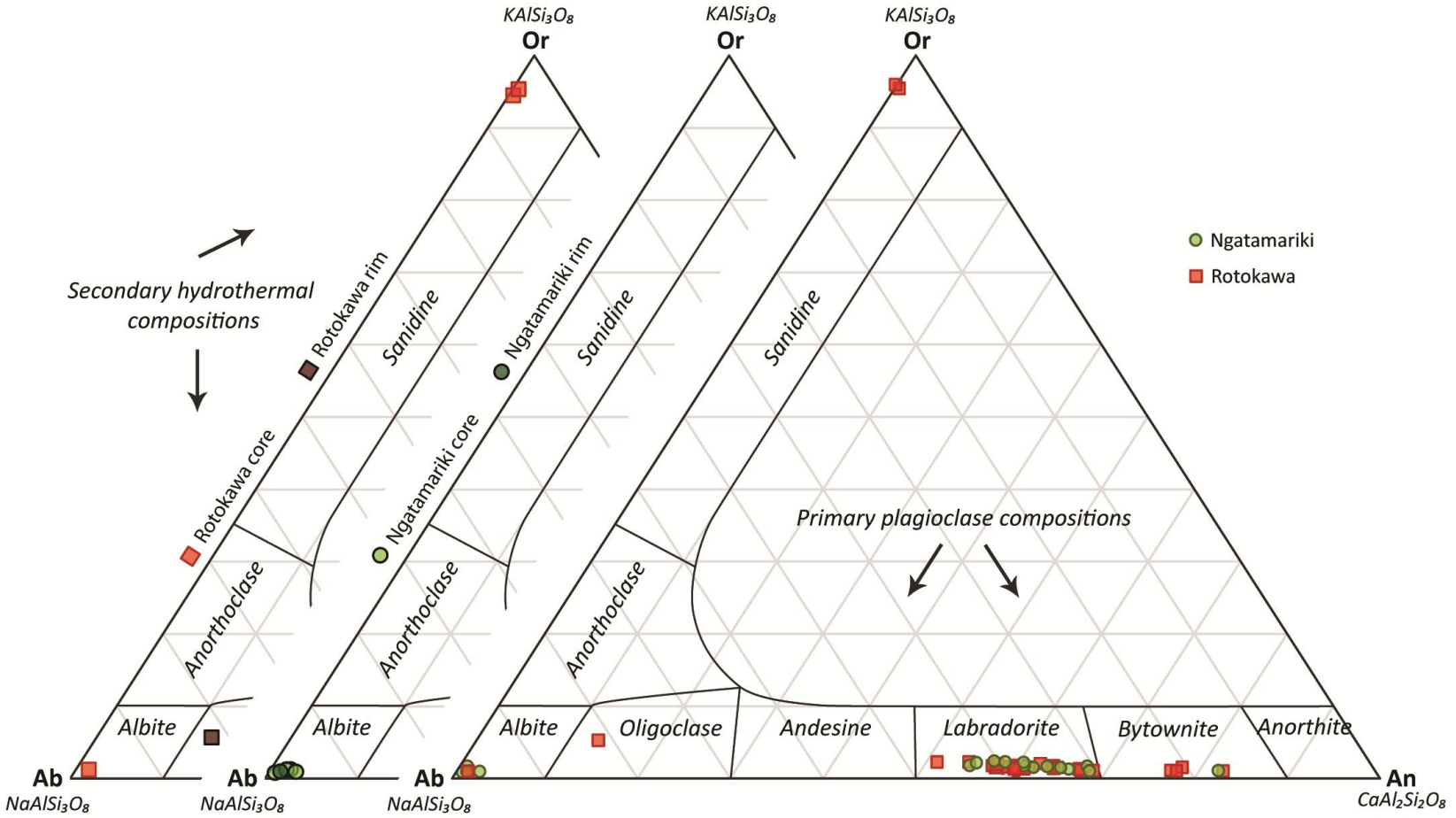

Figure 4.7: Plagioclase and secondary feldspar compositions obtained by microprobing (Appendix 1). The secondary feldspars have been divided into occurrences at Ngatamariki and Rotokawa, and also core and rim measurements where available.

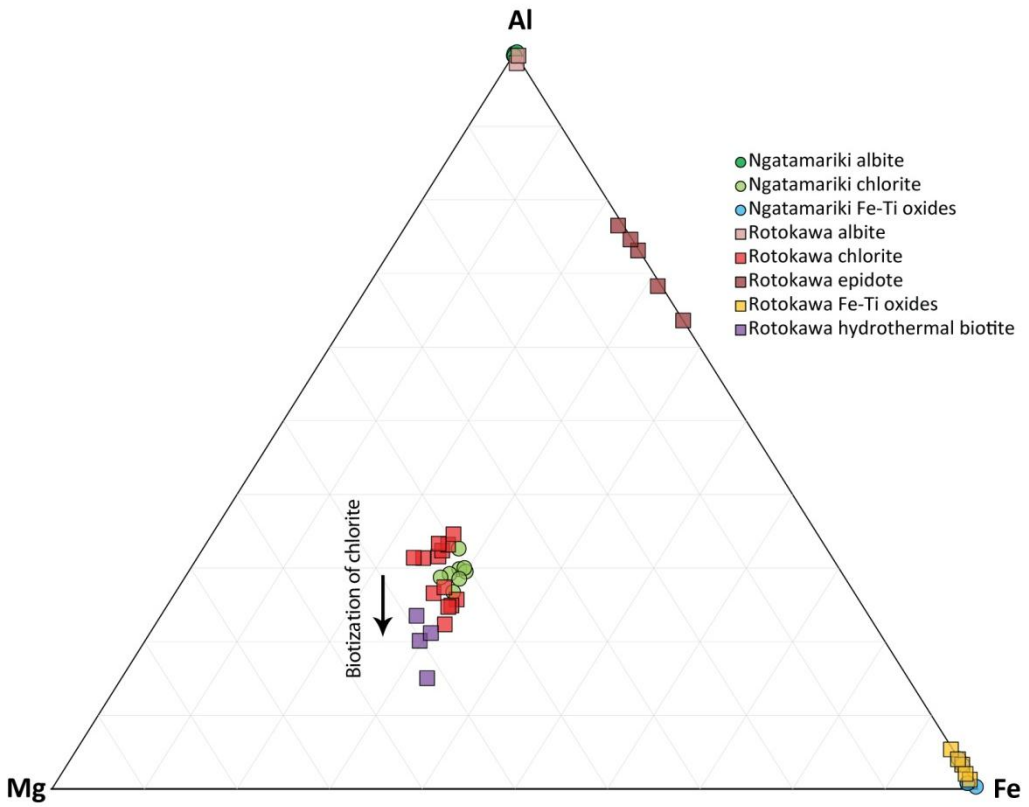

Figure 4.8: Al-Fe-Mg cation plot showing differences in alteration minerals at Ngatamariki and Rotokawa (based on diagram from Gifkins et al., 2005). Data is from Appendix 1.

The transformation from plagioclase takes place when Ca is removed from the plagioclase phenocryst and instead it is enriched in either Na or K (e.g. adularia, albite, oligoclase). The analysed albite phenocrysts at Ngatamariki range from Ab_{97-99} and An_{51-82} in composition. At Rotokawa, both albite and adularia were analysed, and the albite phenocryst had zoning with a Na-rich core (Ab_{98}) and a Ca-rich rim (Ab_{82}) while adularia ranged in composition from Or_{95}-Or_{96}. Other secondary minerals were plotted on an Al-Mg-Fe cation ternary diagram to visualize differences in compositions (Fig. 4.8). Epidote and hydrothermal biotite were only analysed at Rotokawa. There is a slightly wider range in Al-content of chlorite and Fe-Ti oxides at Rotokawa compared to Ngatamariki. The diagram also shows the path of alteration from chlorite to hydrothermal biotite, with decreasing Al-content.

In the following section, alteration minerals which have been identified at Ngatamariki and Rotokawa will be categorised under four main alteration styles;

argillic, advanced argillic, potassic and propylitic. Petrographical observations are supported by XRD data in samples where this has been obtained (Appendix 6).

4.3.2 Argillic mineral assemblage

An overview of clay occurrences at Ngatamariki and Rotokawa is summarised in Fig. 4.5, Section. Most clays form in different environments (e.g. temperature, pH-level), but they may also co-exist due to changing conditions in the geothermal system (Table 4.8).

Illite

Illite is very fine-grained and colourless, although contamination of iron oxides or hydroxides may result in yellow, green or brown discolouration and weak pleochroism. Illite has been identified by XRD analysis in well NM6 between 2210 and 3035 mRF at Ngatamariki, and in well RK21 at 1850 mRF at Rotokawa (Table 4.8).

Smectite

Smectite normally occurs in shallow levels at Ngatamariki and Rotokawa, where the reservoir temperatures are cooler. However, it can occur together with chlorite in mixed clay layers to fill vugs or replace ferromagnesian minerals, and is recognised by a brownish colouring. Mixed layers have been identified in well NM6 between 1530 and 2400 mRF at Ngatamariki and in well RK27 between 2150 and 2152 mRF at Rotokawa (Table 4.8).

Table 4.8: A summary of clay minerals in samples from Ngatamariki and Rotokawa (data from Appendix 6). Chlorite and kaolinite are included in this table, although they are advanced argillic and propylitic alteration types, respectively.

Sample no	Well	Depth	Chlorite	Illite	Kaolinitie	Mixed layer
Ngatamariki						
LA.5	NM6	2686-2689	○		○	
LA.7	NM6	3032-3035	○	○	○	
LA.15	NM6	2210	○	○		
LA.17	NM6	2300	○	○	○	
LA.19	NM6	2400			○	○
LA.22	NM6	2550	○			
LA.23	RK21	1250	○			
LA.27	RK21	1450	○			
Rotokawa						
LA.31	RK21	1650	○			
LA.35	RK21	1850	○	○		
LA.39	RK21	2050	○			
LA.44	RK21	2300	○			
LA.53	RK27 #2	2147	○		○	
LA.54	RK27 #2	2148	○		○	
LA.55	RK27 #2	2149	○		○	
LA.56	RK27 #2	2150				○
LA.57	RK27 #2	2151				○
LA.58	RK27 #2	2152				○
LA.78	NM6	1330	○			
LA.82	NM6	1530				○

4.3.3 Advanced argillic mineral assemblage

Anhydrite

At Ngatamariki and Rotokawa, anhydrite is rare but occurs as infilling of vugs or veins (Fig. 4.9) at both shallow and deep levels (e.g. RK4 at ~185 mRF, NM4 at 2208 and 2461 mRF, RK24 at 1820 mRF and RK27 at 2147 mRF) although it is often overprinted by calcite, indicating a change to less acid geothermal fluids. It is colourless in plain polarised light, and has strong pastel interference colours (pink, yellow, blue and violet) in cross-polarised light.

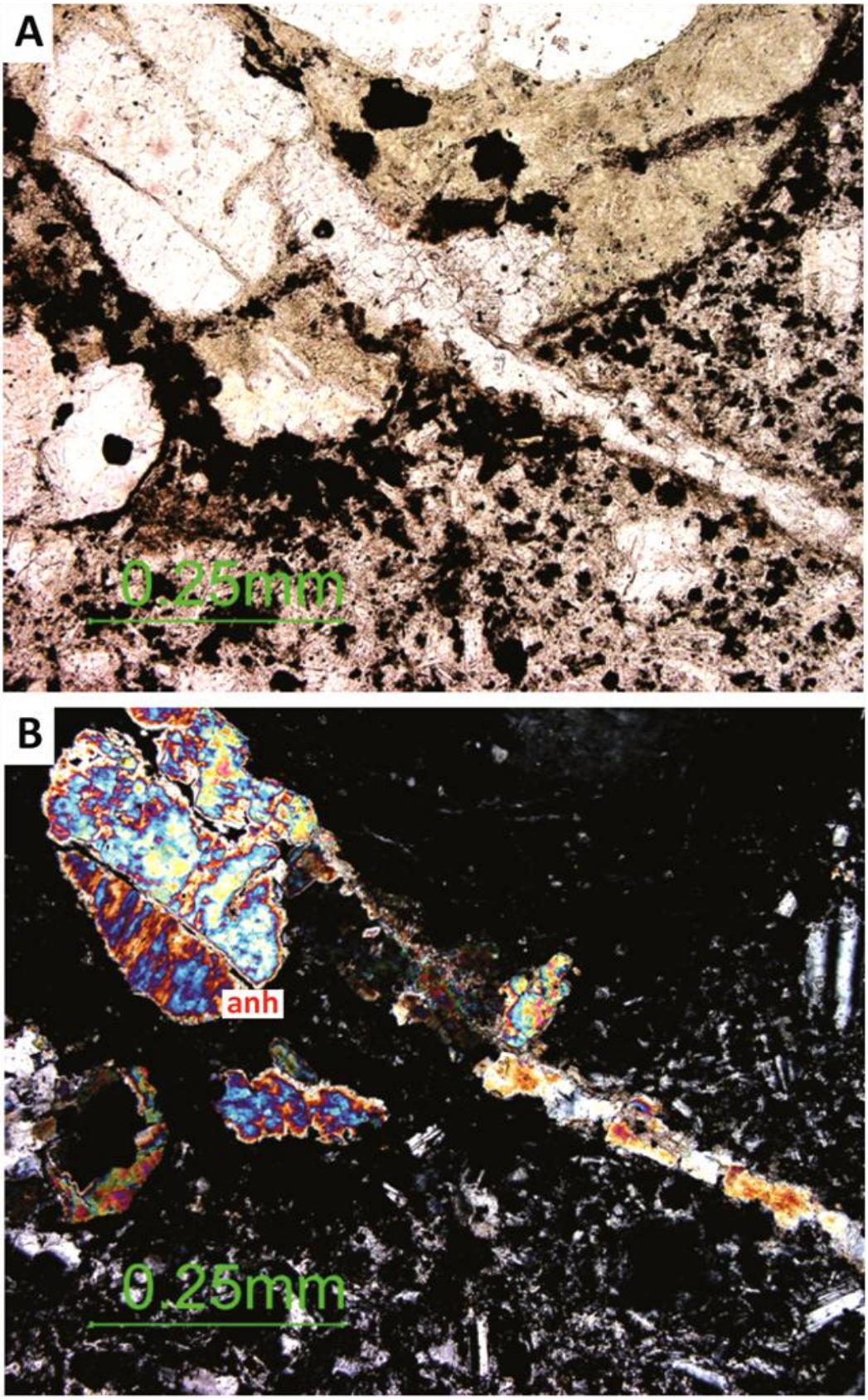

Figure 4.9: Anhydrite vein and replacement of phenocryst with unknown original composition in well RK24 at 1820 mRF (sample LA.51). A = PPL, B = XPL.

Hematite

Hematite has mainly been observed in samples retrieved from Rotokawa (RK18 at 2221 mRF, RK27 at 1850-53 and 2147-53 mRF). Fine-grained hematite may give patches in andesite lava or whole breccia clasts a pink colouring, and it also occurs in veins. In well RK27, hematite coats smooth slip surfaces in fractures with an angle ~40° to core axis (smileys). Hematite is normally opaque in thin section, but thin, platy hematite may appear red in plain polarised light (Fig. 4.10).

Limonite

Limonite is rare at Rotokawa, but has been observed in wells at Ngatamariki (NM6 at 2210 and 2300 mRF) as brownish yellow flakes in plain polarized light on rims or filling voids between grouped, altered feldspar and pyroxene (Fig. 4.11).

Kaolinite

Kaolinite mostly occurs at shallow depths (<200 mRF) near surface features at Ngatamariki and Rotokawa fields (Fig. 4.5). It may also occur at deeper levels in rare cases, where acid fluids have permeated down along faults and fractures. Kaolinite has been identified in XRD graphs at Ngatamariki in well NM6 between 2686 and 3035 mRF, and at Rotokawa in well RK27 between 2147 and 2149 mRF (Table 4.8).

Quartz

Quartz has been identified in XRD graphs all samples by its Ångstrom position at 3.34 and 4.26 (Appendix 6). Microcrystalline quartz is a common replacement mineral for volcanic glass and plagioclase or as infilling in veins at both Ngatamariki and Rotokawa. Quartz can fill the vein completely with a polycrystalline structure (Fig. 4.12) or radiate out from the vein wall in a fibrous habit (Fig. 4.13). CL-imaging was used on the sample containing fibrous quartz.

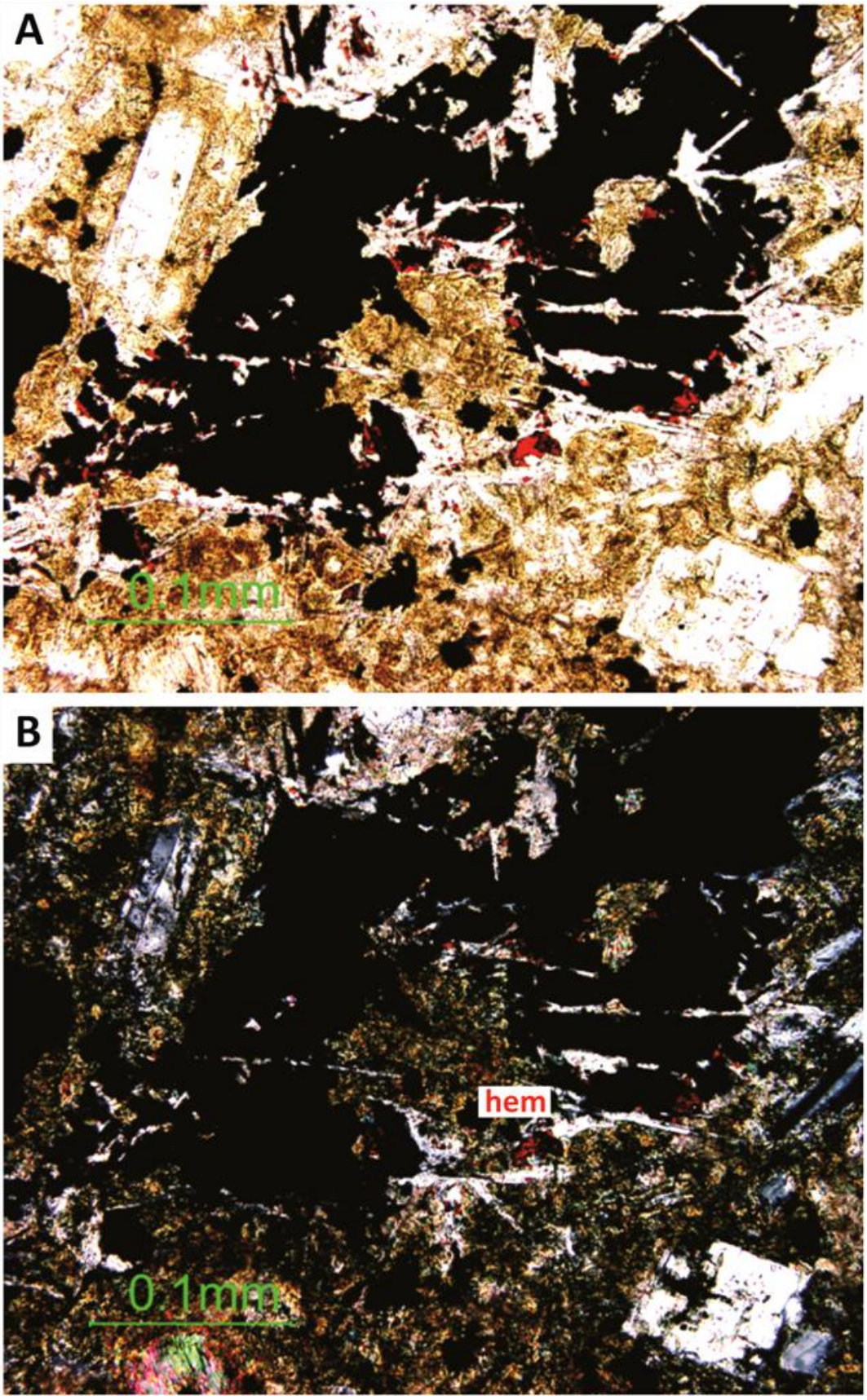

Figure 4.10: Opaque hematite vein in well RK18 at 2219-2221 mRF, with thinner, red flakes along the edges (sample LA.14). A = PPL, B = XPL.

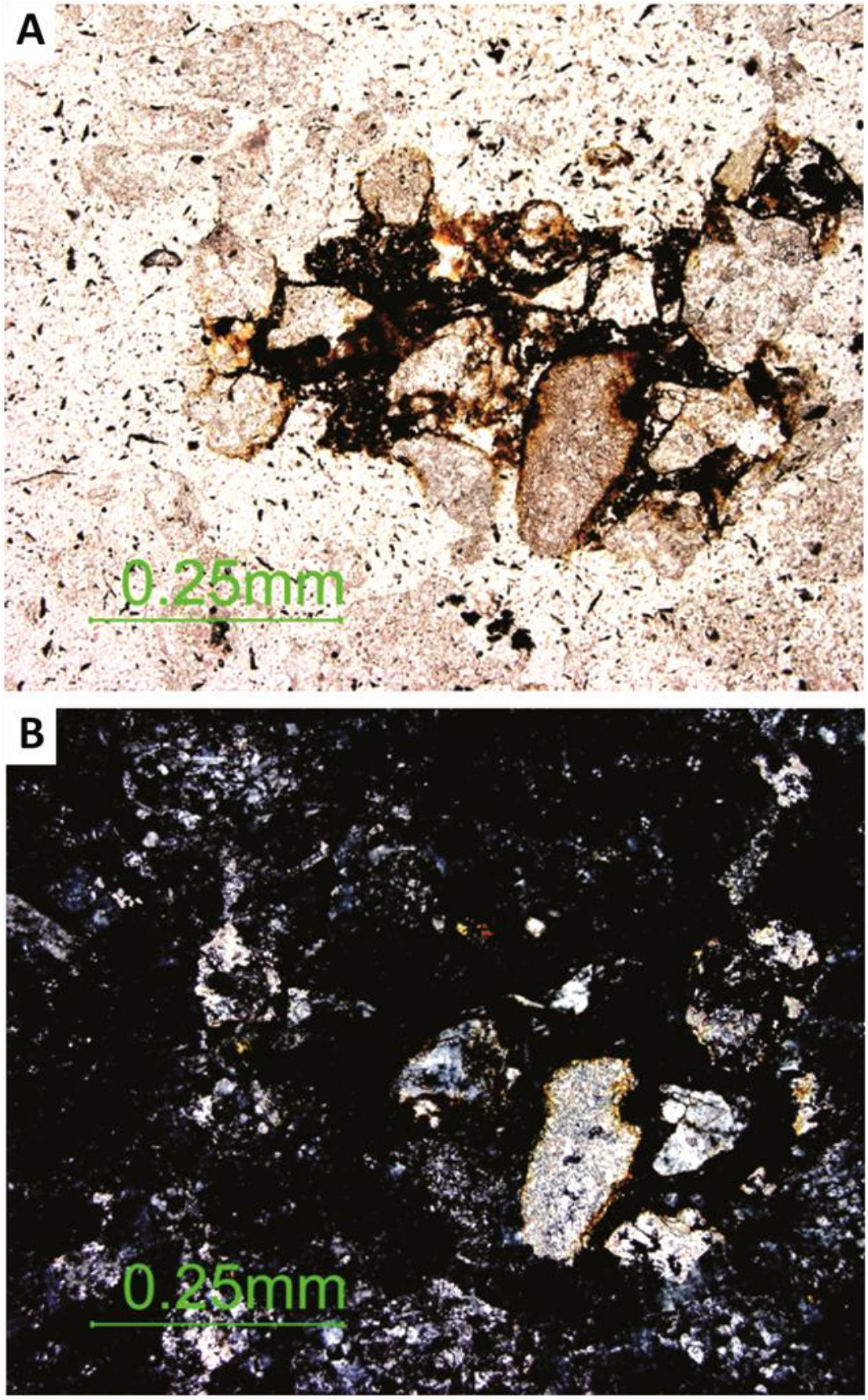

Figure 4.11: Yellowish brown limonite between fragments of altered feldspar, cuttings retrieved from NM6 at 2210 mRF (sample LA.15). A = PPL, B = XPL.

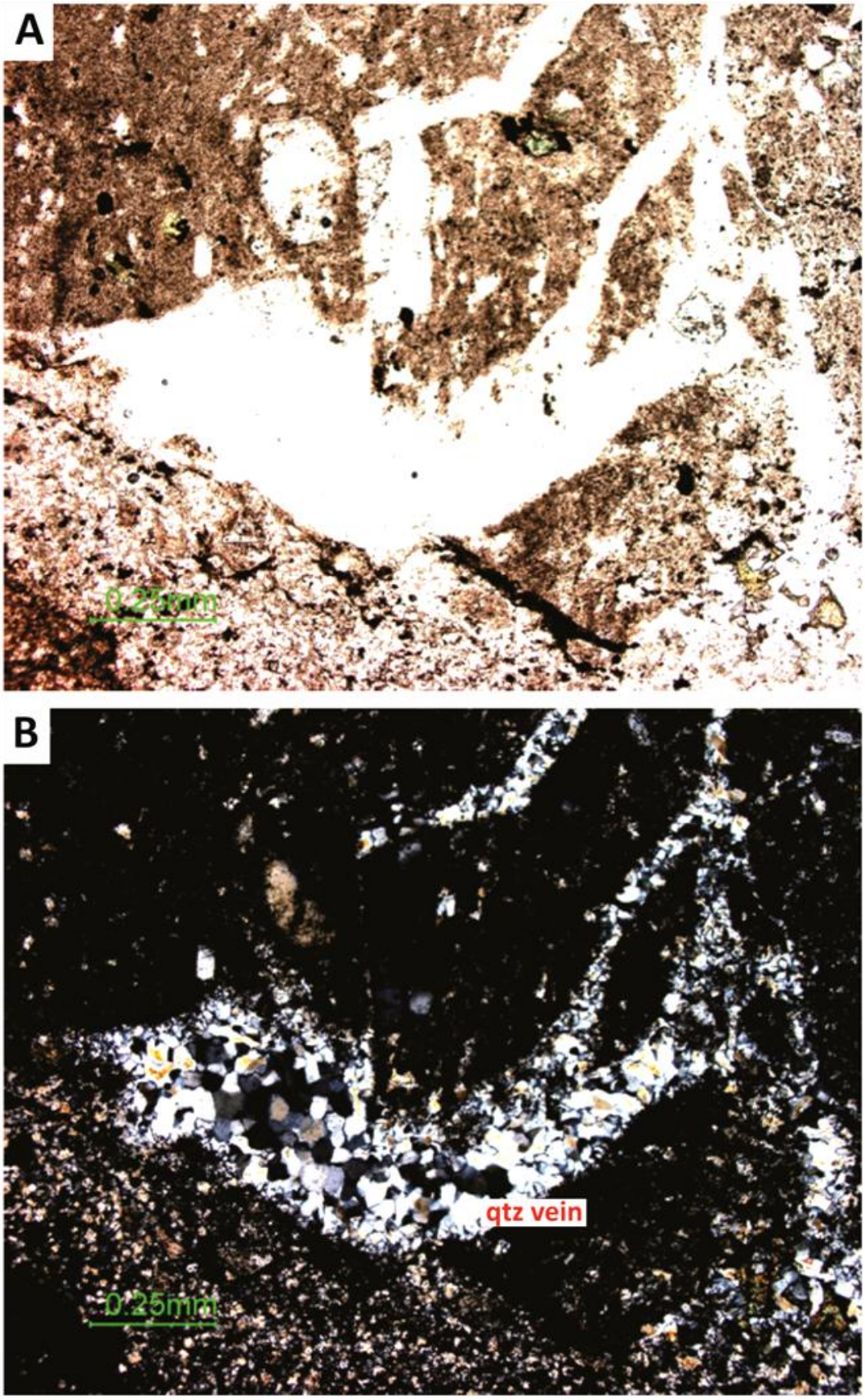

Figure 4.12: Polycrystalline quartz vein, retrieved from Ngatamariki well NM7 at 2181 mRF (sample LA.46). A = PPL, B = XPL.

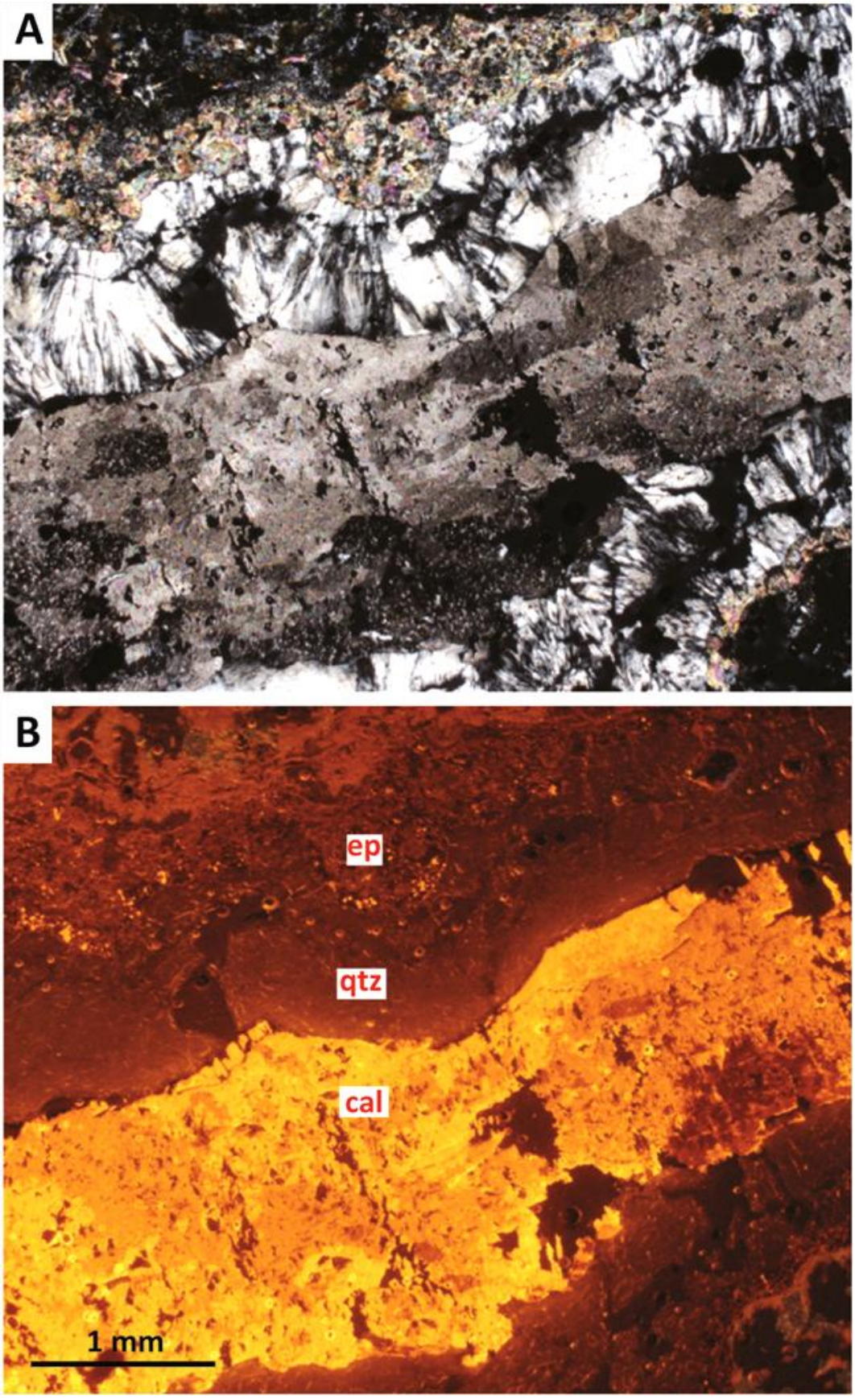

Figure 4.13: Vein with layered infill of epidote, quartz and calcite retrieved from well RK25 at 2000 mRF (sample LA.48). A = XPL, B = CL. Alteration minerals show luminescence by CL-imaging.

Like many other alteration minerals, quartz emits a red luminescence colour in CL, but it is possible to distinguish between the outer layer of brownish red epidote followed by duller greyish red quartz and lastly bright yellow-orange calcite crystals in the middle.

Cristobalite

Cristobalite has not been petrographically identified in thin sections of samples from Ngatamariki and Rotokawa, although its presence has been identified in all XRD graphs by its Ångstrom position at 4.05, 3.1 and 2.84 (Appendix 6). This may be explained by its small grain size, similar colour and cleavage habit as quartz.

4.3.4 Potassic mineral assemblage

Hydrothermal biotite

Both igneous and hydrothermal biotite, replacing ferromagnesian minerals, is common at Rotokawa, although rare to non-existent at Ngatamariki. Hydrothermal biotite is tabular and pleochroic in shades of green and brown, with an average length of ~0.5 mm although some can grow up to 1 mm. It has straight extinction, excellent cleavage and is easily recognised by its undulating, mottled extinction (Fig. 4.14). The interference colours are of high second order but are masked by the colour of the mineral. The most abundant occurrence is in well RK18. At 2219 mRF, the andesite lava has moderate alteration intensity and hydrothermal biotite is abundant as all pyroxene has been replaced. At 2221 mRF, hydrothermal biotite is rare and co-exists with igneous biotite, although the latter has been partly to completely replaced by chlorite.

K-feldspar (Adularia)

Adularia has been analysed by microprobe in two samples from Rotokawa, in wells RK25 at 2000 mRF and RK27 at 2147 mRF, ranging from Or_{95-96} in composition (Table 4.7, Fig. 4.7). Secondary feldspar is however common at both Ngatamariki and Rotokawa, but it can be difficult to distinguish between albite and adularia due to core textures and alterations to epidote.

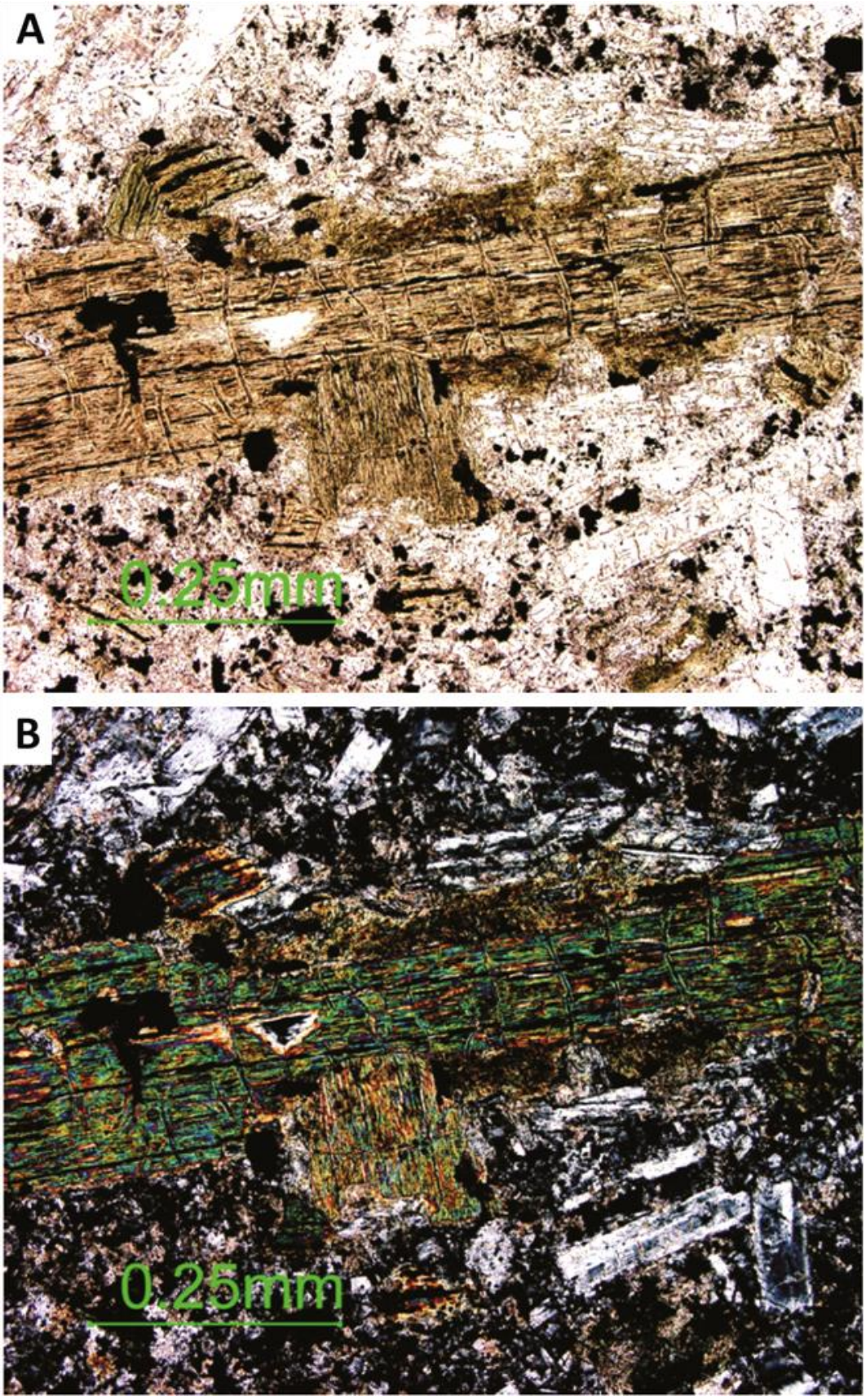

Figure 4.14: Hydrothermal biotite with green and brown pleochroism and a characteristically undulating extinction, surrounded by small, abundant grains of Fe-Ti oxides. Retrieved from RK18 at 2219 mRF (sample LA.12). A = PPL, B = XPL.

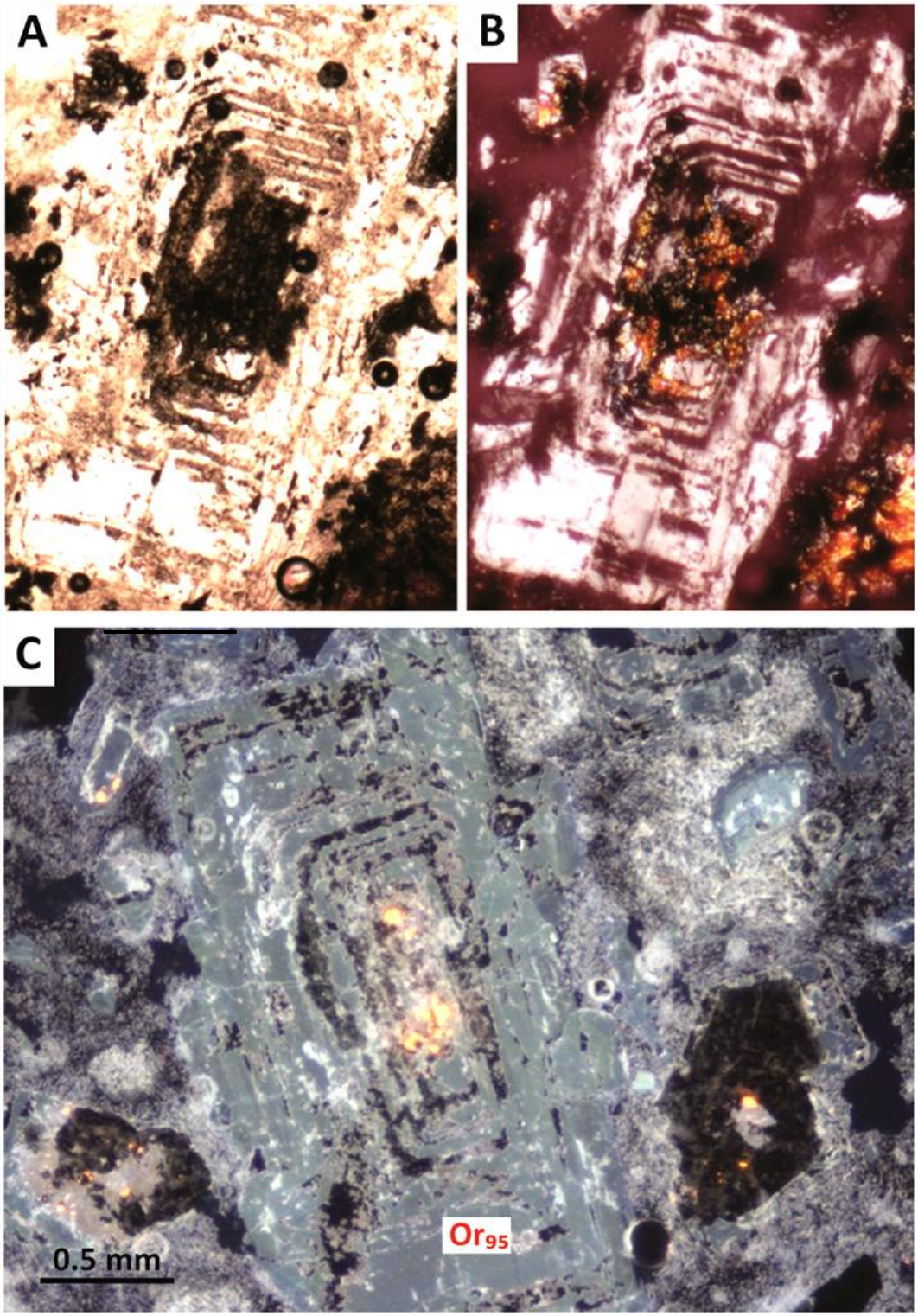

Figure 4.15: Zoned adularia with bluish-green luminescence while yellow luminescence captured by CL imaging suggests replacement by calcite in the core. Retrieved from Rotokawa well RK25 at 2000 mRF (sample LA.48). A = PPL, B = XPL, C = CL.

Adularia is recognised by wavy extinction and a mottled appearance, twinning is patchy if present. It has an anomalous faded bluish colour in CL-imaging, typical of secondary feldspar (Fig. 4.15).

4.3.5 Propylitic mineral assemblage

Na-feldspar (Albite)

Albite is present in samples from both Ngatamariki and Rotokawa, with values of Ab_{97-99} (Table 4.7, Fig. 4.7). One sample (LA.53) showed normal zoning with a Na-rich core and Ca-rich rim, where the composition was similar to oligioclase (Ab_{82}) (Fig. 4.16). Albite is recognised by the brownish dust covering its surface, giving it a cloudy appearance. The twinning in albite is often absent, depending on the viewed angle. Albite has a light brownish luminescence colour in CL-imaging, which is different from the fade blue of adularia and the strong green colour of plagioclase.

Calcite

Calcite is present in almost all samples from Ngatamariki and Rotokawa as it is an early alteration product of plagioclase and volcanic glass, plus it has a wide range of temperature stability. Calcite is colourless in plain polorised light, and has a characteristic light pastel, or “oil-slick” colour in cross-polarized light. Fine grains is a common infill in veins or vugs, but may also occur as large, platy crystals (Fig. 4.17).

Chlorite

Chlorite together with calcite is the first sign of alteration in the Ngatamariki and Rotokawa Andesites. They often occur together with epidote as layered infill in veins and vugs (Fig. 4.18). Chlorite is abundant in altered rocks, and even in weakly altered samples it may comprise up to 6% of the total rock composition (Chapter 3, Table 3.3). The chemical composition is similar at both fields, typically an Mg-Fe chlorite with a single cleavage, weak, pale green pleochroism and blackish interference colour (Table 4.7).

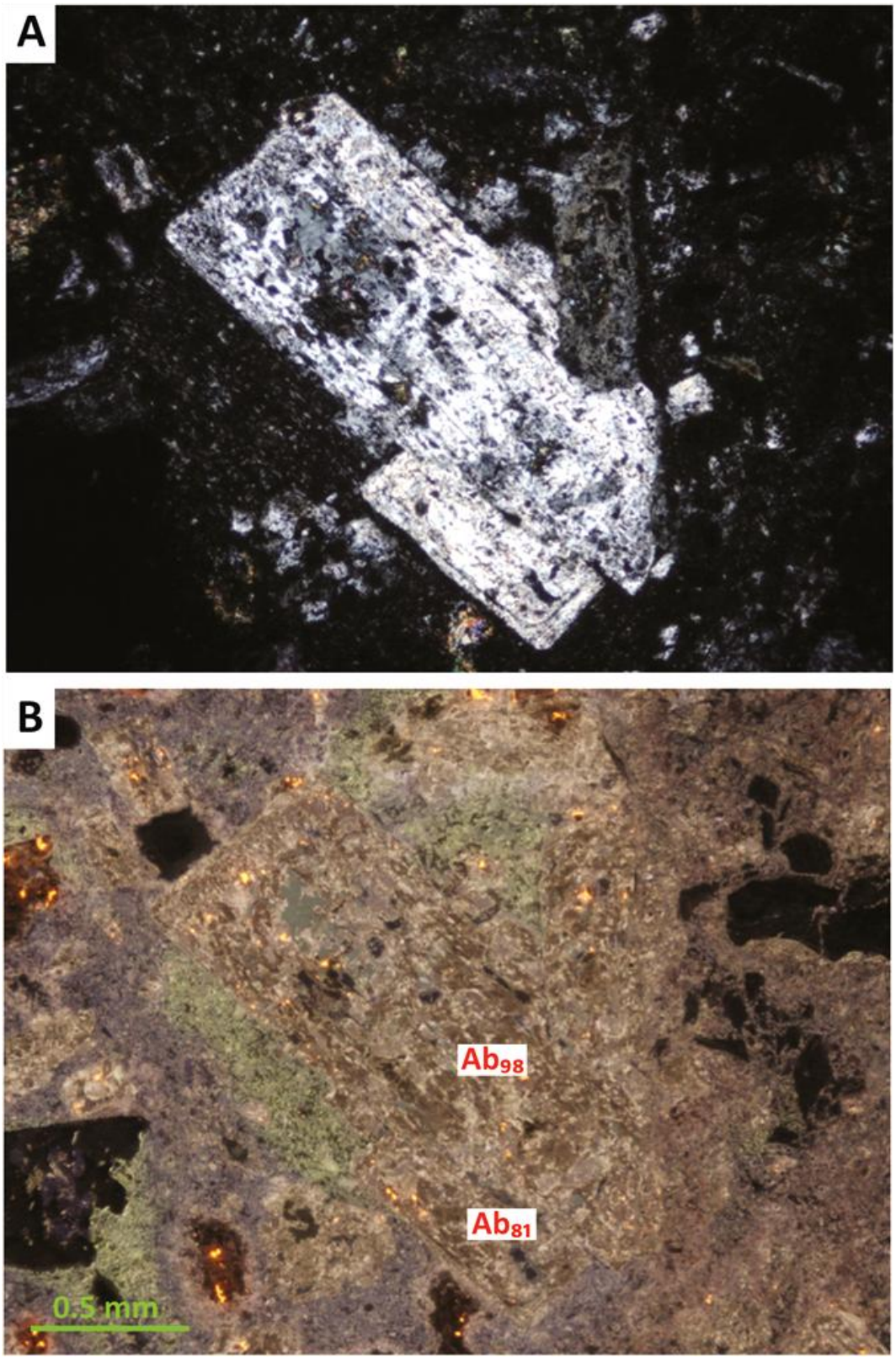

Figure 4.16: Brownish albite in CL, retrieved from Rotokawa well RK27 at 2147 mRF (sample LA.53). This phenocryst display normal zoning with a Na-rich core with Ca-enriched rim. Sprinkles of yellow-orange calcite occur in the feldspar, but is absent in the groundmass. A = XPL, B = CL.

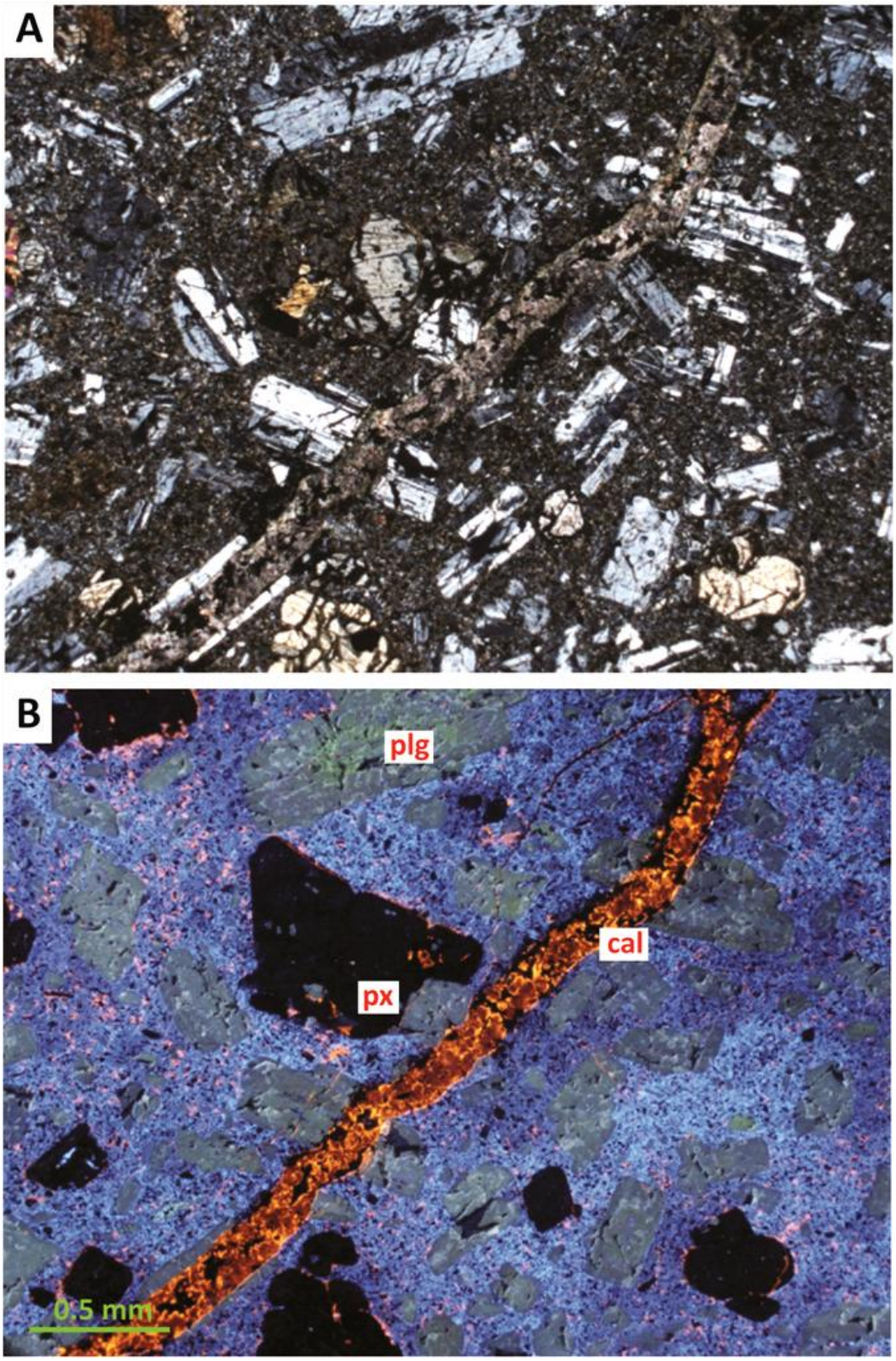

Figure 4.17: Orange-coloured calcite vein with CL-imaging in an otherwise weakly altered sample, running through plagioclase phenocrysts and has partly replaced groundmass and pyroxene. Retrieved from Rotokawa well RK27 at 2153 mRF (sample LA.58). A = XPL, B = CL.

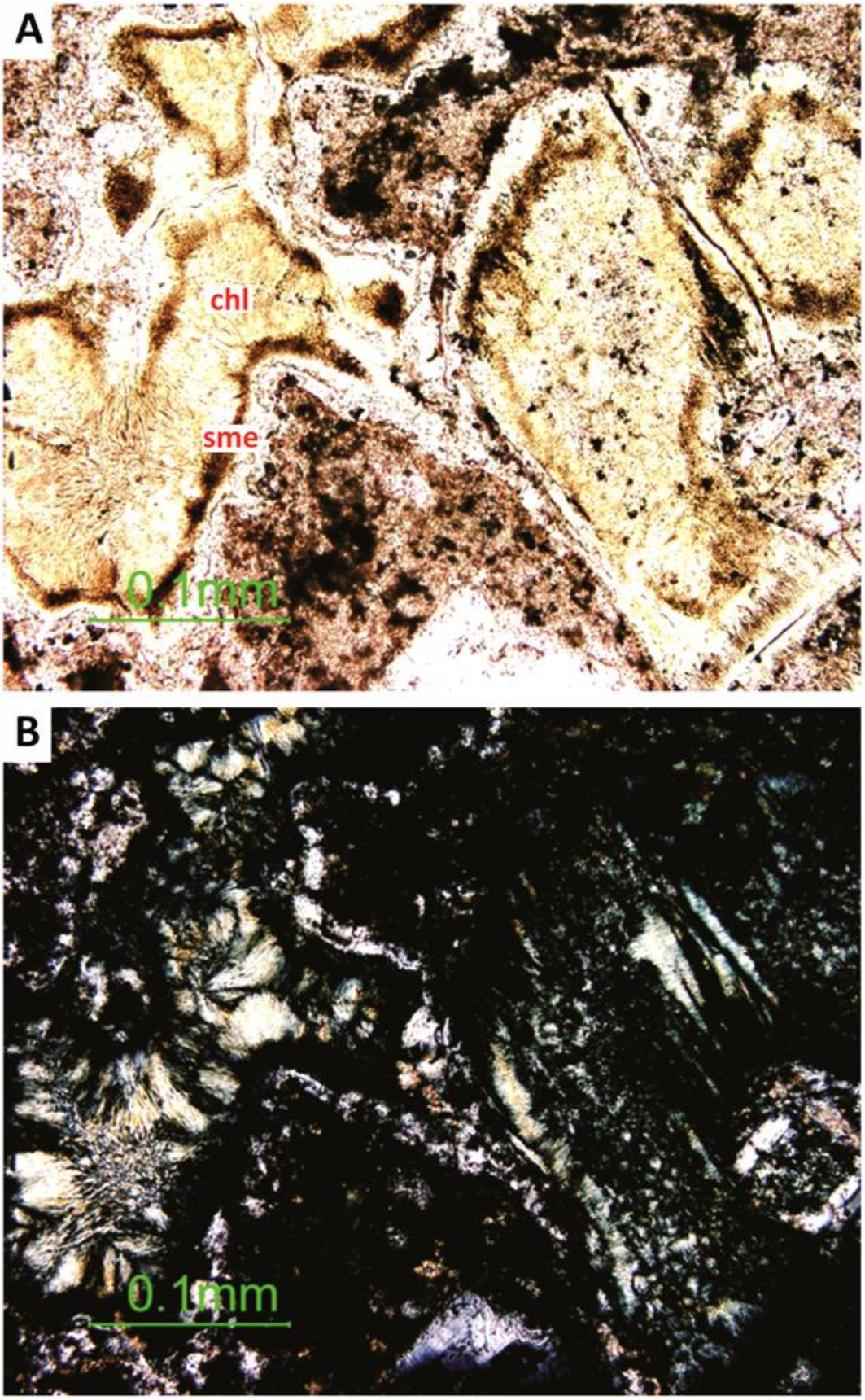

Figure 4.18: Green chlorite replacing a ferromagnesian mineral and filling the centre of a vug, retrieved from RK21 at 1876 mRF (sample LA.1). The presence of smectite is causing the brown colouring at the outer rims of vug and phenocryst. A = PPL, B = XPL.

The chemical composition reflects that of the primary mineral. For example, the chlorite has a slightly higher Mg-content when replacing orthopyroxene (LA.4), compared to when replacing clinopyroxene (LA.58).

Epidote

Epidote is a common alteration mineral at both Ngatamariki and Rotokawa, often replacing feldspar or filling vugs and veins. It has a weak, greenish yellow pleochroism with a high relief and a distinctive bright pink and green colouring in cross-polarised light (Fig. 4.19). Epidote is normally fine-grained, but large (~0.5 mm), randomly ordered crystals was observed in a vein in well RK25 at 2000 mRF (Fig. 4.20).

Green amphibole

Green amphibole is relatively common at Ngatamariki, with a modal abundance of 0-8 % (Chapter 3, Table 3.3). The crystal shape is prismatic and varies in length from 0.3-0.7 mm (Fig. 4.21). Green amphibole is recognised by the characteristic 60-120° cleavage angle, pleochroism in shades of green and an oblique extinction angle. The interference colours are middle second order, often yellow to orange. The chemical composition of this type of amphibole is unknown due to lack of microprobe data.

Amphibole is rare at Rotokawa, although yellowish brown amphibole (Fig. 4.22) is occasionally replacing orthopyroxene along fractures and/or cleavages which facilitate the movement of geothermal fluids. The amphibole has a chemical composition similar to magnesio-hornblende rather than actinolite (Table 4.7).

Opaques (galena, sphalerite and chalcopyrite)

Disseminated grains of galena and sphalerite with inclusions of chalcopyrite (Fig. 4.23) have been found in a strongly altered sample retrieved from Ngatamariki (NM5A at 2905 mRF). These opaques can be both potassic and propylitic alteration products. Galena is white in reflected light and isotropic transmitted light, with an anhedral to subhedral crystal shape <0.1 mm in length.

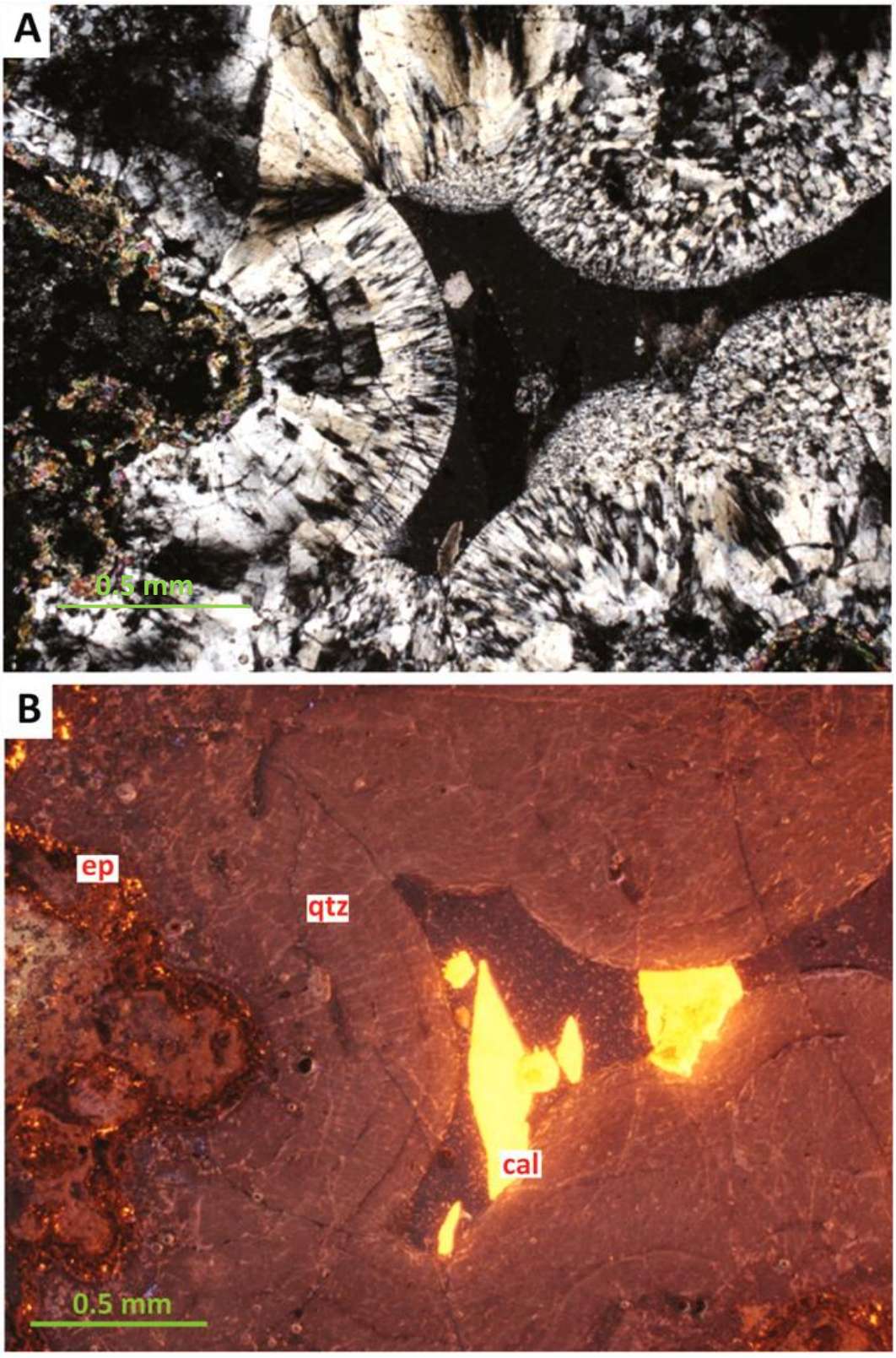

Figure 4.19: Partly infilled vein where alteration minerals show luminescence by CL-imaging. Although alteration minerals receive a red colour in CL, it is possible to distinguish between the outer layer of brownish red epidote followed by duller greyish quartz and large orange-yellow calcite crystals in the centre. Retrieved from RK25 at 2000 mRF (sample LA.48). A = XPL, B = CL.

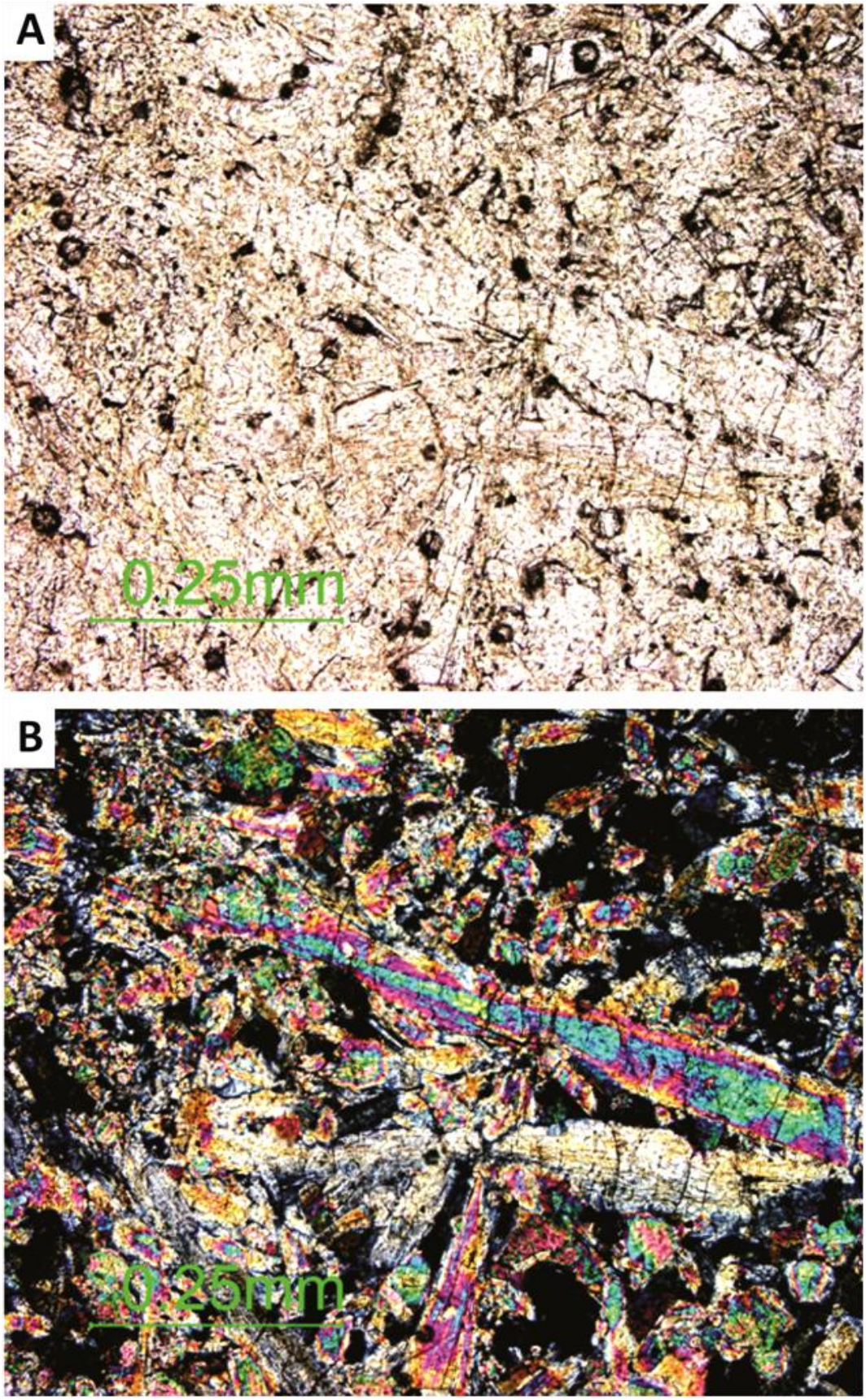

Figure 4.20: Large, free-growing epidote crystals in a vein (sample LA.48). A= PPL, B = XPL.

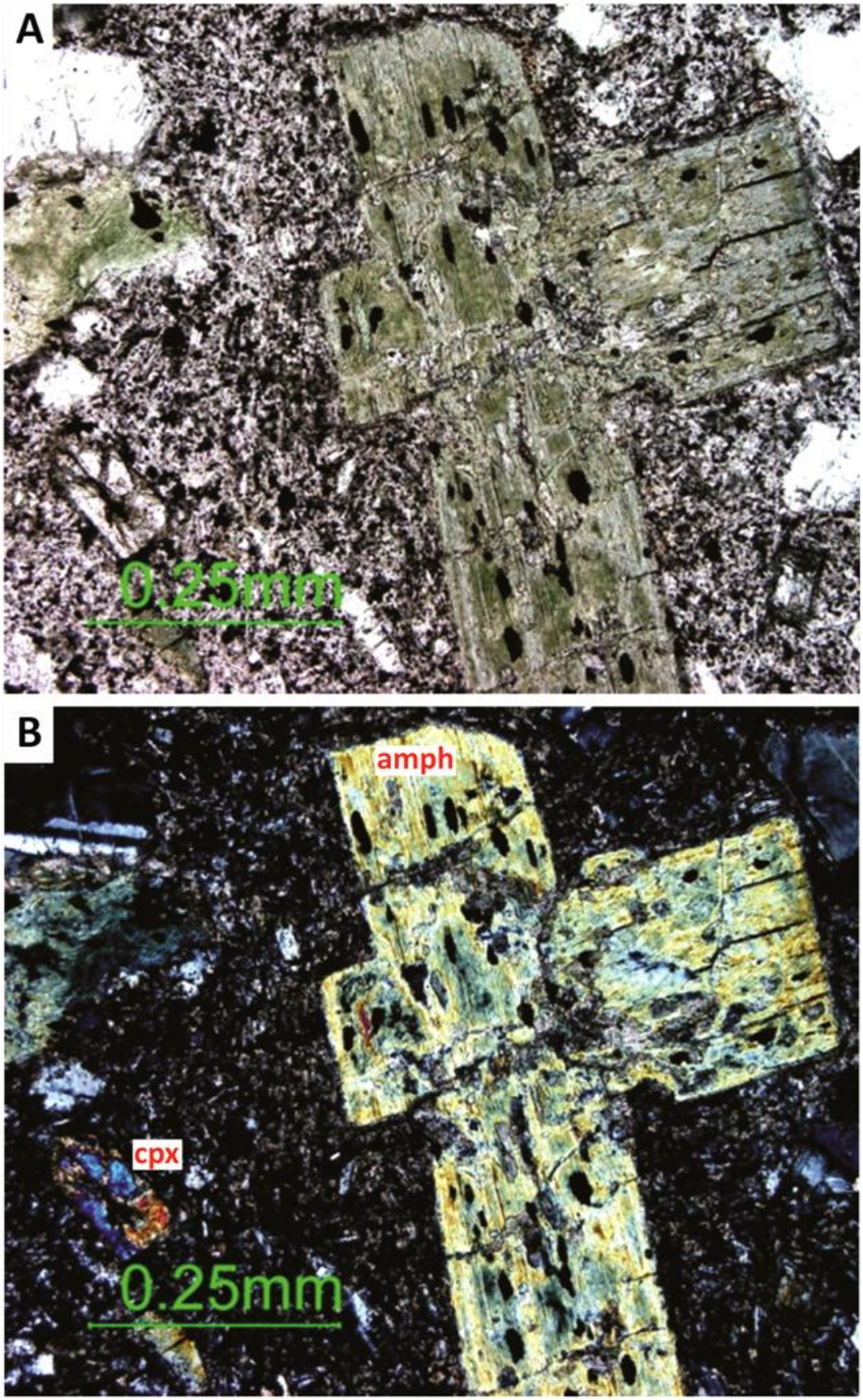

Figure 4.21: Green amphibole (amph) has replaced intergrown phenocrysts, possibly orthopyroxene since clinopyroxene (cpx) is unaltered in this sample. Retrieved from NM5 at 2575-78 mRF (sample LA.4). A=PPL, B = XPL.

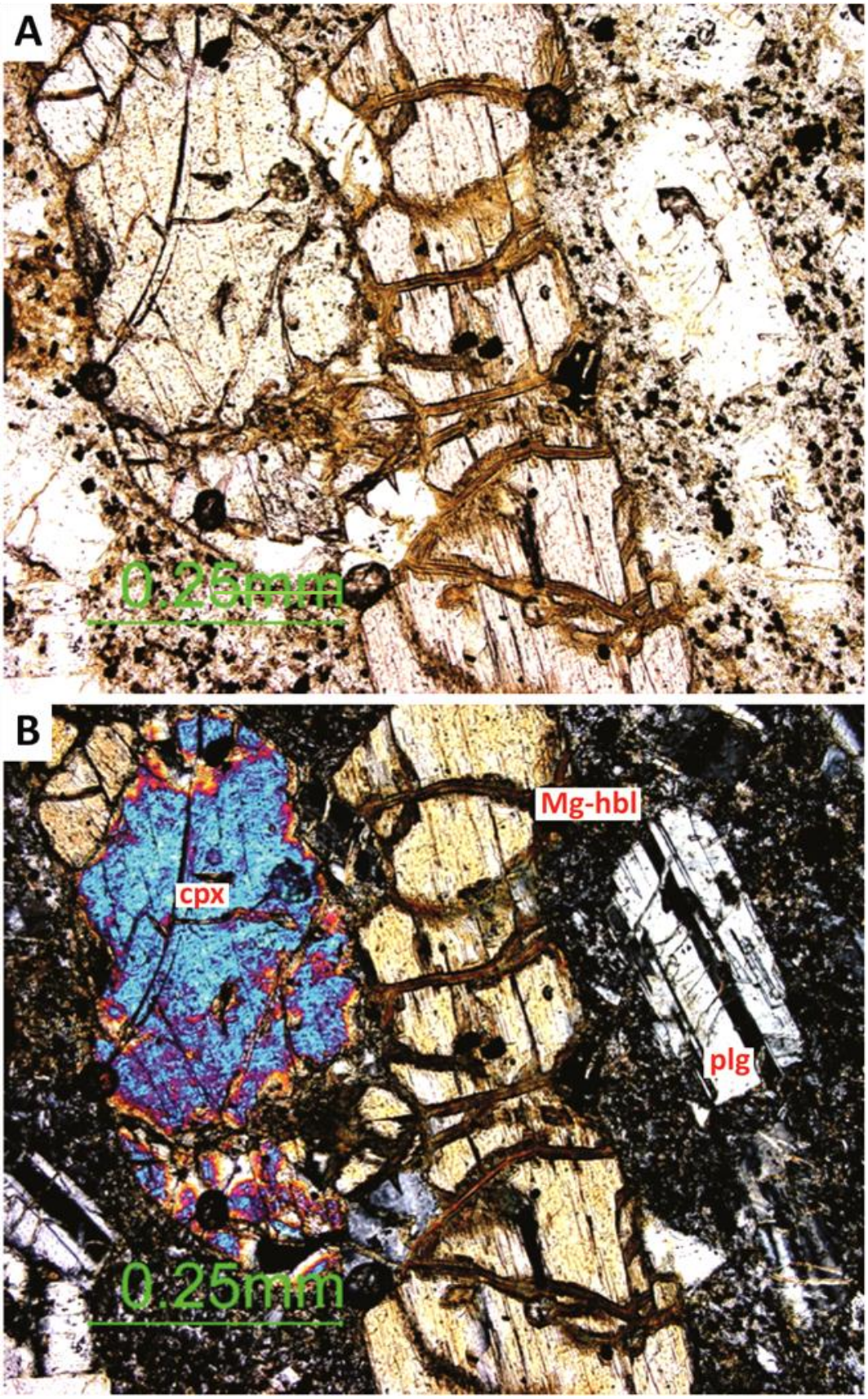

Figure 4.22: Yellowish brown magnesio-hornblende replacing orthopyroxene in cleavages, while the nearby plagioclase and clinopyroxene are less altered. Retrieved from RK27 at 2153 mRF (sample LA.58). A = PPL, B = XPL.

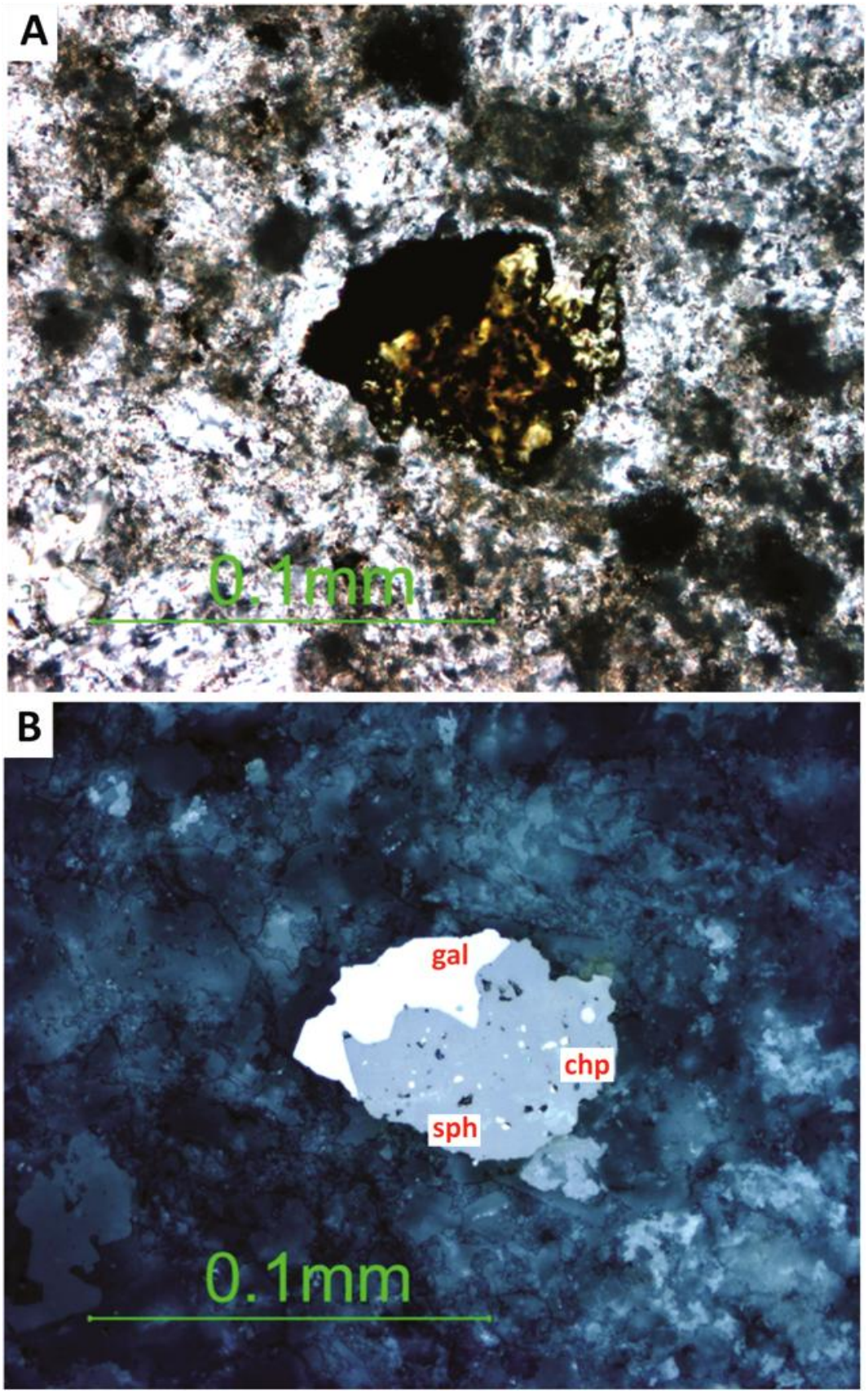

Figure 4.23: White galena and grey sphalerite, with small inclusions of yellow chalcopyrite, retrieved from NM5A at 2905 mRF (sample LA.59). A = PPL, B = RL.

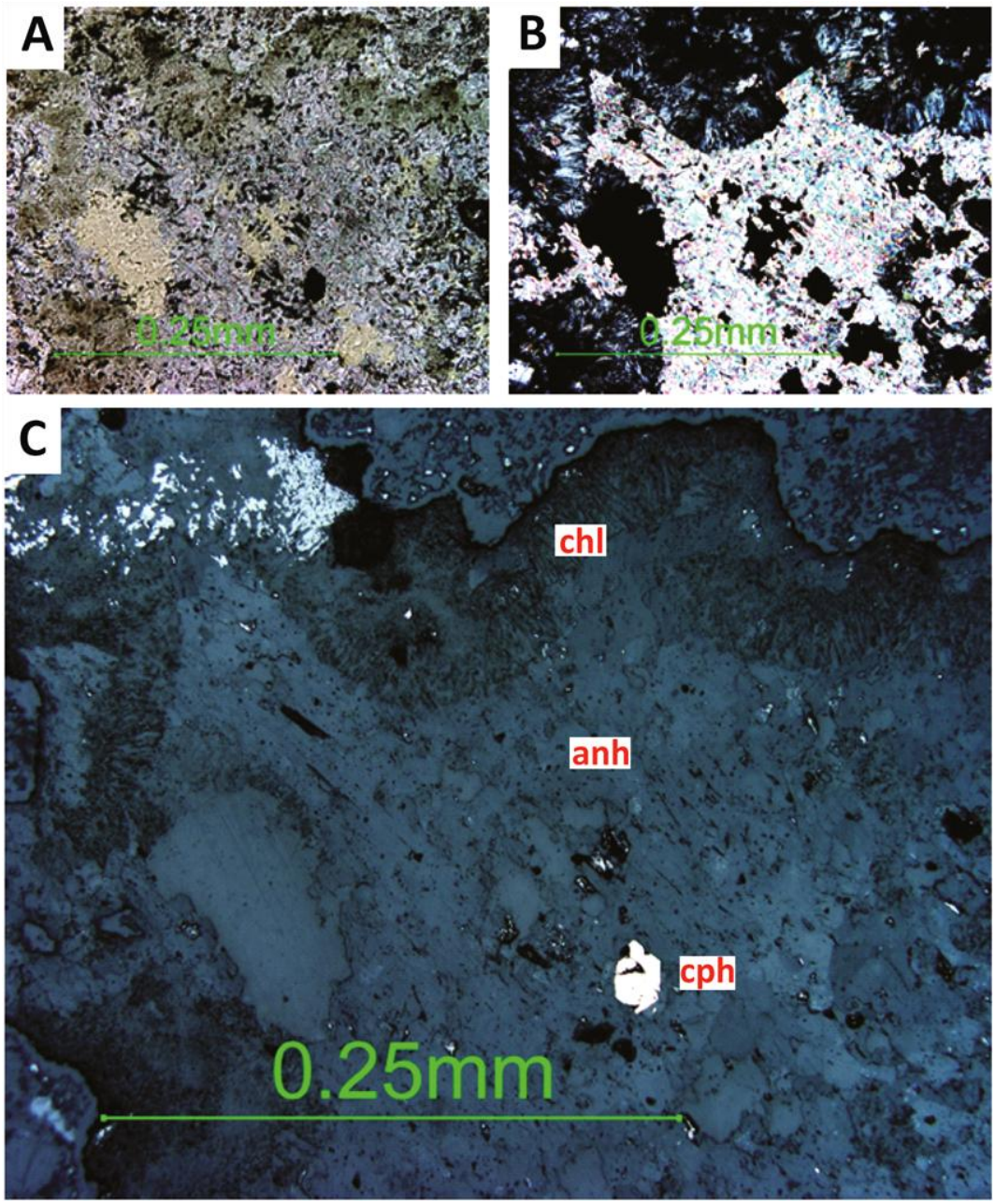

Figure 4.24: Pale yellow chalcopyrite (chp) in a vug with layered infill of chlorite (chl) and anhydrite (anh), retrieved from RK21 at 1876 mRF (sample LA.1). A = PPL, B = XPL, C = RL.

It has cleavage in three directions forming cubes, and is recognised by black triangular shapes in the crystal which is created by plucking out along cleavages. Sphalerite has a greyish colour and a granular, anhedral crystal shape <0.1 mm length. Tiny inclusions (<0.01 mm) of chalcopyrite are yellow in colour with an anhedral to subhedral crystal shape. These three sulphides are often associated with each other and indicate the presence of low grade epithermal ore deposits. Single grains (<0.04 mm) of rare chalcopyrite in a strongly altered sample

retrieved from Rotokawa (RK21 at 1876 mRF) are yellow in colour with an anhedral to subhedral crystal shape (Fig. 4.24). Humidity tends to tarnish chalcopyrite and give it a strong pastel colour.

4.4 Mineral time sequence

The order in which secondary minerals have formed within a host rock may indicate the evolution of the geothermal system, with regard to fluid composition, temperature and hydrological pathways. A 6 m core recovered from RK27 2147-2153 mRF display variations in both composition and alteration intensity, as it retrogrades from a strongly altered andesite breccia to a subtle altered andesite lava over these few meters (Fig. 4.25). It is a good example of the types of alteration present at both Ngatamariki and Rotokawa fields, and layered infill in vugs and veins in addition to overprinting may give an insight to the changing conditions in the geothermal system

4.4.1 Rotokawa well RK27

2147-2147.8 mRF

The top part of the retrieved 6 m core is an olive green hydrothermal andesite breccia, set in a pink matrix with strong alteration intensity (Fig. 4.26). The clasts consist of abundant green alteration minerals. Albite has been partly to completely altered to epidote and with patches of calcite, whereas ferromagnesian minerals have been completely altered to chlorite with occasional anhydrite. These secondary minerals have also replaced the groundmass. The mineral sequence of vugs in the clasts is:

epidote → chlorite

The outer layer of epidote indicates an initial high-temperature (>240°C) propylitic alteration style of the brecciated rocks, while the later infill of chlorite has a wider range of temperature stability (~100-300°C) so it cannot be used for geothermometry. Veins in the clasts are only filled with epidote.

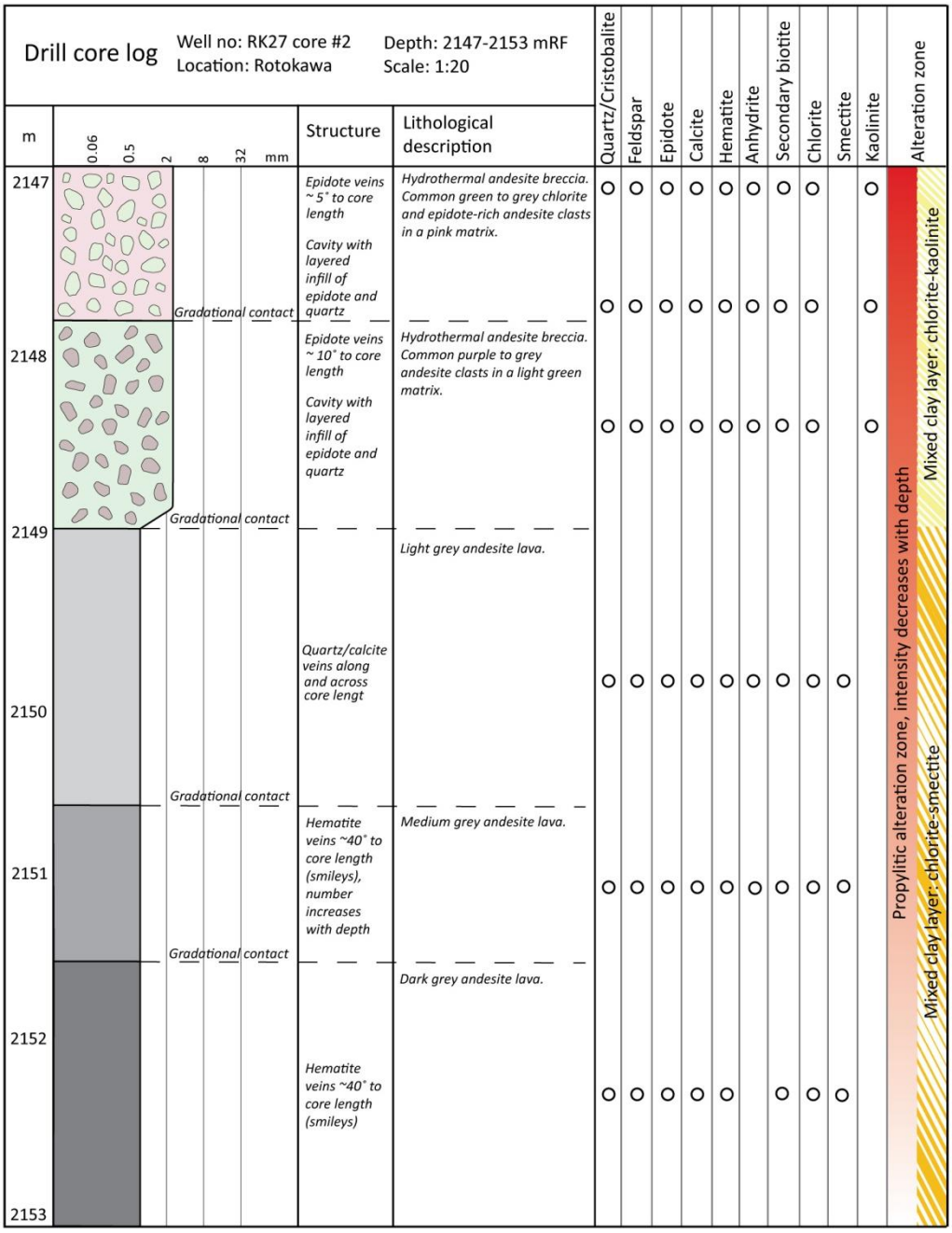

Figure 4.25: Stratigraphic column of a 6 m core recovered from RK27 at a depth of 2147-2153 mRF, Rotokawa. Mineral identification based on XRD-data (LA.54 and LA.56 can be found in Appendix 2, other XRD-graphs are available on CD-rom, Appendix 6) and petrographical examination.

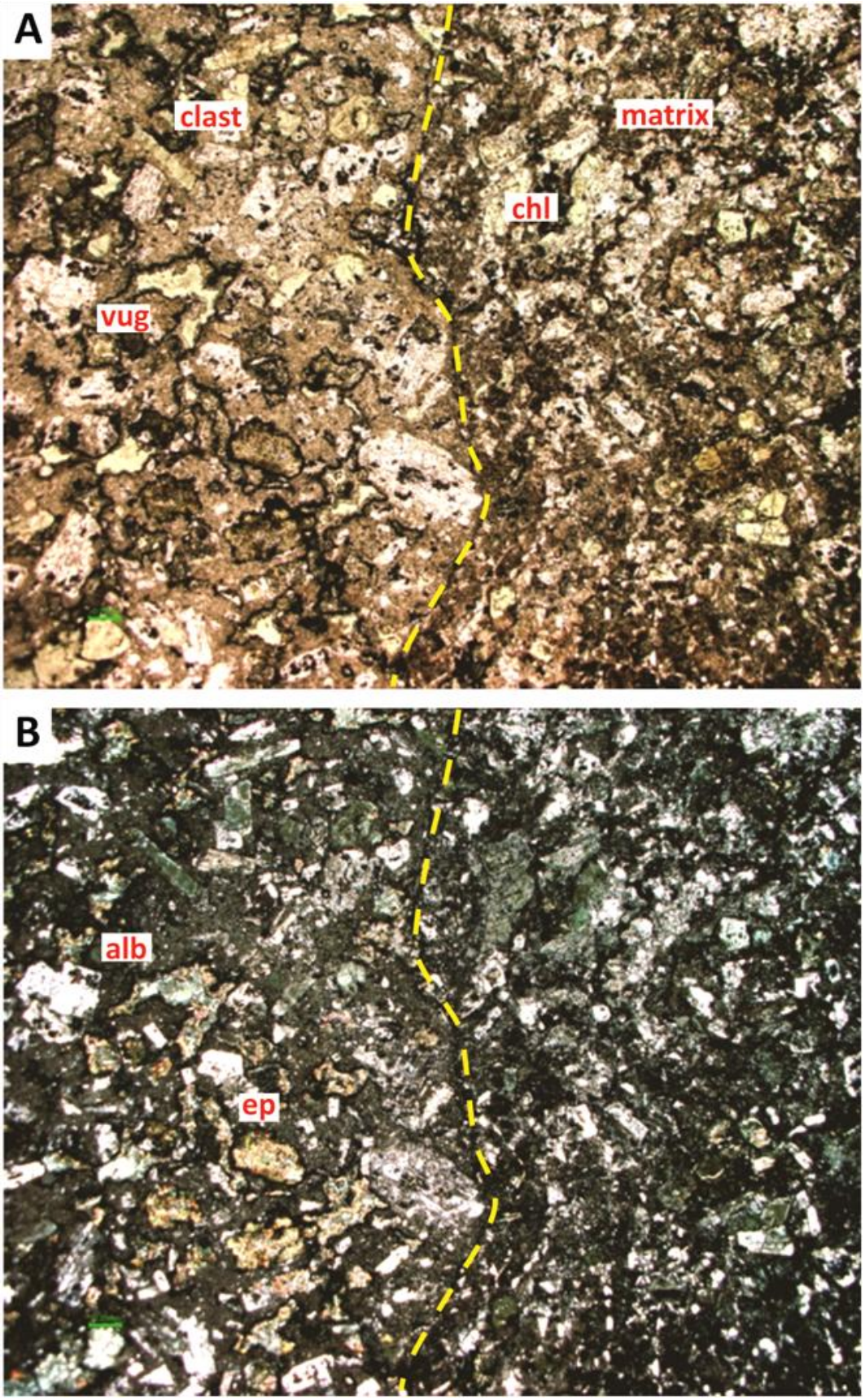

Figure 4.26: Breccia clast with abundant chlorite (chl) and epidote (ep) replacing ferromagnesian minerals and albite, while primary minerals in the matrix have been replaced by albite (alb) and chlorite (chl) (sample LA.53). A=PPL, B=XPL.

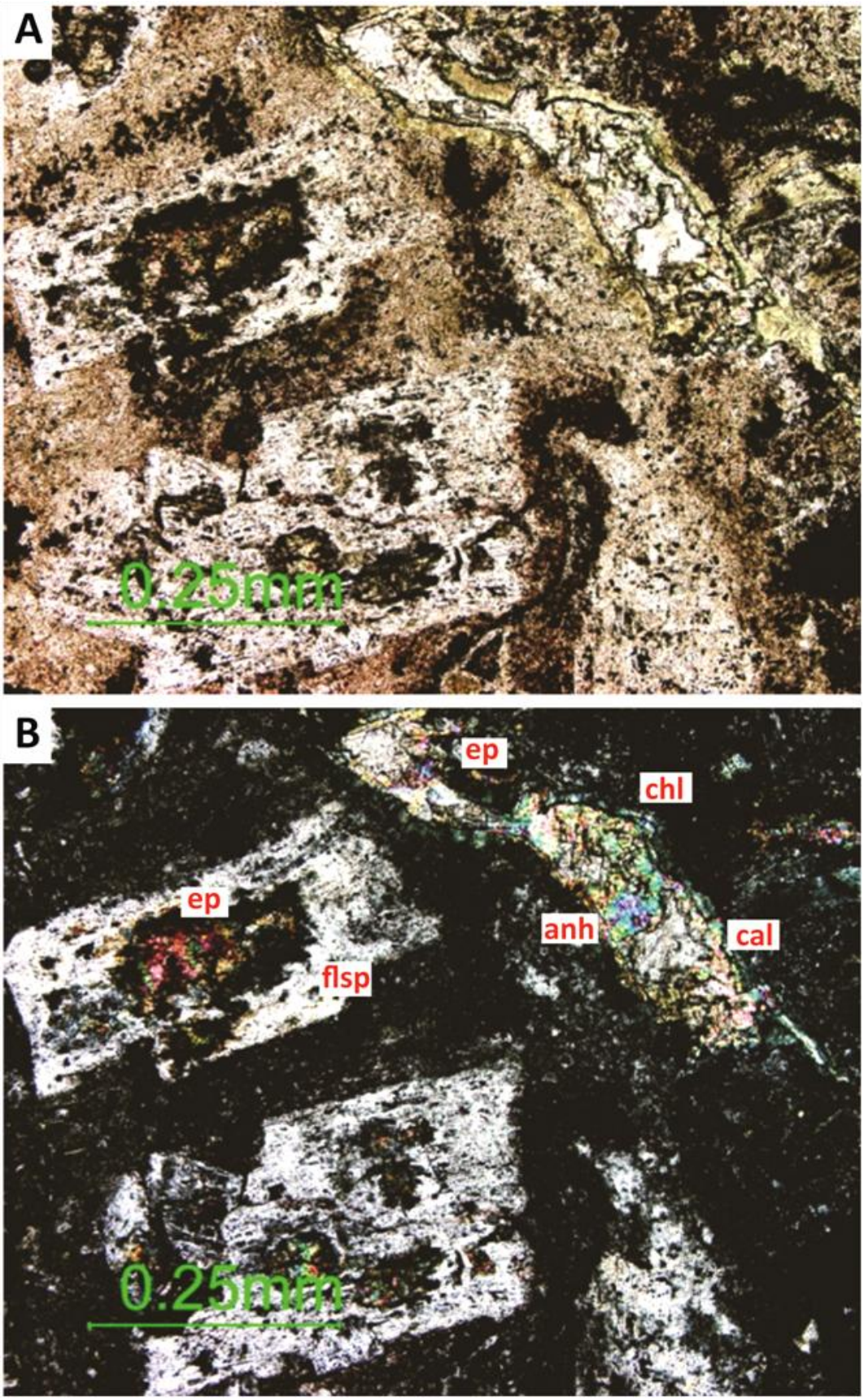

Figure 4.27: Secondary feldspar where the core has been replaced by epidote, and a vug lined with chlorite, epidote, anhydrite (anh) and calcite (cal) (sample LA.53). A=PPL, B=XPL.

In the breccia matrix, cores of albite are commonly replaced by epidote, and one albite crystal has an epidote-vein running through it. Ferromagnesian minerals have mainly been replaced by chlorite, and many are rimmed with microcrystalline quartz.

Fine-grained leucoxene in addition to hematite in the groundmass causes the pink colouring of the matrix. The mineral sequence lining the walls of vugs in the matrix is (Fig. 4.27):

chlorite → epidote → anhydrite → calcite

2147.8-2149 mRF

The colouring of the andesite breccia changes with depth, as the clasts here are purple to grey and set in a light green matrix. This is probably caused by more moderate alteration intensity rather than a change in primary composition. The breccia clasts are less altered than the matrix. Plagioclase in the breccia clasts has been altered to albite with patches of epidote and calcite, while ferromagnesian minerals have been replaced by chlorite, hydrothermal biotite, anhydrite and calcite. Vugs in this part of the core are filled with chlorite, while the mineral sequence in veins is:

epidote → chlorite → calcite

Again, the primary minerals in the breccia matrix have mainly been replaced by chlorite, and veins are also cutting through phenocrysts. The mineral sequence of vugs in the matrix is (Fig. 4.28):

chlorite → epidote → anhydrite → calcite

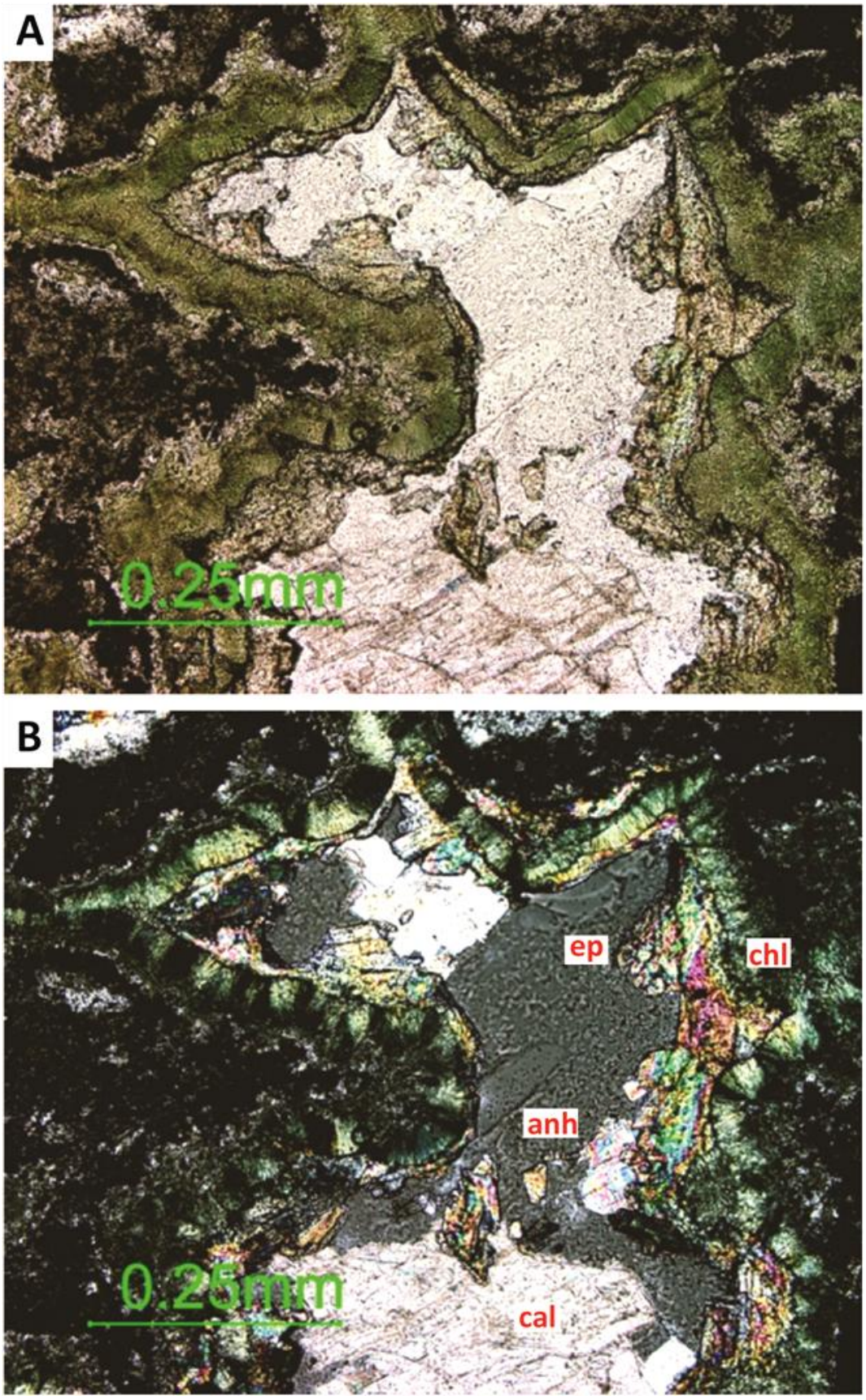

Figure 4.28: Vug with layered infill of chlorite, epidote, anhydrite, which is being replaced by calcite (sample LA.54). A=PPL, B=XPL.

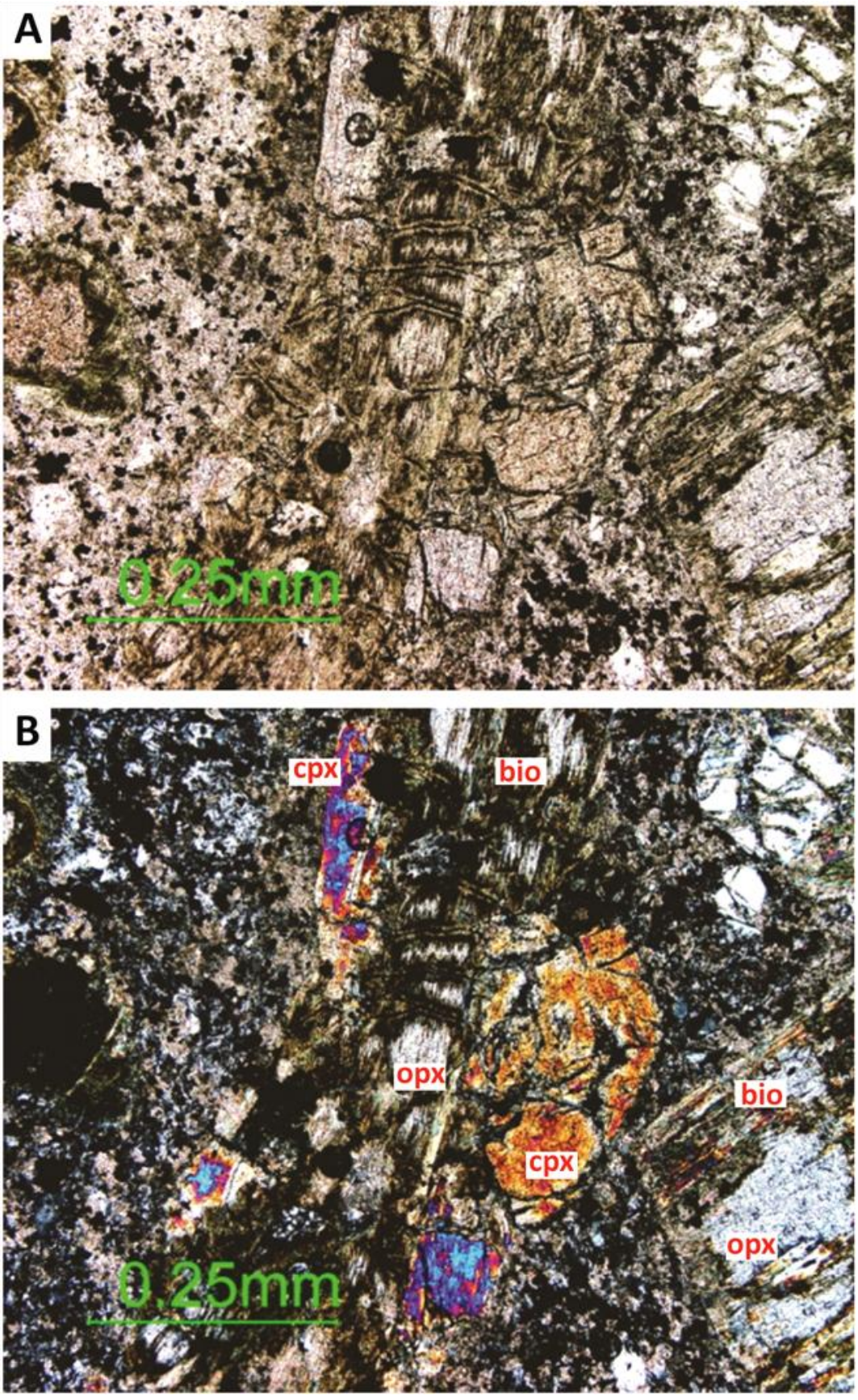

Figure 4.29: Orthopyroxene (opx) and clinopyroxene (cpx) are partially altered to hydrothermal biotite (bio) along fractures and cleavages (sample LA.56). A=PPL, B=XPL.

2149-2150.6 mRF

The breccia overlies light grey, weakly altered andesite lava. Plagioclase has patches of calcite and epidote, while ferromagnesian minerals are partly to completely replaced by chlorite and hydrothermal biotite (Fig. 4.29). The same alteration minerals are also replacing the groundmass, in addition to leucoxene and limonite. Thin veins of calcite and quartz are running across the core.

2150.6-2151.5 mRF

The andesite lava progressively becomes less altered with depth. The andesite is medium grey with a weak to subtle alteration intensity. Plagioclase has patches of calcite and epidote, while ferromagnesian minerals are partially replaced by hydrothermal biotite and chlorite (Fig. 4.30). The same alteration minerals are present in the groundmass in small amounts. Hematite which was previously present as fine grains in the groundmass of the matrix now forms prominent veins which are ~40° angle to the core axis (Fig. 4.31). Note that RK 27 is a deviated well towards north-east, with a final azimuth of 060°. Hematite commonly replaces magnetite in reducing conditions, so at some stage there have been fluids with an acid composition running through the fracture. The hematite vein comprises plagioclase and pyroxene with only minor alteration to red hematite in fractures, and the centre of the vein contains a thin layer of calcite.

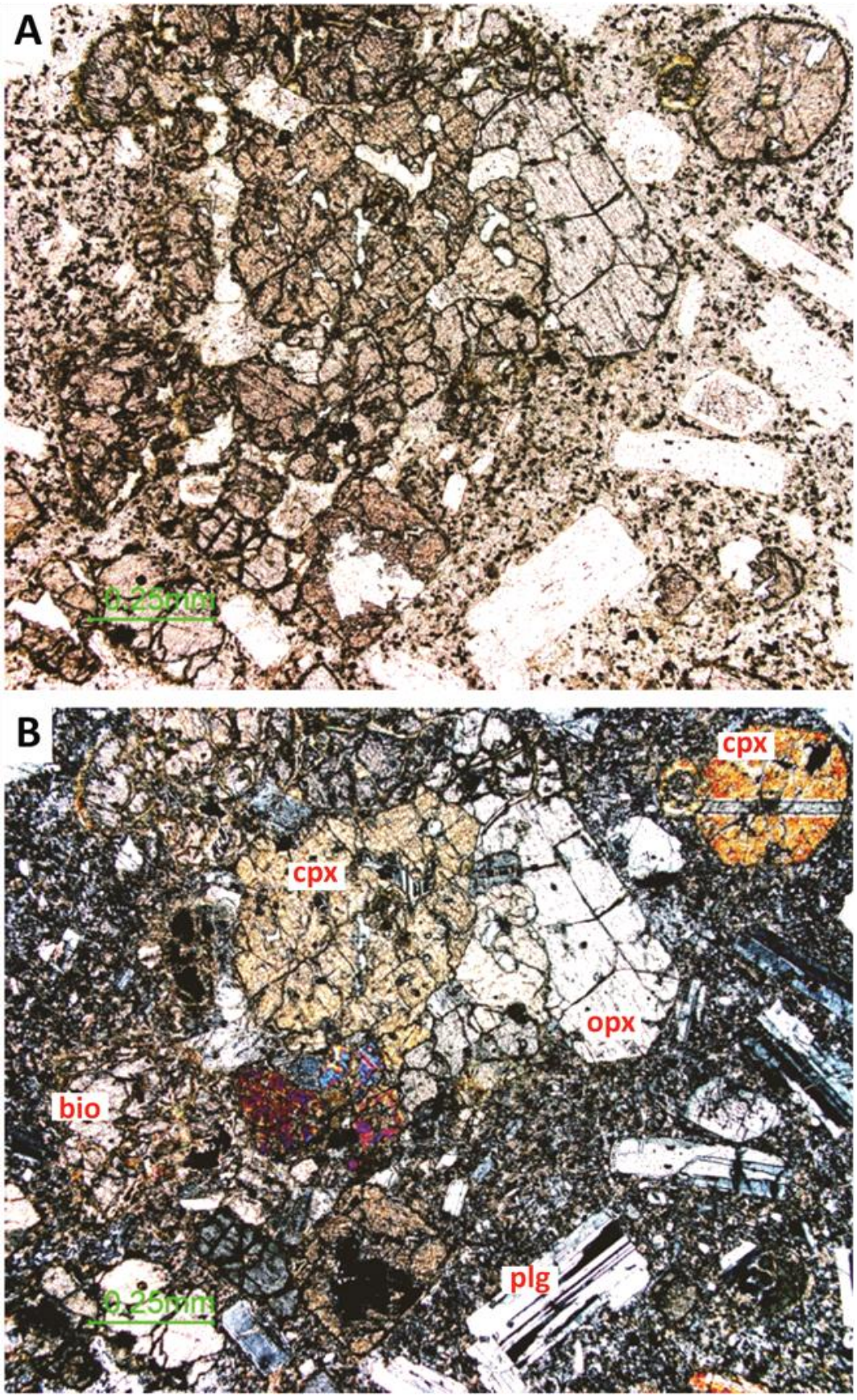

Figure 4.30: Glomeroporphyritic pyroxene, with minor alteration to hydrothermal biotite of the orthopyroxene crystal (sample LA.57). A=PPL, B=XPL.

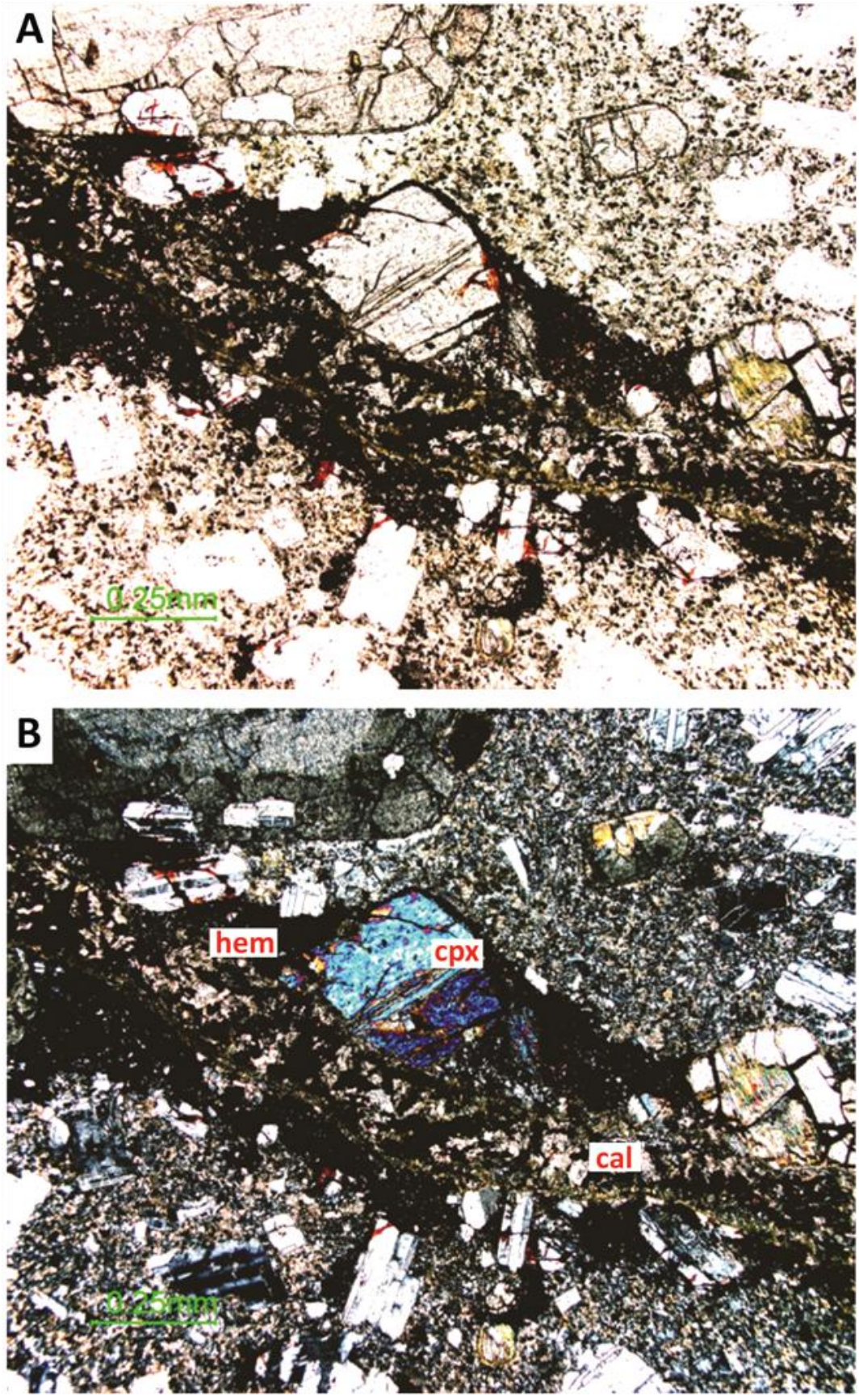

Figure 4.31: Hematite vein with a thinner calcite vein in its centre, in addition to primary phenocrysts of plagioclase and pyroxene (sample LA.57). A=PPL, B=XPL.

2151.5-2153 mRF

The andesite is dark grey with subtle alteration intensity. Plagioclase has minor patches of calcite and epidote. Clinopyroxene is unaltered, while orthopyroxene is partially altered to hydrothermal biotite and chlorite. The same alteration minerals are present in the groundmass in small amounts. There are hematite veins ~40° angle to the core axis.

4.4.2 Ngatamariki well NM6

Alteration textures in two separate units of andesitic lava from 2686-2689 mRF and 3032-3035 mRF offer an opportunity to study the mineral deposit order at Ngatamariki.

2686-2689 mRF

In hand specimen, the rock is greyish green with pinkish areas. Plagioclase has patches of calcite and epidote and show core texture, while ferromagnesian minerals have been altered to chlorite (Fig. 4.32). The groundmass is completely altered by primarily brown hematite (causing the pink staining), near-black irregular grains of leucoxene and vugs. The mineral sequence in vugs is:

quartz → chlorite → calcite

Quartz was the first mineral to line the vug, which was followed by complete infill of chlorite. A calcite vein has afterwards cut through the vug, and therefore represents the latest alteration event in this part of the rock.

3032-3035 mRF

The rock is light grey in hand specimen. All original minerals have been replaced, although outlines of tabular feldspar and prismatic clinopyroxene can be distinguished in the thin section (Fig. 4.33). Secondary minerals consist of mainly finegrained chlorite, calcite, quartz and epidote. Fe-Ti oxides have been altered to leucoxene or pyrite.

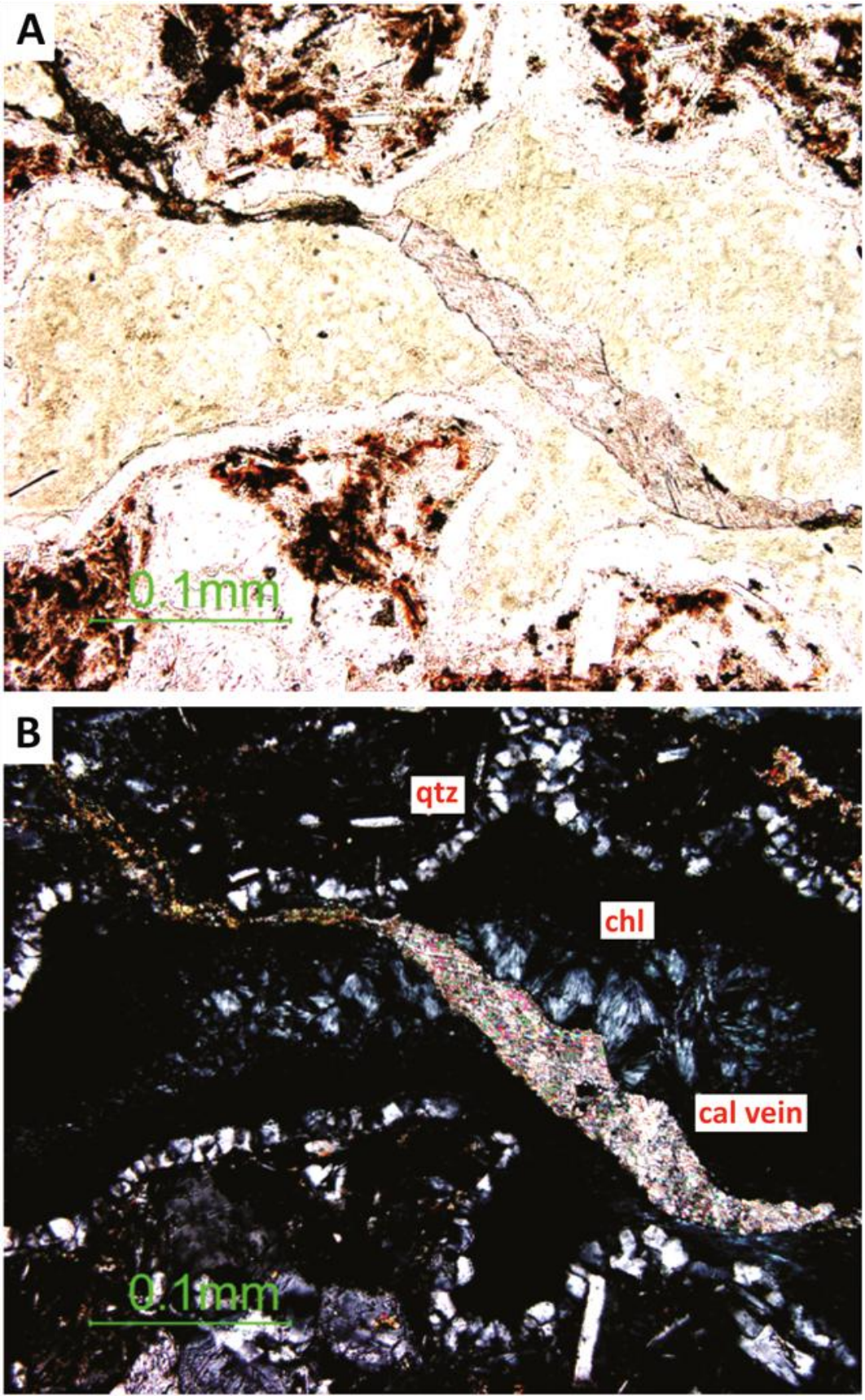

Figure 4.32: Vug in a moderately altered rock sample from well NM6 at 2686-2689 mRF, with layered infill of quartz and chlorite which is cut though by a calcite vein (sample LA.6). A = PPL, B = XPL.

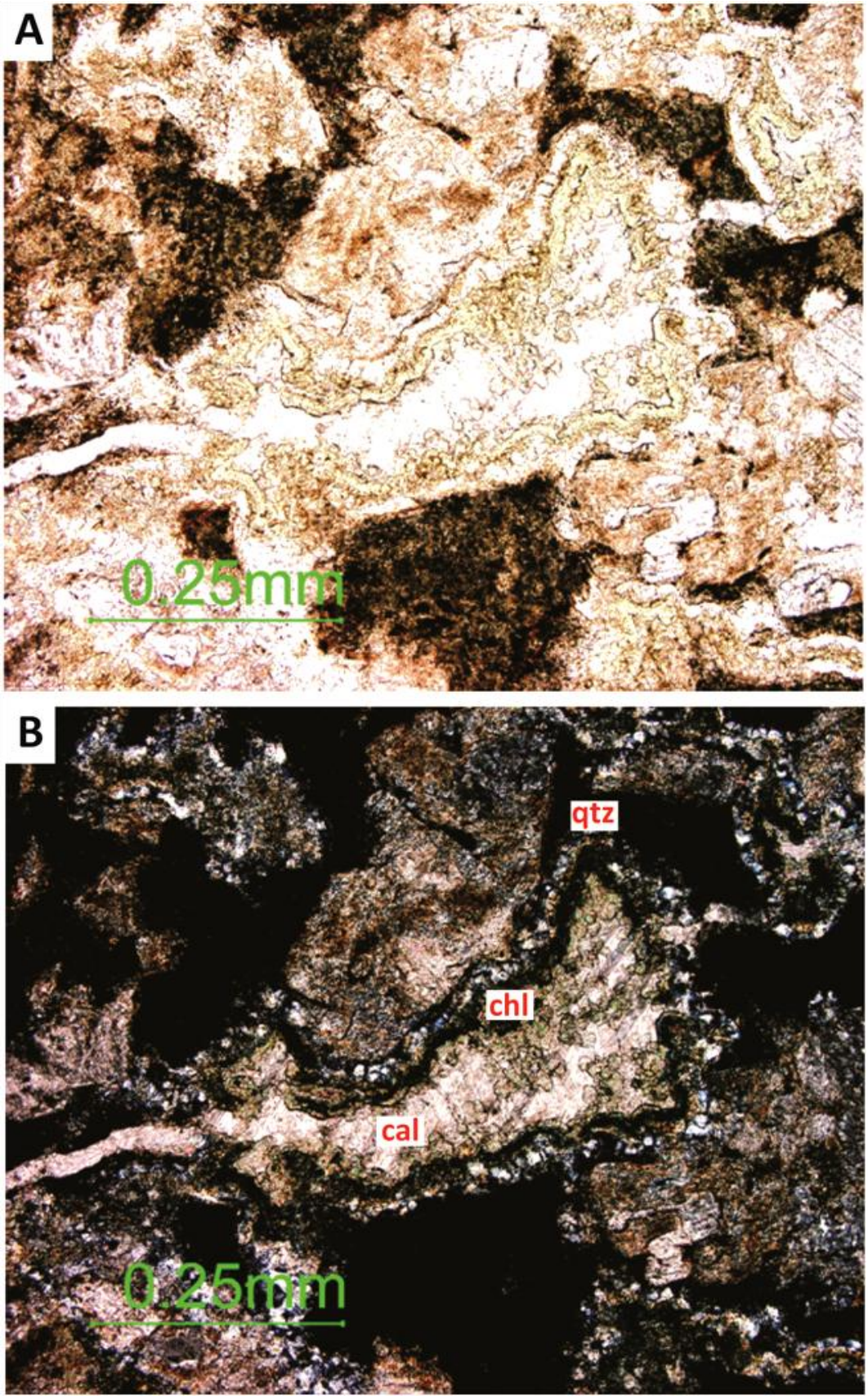

Figure 4.33: Vug in an intensely altered rock sample from well NM6 at 3032-3035 mRF, with layered infill of quartz, chlorite and calcite (sample LA.7). A = PPL, B = XPL.

The mineral sequence in vugs is:

quartz → chlorite → calcite

This is the same depositional order as in the overlying sample. The difference is that chlorite merely lines the vug in this sample, with a final and complete infill of calcite.

4.5 Discussion

4.5.1 Mineral time sequence

By studying a range of alteration intensity and style in the 6 m core from RK27, it has been possible to re-create the order in which secondary minerals have been formed at this location.

Andesite breccia in the upper part of the core (2147-2149 mRF) has the appearance of pseudobreccia described in Chapter 4.1.2.3. Coherent lava can have different but coexisting alteration assemblages, which may create the illusion of pseudoclasts and pseudobreccia (Allen, 1988). The main distinction between breccia clasts and matrix in the core from RK27 is different alteration styles, and the clast boundaries are not clearly defined by broken or aligned phenocrysts. However, the crystals are smaller in the matrix which suggests that the breccia is derived from two different andesitic lava types. The mineral type and sequence observed in vugs revealed a simple propylitic alteration style (epidote → chlorite) in clasts, while the matrix had been subjected to an initial propylitic alteration, followed by an advanced argillic alteration which subsequently was overprinted by propylitic alteration again (chlorite → epidote → anhydrite → calcite). These observations point to a hydrothermal breccia, where the clasts are likely to originate from the underlying, less altered andesite lava.

The more complex alteration of the breccia matrix can be explained by the conditions caused by a hydrothermal eruption. This is a common event at hot geothermal fields, and there have been numerous small eruptions within the TVZ in historic times. Hydrothermal eruptions take place close to the ground surface (<450 m depth) as a result of a rapid reduction in pressure (Browne & Lawless, 2000). This creates large amounts of steam with enough energy to break through layers of rocks and eject fragments into the air. In fact, one of the largest known hydrothermal eruptions in New Zealand took place at Rotokawa 6060 ± 60 years ago where the current Lake Rotokawa is located. The eruption created a deposit with a maximum thickness of 11 m and a diameter of 4 km. A much smaller eruption took place at Ngatamariki in 1948. Breccia is often poorly sorted and invariably matrix-supported due to rapid settling velocity. The clast sizes ranges from fine grains to large blocks of fragmented host rock, and they are often subrounded as they probably grind against the vent wall before being ejected Clasts are commonly hydrothermally altered and hydraulically brecciated before the eruption due to fluid/rock interaction of host rock and geothermal fluids (Fig. 4.34). The focal depth of the eruption depends on several factors, such as near-vertical fluid pathways, depth of piezometric surface and availability of meteoric waters. Reservoir rocks with high permeability often have the largest focal depth as this provides large quantities of water that can flash to steam. The sudden increase in permeability and steep temperature gradient result in rapid formation of alteration minerals and also cementing of clasts, creating brittle but coherent volcanic rocks. The finer grained fragments will form the new breccia matrix, and with high porosity they will be easily altered to an advanced argillic mineral assemblage by the interaction with acid surface fluids.

This scenario explains why the alteration style of the breccia clasts are propylitic, while in the breccia matrix changes from propylitic, to advanced argillic and back to propylitic (Fig. 4.27, 4.28). As the breccia is buried with time it has been exposed to the hot and more neutral chloride fluids deeper down in the reservoir, and propylitic minerals have overprinted earlier assemblages.

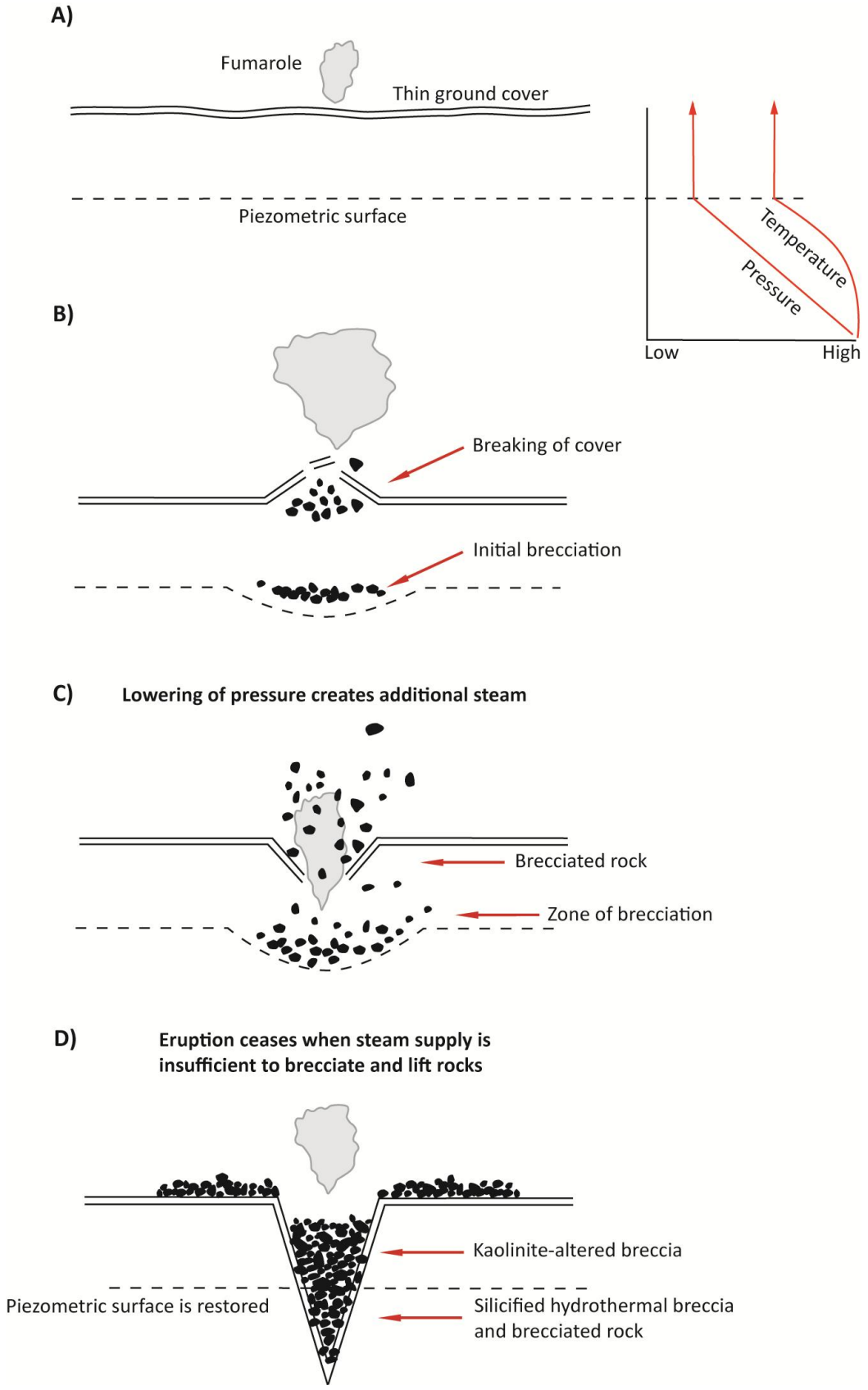

Figure 4.34: Image a-d) Progress of a hydrothermal eruption (modified from Browne & Lawless, 2000). The piezometric surface changes in a hot geothermal field with a steam cover, during the course of the eruption. Steam provides the necessary energy for lifting ejecting rocks out of the vent. In the last image, the piezometric surface is restored and the onset of hydrothermal alteration causes sealing.

The key minerals of the underlying, weakly altered andesite lava (2149-2153 mRF) are medium-temperature clays chlorite-smectite (~160-210°C) and high-temperature epidote (>240°C) and hydrothermal biotite (>280°C). Veins are present in the lava, and the mineral sequence is (Fig. 4.30):

Hematite → calcite

The hematite is primarily an alteration product of titanomagnetite or ilmenite. The andesite lava may have contained veins of these minerals prior to the hydrothermal eruption which resulted in the overlying andesite breccia. An influx of the acid surface waters would have promoted alteration to hematite. Primary phenocrysts included in the vein are almost unaltered, except for minor red hematite in fractures. This suggests that the reducing conditions were short-lived. The vein has at a later stage been infilled with a layer of fine-grained hydrothermal biotite probably caused by an influx of hot, K-rich fluids followed by calcite in the centre as the geothermal fluids returned to near-neutral pH-levels.

4.6 Summary

Secondary minerals are commonly used to estimate well temperatures in geothermal systems (Browne, 1970, 1993; Giggenbach, 1980, 1981, 1988; Arnorsson, 1983; Reed & Spycher, 1984; Harvey & Browne, 1991). In neutral pH-conditions, temperature-sensitive clay minerals such as smectite and illite may be used to identify cool (<140°C) vs. hot (>210°C) thermal regimes. Calc-silicates may also be used to define subzones within these regimes, such as cristobalite (<50°C) or epidote, green amphibole and hydrothermal biotite (>240°C).

A propylitic mineral assemblage represents the most widespread alterationstyle of Ngatamariki and Rotokawa andesites, comprising albite, calcite, chlorite, epidote and green amphibole in addition to rare galena, sphalerite and chalcopyrite. These minerals usually form from the dissolution of plagioclase and

ferromagnesian minerals. Propylitic alteration is characteristic for an environment where hot (>240°C), deep, chloride fluids with neutral pH (5.5-6.5) and low CO_2-content interacts with the host rock (Fig. 4.35). Mineral assemblages representing advanced argillic and potassic alteration styles are less common at Ngatamariki and Rotokawa. Potassic mineral assemblage typically represents the alteration style with highest temperatures (>280°C), forming deep down in the geothermal system. It comprises adularia and hydrothermal biotite which is formed by interaction of K-enriched, hot fluids with the host rock.

Advanced argillic alteration is very rare in the andesites, as associated minerals anhydrite and kaolinite are formed by low pH-level (2-5), near-surface fluids with an intermediate to cool temperature level (<180°C). This requires fluid pathways to the deeper stratigraphic units, such as faults or fractures. The distribution of key minerals at Ngatamariki and Rotokawa is summarized in Fig. 4.5.

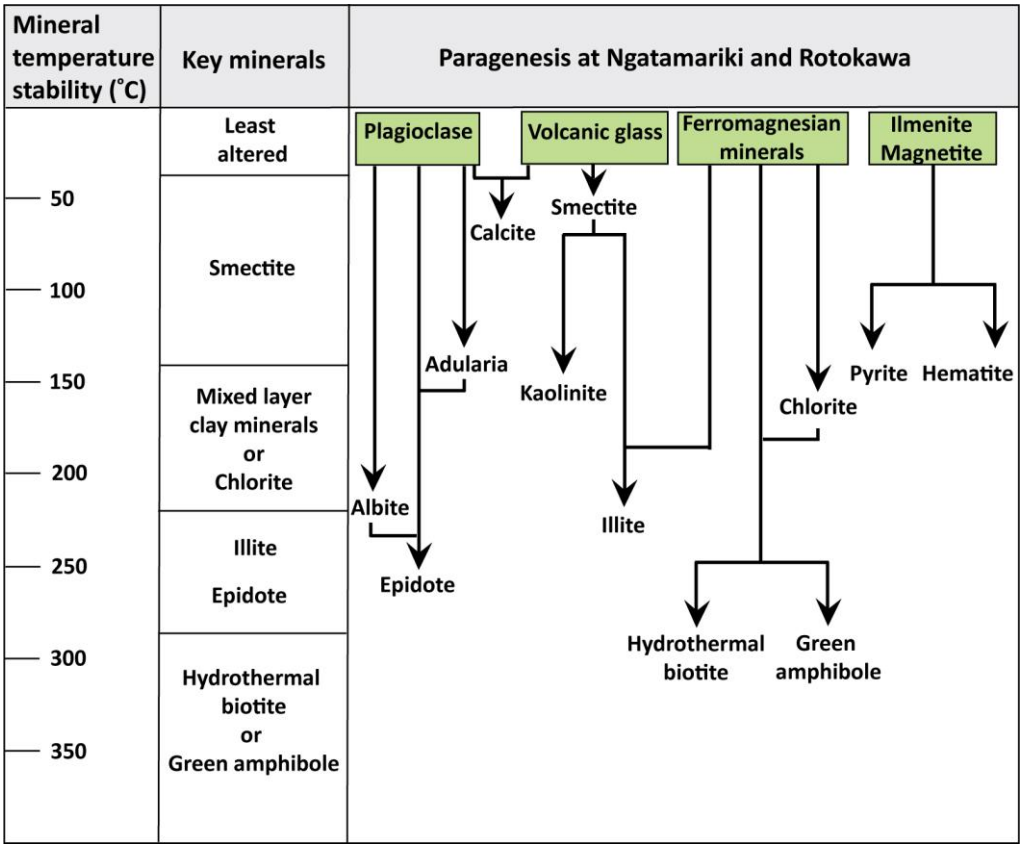

Figure 4.35: Temperature ranges of key alteration minerals and their paragenesis, based on observations during this study.

The same type of alteration mineral assemblages occurs in both Ngatamariki and Rotokawa andesites. An exception is green amphibole and hydrothermal biotite. These high-temperature (>280°C) minerals form indiscriminately of host rock composition, and can therefore not be used to infer differences in original compositions (Browne, 1978). The presence of green amphibole at Ngatamariki is merely a result of increased fluid/rock ratio while hydrothermal biotite at Rotokawa has been caused by the presence of K-rich fluids.

The use of key minerals to estimate well temperatures may be more precise at Ngatamariki than Rotokawa. Fluid chemistry studies of Ngatamariki have indicated that alteration minerals and the geothermal fluid are in equilibrium, with an estimated temperature range between 280 and 320°C (O'Brien, 2010). However, measured well temperatures (>300°C) do not correspond to the mineral stability of the current propylitic mineral assemblage at Rotokawa. This indicates disequilibrium between alteration minerals and geothermal fluids caused either by low permeability at depth or by being a young system where equilibrium has not been reached yet (Rae, 2007). The overall distribution of temperature-sensitive alteration minerals, in addition to overprinting also indicates ongoing changes to the thermal regime at these geothermal fields. At Ngatamariki, overprinting by low-temperature minerals in peripheral wells is a sign that the geothermal system is contracting (Bignall, 2009), whereas the southern end of Rotokawa has experienced an increased (+30-60°C) temperature in recent years (Rae, 2007).

Chapter 5
Geochemistry

5.1 Introduction

There are several processes which control the chemical composition of volcanic rocks (Fig. 5.1). The most important one is the composition and mineralogy of the source region, which is believed to be in the mantle wedge above the subducting Pacific plate, ~80 km below the TVZ (Grove & Kinzler, 1986; McCulloch & Gamble, 1991). A melt is created when fluids from the dehydrating plate becomes buoyant and induce melting of the overlying mantle wedge (Hawkesworth et al., 1979; Arculus & Powell, 1986; Turner et al., 1997; Ayers, 1998). Major- and trace element contents in this primary melt depends on several factors, such as the degree of partial melting or crustal contamination. On its way to the surface, additional modifications take place when the melt interacts with overlying lithosphere and is filtered through a magma chamber. During accumulation and storage time, the melt is subjected to processes such as fractional crystallization and magma mixing. Following the eruption, volcanic rocks may experience weathering or interaction with groundwater (Graham & Hackett, 1987; Graham et al., 1995; Dungan et al., 2001).

All these processes may be reconstructed by geochemical analysis of major- and trace elements. This information is commonly used for classification of volcanic rocks by characteristics such as magma affinity, rock composition or type of magmatic differentiation and it may also reveal petrogenetic relationships between rock units. Geochemical data in combination with petrological observation is an especially valuable tool when studying altered volcanic rocks, where complex textural and compositional modifications of primary minerals or even the formation of secondary minerals tend to make identification of rocks difficult.

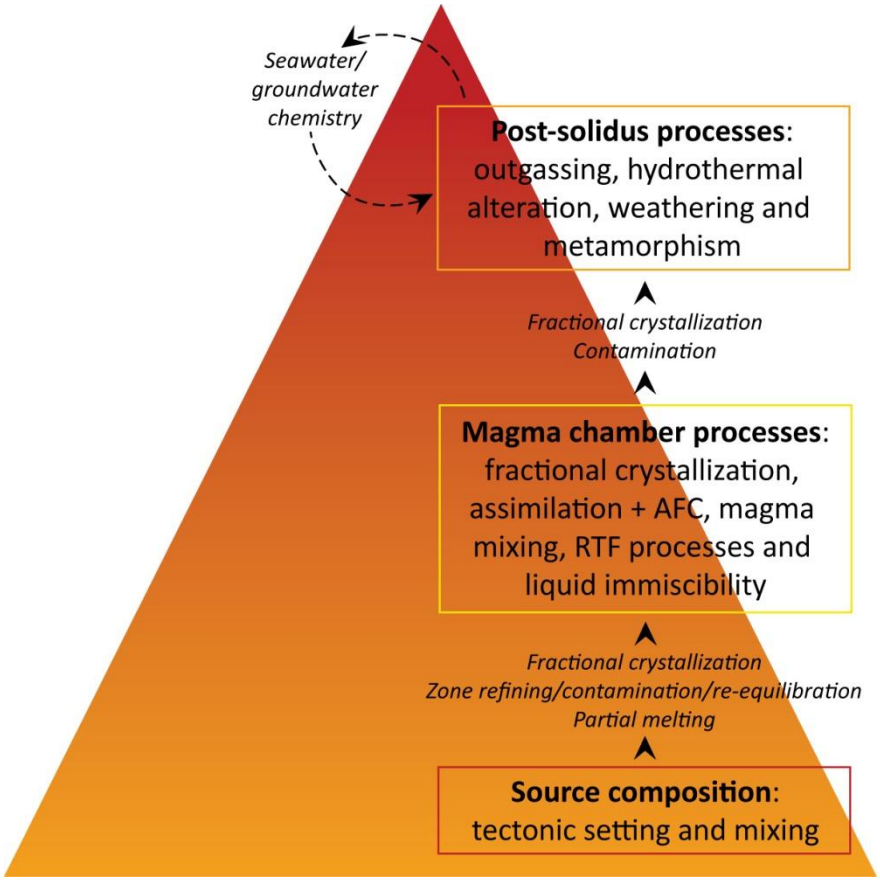

Figure 5.1: Flow diagram of processes which control the chemical composition of volcanic rocks (modified from Rollinson, 1993).

Major elements which have traditionally been used for classifying rocks (i. e. SiO_2, Na_2O, K_2O, Fe_2O_3, MgO, CaO) are known to be mobile during hydrothermal alteration, where compositional changes may outweigh their primary variations. The immobility of high-field-strength (HFS) elements (i.e. Ti, Zr, Y, Nb) has been documented by several studies (e.g. Pearce & Cann, 1973; Floyd & Winchester, 1975; Winchester & Floyd, 1977; MacLean & Kranidiotis, 1987), and variation diagrams of these elements may be used instead for the classifications mentioned above.

The behaviour of an element during hydrothermal alteration is related to its ionic potential (ratio of ionic charge vs. radius of an ion) as elements with low ionic potential (<3) are easily hydrated and become mobile under a range of conditions whereas elements with high ionic potential (>10) form soluble complexes and dissolve easily (Pearce, 1996). Elements with intermediate ionic

potential are relatively insoluble and tend to remain in the rock during alteration. These include Th, Pb, Zr, Hf, Ti, Nb, U and some rare earth elements (REE), except Eu, Ce and La, Cr, V, W (Fig. 5.2). However, a change in fluid composition, deep weathering, temperature or rate of fluid throughput can make even these elements mobile (McCulloch & Gamble, 1991).

Depending on the compatibility of an element, its behaviour will also vary in melts of different compositions, regardless of hydrothermal alteration. A compatible element is one that it is preferentially taken up by mineral phases during crystallization in the magma chamber. The element will therefore be depleted from the melt as fractionation proceeds.

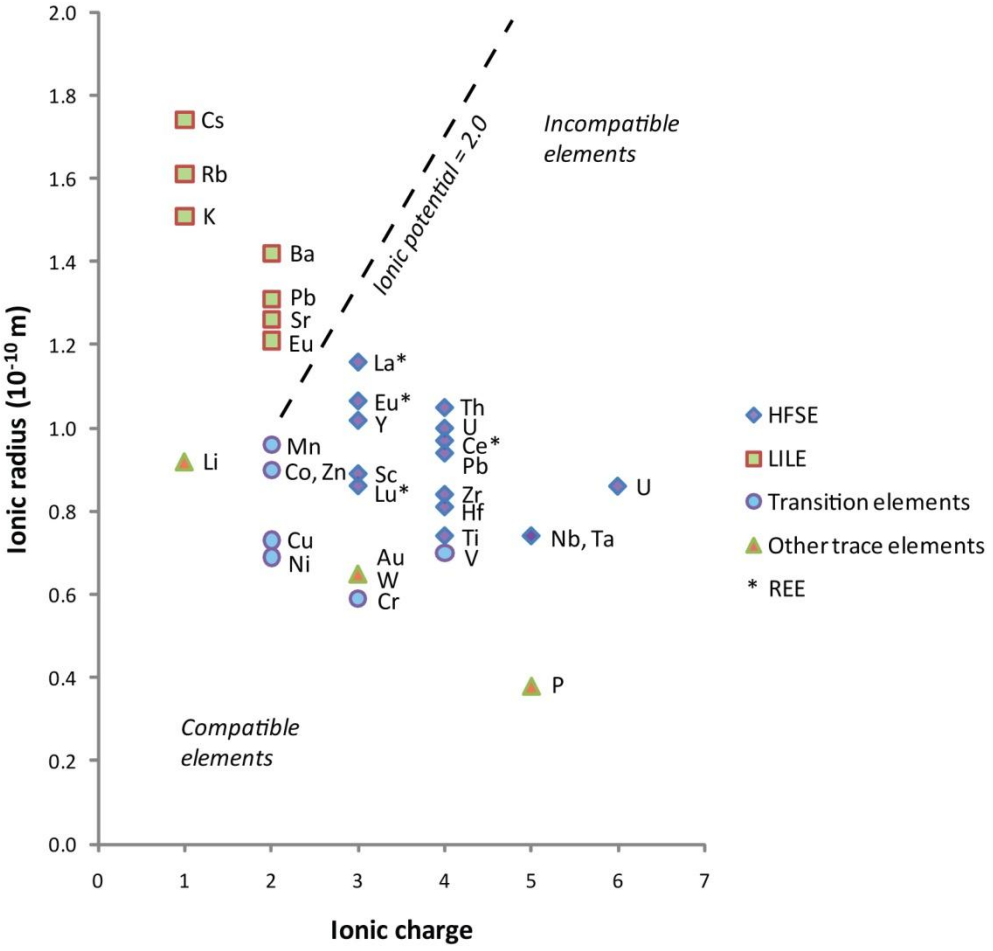

Figure 5.2: Plot of ionic radius vs. ionic charge for trace elements commonly used in lithogeochemistry (Shannon, 1976). The large ion lithophile (LIL) elements are subdivided from high field strength (HFS) elements by an ionic potential (ionic radius/ionic charge ratio) of 2.0. Compatible elements have a low (<3) or high ionic potential ratio (>10), while incompatible elements have an intermediate ionic potential.

The opposite will happen with an incompatible element, which will be rejected from the lattice of crystallizing minerals and its quantity will increase in the melt (Winter, 2001).

Different petrographical types have been identified at Ngatamariki and Rotokawa, i.e. pyroxene-, hornblende-, biotite- and quartz andesites (Chapter 3). However, it was impossible to identify the primary mineralogy of all samples as they had been variably replaced by propylitic, potassic and argillic alteration assemblages (Chapter 4). Geochemical techniques involving immobile elements will therefore be used in an attempt to see through the effects of hydrothermal alteration. MacLean & Barrett (1993) described a step-wise procedure for this specific purpose where a few, least altered samples are used to limit the influence of hydrothermal alteration on geochemical analyses (Fig. 5.3). There are two different approaches, depending on if the samples represent a homogenous rock unit (single precursor system) or continuous volcanic series (multiple precursor system). This study will use the approach for multiple precursor systems, based on the lateral and vertical extent of sample locations in addition to the different petrographical types identified by thin-section analysis.

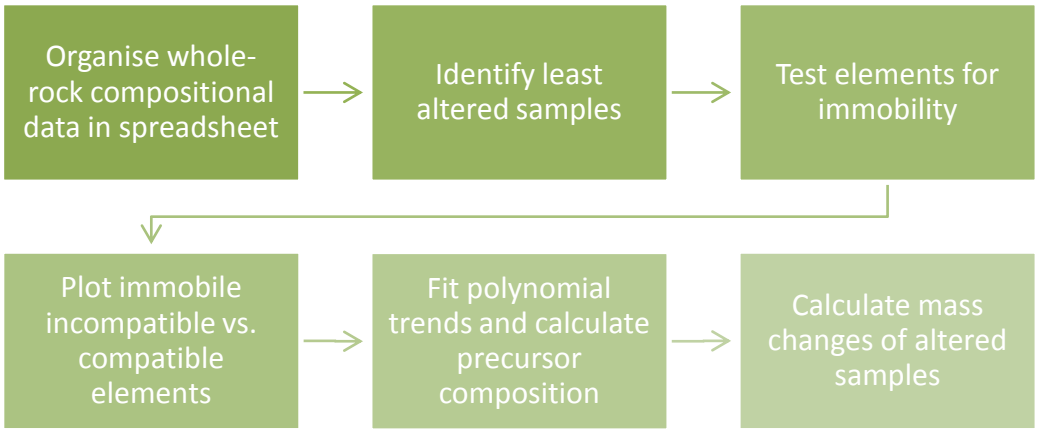

Figure 5.3: Flow chart of a geochemical technique using immobile elements (modified from MacLean & Barrett, 1993).

Previous studies utilizing immobile elements to characterize volcanic rocks in the TVZ have been carried out by for example Ewart (1977), Price et al. (1992) and Gamble et al. (1993). Browne et al. (1992) described the Ngatamariki and Rotokawa andesites as calc-alkaline, low- to medium K, with high Cr and Ni contents and high HFS elements (P, Ti, Y). The Sr isotopic range is from 0.70481 to 0.70553, similar to Tongariro volcanic rocks. The aim of this chapter is to obtain a more extensive and precise rock classification, investigate petrogenetic relationships between the fields and get an insight to the magmatic processes which have created these andesites.

5.2 Methodology

A total of 123 samples have been collected from the Ngatamariki and Rotokawa fields. 17 of the samples are not used, as they either are from the overlying Tahorakuri Formation (LA.60-65, 79-80, 85), rhyolite lava (LA.74-76), or the greywacke basement (LA.100-104). Trace element data has been obtained from all samples by XRF, while only 15 of them were analysed for major elements. Major- and trace element data of another 16 samples obtained by Browne et al. (1992) from some of the early wells drilled in the 1980's is also used in this study to provide a wider range of the rock compositions at the Ngatamariki and Rotokawa fields. They will be denoted with a * in order to separate them from samples collected in this study. Major elements are commonly used for:

- ✧ classification diagrams of magma affinity and rock type;
- ✧ identifying least altered samples which may be used for precursor compositions, and
- ✧ mass-change calculations of net gain/loss caused by alteration.

Due to the extensive hydrothermal alteration of the andesites, only a few least altered samples per well were selected for major element analysis. Trace elements are used for several purposes:

- ✧ bivariate plots of trace elements against a proven immobile element (i.e Zr) to test for scatter and mobility;
- ✧ multivariate diagrams to visualize mass changes, and
- ✧ chondrite-normalised patterns to identify tectonic setting.

The XRF instrument used for the analysis was a Spectro X-Lab 2000 located at the University of Waikato. Major element (Na_2O, MgO, Al_2O_3, SiO_2, P_2O_5, K_2O, CaO, TiO_2, MnO, Fe_2O_3) and trace element (Rb, Ba, Th, La, Pb, Sr, Zr, Y, V, Cr, Ni, Cu, Zn, Nb, Cl, Co, Ga, Ge, Se, Br, Mo, Cs, Ce, Hf, W, Tl, Bi, U, S) data are presented in Appendix 3.

Samples were crushed in a tungsten carbide mill until they have a texture of talcum powder in order to homogenise them. The parts of the mill and any containers and spatulas are carefully cleaned or disposed of to prevent contamination between samples. The powdered rock can then be prepared in two ways; fused discs for major element analysis and pressed pellets for trace element analysis.

5.2.1 Major element analysis

0.35 g of sample is mixed with 2.50 - 2.55 g of flux type 1.2:2.2 (35% Li-tetraborate, 65% Li-metaborate normally used for basaltic andesites) in a platinum alloy crucible. The sample is then step heated (to break the SiO_2 bonds) with intervals of 15 minutes in a Bradway Fusion Furnace at 700°C, 800°C, and finally 1040°C with the furnace shaker on. When the 45 minutes of heating is complete, a pinch of ammonium iodide is added to the sample as a wetting agent to prevent the melt from sticking to the crucible. The sample is then poured onto a graphite disc on a press, situated on a hot plate which is set to 230°C. The molten samples are pressed into glass discs, then step-cooled from 230°C to 180°C, making the glass more durable and less likely to shatter when subjected to change in temperature or mechanical shock. Once cooled, the

samples are labeled with a sticker and the edges trimmed to fit into the sample tray of the XRF.

5.2.2 Trace element analysis

To prepare pressed pellets, 5 g of powdered sample was mixed with 13-15 drops of PVA binder in separate paper cups and stirred with a wooden spatula. The mixture was poured into a metallic container which was then placed in a pneumatic press and the powder is compressed into the container at 90 bar. A flat surface of the pellets is vital for the quality of the analysis. The sample is then dried at 70°C for 2 hours to evaporate the PVA binder before analysis

5.2.3 Loss on ignition

The last step of the XRF analysis is to determine the Loss of Ignition (LOI) for each of the samples, using ~2 g of powdered sample heated in the furnace at 1000°C for 1 hour. The samples are then cooled for 10 minutes before weighing. The dry weight is compared to the initial weight of the sample and LOI calculated. Two control samples were re-run to ensure the quality of the analysis.

5.3 Least altered samples

The identification of least altered samples is an important part of this chapter, as they will be used to confirm the immobility of HFS-elements, link the immobile element ratios of altered rocks to precursor rock types and also provide the basis for mass change calculations. Whole-rock compositional data of representative samples from Ngatamariki and Rotokawa is compiled in Table 5.1, to give an idea of the compositional variations between least altered and altered rocks.

As a part of the petrological investigation in Chapter 3, samples from this study have been assigned alteration intensity terms.

Table 5.1: Whole-rock chemistry of representative samples from Ngatamariki and Rotokawa. * = samples from Browne et al. (1992). TiO_2/Zr ratios are: <15 = rhyolite, 16-23 = dacite, 24-53 = andesite, 54-119 = basaltic andesite. Zr/Y ratios are: <4 = tholeiitic, 4-7 = transitional, >7 = calc-alkaline magma affinity (data from Appendix 3).

Sample	**3***	**4***	**LA.7**	**16***	**LA.4**	**LA.5**	**13***	**14***	**15***	**LA.15**
Well	**RK4**	**RK5**	**NM6**	**NM4**	**NM5A**	**NM6**	**RK6**	**NM2**	**NM3**	**NM6**
Depth (mRF)	**1429**	**2349**	**3032-35**	**2460**	**2575-78**	**2686-89**	**1861**	**2000**	**1991**	**2210**
Rock type	Basaltic-andesite	Basaltic andesite	Basaltic andesite	Basaltic andesite (micro diorite)	Andesite	Andesite	Andesite	Andesite-dacite	Andesite-dacite	Andesite-dacite
Alteration intensity	Low degree of alteration	Low degree of alteration	Intense	Altered	Subtle	Weak	Altered	Low degree of alteration	Low degree of alteration	Weak
Major oxides (wt. %)										
SiO_2	57.14	57.26	51.03	57.09	55.01	56.62	62.16	56.88	61.80	61.84
TiO_2	0.65	0.67	0.65	0.88	0.63	0.64	0.46	1.10	0.88	0.59
Al_2O_3	17.17	17.60	16.64	16.63	16.19	18.06	15.59	18.27	16.38	13.37
Fe_2O_3	7.40	7.20	6.98	8.63	6.13	6.52	6.23	7.37	6.31	4.84
MnO	0.12	0.14	0.16	0.17	0.14	0.10	0.08	0.18	0.21	0.09
MgO	5.01	4.45	3.52	3.35	3.14	2.69	5.02	3.10	3.30	2.18
CaO	8.28	8.70	7.38	7.00	7.93	7.75	6.17	7.43	6.28	5.25
Na_2O	2.86	2.69	1.73	5.27	2.50	2.46	2.41	4.51	3.30	2.99
K_2O	1.24	1.15	2.12	0.71	1.70	1.45	1.76	0.84	1.38	1.71
P_2O_5	0.13	0.12	0.09	0.27	0.18	0.12	0.12	0.30	0.18	0.12
H_2O	0.50	0.20	na	0.00	na	na	0.20	0.10	0.10	na
LOI	1.00	2.70	8.92	0.40	4.55	3.02	3.80	1.60	1.80	6.22
TOTAL	**100.00**	**100.12**	**99.21**	**99.81**	**98.10**	**99.44**	**100.11**	**99.30**	**99.54**	**99.20**
Trace elements (ppm)										
V	212	221	224	185	183	191	158	157	134	100
Cr	70	52	30	11	126	11	252	20	45	58
Ni	37	26	22	n/a	40	6	56	7	11	14
Cu	43	35	42	36	24	31	17	8	26	20
Zn	75	76	73	207	58	75	58	95	123	58
Rb	71	53	101	15	47	36	54	23	43	68
Sr	284	299	236	248	273	236	275	371	295	205
Y	16	16	19	42	22	20	14	24	24	23
Zr	71	77	78	96	124	96	96	255	210	160
Nb	na	na	4	na	6	5	na	na	na	7
Ba	251	278	281	300	333	257	373	227	516	367
La	10	9	< 4.9	20	7	10	16	11	16	13
Ce	na	na	9	na	19	17	na	na	na	30
Hf	na	na	3	na	6	6	na	na	na	5
W	na	na	74	na	412	204	na	na	na	184
Pb	28	12	6	84	8	9	16	18	13	10
Th	14	<2	6	10	9	8	6	4	<2	9
U	na	na	6	na	6	6	na	na	na	6
TiO2/Zr	55	52	50	55	31	40	29	26	25	22
Zr/Y	4	5	4	2	6	5	7	11	9	7
$^{87}Sr/^{86}Sr$	0.70512	0.70515	na	0.70510	na	na	0.70485	na	na	na
$^{87}Sr/^{86}Sr$ (L)	0.70509	0.70500	na	0.70507	na	na	0.70481	na	na	na

The different categories range from subtle, weak, moderate, and strong to intense based on the extent of destruction of primary minerals and the growth of secondary minerals (see Chapter 4.1.2.1 for category description). Almost half of the samples were assessed to have subtle to weak alteration intensity where major elements have been obtained, while 8 out of 16 samples from Browne et al. (1992) were described as having a low degree of alteration, based on petrology and low LOI (<2%). These will represent least altered samples for the ensuing geochemical analyses.

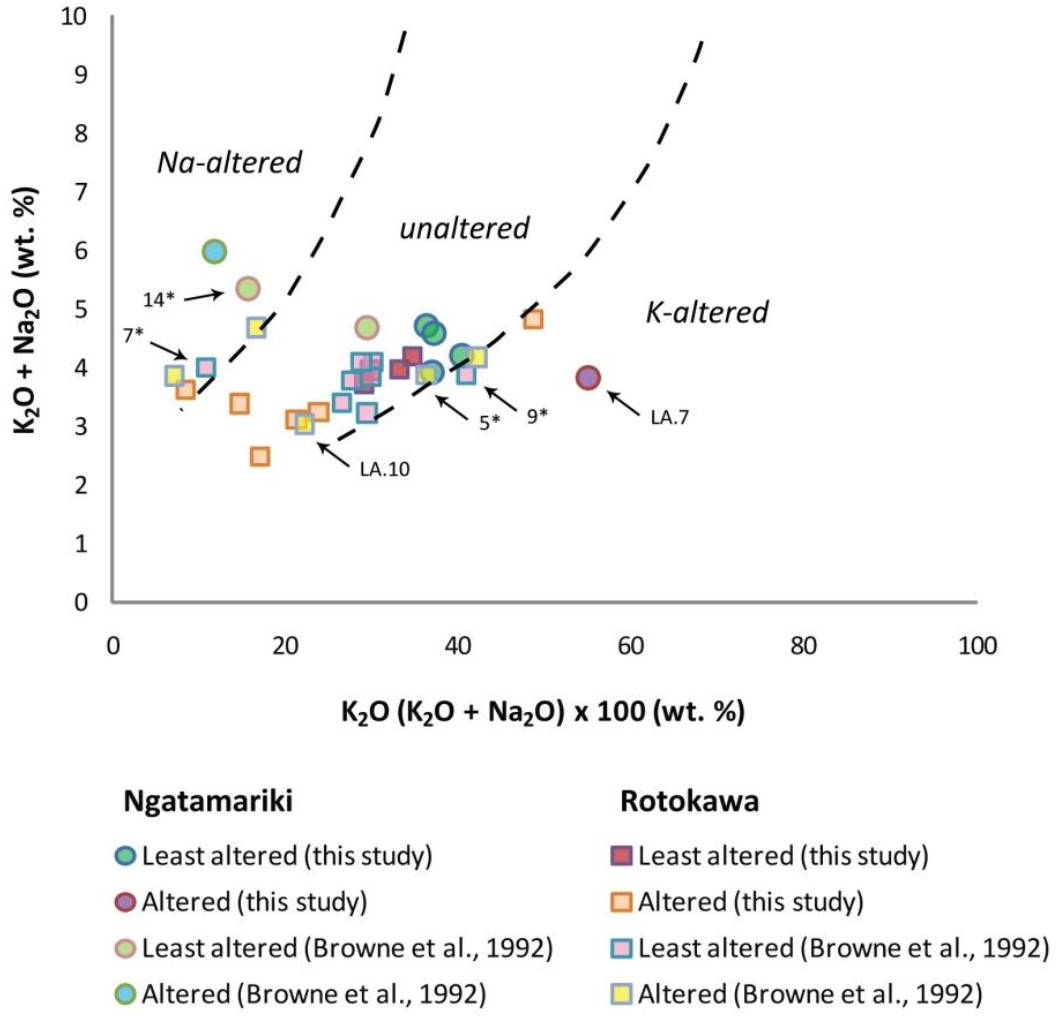

Figure 5.4: A plot of 31 samples where major elements have been obtained, in this study and by Browne et al. (1992) (Appendix 3). Samples previously classified in this study by petrography as least altered plot within Hughes igneous spectrum (Hughes, 1973). Some samples from Browne et al. (1992) classified as altered plot within the spectrum (i. e. 5*), and samples classified as least altered plot as Na-altered (i.e. 7* and 14*) or K-altered (i.e. 9*).

By using a geochemical tool for identifying least altered samples, Hughes igneous spectrum (Hughes, 1973), it is possible to confirm the initial petrological assessment of samples where major element data has been obtained (Fig. 5.4). The igneous spectrum is a bivariate diagram of Na_2O vs. K_2O where altered samples with an anomalous alkali distribution plot either to the right or left of the spectrum, while least altered samples plot within it.

According to this diagram, total alkali ranges between 3-5 wt. % for least altered samples and 2-6 wt. % for altered samples. Ngatamariki samples have in general a larger amount of total alkali, probably due to a more evolved composition with K- and Na-bearing silicates. Some samples from Browne et al. (1992) which were initially assessed as having low alteration intensity (7*, 9*, 14) plot outside the spectrum.

The alteration styles at both Ngatamariki and Rotokawa fields are mainly propylitic (albite, chlorite, calcite, epidote, green amphibole) with less common argillic (clay minerals) and potassic (hydrothermal biotite, K-feldspar, adularia) (Chapter 4). The altered samples in the diagram mainly show an enrichment of Na, which may indicate albitization of plagioclase crystals. The altered sample from Rotokawa (LA.10) is a breccia with strong alteration intensity, where plagioclase has indeed been altered to albite with patches of calcite and epidote while pyroxene has been altered to chlorite with occasional leucoxene. A few samples showing an enrichment of K may be due to replacement by K-feldspar or illite. The altered sample from Ngatamariki (LA.7) with K-enrichment is intensely altered with all primary minerals replaced by calcite, chlorite, epidote, quartz or clays, so the high level of K may be caused by the presence of illite.

By re-classifying the three least altered samples from Browne et al. (1992), 15 out of 31 samples have been confirmed by the igneous spectrum as least altered (Table 5.2).

Table 5.2: List of least altered samples at Ngatamariki and Rotokawa according to Hughes igneous spectrum (Fig. 5.4). Altered samples LA.7 and LA.10 are included for comparison (data from Appendix 3).

Sample	Well	Depth (mRF)	Rock type	Alteration intensity	Na_2O (wt. %)	K_2O (wt. %)
Ngatamariki						
LA.4	NM5A	2575-78	Andesite	Weak	2.50	1.70
LA.5	NM6	2686-89	Andesite	Weak	2.46	1.45
LA.15	NM6	2210	Andesite-dacite	Weak	2.99	1.71
LA.22	NM6	2550	Andesite	Weak	2.88	1.71
15*	NM3	1991	Andesite-dacite	Least altered	3.30	1.38
LA.7	*NM6*	*3032-35*	*Basaltic andesite*	*Intense*	*1.73*	*2.12*
Rotokawa						
LA.3	RK21	1876	Basaltic andesite	Subtle	2.65	1.32
LA.14	RK18	2219-21	Basaltic andesite	Weak	2.74	1.46
LA.23	RK21	1250	Basaltic andesite	Weak	2.77	1.19
LA.58	RK27 #2	2152	Basaltic andesite	Subtle	2.64	1.09
2*	RK8	2219	Basaltic andesite	Least altered	2.27	0.95
3*	RK4	1429	Basaltic andesite	Least altered	2.86	1.24
4*	RK5	2349	Basaltic andesite	Least altered	2.69	1.15
6*	RK4	1630	Basaltic andesite	Least altered	2.49	0.90
8*	RK5	2655	Basaltic andesite	Least altered	2.91	1.18
10*	RK5	2003	Basaltic andesite	Least altered	2.73	1.05
LA.10	*RK27*	*1853-56*	*Basaltic andesite*	*Strong*	*3.3*	*0.31*

5.3.1 Rock classification with major element data

SiO_2 vs. K_2O, Total Alkalis (TAS) and Al, Mg, Fe (AMF) diagrams are not recommended for weathered, altered or metamorphosed rocks in the literature (Rollinson, 1993). Alkalis (K_2O and Na_2O) are known to become mobilized in potassic-rich or altered rocks. The AMF (Al, Mg and Fe) diagram is stable during low grades of metamorphism, but extensive hydrothermal alteration of ferromagnesian minerals causes compositional variations of these precise elements. The weaknesses of these diagrams may however be useful in this study, as altered samples create scattered plots and are therefore easily recognized when comparing different classification diagrams of magma series and/or rock types.

Magma series may be divided into sub-alkaline or alkaline groups (Winchester and Floyd, 1977). The sub-alkaline group may be further divided into tholeiitic basalt- and calc-alkali series whereas the alkaline group have two members; the alkali olivine basalt- and shoshonite series.

The composition of arc magmas occurring in a subduction setting vary both with the stage of evolution and with interaction with the crust. Tholeiitic magmas are often the first to occur at a volcanic arc, and also closest to the Benioff Zone. Therefore, it is dominant in young oceanic island arcs, while calc-alkaline magmas are most common in mature oceanic or continental arcs, where the composition may range from mafic basalt to felsic rhyolite (Pearce & Cann, 1973). The andesitic volcanoes located within the TVZ (e.g. Ruapehu and Tongariro) for example, are often described as medium-K, calc-alkaline (Cole, 1978; Cole et al., 1983). The term 'calc-alkaline' was first used by Peacock (1931) to define a calc-alkalic group where the SiO_2-value at which CaO and alkali (Na_2O + K_2O) trends intersected (at 56-61 wt. %). This definition is no longer valid. Also, the term 'tholeiitic' should not be confused with 'tholeiite', which is an olivine-hypersthene basaltic rock.

SiO_2 vs. K_2O and TAS diagram

The origin and evolution of magmas has traditionally been a much debated topic in scientific literature. The earliest attempt of classifying magma series by Bowen (1928) suggested enrichment of silica as a sign of magma evolution, while Fenner (1931) believed iron enrichment was a better indicator. Two of the most common classification diagrams for volcanic rocks today are based on total alkali vs. SiO_2 (TAS) from LeMaitre et al. (1989) and SiO_2 vs. K_2O (Peccerillo & Taylor, 1976). The TAS diagram divides rocks into alkaline or sub-alkaline magma series based on their Na_2O and K_2O concentrations, and ultrabasic to acid rock types depending on SiO_2. Silica is the most abundant element oxide in most volcanic rocks and is mainly controlled by the degree of differentiation in a magma chamber which gives it an excellent diagnostic value. Sub-alkaline rocks can be further subdivided by the SiO_2 vs. K_2O diagram into tholeiitic, calc-alkaline, high-K or shoshonitic magma series, based on the concentration of K_2O only. Potassium is added to volcanic rocks via large ion lithophile element (LILE)-enriched fluids which are released from the dehydrating subducted plate to the overlying mantle wedge (Winter, 2001). It is believed that the thick, continental crust of mature island arcs promote deep-level fractional crystallization and other

processes, which results in more evolved and enriched magmas, compared to young island arcs with a thin crust.

Least altered samples from Ngatamariki and Rotokawa plots within the sub-alkaline magma series (Fig. 5.5a) or more specifically calc-alkaline (Fig. 5.5b), similar to other andesites from the TVZ. The rock types range from basaltic andesite to andesite. The altered samples plot in a wider range, from low- to high-K magma series and even as basaltic rock types. Large scatter along the total alkalis-axis could be due to alteration of plagioclase to albite or K-feldspar as discussed previously regarding Hughes igneous spectrum (Fig. 5.4). Scattering along the SiO_2-axis can be caused by both primary and secondary processes. An increased amount of SiO_2 in magma may be caused during its generation, for example mantle melting at low pressures (Lee et al., 2005) or high-pressure fractionation where garnet is present (Macpherson et al., 2006). This can result in a variety of silicic primary magma of which most will plot within the calc-alkaline field regardless of evolution. Secondary processes such as hydrothermal alteration may both increase and decrease the amount of SiO_2 in volcanic rocks. High-temperature geothermal fluids increase the solubility of silica which will consequently leach out from the rock, while low temperature will cause silica-rich minerals to precipitate out of solution.

Least altered samples from Ngatamariki and Rotokawa have an intermediate rock composition, with SiO_2-values ranging from 55.01 to 61.84 wt. % and 54.72 to 59.44 wt. %, respectively (Appendix 3). Primary silicic minerals such as quartz phenocrysts will therefore not affect the rock classification with regards to SiO_2-content. The large scatter of altered samples in the two diagrams utilising this element is therefore attributed to hydrothermal alteration. Least altered samples have a consistent behaviour in both diagrams, which confirms their lack of compositional changes.

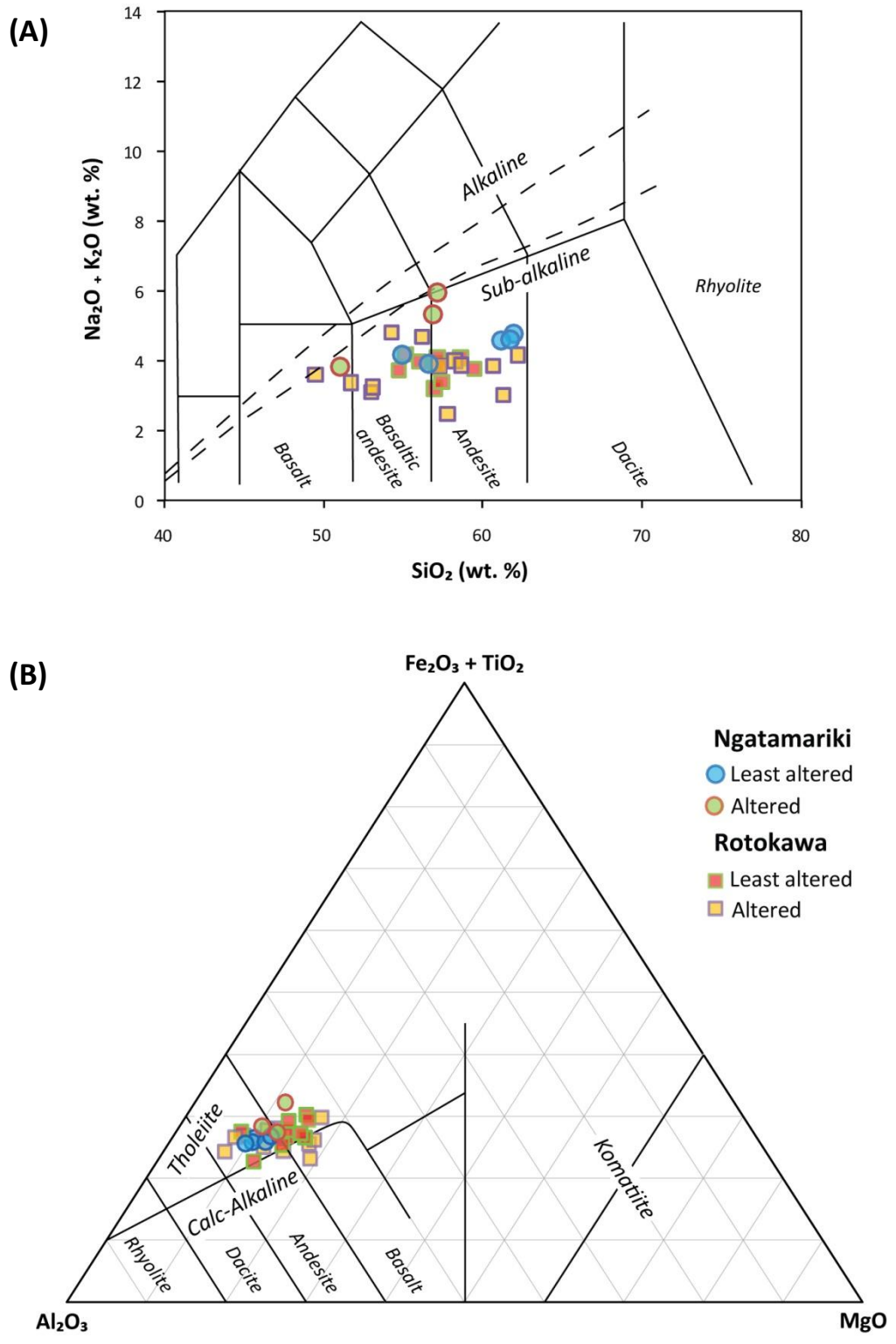

Figure 5.5: a) Rock classification plot of total alkali vs. silica oxide (TAS), diagram is from LeMaitre et al. (1989) and approx. magma series boundary from Rickwood (1989). b) Plot of K_2O vs. SiO_2 in comparison with other volcanic rocks from TVZ. Data sources for TVZ are high-alumina basalt (HAB) from Gamble et al. (1990); Ruapehu rock types 1-4 and 6 from Graham & Hackett (1987); Tongariro Volcanic Centre (TgVC) from Cole (1978), Cashman (1979), IJG unpublished data; Ruapehu rock type 5 including Titiraupenga, Pureora and Karangahape from Graham and Hackett (1987), Cole (1978), Froude & Cole (1985); White Island from Graham & Cole (1991); Rolles Peak, Tauhara andesite and dacite, TVZ silicic volcanic from Cole, (1979), Graham & Worthington (1988). Diagram is from Peccerillo & Taylor (1976).

AFM diagram

The AFM ternary diagram is another tool for rock classification, which plot alkalis ($Na_2O + K_2O$) vs. Fe oxides ($Fe + Fe_2O_3$) vs. MgO (Irvine & Baragar, 1971). These elements were chosen partly due to their stability under low grades of metamorphism. The diagram mainly uses enrichment or depletion of Fe to assign rocks into tholeiitic or calc-alkaline magma series, respectively. This is a rather simplified approach, since magmas display a continuum of Fe-enrichment in a variety of tectonic settings. Even though most subduction zone volcanism is calc-alkaline with characteristic low Fe-contents, there are exceptions such as the Kermadec and Aleutian arcs (Zimmer et al., 2010). A common problem with this original diagram is that all Fe should be converted to FeO which some studies overlook by presenting a sum of all unconverted Fe in wt. %, thus making comparisons unreliable (Rollinson, 1993). A modified version of the AFM diagram by Jensen (1976) utilises elements $Fe_2O_3 + TiO_2$ vs. Al_2O_3 vs. MgO as variables, because he was of the opinion that the alkali component would be affected by alteration processes. The diagram also has the benefit of presenting the data as cation percentage and therefore avoids the conflict of converting Fe.

In this diagram, the least altered samples from Ngatamariki and Rotokawa plot within the basaltic to andesitic fields, belonging mainly to the tholeiitic magma series although with some overlap to calc-alkaline (Fig. 5.6). It appears as even the least altered samples have been reduced in Mg while Fe + Ti contents are higher than normal. The varying classifications of magma series between this diagram and the SiO_2 vs. K_2O or TAS diagrams may be explained by the type of alteration minerals present at Ngatamariki and Rotokawa. Ferromagnesian minerals become unstable at lower temperatures than plagioclase (Chapter 4), so alteration minerals like chlorite occur at early stages in greater abundance compared to those which replace plagioclase, such as K- or Na feldspar. This is why false classification by the AFM diagram at weak alteration intensity is not unexpected. The different results from these three classification diagrams (Fig. 5.4-6) emphasize the mobility of major elements even in least altered samples.

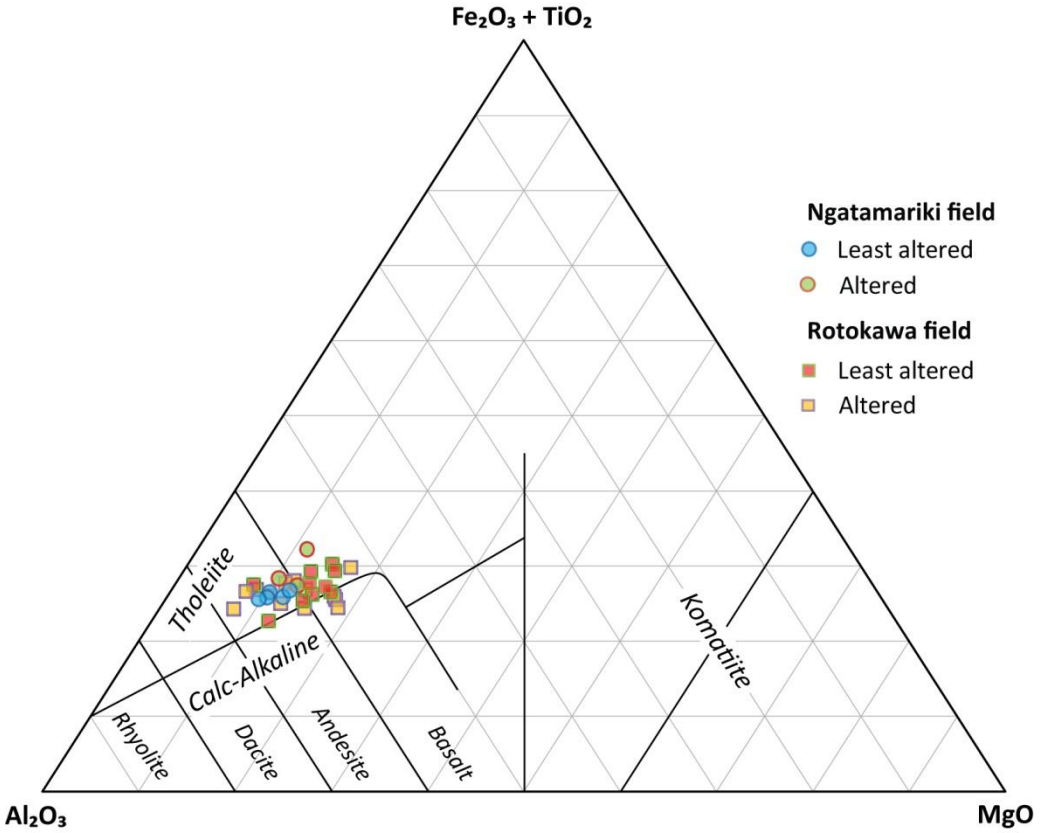

Figure 5.6: Al, FeO and MgO (AFM) ternary diagram (from Irvine & Baragar, 1971, modified by Jensen, 1976).

5.3.2 Rock classification with trace elements

Rock classification diagrams utilising ratios of HFS elements were developed in the 1970's (e.g. Pearce & Cann, 1973; Winchester & Floyd, 1977) to identify the original tectonic setting and primary composition of altered volcanic rocks. This is done by comparing trace element concentrations of altered rock with unaltered rock, for which the tectonic setting has been established by traditional methods. The trace elements chosen for this purpose need to have greater concentration variations between magma types than between rocks of the same magma type, be easy to measure and insensitive to alteration. Diagrams of this type commonly plot immobile elements such as TiO_2, Zr, Nb and Y. Pearce & Cann (1973) recognised the sensitivity of Nb/Y in relation to tectonic settings, as the ratio increases from tholeiitic to alkaline magma series.

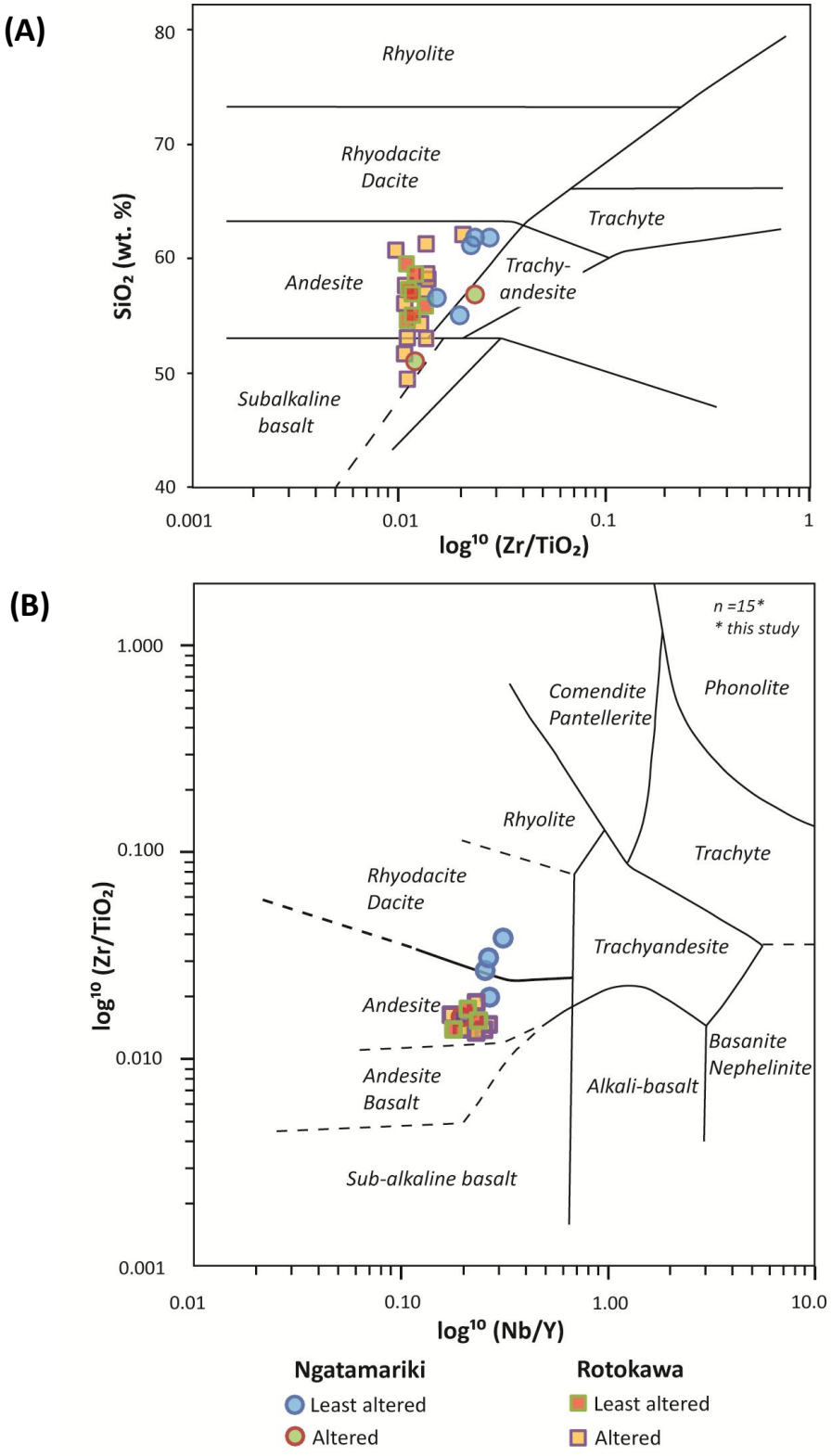

Figure 5.7: a) Rock classification plot of SiO_2 vs. ratio of Zr/TiO_2. Least altered samples from Rotokawa and most from Ngatamariki plots within the andesitic field (from Winchester & Floyd, 1977); b) Rock classification plot of ratios Zr/TiO_2 vs. Nb/Y. Least altered samples from Rotokawa form a small cluster in the andesitic field together with all altered samples, while least altered samples from Ngatamariki form a linear trend from andesitic to dacitic fields (from Winchester & Floyd, 1977).

A plot of SiO_2 vs. Zr/TiO_2 was originally used for testing the sensitivity of Zr/TiO_2 to differentiation of basic magma (Winchester & Floyd, 1977). The ratio was found to increase in relation to SiO_2 from basalts to rhyolites, reflecting the decline of TiO_2-content in felsic rocks. Also, a strong concentration of Zr in alkaline rocks caused an increased ratio compared with tholeiitic rocks. A combination of the two ratios, Nb/Y vs. Zr/TiO_2, will return both rock composition and magma series.

Whereas least altered samples from Ngatamariki and Rotokawa showed a large scatter from basaltic to andesitic composition in classification diagrams based on major elements, they are now plotting in smaller clusters within the andesitic (Fig. 5.7a) or andesitic to dacitic (Fig. 5.7b) fields belonging to the sub-alkaline magma series. Altered samples still have a large range along the SiO_2-axis in Fig. 5.7a due to silica depletion or enrichment. The same samples are however tightly clustered together in Fig. 5.7b, while least altered samples spread out along the Zr/TiO_2-axis. This is a result of increasingly evolved rock compositions rather than hydrothermal alteration, with the more felsic samples from Ngatamariki plotting correctly within the dacitic field and less felsic samples from Rotokawa within the andesitic field. With no sign of scattering, HFS elements Zr, Ti, Nb and Y appear to be unaffected by hydrothermal alteration.

Barrett et al. (2005) created a simplified version of the diagrams by Winchester & Floyd (1977), a plot of Zr vs. Y where the ratio varies distinctively with magma series. Tholeiitic and transitional rocks typically have a linear trend in this diagram caused by increasing incompatible enrichment from basalts to rhyolites, whereas plots of calc-alkaline rocks are scattered with poor correlation due to varying compatibility of the two elements. The least altered samples from Ngatamariki and Rotokawa plot differently, as Ngatamariki samples plot in a linear trend from transitional to calc-alkaline magma series, while Rotokawa plot in a tight cluster in the transitional magma series (Fig. 5.8).

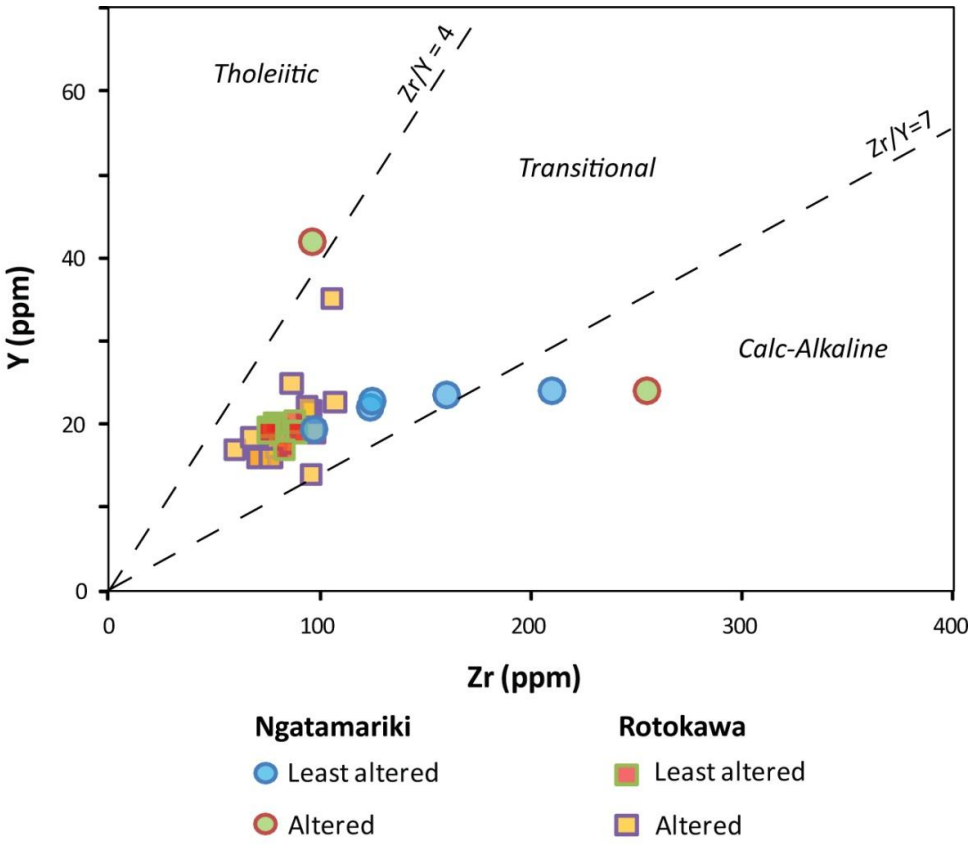

Figure 5.8: Rock classification diagram of magma affinities with Zr vs. Y, where the ratios are <4 for tholeiites, 4-7 for transitional and >7 for calc-alkaline rocks (from Barrett et al., 2005).

5.3.3 Summary

All of the rock classification diagrams have plotted the least altered samples from both fields as sub-alkaline. Diagrams based on major elements were expected to return false classifications due to mobilization during alteration, with one diagram (SiO_2 vs. K_2O) identifying them as calc-alkaline and another (AFM ternary diagram) as mainly tholeiitic. A third diagram based on presumably immobile trace elements (Zr vs. Y) classified them to be transitional to calc-alkaline in nature. Suggestions of rock types ranged from basaltic to dacitic, although the diagram utilizing immobile elements (Nb/Y vs. Zr/TiO_2) showed the least amount of scattering. It identified samples from Rotokawa as andesitic and Ngatamariki as andesitic to dacitic.

Of the 15 least altered samples from Hughes igneous spectrum, almost all have plotted in a relatively small cluster without noteworthy reactions to major- or

trace elements used in the classification diagrams. Least altered samples from Ngatamariki have plotted in a linear trend along the axis where Zr has been used alone or in combination with TiO_2. This is probably due to variation in primary composition rather than alteration, as the petrological investigation in Chapter 3 revealed a more felsic mineralogy compared to Rotokawa. The least altered samples summarised in Table 5.2 can now be used for confirming immobile elements and to calculate precursor compositions.

5.4 Immobile elements

In order to correlate rock units and for calculating mass changes of altered rocks, immobile element pairs (e.g. HFSE) are required in addition to least altered samples. The mobility of trace elements is mainly controlled by mineralogical changes caused by hydrothermal alteration and the nature of the fluid phase (Rollinson, 1993). As a rule of thumb, elements with intermediate ionic potential (3-10) are relatively insoluble and tend to remain in the rock during alteration (e.g. HFSE and some REE). Exceptions do however occur; a study of the Kermadec Arc found slightly increased mobilization of the HFS element Hf in a sediment-rich subduction zone (Todd et al., 2010). The immobility of Ti, Zr, Y and Nb has however been well documented as discussed in previously in this chapter, and is often used in classification diagrams of altered volcanic rocks in TVZ and elsewhere (e.g. Ewart, 1977; Mc Culloch & Gamble, 1992; Gamble et al., 1993).

The most basic test to confirm immobility is by plotting potential elemental pairs on bivariate diagrams and check for correlation coefficients (r) exceeding ~0.85 (MacLean & Barrett, 1993). If the elemental pair is immobile, variably altered samples from a single precursor system should form a highly correlated line from the origin and through least altered samples. The linear trend is a result of mass gain or loss of mobile elements in the altered samples (Gifkins, 2005). If the dataset is large, there are more efficient element analysis methods to use. Both covariance and correlation matrixes may be employed to find linear relationships of elements and samples with some sort of association.

Table 5.3: Correlation matrix of potential immobile elements in samples from Ngatamariki and Rotokawa fields. MgO and K_2O are added as examples of correlation between mobile elements. Calculated from major- and trace element data in Appendix 3.

	TiO_2	Al_2O3	MgO	K_2O	Th	Pb	Zr	Y	V	Cr	Nb	Ce	Hf	U	W
TiO_2	-														
Al_2O_3	0.51	-													
MgO	-0.17	0.04	-												
K_2O	-0.34	-0.48	-0.23	-											
Th	-0.29	-0.19	0.23	-0.15	-										
Pb	0.03	-0.10	-0.04	-0.33	0.19	-									
Zr	0.58	-0.13	-0.36	0.14	-0.25	-0.13	-								
Y	0.48	0.03	-0.48	-0.06	-0.04	0.26	0.32	-							
V	0.00	0.54	0.25	-0.22	-0.06	0.00	-0.65	-0.21	-						
Cr	-0.61	-0.34	0.37	0.17	0.14	-0.05	-0.16	-0.46	-0.13	-					
Nb	-0.35	-0.36	-0.50	0.31	**0.86**	-0.27	**0.97**	0.69	**-0.72**	0.18	-				
Ce	-0.17	-0.34	-0.21	0.04	0.64	-0.13	**0.79**	0.53	-0.54	0.22	**0.78**	-			
Hf	-0.26	-0.16	-0.35	0.32	0.63	-0.52	0.61	0.38	-0.36	0.19	0.65	0.32			
U	-0.20	-0.18	-0.04	0.41	0.67	-0.32	0.49	0.31	-0.31	-0.11	0.54	0.30	0.51		
W	-0.22	-0.20	-0.02	-0.07	0.22	0.12	0.09	0.07	-0.26	0.52	0.06	0.13	0.06	-0.20	-

Covariance relationships are however affected by the magnitude of elements and will therefore blow up the importance of these elements. Association should therefore be measured by a correlation matrix which represents the inter-element correlations only, and all elements have equal representation (Davis, 1986).

Compatible vs. incompatible pairs such as TiO_2 vs. Zr which are normally reliable immobile elements show a weak correlation in this dataset (Table 5.3). The reason for this is probably due to the range of rock types (basaltic andesite-dacite) as they will have different fractionation processes, so a good correlation is not expected between compatible vs. incompatible elements. Ti, for example, is preferentially taken up by Fe-Ti oxide phases (compatible) during crystallization of mafic magma and will therefore be depleted in the melt at late stage fractionation of felsic magma (incompatible). The opposite happens to Zr, which is progressively enriched in early stage fractionation and will only be included into the lattice of crystallizing zircon. A key factor is that the correlation matrix indicates a good correlation of incompatible HFS elemental pairs such as Zr vs. Nb, Zr vs. Ce and Nb vs. Th, which confirms their resistance to hydrothermal alteration at Ngatamariki and Rotokawa.

Plotted lines representing elemental content of samples show a consistent behaviour of major elements Al_2O_3 and TiO_2 and trace elements V, Ce, Nb and U in both least altered and altered samples, with only minor variations (Fig. 5.9). Others trace elements such as Cr and Pb have large variations, but it occurs in both least altered and altered samples. Major elements MgO and K_2O which were added to the diagram as examples of mobile elements, display large variations in altered samples as expected. An interesting observation is that plotted lines of Zr and Y follow almost an identical pattern in this diagram.

The variation in trace element concentrations can be explained by partition coefficients. Partition coefficients are often used to describe the distribution of trace elements between melt and minerals (Rollinson, 1993). It is calculated by:

$$Kd = C \text{ mineral element}i/\text{melt element}i$$

where *Kd* is the Nernst partition coefficient, and *C* is the concentration of the trace element *i* in ppm or wt. %. A mineral/melt partition coefficient of 1 indicates that the trace element is equally distributed between the mineral and melt. A trace element is regarded to have a preference for the melt if the value <1 and a preference for the mineral if the value is > 1 (Table 5.4). There are many physical variables that may affect the partition coefficients, such as melt composition, temperature, pressure and water content in the melt.

There are a few samples in this study with high Pb-content (16* and LA.44). According to Price et al. (1992) enrichments in Pb relative to Ce and strong depletions of Nb relative to La are typical arc-like signatures of TVZ. Enrichment of Pb can be caused by the involvement of sediment, either directly, through melting in the subducted slab or extracted fluids from the slab. Browne et al. (1992) suggested that the high Pb-value (84 ppm) in sample 16* (micro diorite) could be caused by the presence of galena and sphalerite.

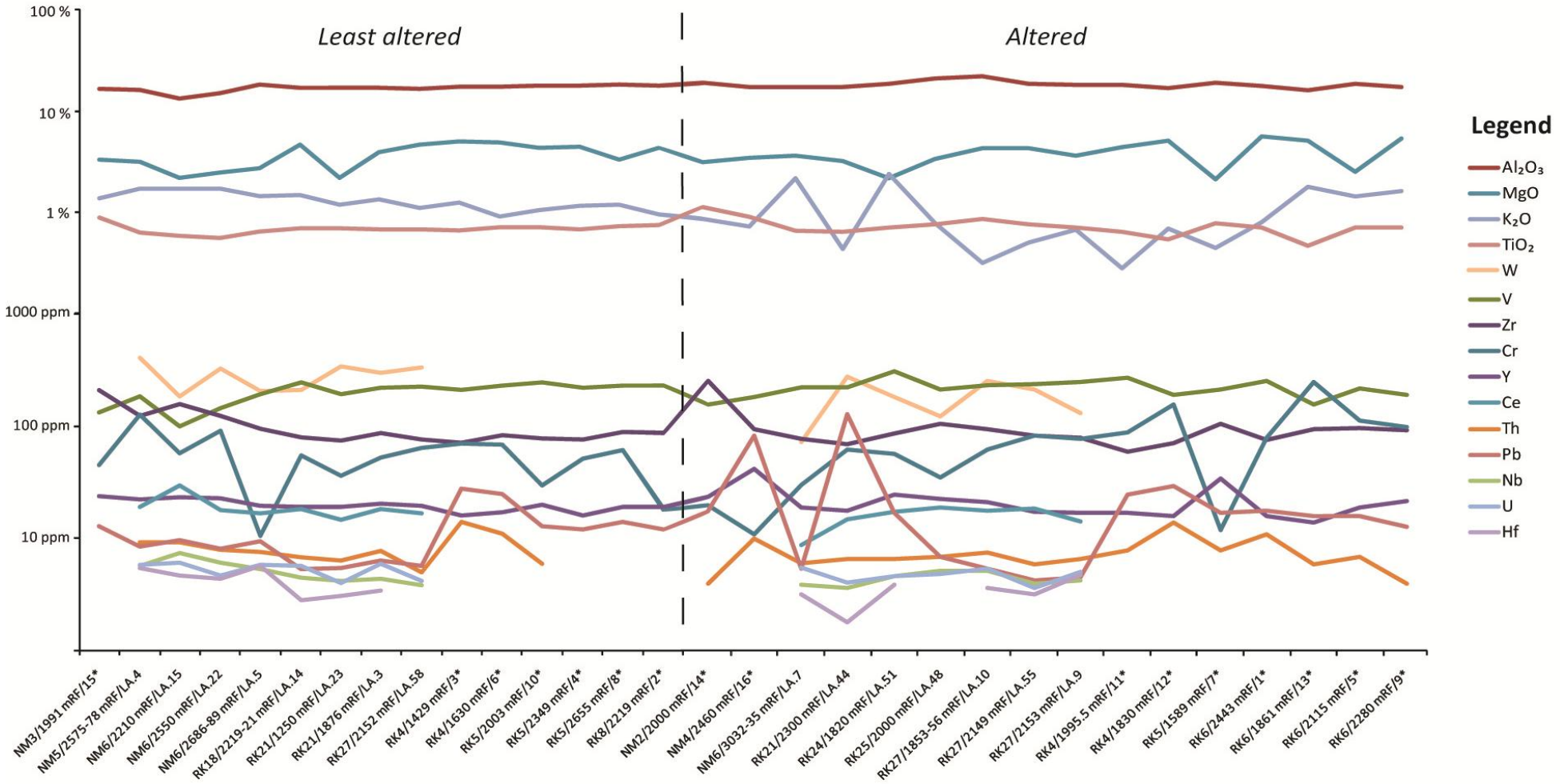

Figure 5.9: Spider diagram of potential immobile elements, K_2O and MgO are included as examples of typical mobile elements. Data from Appendix 3. * = samples from Browne et al. (1992).

The large variations in Cr observed in some samples (LA.7, 7* and 16*) has also been reported in other studies of TVZ andesites (e.g. Cole et al., 1983), where it was attributed to differences in modal content of pyroxene. Cr has a very high partition coefficient (>13) in mafic minerals in andesitic rocks and behaves as a compatible element. The almost identical pattern of Zr and Y suggest that they have similar bulk partition coefficients and are highly incompatible. This means that their content is not likely to change due to fractional crystallization or batch partial melting (Rollinson, 1993).

Table 5.4: Partition coefficients (Conc. mineral element/Conc. melt element) for less mobile trace elements in basaltic andesite, andesite and dacite/rhyolite rocks (data from Rollinson, 1993).

Element	Melt	Clinopyroxene	Orthopyroxene	Hornblende	Biotite	Plagioclase	K-feldspar	Magnetite
V	*Andesite*	1.10	1.10	32.00	-	0.01	-	30.00
Zr	*Andesite*	0.27	0.10	1.40	-	0.01	-	0.20
Cr	*Andesite*	30.00	13.00	30.00	-	0.01	-	32.00
Y	*Andesite*	1.50	0.45	2.50	-	0.06	-	0.50
Ce	*Andesite*	0.25	0.05	-	-	0.20	-	0.20
Th	*Andesite*	0.01	0.05	0.15	-	0.01	-	0.10
Pb	*Dacite/ Rhyolite*	-	-	-	0.77	0.97	2.47	-
Nb	*Andesite*	0.30	0.35	1.30	-	0.03	-	1.00
Hf	*Andesite*	0.25	0.10	-	-	0.02	-	-
U	*Basaltic andesite*	0.04	-	0.10	-	0.01	-	-

5.4.1 Geochemical mapping

Petrographical and geochemical data suggests that there are a wide range of rock types at Ngatamariki and Rotokawa. The rock units with different compositions can be located by transferring plots of the immobile elements to geological cross-sections. As discussed previously in this chapter, a bivariate diagram of immobile incompatible vs. incompatible elements (e.g Zr/Y) normally results in a combined alteration and fractionation line for rock units with similar magma affinity.

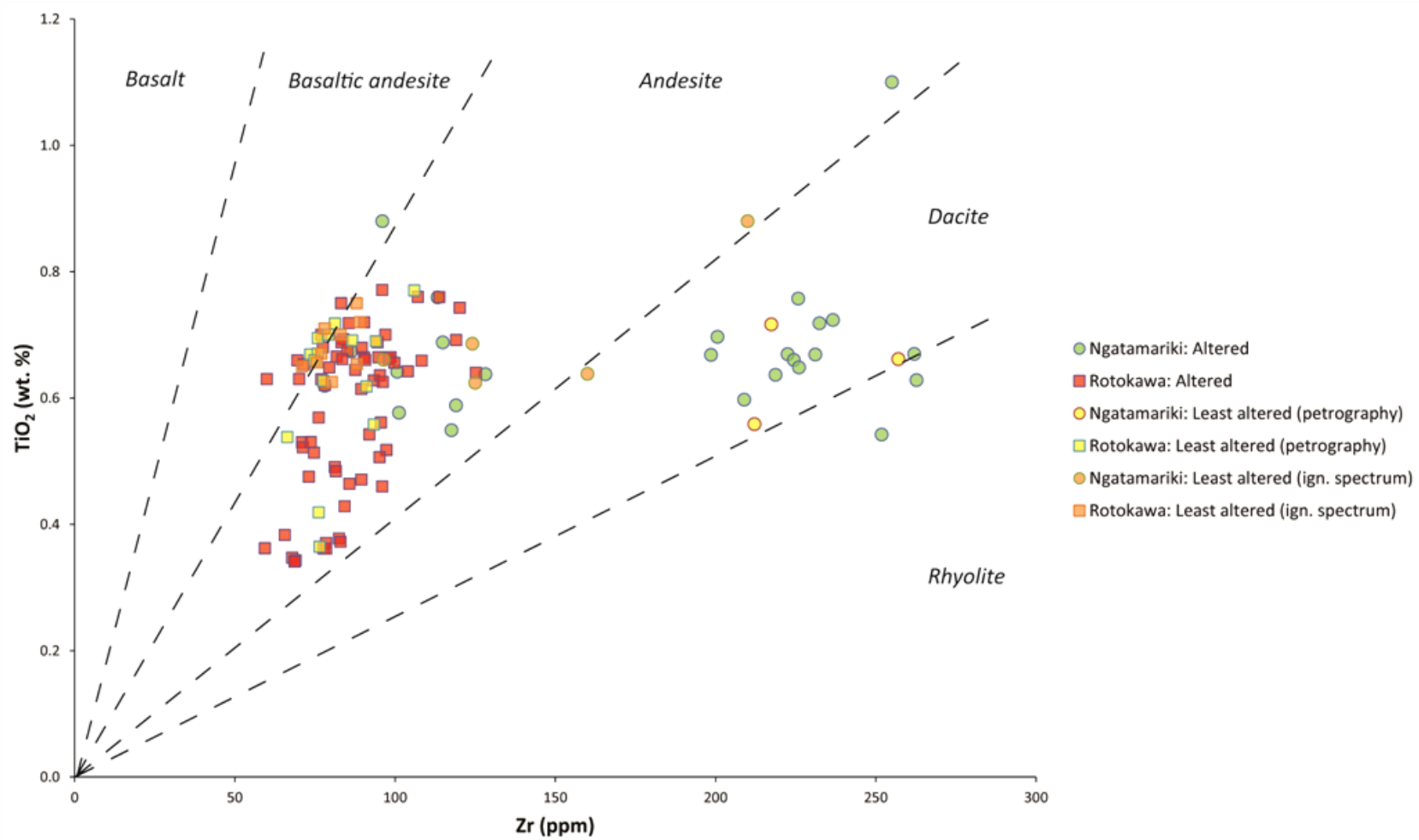

Figure 5.10: Plot of immobile compatible vs. incompatible element pair (TiO_2 vs. Zr), of all samples in this study and in Browne et al. (1992). TiO_2/Zr ratio is obtained by converting TiO_2 wt. % to ppm, multiplying wt. % by 5995. Basalt is <119, basaltic andesite is 54-119, andesite is 24-53, dacite is 16-23 and rhyolite is <16 (Ratios for basalt and dacite are from Winchester & Floyd, 1977; basaltic andesite and andesite are from Hallberg, 2001). Data from Appendix 3.

A similar diagram of immobile compatible vs. incompatible elements (e.g. TiO_2/Zr) create separate alteration lines for each homogenous rock unit, thus making it possible to identify samples with similar compositions which can be used for geochemical mapping. The rock classification diagram Zr/Ti vs. Nb/Y shown in Fig. 5.7b in previous section returned the least amount of scattering among the selected Ngatamariki and Rotokawa samples. Zr was confirmed immobile by a high correlation coefficient (>0.79) despite the range of rock types included in the correlation matrix (Table 5.3), while TiO_2 displayed a uniform behaviour in least altered and altered samples (Fig. 5.9). These elements will therefore be used for a more detailed and extended rock classification of Ngatamariki and Rotokawa samples. All samples from this study and Browne et al. (1992) have been included into the bivariate diagram of TiO_2 vs. Zr (Fig. 5.10), and they have been divided into three main groups:

- ✧ least altered as established by Hughes igneous spectrum (Fig. 5.4);
- ✧ least altered samples according to petrography, and
- ✧ all other samples, ranging from moderate to intense alteration.

There is a large scatter in the diagram, and outliers from Ngatamariki are found amongst Rotokawa samples. There is a boundary separating Rotokawa and most of Ngatamariki samples at ~125 Zr (ppm). Rotokawa samples appear to have a predominant andesitic composition with a high TiO_2/Zr ratio (27 to 63), while most Ngatamariki plot on the right hand side and hence have a low TiO_2/Zr ratio (13 to 24). The outliers from Ngatamariki with a more mafic composition have similar TiO_2/Zr ratios as Rotokawa (28-55). Least altered together with altered samples from Rotokawa form a cluster towards the boundary between the basaltic andesite and andesite categories, while least altered samples from Ngatamariki are scattered from andesite to rhyolite categories. However, only 31 of 122 samples were classified into unaltered vs. altered samples by Hughes igneous spectrum, so there might be additional least altered samples which have been overlooked by the petrographical investigation.

By comparing TiO_2/Zr ratios and stratigraphical positions of the samples, the large group of basaltic andesites and andesites were divided into two new groups at a TiO_2/Zr ratio of 42, while dacitic to rhyolitic groups were divided at a TiO_2/Zr ratio of 12. The newly identified five subgroups of the Ngatamariki and Rotokawa andesites (Fig. 5.11) consist of:

- *basaltic andesite*- these samples have a composition close to basaltic andesite with a TiO_2/Zr ratio between 42 to 63, occurring at most depths in well RK21 (1250-2300 mRF) in the southern end of the Rotokawa field whilst becoming progressively deeper towards the north where the last occurrence is below 2686 mRF in well NM6 in the southern end of Ngatamariki;
- *andesite* – these samples have a TiO_2/Zr ratio between 27 and 41 with more scattered locations, interlayering basaltic andesite in well RK21 in the southern end of the Rotokawa field while overlying the basaltic andesites towards north with the last occurence below 2575 mRF in well NM5;
- *andesite-dacite* – there are very few samples with this composition (TiO_2/Zr ratio between 24 and 26), but they seem to form a thin layer above andesitic units at Ngatamariki;
- *dacite* – these samples have a TiO_2/Zr ratio between 16 to 21, typical of the shallow units at Ngatamariki; and
- *rhyolite* – these few samples have a TiO_2/Zr ratio between 13 and 15 and form a thin unit in well NM6 at 1480-1630 mRF.

The diorite encountered in well NM4 has a ratio of 55, similar to the basaltic andesites found at Rotokawa and the southern end of Ngatamariki field.

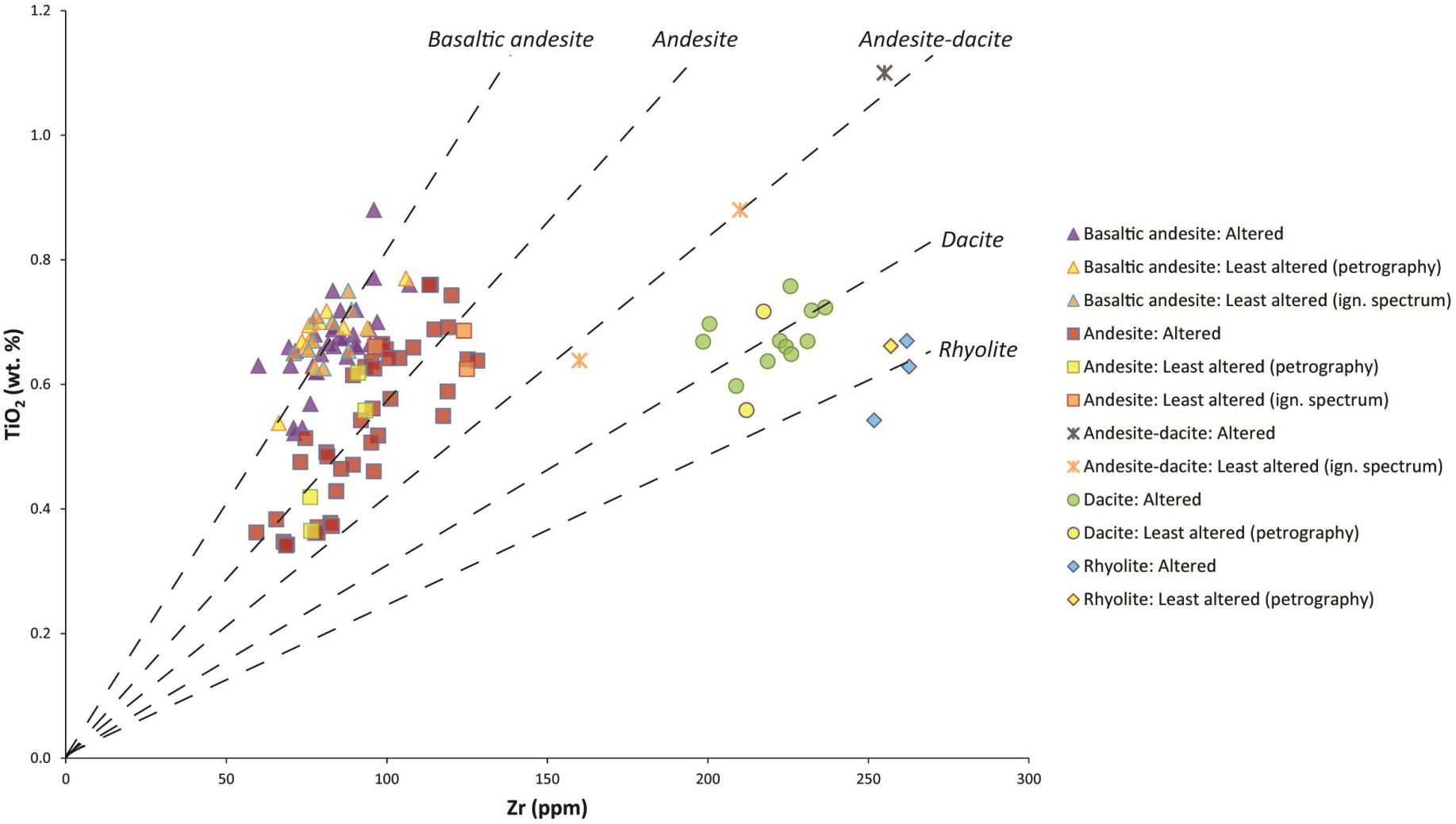

Figure 5.11: A modified version of the classification diagram in Fig. 5.10, with the five subgroups highlighted by different markers. Clusters with similar TiO_2/Zr ratios suggest that rock groups at Ngatamariki and Rotokawa consist of basaltic andesite (42-63), andesite (27-41), andesite-dacite (24-26), dacite (16-21) and rhyolite (13-15).

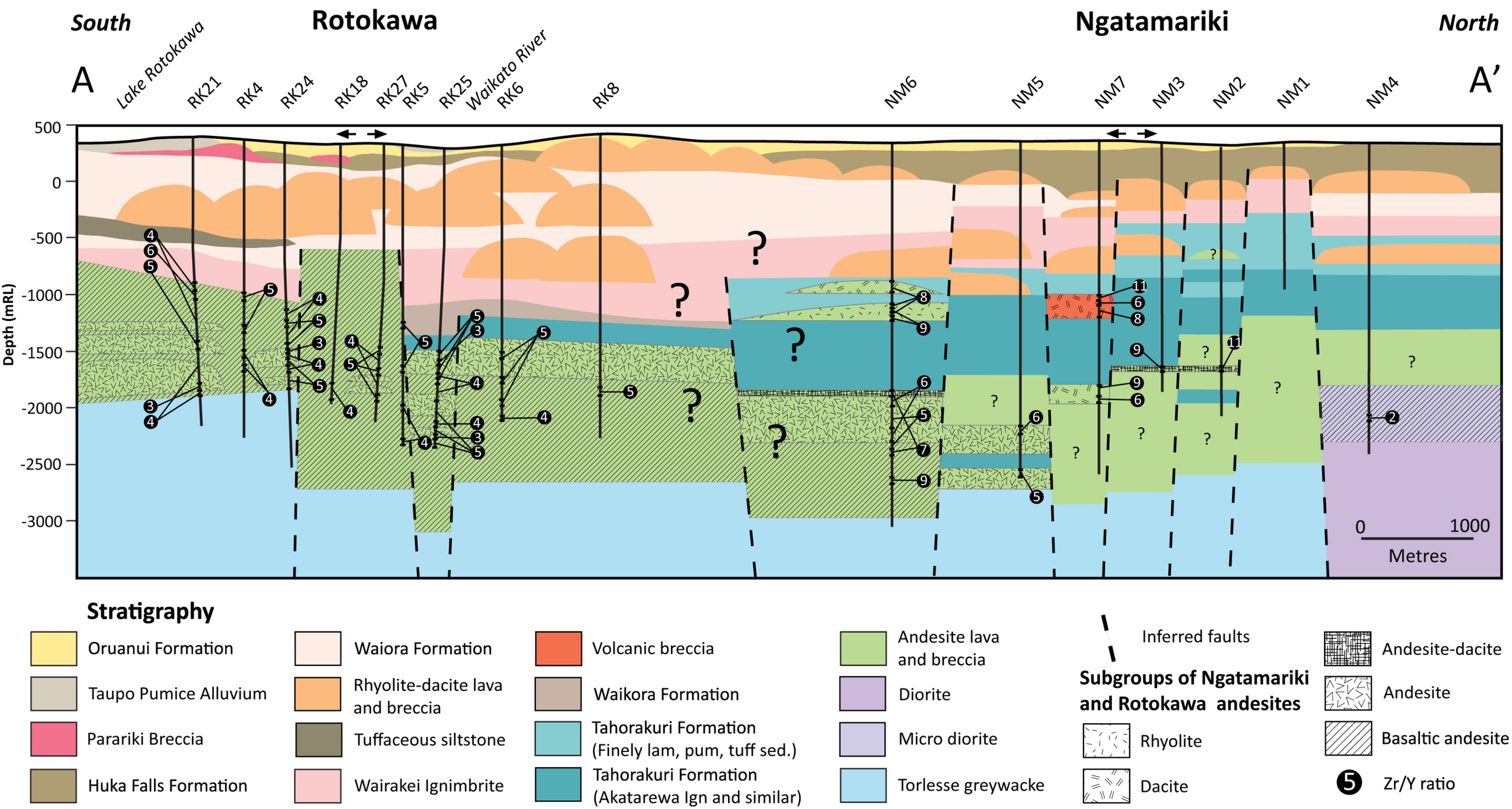

Figure 5.12: Cross –section of field area with TiO_2/Zr and Zr/Y ratios for rock classification and indication of magma affinity (data from Appendix 3).

Some of the samples were collected in regular down-hole intervals in wells NM6, NM7, RK21, RK24, RK25 and RK27. Samples cover 650 to 900 m in each of the Rotokawa wells, although samples are scarce from Ngatamariki wells. Samples cover 300 m of deep and 600 m of shallow rock units from NM6 (separated by a unit of ignimbrite) in addition to 70 m of volcanic breccia from NM7. By creating a simple scatterplot of the ratios, it is possible to see how the rock composition has changed with depth over time (Fig. 5.13-15).

RK21 (1250-2300 mRF)

This well is located at the southern end of the Rotokawa field. The Rotokawa Andesite has been described as a hornblende-pyroxene andesite lava (Ramirez et al., 2008). Starting from the lowermost point where the unit rests directly above greywacke basement, the first 50 m consist of a layer where the composition changes sharply from basaltic andesite to andesite (Fig. 5.13a). This is followed by a 500 m thick andesitic layer with an average TiO_2/Zr ratio of 30. The ratio increases to 53 over the next 350 m as the rocks become progressively younger, which borders to a composition of basaltic andesite. During the final 200 m, the ratio stabilizes at an average of 50. Next in the stratigraphy is the 330 ka Wairakei Ignimbrite, followed by the Waiora Formation, Haparangi Rhyolite and surficial deposits of hydrothermal breccias and fluvial sediments.

RK24 (1505-2155 mRF)

Although this well is situated ~1 km to the northeast of RK21, the Rotokawa Andesite is in the same stratigraphical position. The unit has been described as a pyroxene andesite lava with intercalated andesite tuff and breccias (Ramirez & Rae, 2009), which is consistent with the geochemical composition. The lowermost samples reveal a 500 m thick andesitic unit with an average TiO_2/Zr ratio of 41, while the uppermost 200 m is a basaltic andesite with an average ratio of 54 (Fig. 5.13b).

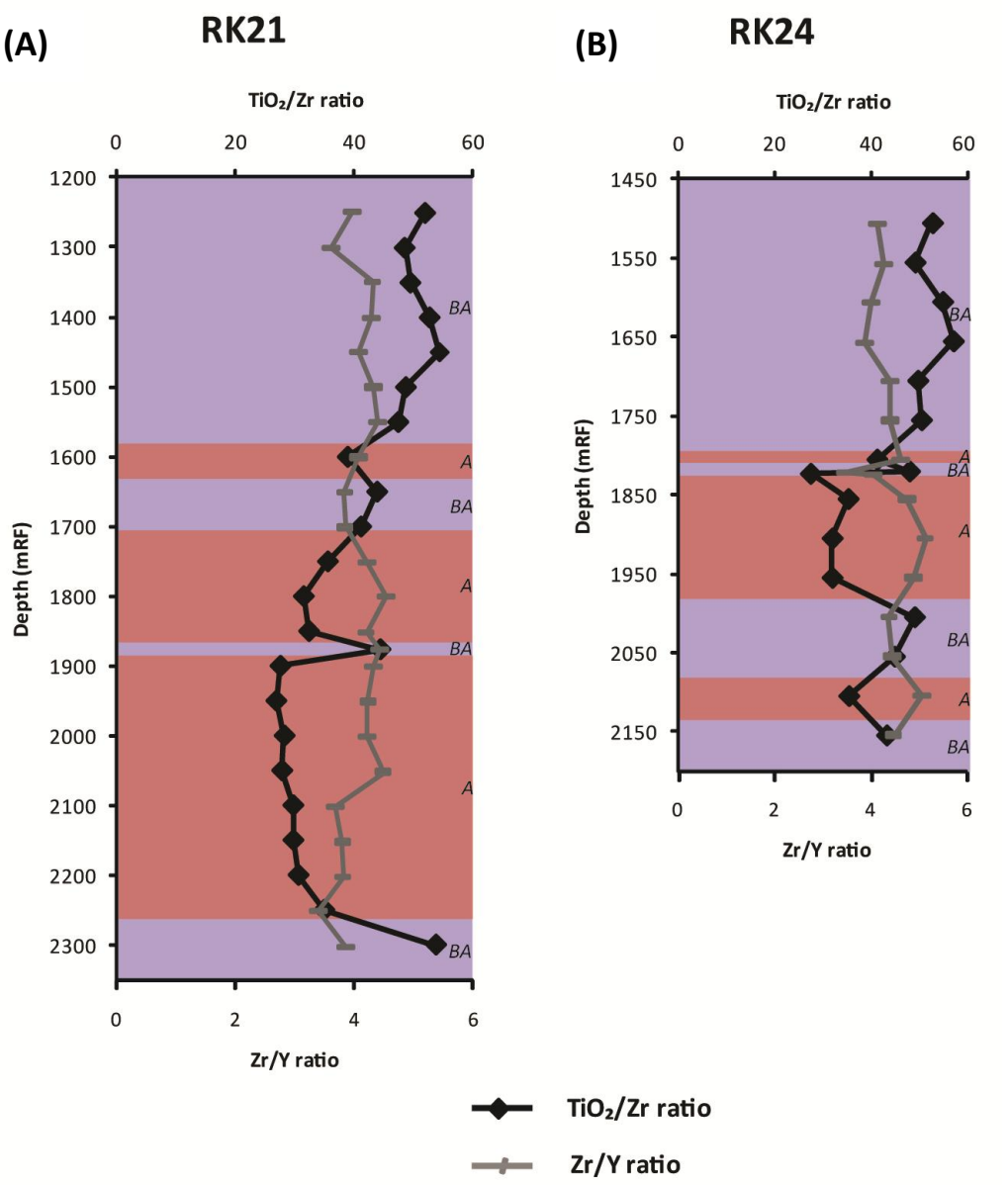

Figure 5.13: Down-hole ratios of TiO_2/Zr and Zr/Y in well a) RK21 and b) RK24 at the Rotokawa field (data from Appendix 3). BA = basaltic andesite, A = andesite.

RK25 (1835-2705 mRF)

Another ~1 km to the north-northwest of RK24, the Rotokawa Andesite is deeper down in the ground compared to RK21 and RK24. Drilling ended in andesite at 2705 mRF instead of greywacke basement, so the well might be situated above a down-faulted section of the field. This unit has been described as a pyroxene-andesite lava with intercalated andesite tuff/breccia (Ramirez et al., 2008) which is consistent with

the geochemical composition. Samples here have smaller, evenly spaced variations within an andesitic rock composition, the TiO_2/Zr ratio ranging between 30 and 47 every few hundred meters (Fig. 5.14a).

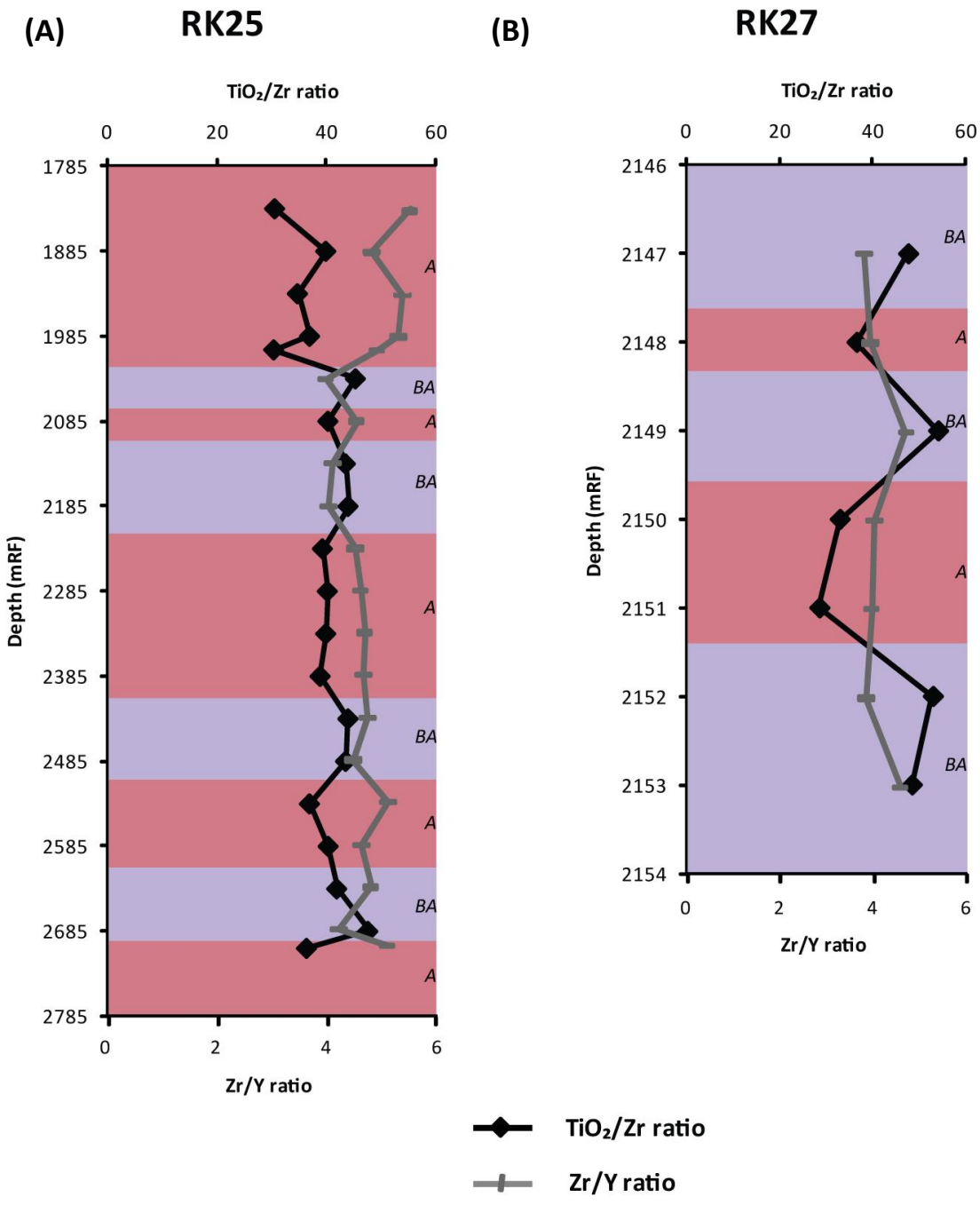

Figure 5.14: Down-hole ratios of TiO_2/Zr in well a) RK25 and b) RK27 at the Rotokawa field (data from Appendix 3). BA = basaltic andesite, A = andesite.

RK27 core #2 (2147-2153 mRF)

A 6 m-core was retrieved from RK27, which is located in the southwestern side of the Rotokawa field (Fig. 5.14b). The total thickness of the rock unit has not been established due to circulation losses below the Tahorakuri Formation at 1797 mRF. The recovered core has been described as a greenish grey porphyritic andesite lava and breccia, with clasts of andesite (Rae et al., 2009). TiO_2/Zr ratios indicate compositional changes almost every meter, from basaltic andesite to andesite. The core has been described in detail in Chapter 4.4.

NM6 (1280-1330, 1480-1630, 2210-2550, 2686-3035 mRF)

This well is located in the southern end of Ngatamariki field. Drilling intersected a shallow and a deep andesitic unit of Ngatamariki Andesite, separated by ~500 m of Tahorakuri Formation ignimbrite (Fig. 5.15a). The shallow unit is really two thin layers interlayered with Tahorakuri Formation tuff, the topmost described as andesite lava and breccia and the underlying layer as andesite/dacite lava and breccia (Rae et al., 2009). According to TiO_2/Zr ratios, the rock composition of the topmost lava and breccias is dacitic (average ratio of 19), while the lower unit is rhyolitic (average ratio of 15). The lower unit has been described as pale grey porphyritic pyroxene-andesite lava (Rae et al., 2009), which correlates with the TiO_2/Zr ratio. The uppermost samples have an average ratio of 23, which increases to 30 with depth and with only small variations. Below a zone of circulation losses, the final ~250 m of the rock unit have the composition of basaltic andesite.

NM7 (1390-1460, 2179-2184 mRF)

~ 2 km north of NM6, drilling intersected a shallow unit of pale grey, weakly porphyritic volcanic breccia (Rae et al., 2009). The primary composition could not be determined due to intense hydrothermal alteration. According to its TiO_2/Zr ratio of 18, the unit has a consistent, dacitic composition with only minor variations (±2) at either end (Fig. 5.15b).

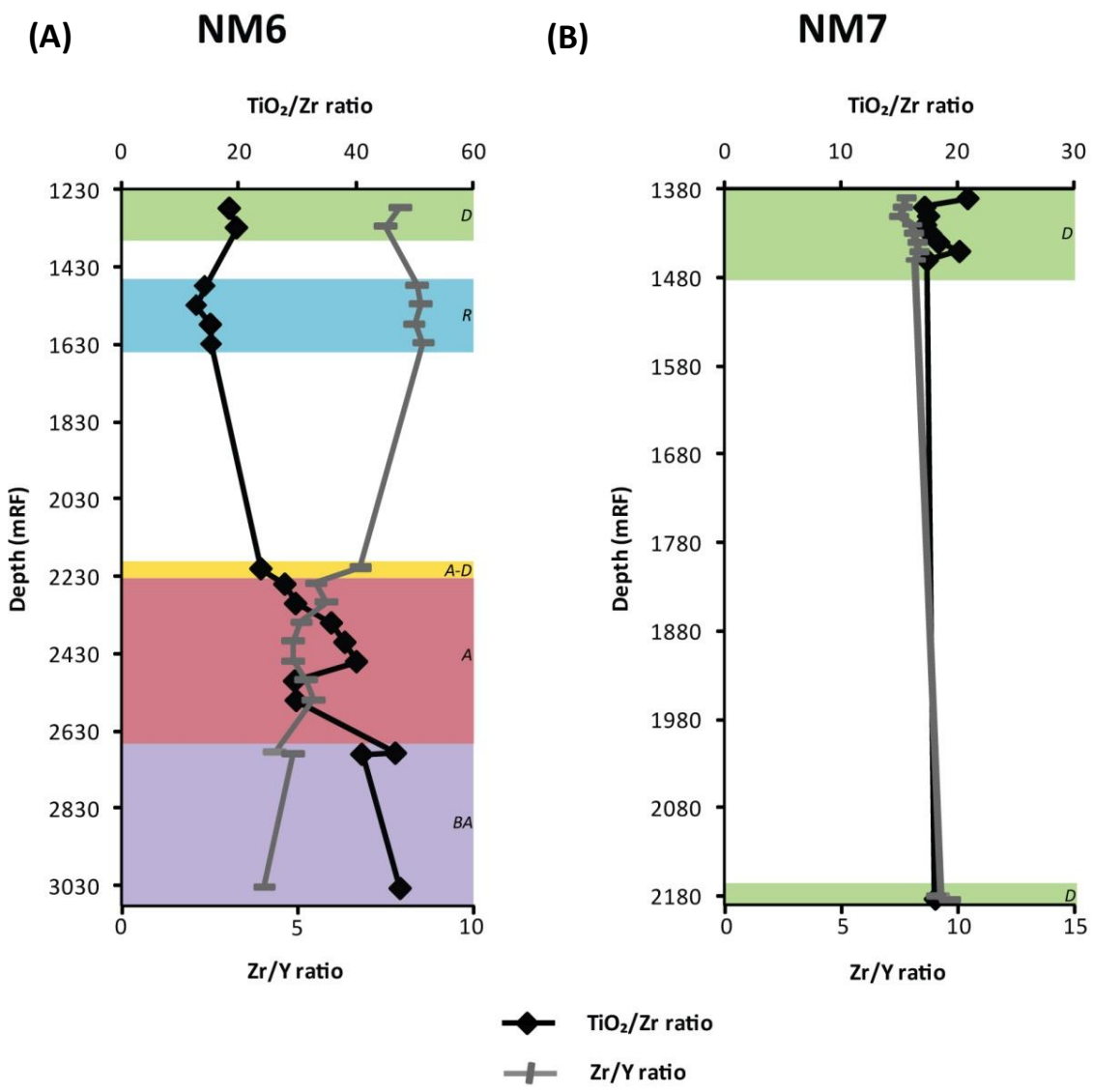

Figure 5.15: Down-hole ratios of TiO_2/Zr and Zr/Y in well a) NM6 and b) NM7 at Ngatamariki field (data from Appendix 3). BA = basaltic andesite, A = andesite, A-D = andesite-dacite, D = Dacite, R = rhyolite.

A few, deeper samples of andesite breccia with clasts of greywacke, granite, diorite, andesite and rhyolite has the same composition as the shallow unit.

5.4.2 Summary

The 10 samples that were identified as altered by Hughes igneous plot (Fig. 5.4) are widely scattered within the units, representing sodic and potassic alteration zones:

- ✧ *Na-altered* – 1* from RK6 at 2443 mRF, 7* from RK5 at 1589 mRF, LA.10 from RK27 at 1853 mRF, 11* from RK4 at 1995 mRF, 14* from NM2 at 2000 mRF, 16* from NM4 at 2460 mRF, and
- ✧ *K-altered* – LA.7 from NM6 at 3032 mRF, 9* from RK6 at 2280 mRF, 13* from RK6 at 1861 mRF and LA.51 from RK24 at 1820 mRF.

By mapping the geochemical composition of rocks, it is possible to correctly identify geological units regardless of the effects of hydrothermal alteration. The TiO_2/Zr-ratios suggest that the volcanic rocks at Rotokawa and Ngatamariki which were initially described as andesitic, instead ranges in composition from basaltic andesite to rhyolite (Fig. 5.12). There are similar variations in TiO_2/Zr ratios between wells at the Rotokawa field, especially RK21 and RK24, whereas RK25 has an extra underlying and overlying unit of andesitic magma. A correlation is therefore more uncertain because of the lack of stratigraphic control. There is a more likely stratigraphic relation between the top basaltic and andesitic units at RK25 and the lower lying units at NM6, the southernmost well at Ngatamariki (Fig. 5.16). The groupings of least altered and altered samples (Fig. 5.11) with unique TiO_2/Zr ratios are likely to represent different rock types at these fields, and least altered samples may therefore be used for estimating the original composition of altered samples in each rock type group.

5.5 Fractionation curves and precursor composition

Precursor composition and hence mass change calculations are based on fractionation curves fitted to plots of major- and trace elements in variation diagrams. The first and still most commonly used variation diagram was created by Harker (1909), which plots silica as abscissa vs. other major elements in an x-y diagram. Harker's theory was that SiO_2 increased with magmatic evolution, and the abscissa would therefore indicate how differentiated a rock sample would be within

a range of mafic to felsic composition. In this study, a ratio of immobile elements (TiO_2/Zr) has proved to be a good indicator of magma differentiation with a low ratio for felsic rocks and a high ratio for mafic rocks, and is therefore used as abscissa instead of a mobile element such as SiO_2. The advantage with the variation diagram is that trends are easily observed within large datasets, and by fitting a fractionation curve to the plots it is possible to determine the kind of process by which magma differentiates (e.g. fractional crystallisation, magma mixing or assimilation). For this study, a 2^{nd} order polynomial trend line is used as it fits the concave fractionation curve created by depletion of compatible elements. The resulting regression equation represents the precursor composition of a specific element.

The regression equation is created by selecting the ratio of an immobile monitor (e.g. TiO_2/Zr) and an element in the dataset of *least altered samples*, create a scatter plot and add the trend line (Fig. 5.17).

Choose to display the regression equation on the diagram, its standard form is:

$$\text{Element} = ax^2+bx+c$$

where *x* is the ratio of immobile monitor. This procedure is repeated for all elements, so they all have a regression equation. By inserting the ratio of immobile monitor from *altered samples* into these equations, the reconstructed composition of each element is returned. Lastly, the mass change is calculated by:

$$\text{Mass change} = \text{Reconstructed composition} - \text{Precursor composition}$$

This technique is based on the behavior of unaltered samples in diagrams where immobile compatible vs. incompatible elements are plotted. Normally, the plotted

points follow a fractionation curve as they are included or rejected from crystallization phases in evolving magma.

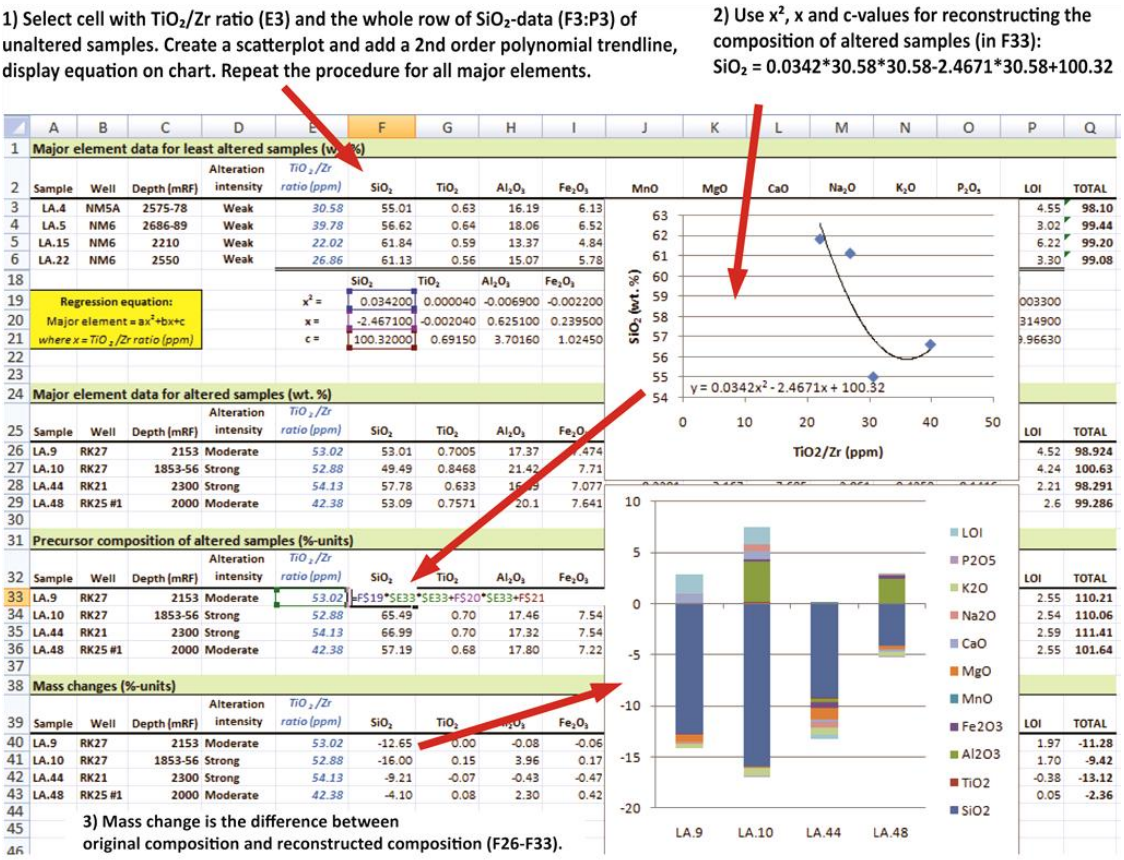

Figure 5.17: Example of layout and calculation of mass changes by multiple precursor method for 4 samples from Ngatamariki and Rotokawa fields.

During alteration, the concentration of certain elements may either be depleted or concentrated, which will move the plotted points and create a secondary alteration line that passes through the fractionation curve. This intersection point represents the precursor composition. But when mobile elements such as SiO_2 and MgO are included into the diagram, the plotted points are displaced randomly without creating an alteration line. So instead of locating the intersection point of a fractionation curve and alteration line for an element to obtain the precursor composition, the ratio of immobile monitor (e.g. TiO_2/Zr) from an altered sample is inserted into the established regression equation which represents the precursor

composition, based on a number of least altered samples. It will return an element's precursor composition at a given ratio of immobile element. In this study, mass change calculations will be performed on major- and trace elements, so precursor compositions will be obtained for both types.

5.5.1 Major elements

The trends observed of major elements in this dataset indicate that a succession of minerals are separated out from the melt with an increasingly felsic composition. This is consistent with Bowen's (1928) theory of a liquid line of descent, which describes the path of residual liquids as minerals crystallises and settles within the chamber at different stages of magma evolution.

A polynomial trendline has been fitted to least altered samples in the diagram. This is not a fractionation line *per se*; it is only tracing the average composition of least altered samples which is then used to calculate precursor composition for the altered samples (Fig. 5.18). Nevertheless, the plots of least altered samples appear to follow a fractionation line seen in many igneous rock suites. At high TiO_2/Zr ratios where the rock composition is near to basaltic andesite (~50), the content of elements MgO and Fe_2O_3 decrease due to the early crystallisation of mafic minerals, such as pyroxene and magnetite and thereby creates a negative trend. The content of elements K_2O, and in lesser extent Na_2O, increases towards a dacitic rock composition (~20); this is because they are concentrated in the melt after all other elements have been removed due to crystallisation and therefore represents a greater proportion of the remaining melt.

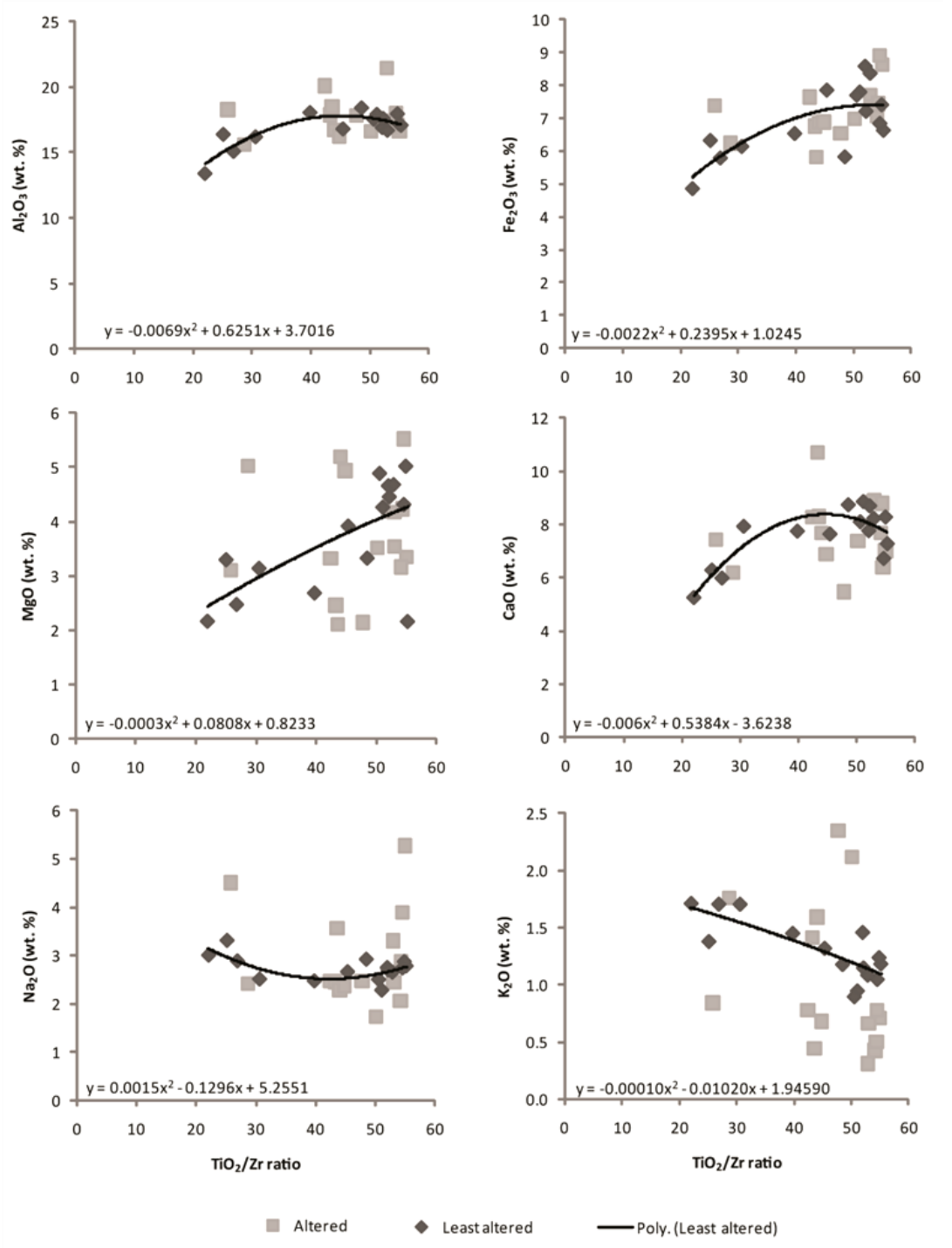

Figure 5.18: Variation diagrams of selected major elements in both least altered and altered samples. TiO_2/Zr ratio replaces SiO_2 as immobile monitor along x-axis. Ratios in this figure are: <16 rhyolite, 16 to 23 dacite, 24 to 53 andesite, 54 to 119 basaltic andesite, >119 basalt. A polynomial trendline and regression equation has been fitted to least altered samples in the diagram. Equations are summarised in Table 5.5. Note that the curves are *not* fractionation lines.

Table 5.5: Regression equations for major element composition derived from least altered samples, where x= TiO_2/Zr (data from Appendix 3).

Element	Regression equation	Element	Regression equation
SiO_2	$y = 0.0129x^2 - 1.1344x + 80.921$	**CaO**	$y = -0.006x^2 + 0.5384x - 3.6238$
TiO_2	$y = 0.00004x^2 - 0.00204x + 0.69150$	**Na_2O**	$y = 0.0015x^2 - 0.1296x + 5.2551$
Al_2O_3	$y = -0.0069x^2 + 0.6251x + 3.7016$	**K_2O**	$y = -0.00010x^2 - 0.01020x + 1.94590$
Fe_2O_3	$y = -0.0022x^2 + 0.2395x + 1.0245$	**P_2O_5**	$y = -0.00006x^2 + 0.00492x + 0.05992$
MnO	$y = -0.00000048x^2 - 0.00021589x + 0.13635920$	**H_2O**	$y = 0.00126x^2 - 0.09357x + 1.65674$
MgO	$y = -0.0003x^2 + 0.0808x + 0.8233$	**LOI**	$y = 0.0033x^2 - 0.3149x + 9.9663$

5.5.2 Trace elements

The variation diagrams of trace elements in unaltered rocks (Fig. 5.19) show trends which indicate that one of the main magmatic processes at Ngatamariki and Rotokawa is fractional crystallisation. This observation is based on the negative slope of compatible (Cr, Sr, V) elements and a positive slope of incompatible elements (Ba, Rb, Y) (Best, 2003). Some elements do however display large scattering in the diagrams. The variation in trace element concentrations can best be explained in terms of partition coefficients, as discussed in Chapter 5.3.2 (Rollinson, 1993; Winter, 2001). A partition coefficient (K_D) defines the concentration of trace element in mineral versus concentration of trace element in melt.

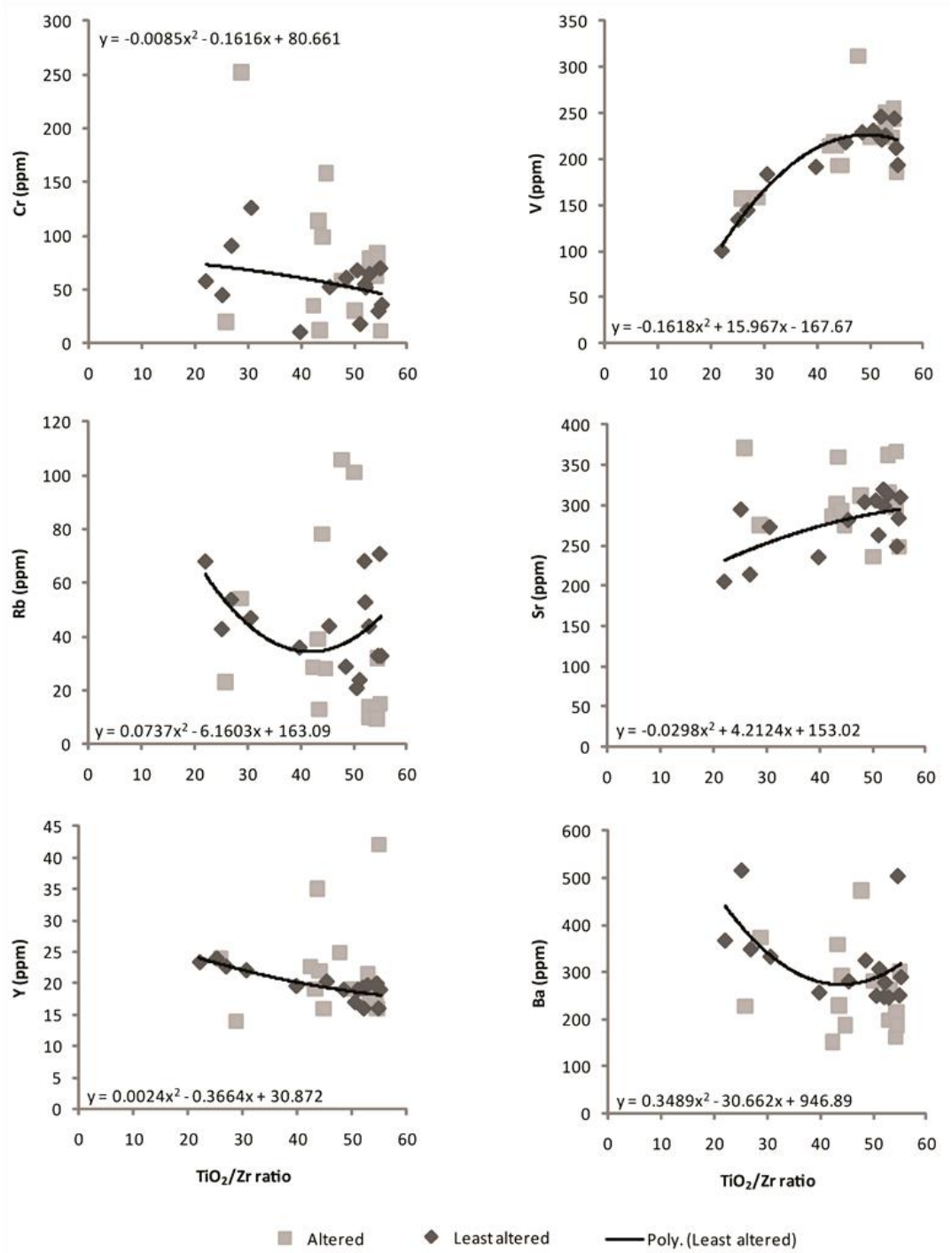

Figure 5.19: Harker variation diagrams of selected trace elements in least altered samples. TiO_2/Zr ratio replaces SiO_2 as immobile monitor along x-axis. Ratios in this figure are: <15 is rhyolite, 16 to 23 is dacite, 24 to 53 is andesite, 54 to 119 is basaltic andesite, >120 is basalt. A polynomial trendline and regression equation has been added to the diagram, this is used to calculate precursor composition for all altered samples. Equations are summarised in Table 5.6. Note that the curves are not fractionation lines.

It is controlled by several factors, such as melt composition, temperature, pressure or ionic potential. Trace elements can either be compatible (K_D >1) or incompatible (K_D <1). Cr for example, has a very high partition coefficient in andesite and normally behaves as a compatible element by being included into the lattice of ferromagnesian minerals, such as clinopyroxene. Sr is another compatible element, which is concentrated in plagioclase at low pressures. Both Cr and Sr show large scatter in their variation diagrams, and Cr even appears to become more abundant in felsic rocks (TiO_2/Zr ratio 20-30) than in mafic rocks (TiO_2/Zr ratio >50).

Table 5.6: Regression equations for trace elements derived from least altered samples, where x= TiO_2/Zr (data from Appendix 3).

Element	Regression equation	Element	Regression equation
V	$y = -0.1618x^2 + 15.967x - 167.67$	**Nb**	$y = 0.0023x^2 - 0.2677x + 11.936$
Cr	$y = -0.0085x^2 - 0.1616x + 80.661$	**Ba**	$y = 0.3489x^2 - 30.662x + 946.89$
Ni	$y = 0.0075x^2 - 0.3691x + 23.517$	**La**	$y = 0.0071x^2 - 0.6542x + 23.886$
Cu	$y = 0.0402x^2 - 2.4434x + 60.182$	**Ce**	$y = 0.0178x^2 - 1.6435x + 53.751$
Zn	$y = 0.0067x^2 - 0.5463x + 84.876$	**Hf**	$y = -0.0048x^2 + 0.3097x + 0.1204$
Rb	$y = 0.0737x^2 - 6.1603x + 163.09$	**W**	$y = -0.0853x^2 + 7.3188x + 145.34$
Sr	$y = -0.0298x^2 + 4.2124x + 153.02$	**Pb**	$y = 0.012x^2 - 0.8174x + 22.865$
Y	$y = 0.0024x^2 - 0.3664x + 30.872$	**Th**	$y = 0.0033x^2 - 0.2906x + 14.061$
Zr	$y = 0.0818x^2 - 9.3062x + 341.87$	**U**	$y = -0.0033x^2 + 0.2265x + 2.0076$

5.6 Mass change calculations

By comparing the compositions of least altered and altered samples, it is possible to calculate mass changes in major- and trace elements that take place during hydrothermal alteration. This is a mathematical technique where the composition of an altered sample deviates from 100% (precursor composition), depending on the degree of alteration intensity. This value may be either negative (mass loss) or positive (mass gain). For example, a gain in a mobile element (X) may decrease the proportion of an immobile element (Z) by dilution. By multiplying all elements in the rock by a ratio of least altered vs. altered content of the immobile element (Z^o/Z^a), it is possible to reconstruct the composition of the altered rock (Fig. 5.20). The net mass gain/loss is then calculated by subtracting the reconstructed composition from

the precursor composition and the result may be displayed as bar graphs for visual comparison. Both precursor composition and mass change is preferably reported as %-units so that it is not confused with how chemical data is normally reported. This type of diagram can be very useful in mineral exploration to locate alteration zones which are associated with hydrothermal mineralisation, such as the typical VMS alteration of sericite-chlorite-quartz near massive sulphide horizons (Barrett et al., 2005). Others have used mass changes to compare the geochemical composition of old vs. young members of a volcanic formation (Hildreth, 1981).

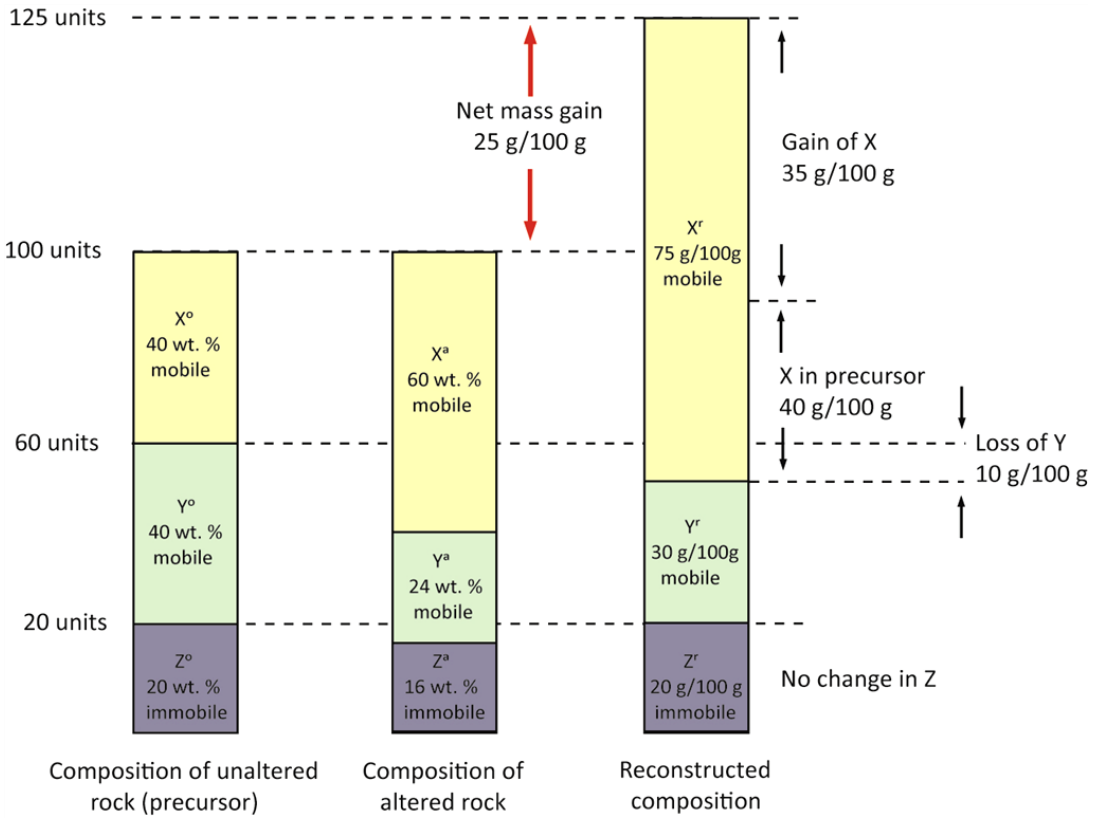

Figure 5.20: Illustration of mass change calculation for an altered rock with an initial mass of 100 units (after Gifkins, 2005). The proportion of immobile element Z^a in the altered rock appears reduced, but has in fact been diluted by the addition of mobile element X^a. To reconstruct the composition of the rock, a factor of Z^o/Z^a is multiplied with all other major elements. In this example, $Z^o/Z^a = 1.25$. If Y^a and X^a is multiplied with this factor there will be a net mass gain of 25 g/100 g.

The most obvious mass change in major elements (Fig. 5.21), is a large gain in Na_2O in samples from Ngatamariki with a basaltic andesite to andesitic composition (14* and 16*). Overall, the largest variations are as both mass gain/loss in SiO_2, followed by lesser amounts of Al_2O_3 and Na_2O. An interesting pattern is that in samples where SiO_2 is depleted, Al_2O_3 is enriched and vice versa. The smaller amount of mass change in Na_2O appears to be connected to Al_2O_3, as they are either enriched or depleted together.

Mass change results can easily be correlated with a geological cross-section in order to identify alteration zones. At Ngatamariki, there is a zone of strongly depleted SiO_2 in the southern end of Ngatamariki field (NM6, -5.4%) near the greywacke basement. Another zone is identified in the centre of the Rotokawa field (RK27, -7.5%) while there is a zone of strongly enriched SiO_2 close to the greywacke basement in the southern end of the Rotokawa field (RK4, +5.9%).

Among trace elements, Ba experiences the most frequent and largest mass changes (on average -58 ppm-units), followed by W (-50 ppm-units) while Zn has the largest mass gains (on average +38 ppm-units). Ba is normally incompatible, but may substitute for K in micas, K-feldspar or hornblende (Winter, 2001).

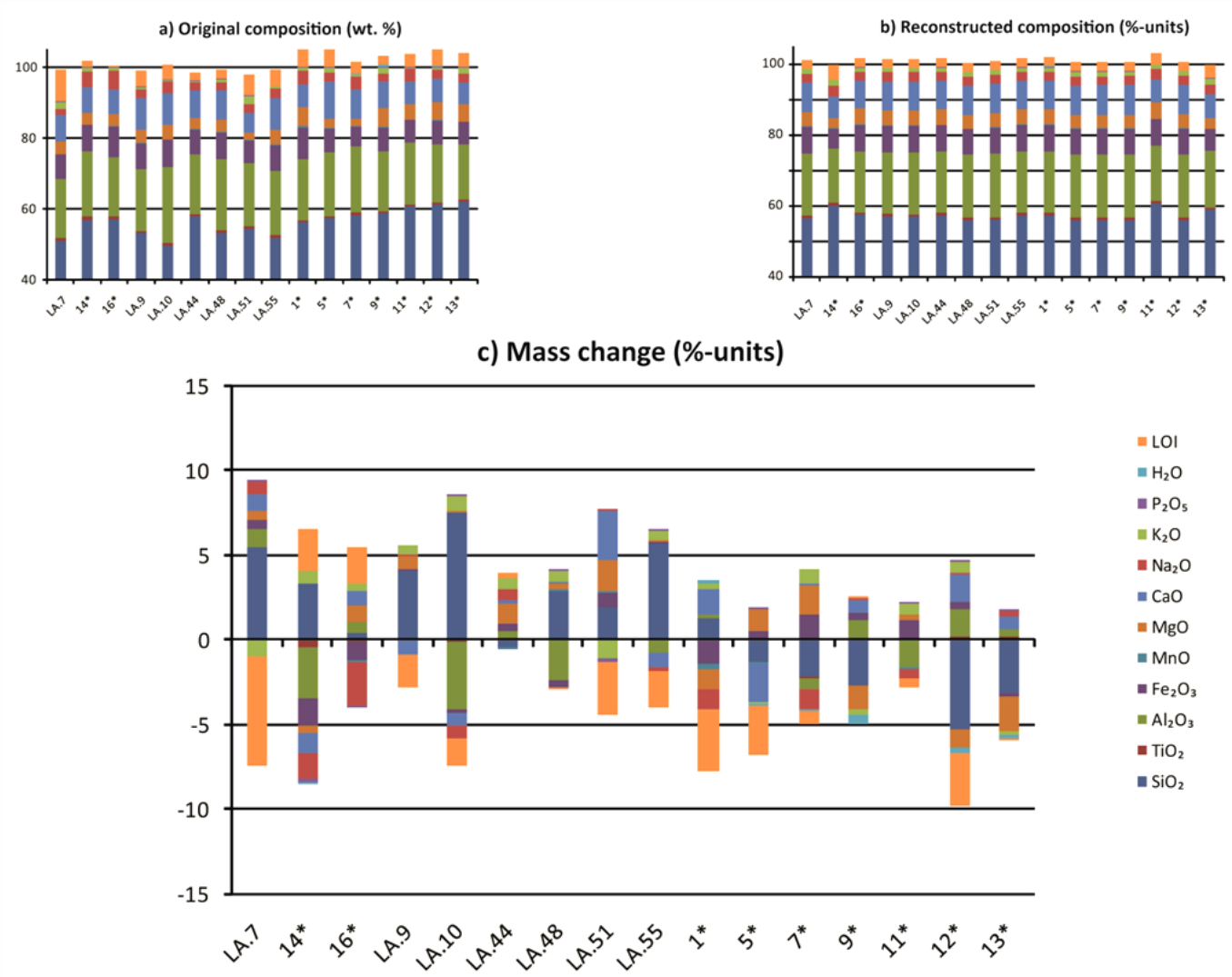

Figure 5.21: a) Original content of major elements where the average sum is 100.71 ±2.04 %, the samples have not been normalised to 100% before mass change calculations. b) Precursor composition of altered samples (%-units), calculated by fitting a 2nd order polynomial trendline to bivariate plots of each major element in unaltered samples vs. TiO_2/Zr ratio (ppm). The resulting regression calculation is then used to calculate the precursor composition of all altered samples. c) Diagram representing mass-change in altered samples (%-units), positive number is mass gain and negative number is mass loss. Numerical results can be found in Appendix 4.

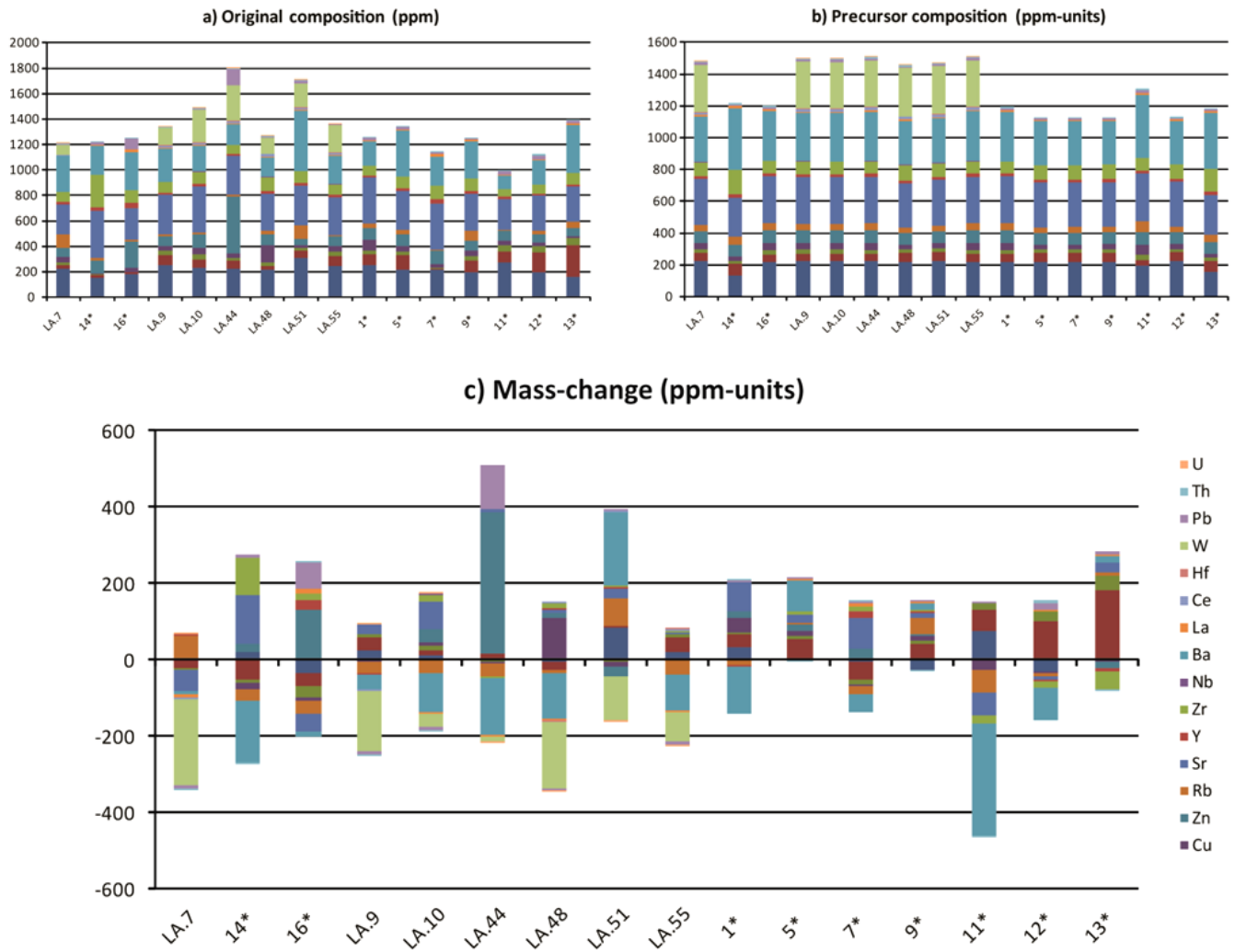

Figure 5.22: a) Original content of trace elements. b) Precursor composition of altered samples (%-units), calculated by fitting a 2nd order polynomial trendline to bivariate plots of each trace element in unaltered samples vs. TiO_2/Zr ratio (ppm). The resulting regression calculation is then used to calculate the precursor composition of all altered samples. c) Diagram representing mass-change in altered samples (%-units), positive number is mass gain and negative number is mass loss. Numerical results can be found in Appendix 4.

Four altered samples from basaltic andesite (TiO_2/Zr ratio 43 to 55) recovered from RK6 give insight of mass change variation with depth, with alternating layers of small (± 2 %-units) mass changes in major elements within a 600 m range (Fig. 5.23). Trace elements Cr, Ba and Sr have experienced a few, larger (<150 ppm-units) variations.

1589 mRF

In the topmost sample (7*), there has been a mass loss of K_2O and Fe_2O_3, MgO and a mass gain in CaO and SiO_2, compared to the precursor composition. This could mean dissolution of ferromagnesian minerals and the formation of silicic minerals instead. There is also a mass gain in Sr which can be concentrated in plagioclase, or less common in adularia.

2115 mRF

Almost the reverse change has taken place in the underlying sample (5*), where there has been a mass loss in CaO and SiO_2, and a mass gain in Fe_2O_3 and MgO. A loss in silica and gain in magnesium is common during the formation of chlorite. A mass gain in Cr suggests large amounts of clinopyroxene, while Ba may be substituting for K in adularia or hornblende.

2280 mRF

This trend has continued in the next sample (9*), except for a zero change in CaO and a small gain in K_2O. Potassic enrichment could mean the formation of adularia or hydrothermal biotite which is commonly iron-rich. A mass gain in Rb could be due to substitution for K in mica or K-feldspar, while a mass loss in V indicates a decreased quantity in Fe-Ti oxides.

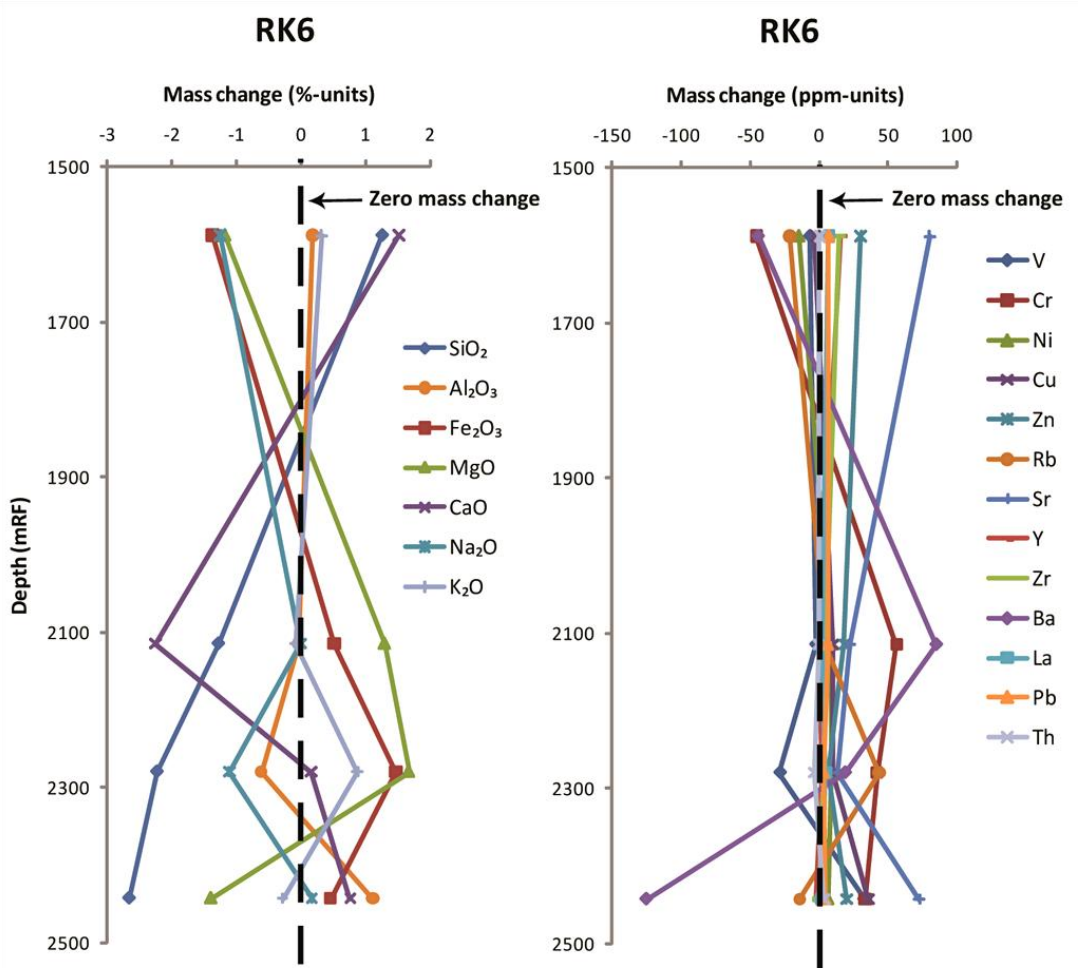

Figure 5.23: Down-hole plot of mass change in well RK6 at Rotokawa (data from Appendix 3). Samples are 1*, 5*, 7* and 9*, from Browne et al. (1992).

2443 mRF

The deepest sample (1*) has the largest mass loss in SiO_2, and there is now a decreasing trend in mafic elements Fe_2O_3 and MgO. Instead, there is a mass gain in Na_2O_3, Al_2O_3 and CaO, suggesting dissolution of ferromagnesian minerals and formation of a propylitic assemblage. A moderate mass gain in Sr suggests more quantities in plagioclase or adularia.

Even though mass change calculation is an easy way to analyse compositional changes in large datasets, it has some restrictions in this study. First, the precursor is based on a small amount of samples, compared to the size of the dataset. Secondly,

Ngatamariki and Rotokawa have been treated as a multiple precursor system, where samples used in the calculations have ranged from basaltic andesite to dacite. This may generate unrealistic mass changes in a rock type of an element which normally would occur in only small amounts. Even so, there seems to be a connection between mass changes to mafic vs. felsic major- and trace elements in the example of well RK6 (Fig. 5.23), so the calculations give reasonable results.

5.7 Summary

The identification of immobile elements in hydrothermally altered rocks is almost a requirement for making correct rock classifications. There are several methods to do this; the one described by MacLean & Barrett (1993) has been used in this study as it is an easy step-wise approach to find least altered samples and immobile elements. From a total of 132 samples, 15 were identified as least altered by a range of rock classification diagrams and Hughes igneous spectrum. These diagrams identified the samples to have a basaltic andesite to dacitic composition of sub-alkaline magma series (transitional to calc-alkaline). At Ngatamariki and Rotokawa, incompatible elemental pairs Zr vs. Nb, Zr vs. Ce and Nb vs. Th had the highest correlation coefficients, and based on this, Zr was selected together with TiO_2 to act as an immobile monitor in calculations of precursor compositions. A plot of TiO_2/Zr was also used for identifying clusters or fractionation trends comprising unaltered and altered samples, which can be interpreted as groups of unique rock types. Five subgroups were identified by this method; basaltic andesite, andesite, andesite-dacite, dacite and rhyolite, with rock units becoming progressively more felsic towards the north and at shallower depths. It could therefore be an advantage to treat these groups as several single precursor systems also described by MacLean & Barrett (1993), as this may reduce any affects that variations in primary mineralogy could have on the calculation of precursor composition. This was however restricted by the small amounts of samples where major elements had been obtained. With the composition of altered samples restored to the original, mass change calculation

identified zones where major- and trace elements had been enriched or depleted depending on alteration style.

Chapter 6
Petrogenesis

6.1 Introduction

TVZ is a volcanic arc and marginal basin of the Taupo-Hikurangi arc-trench system, and a result of the westward subduction of the oceanic Pacific Plate beneath the continental Australian Plate. It was established in Chapter 5 that the Ngatamariki and Rotokawa andesites consist of several units with compositions ranging from basaltic andesite to rhyolite, becoming progressively more felsic towards north, and shallow depths. Magma affinity also varies between units and fields, with mainly a transitional magma type at Rotokawa and a calc-alkaline magma type at Ngatamariki. However, it has not yet been established what kind of magmatic processes that has caused these compositional variations.

The rocks produced by subduction-related volcanism have a complex history which involves multi-level processes and components, making attempts of describing their petrogenesis very challenging. Magmatic processes may however be identified by creating traditional geochemical diagrams (e.g Harker variation and spider diagrams) based on trace elements. This approach will be used in this chapter in order to study the petrogenetic relationship between the Ngatamariki and Rotokawa fields and their associated rock type groups.

6.2 Magmatic processes

The petrogenesis of andesitic rocks has been discussed by several authors (e.g. Gill, 1981; Thorpe, 1982; Winter, 2001). An overview of the petrology and petrogenesis of TVZ volcanic rocks has been published by Graham et al. (1995), while more specific studies have focused mainly on the Tongariro Volcanic Centre (TgVC)

andesites (Cole et al., 1983; Graham & Hackett, 1987; Hackett & Houghton, 1988; Price et al., 2005). Browne et al. (1992) is the only previous study on Ngatamariki and Rotokawa andesites. Based on the distinctive geochemical characteristics of basalts, andesites and rhyolites in the TVZ, it is considered that they have formed by a combination of magmatic processes, such as crystal fractionation, magma mixing, crustal contamination and AFC.

6.2.1 Fractional crystallization

Fractional crystallisation takes place when the parent liquid cools and precipitates out crystals. This creates a melt composition which follows a liquid line of descent on a geochemical diagram as the magma evolves over time (Rollinson, 1993). Sometimes the plots are scattered instead of following a highly correlated line, and the reasons for this may be:

- ✧ highly porphyritic rocks, i. e. accumulation of phenocrysts;
- ✧ samples are not from a single magma;
- ✧ fractionation assemblage has changed during fractional crystallization; and
- ✧ secondary alteration by hydrothermal and weathering processes

Harker variation diagrams of compatible elements (V, Cr) and incompatible elements (Nb, Th) vs. Zr containing all samples from Ngatamariki and Rotokawa are used to identify fractional crystallization, as the multivariate diagram (Fig. 5.8) in Chapter 5 suggested that these elements are little affected by hydrothermal alteration. Zr is used as abscissa instead of SiO_2, as the latter is highly mobile during hydrothermal alteration. There is an overall negative trend of compatible elements V and Cr at both Rotokawa and Ngatamariki (Fig. 6.1). V is compatible in Fe-Ti oxides partial melting and Cr is concentrated in clinopyroxene. Some (dacitic) samples from Ngatamariki have a higher content of V and show a positive trend in the plot of V vs. Zr but more data is necessary to confirm this.

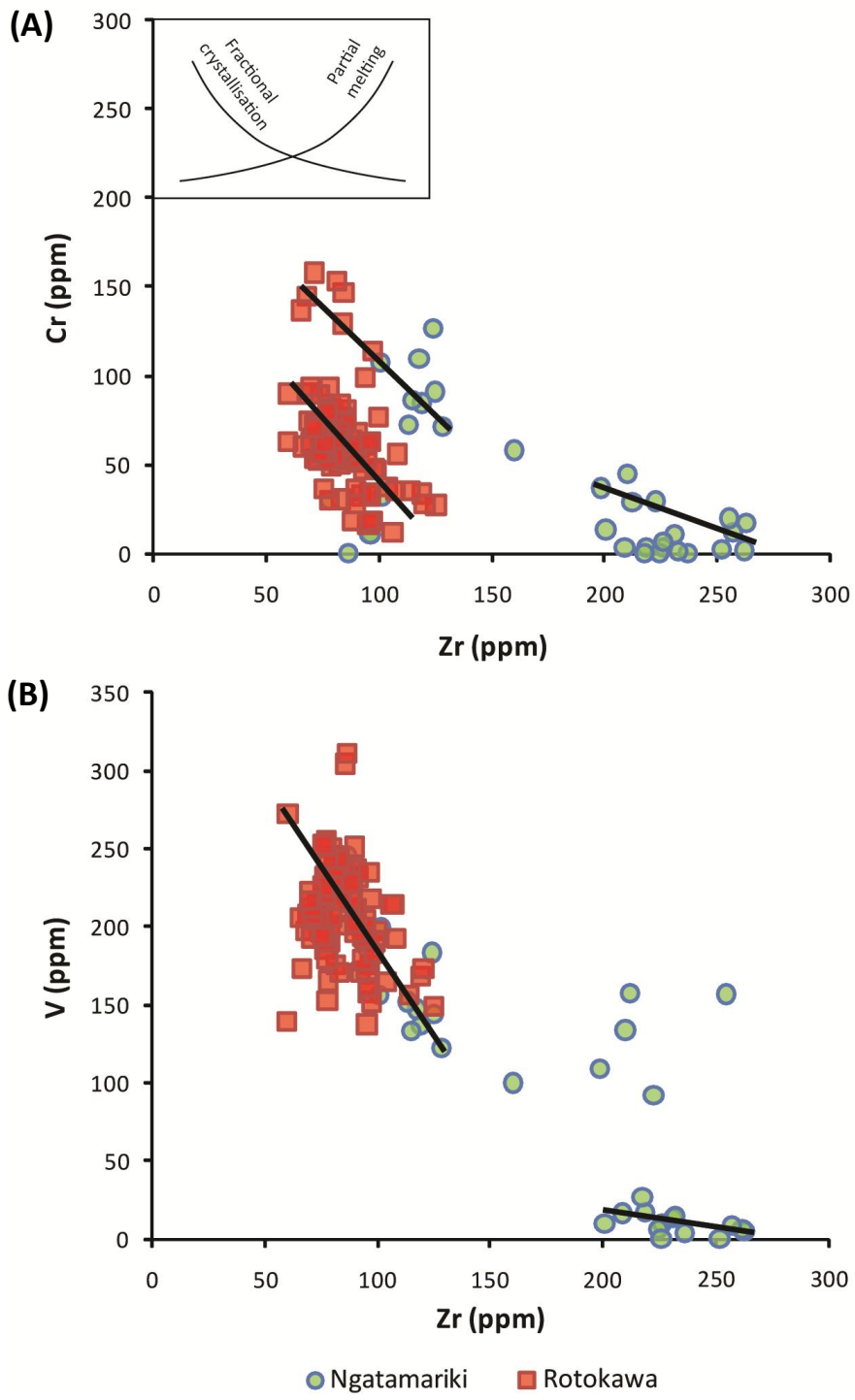

Figure 6.1: a-b) Harker variation diagram of compatible elements Cr and V vs. Zr from Ngatamariki and Rotokawa andesites (data from Appendix 3). Inset shows trends for compatible elements at crystal fractionation and partial melting. The positive trendline in the plot of V vs. Zr is probably scatter and does not represent a fractionation trend.

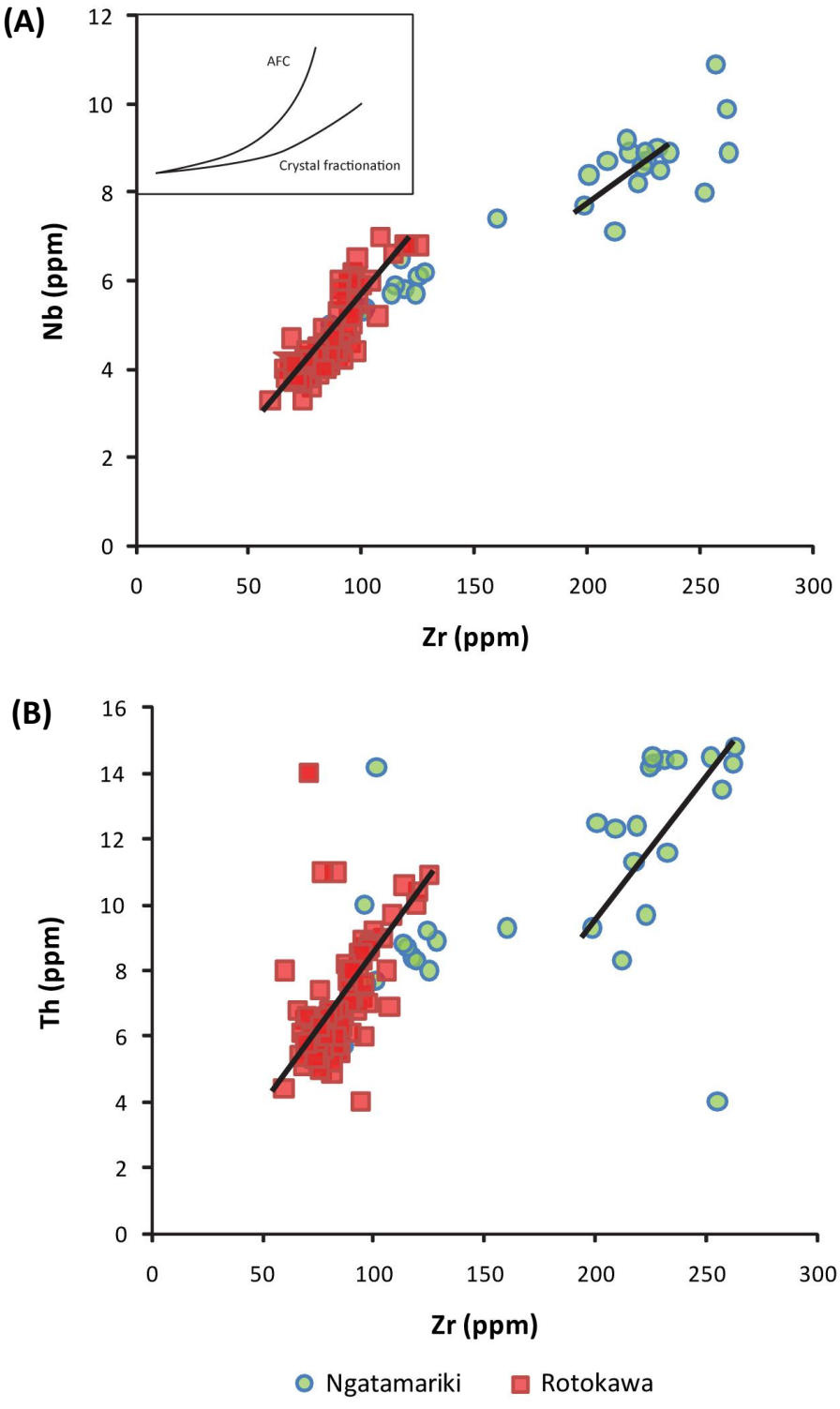

Figure 6.2: a-b) Harker variation diagram of incompatible elements Nb and Th vs. Zr, from Ngatamariki and Rotokawa andesites (data from Appendix 3). Inset shows trends for incompatible elements vs. Zr for crystal fractionation together with crustal assimilation (AFC) and only crystal fractionation. The sharp, positive curve in the plot of Nb vs. Zr is probably scatter and not a fractionation trend. Data from Browne et al. (1992) is excluded from the plot of Nb vs. Zr as Nb was not analysed for those samples.

The positive trend of incompatible elements Nb and Th vs. Zr confirms that fractional crystallisation has been occurring within the magma chamber (Fig. 6.2). A few rhyolitic samples from Ngatamariki show a strong, positive trend line in the plot of Nb vs. Zr, which is characteristic for a combination of assimilation and fractional crystallisation (AFC).

Two main rock groups can be identified in the Harker variation diagrams; basaltic andesites and andesites (<150 Zr) and dacite-andesites to rhyolites (>150 Zr), as they form separate fractionation lines. A third rock group is distinguishable in the plot of Cr vs. Zr, where basaltic andesite to andesite with a higher content of Cr creates its own fractionation line. This suggests that this is a group of lavas that have been derived from a separate batch of magma which has evolved independently.

Normalised multi-element diagrams (spider diagrams) are useful for displaying and comparing the geochemical composition of different rock groups. Primordial mantle values have been used in this study, and the trace elements are plotted from right to left with increasing incompability. Note that the behaviour of mobile LIL elements may reflect a fluid phase while less mobile HFS elements are mainly controlled by the magma source chemistry and magmatic processes which have taken place (Rollinson, 1993).

In the first diagram samples have been divided by field association, i. e. Ngatamariki or Rotokawa, least altered samples have been plotted separately to visualize compositional variations due to hydrothermal alteration (Fig. 6.3). The diagram reveals a typical continental arc-pattern, with enriched LIL elements (Rb, Ba, Th, K), depleted HFS elements and negative Nb anomalies typical of arc magmas. Representative samples from Tongariro Volcanic Centre (TgVC) have also been plotted on the spider diagram for comparison.

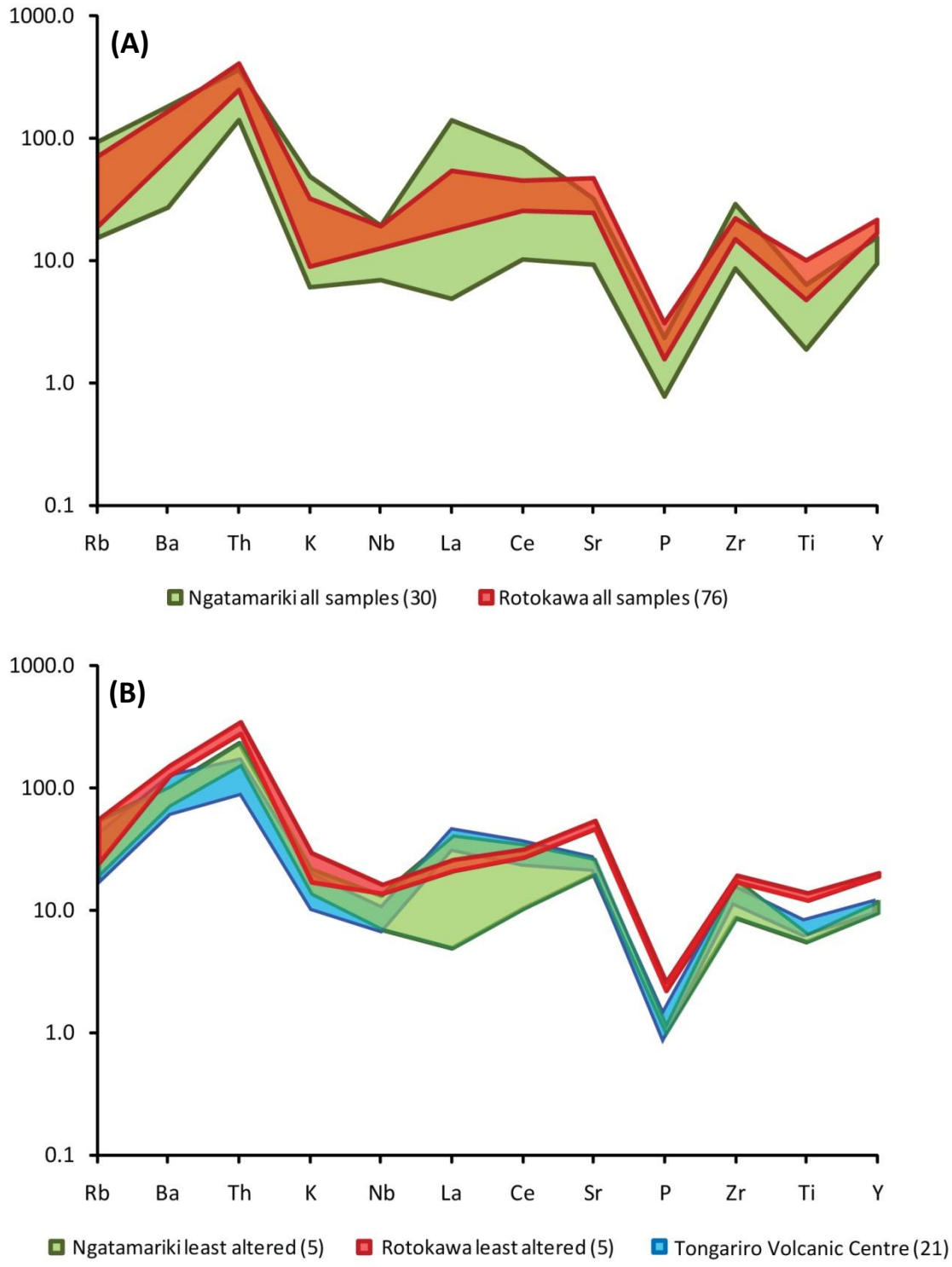

Figure 6.3: Spider diagram of a) all samples and b) least altered samples from Ngatamariki and Rotokawa (data from Appendix 3 but excluding samples from Browne et al., 1992 as analysis was missing for trace element Nb; TgVC data from Gamble et al., 1999 and Price et al., 2010; normalising values from McDonough et al., 1985 - see Appendix 5).

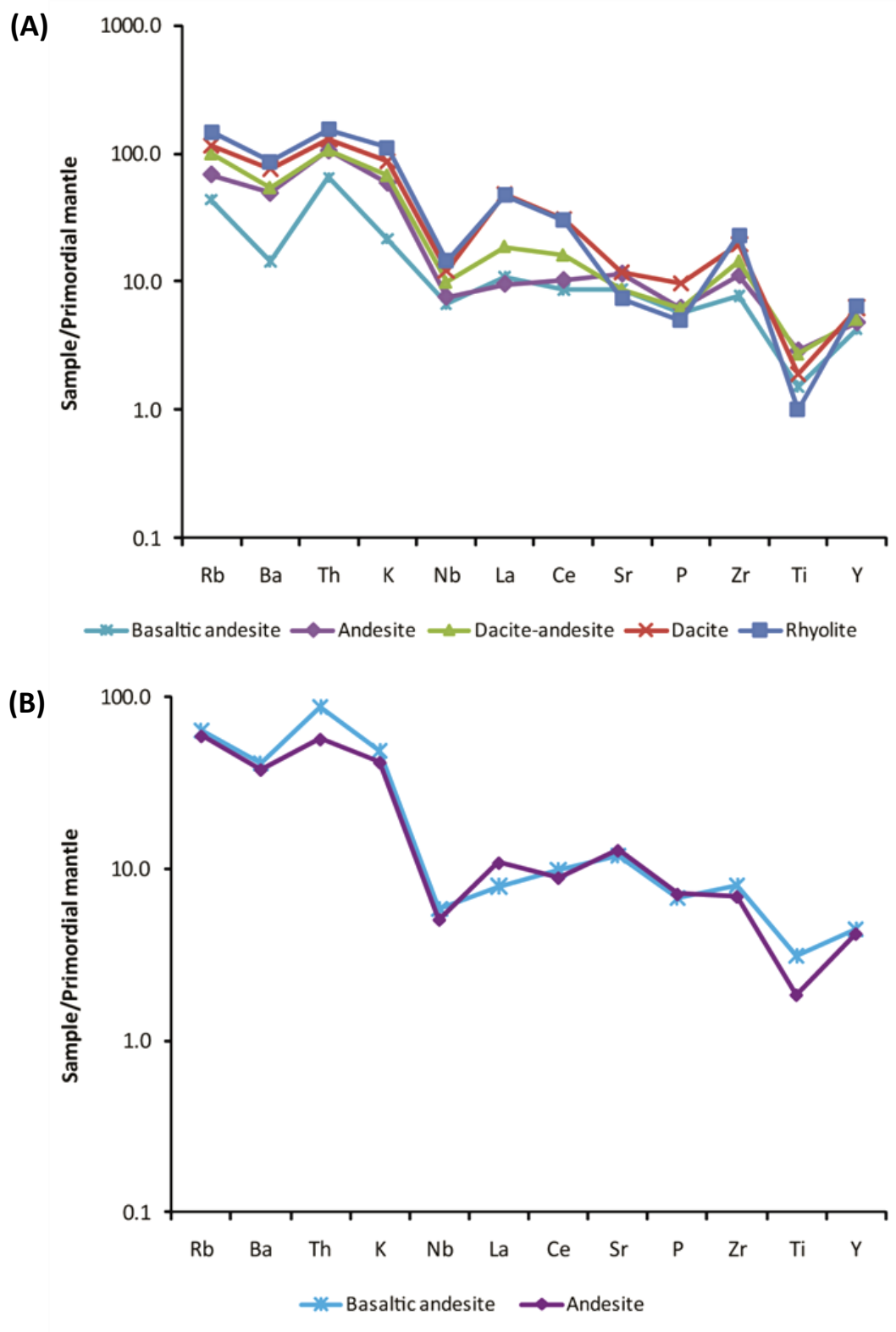

Figure 6.4: Spider diagram of least altered samples in each rock type group at a) Ngatamariki and b) Rotokawa (data from Appendix 3, normalising values from McDonough et al., 1985 – see Appendix 5).

The pattern is remarkably similar to least altered samples from Ngatamariki, with slightly lower LILE content, P and Ti compared to Rotokawa, while there is a small increase in La content.

Spider diagrams have also been created for each rock type group occurring in each field, represented by least altered samples (Fig. 6.4). Compatible and incompatible elements have previously been discussed in Chapter 5. For example, compatible element Sr substitutes for Ca in plagioclase and there are concentrations of Ti in Fe-Ti oxides, while incompatible elements such as Y and Th are rejected from the crystal lattice during fractional crystallisation. Progressive enrichment of incompatible elements as rock types evolve from mafic to felsic compositions will therefore indicate fractional crystallisation. This trend occurs to certain degree among LIL elements at Ngatamariki, but there is overlapping among HFS elements and crossing over of the normalised abundances of compatible elements Sr, P and Ti.

6.2.2 Assimilation and crustal contamination

Differentiation through assimilation means that there has been contamination of magma by rocks from the wall or roof of the magma chamber (Winter, 2001). Contamination may also occur as the basaltic melt ascends through continental crust on its way to the surface, where it easily assimilates components with a low melting point (e.g. silica and alkalis).

An isotopic system such as Rb-Sr may be used to constrain the source of crustal contamination. These heavy elements do not mass fractionate during melting or crystallisation, and the amount of contamination is identified by the fact that continental crust has higher contents of Rb, and therefore also a higher $^{87}Sr/^{86}Sr$ ratio than the mantle (Winter, 2001).

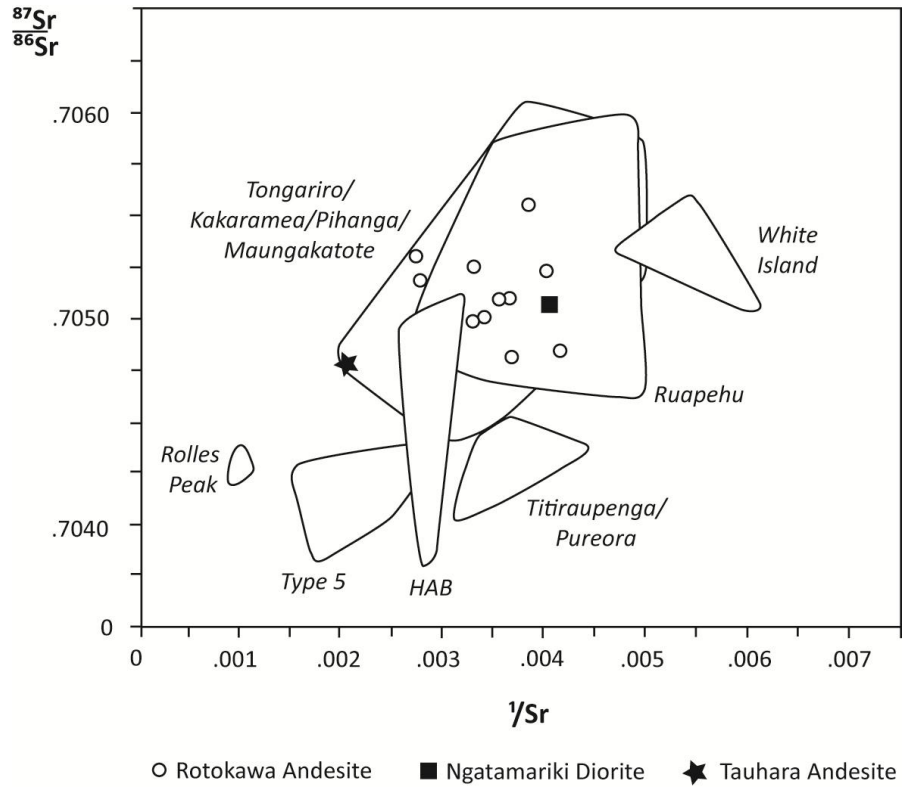

Figure 6.5: $^{87}Sr/^{86}Sr$ vs. 1/Sr for Rotokawa Andesites and Ngatamariki Diorite. Titiraupenga and Pureora which are normally included in Type 5 lavas (Graham & Hackett, 1987), plot separately in this diagram (from Browne et al., 1992).

Assimilation and fractional crystallization may also occur simultaneously (AFC), a process which may be identified by high LILE contents, i. e. K, Rb and Ba (de Paulo, 1981).

The Ngatamariki and Rotokawa andesites rest upon Mesozoic greywacke basement. Two samples were obtained from well RK4 and analysed by Browne et al. (1992) for Sr isotopes. The analysis returned an initial $^{87}Sr/^{86}Sr$ ratio of 0.70778 and an isochron age of 123 Ma (Fig. 6.5). This is similar to the Torlesse Terrane found at the Kaimanawa Ranges ($^{87}Sr/^{86}Sr$ ratio of 0.70735, isochron age of 139 Ma). The Rotokawa Andesites have an $^{87}Sr/^{86}Sr$ ratio ranging between 0.70585 to 0.70549, intermediate values compared to the mantle and continental crust. The occurrence of crustal contamination in Ngatamariki and Rotokawa andesites is confirmed by the negative Nb anomalies seen in previous spider diagrams (Fig. 6.3-4).

6.2.3 Magma mixing

Magma mixing is an important process in the formation of arc magmas. This involves magma recharge and replenishment and takes place in the plumbing system of a volcano at shallow depths (Winter, 2001).

Evidence of magma mixing can be identified by straight-line mixing trends in Harker variation diagrams and also by disequilibrium textures of plagioclase and ferromagnesian minerals, for example glomerocrysts, sieve-texture or normal and reverse zoning. These have all been described as part of the primary mineralogy in the Ngatamariki and Rotokawa andesites (Chapter 3). Plagioclase often has a labradorite core and a calcic-rich bytownite rim, and common glomerocrysts consists either of plagioclases or ferromagnesian minerals.

6.2.4 Discussion

The spatial separation of andesites from rhyolites in TVZ is in itself an indication that magma differentiation is controlled by more than one petrogenetic mechanism. Spinks et al. (2005) observed a general correlation between the amount of extension and the volume and style of eruption in each segment. This study was supported by Price et al. (2005), as they suggested that the varying magma composition within the TVZ could be caused by increased heat flow in the central area where lithospheric extension, asthenospheric upwelling and magma flux from mantle are greatest, thus generating felsic rather than intermediate magmas.

The Ngatamariki and Rotokawa andesites - like other TVZ andesites - show similar compositional characteristics of continental arc lavas globally (Graham et al., 1995). It is therefore likely that they have been created by similar processes, suggested by Gill (1981) to be differentiation of mantle-derived basaltic magmas. Gamble et al. (1990) proposed that parental basaltic magmas have similar compositions, and that secondary processes taking place as the melt ascends through the crust (e.g.

fractional crystallisation and crustal contamination) produce the different types of basalts found in the TVZ. Indeed, some of the first studies about the petrogenesis of TVZ volcanic rocks recognised that the Permian to Jurassic metasediments (e.g. interbedded greywacke, siltstones and shales) underlying lavas and pyroclastics could be a potential source of crustal contamination (Ewart & Stipp, 1968; Stipp 1968). Based on their trace element compositions and $^{87}Sr/^{86}Sr$ ratio, it was suggested that andesites could be created by a combination of the assimilation of sedimentary materials and basaltic magma derived from the upper mantle. Graham & Hackett (1987) argued that lavas at Ruapehu were derived from parental basaltic magmas by crystal fractionation combined with assimilation of continental crust. This was later supported in a study by Price et al. (2001).

A study by Cole et al. (2001) emphasises the importance of mixing and mingling in the evolution of andesitic and dacitic magmas. They found that diorites and micro diorites on the southeastern side of the TVZ had strong petrographical disequilibrium features. Based on the results, they introduced a model of multistage assimilation, differentiation, replenishment and mixing for andesites and dacites in the TVZ.

Several magmatic processes can also be identified in the Ngatamariki and Rotokawa andesites. There are groupings in the Harker variation diagrams with distinguishable fractionation lines, although without coherent trends. Straight, steep trend lines of especially incompatible elements, enrichment of LIL elements and increased $^{87}Sr/^{86}Sr$ ratios compared to the mantle in addition to disequilibrium textures based on petrographic observations suggests that the rocks did not follow a simple liquid line of descent, but reflects a complex process of mixing and AFC. The petrographic differences between Ngatamariki and Rotokawa andesites may suggest that they either originate from the same composite cone, where Ngatamariki is a younger more evolved phase, or from completely separate volcanic sources. In many other

geothermal fields in TVZ, mafic to intermediate volcanic rocks overlain by younger, felsic rocks have been intersected during well drilling (Browne et al., 1992), representing buried basaltic to andesitic volcanoes. Andesitic volcanism is known to precede more evolved rhyolitic systems in TVZ (Price et al., 2005). The transition from andesitic to rhyolitic volcanism is controlled by heat flow, and crustal extension and thinning in this rift zone increases the geothermal gradient significantly. Crustal melting will transform the precursor magmatic system and recycle its andesitic rocks as a rhyolitic system is created. Compositional variations from mafic to felsic lavas originating from the same composite cone have been recognised in other parts of the world, such as the chains of volcanoes in the Cascades, USA (Bacon & Druitt, 1988).

6.3 Volcanic evolution

The TVZ is the latest manifestation of a long history of subduction zone-volcanism in New Zealand (Herzer, 1995; Houghton et al., 1995; Mortimer et al., 2007):

- *23 Ma* - a NW-SE-trending arc developed in Northland;
- *16 Ma* – a change to a NNE-SSW trend which aligned with the Colville and Kermadec arc; and
- *2 Ma* - present day volcanic activity commenced in the TVZ with an onset of sub-alkaline andesitic lava.

6.3.1 Structural control

The southward migration of volcanism and a shift from west to east where the volcanoes are active at the present is a result of the southward propagation of the Havre-Lau volcanic rift zone and also due to TVZ acting as a hinge contact for a clock-wise intraplate rotation (Hochstein & Regenauer-Lieb, 1989; Soengkono et al., 1992; Parson & Wright, 1996).

The central part of the TVZ which is the locus of voluminous felsic volcanism, the lithosphere consist of a brittle upper crust (<8 km thick) and an underlying quartzo-feldspathic mid-crust with high viscosity to a depth of ~16 km followed by another ~14 km of highly modified mafic lower crust (Harrison & White, 2006). In the northern and southern parts where andesitic magmatism is dominant, the lithosphere consists of a brittle upper crust (>8 km thick) and an underlying quartzo-feldspathic viscous lower crust to a depth of ~20 km. Beneath is the upper mantle and source region for the magma (Reyners et al., 2007; Davey, 2010). There is however a difference in rift mechanisms between the two segments. In the north, amagmatic rifting has created a half graben-morphology in the northern TVZ which is characteristic for continental break-up during early stages (Ebinger & Casey, 2001). To the south, extension rates are low and magmatism is concentrated along the axis of the Taupo Fault Belt (TFB), with dike injection related volcanism during periods of increased rifting (Villamor et al., 2007). All these structural styles have a significant effect on magmatism, as the crustal rifting and extension causes mafic and felsic magmatic systems to interact with each other (Rowland et al., 2010).

6.3.2 Volcanic history

The volcano which deposited the Ngatamariki and Rotokawa andesites were once at the front of the propagating rift zone, as the Tongariro Volcanic Centre (TgVC) is today. It is therefore likely that they have been formed during similar circumstances. Several authors have suggested that lavas at Ruapehu were derived through the interaction of mantle-derived arc magmas with lower crust (e.g. Graham & Hackett, 1987; Gamble et al., 1990; Cole et al., 2001; Price et al., 2005). The initial phase of basaltic andesite to andesitic volcanism at Ngatamariki and Rotokawa began as mafic magmas migrated through faults and fractures to the surface ~2 Ma ago. The composite cone would have had a vent location along the western border of the Rotokawa field, and at the peak of its volcanic activity, the lower slopes would have reached the southern end of the Ngatamariki field. This is an estimation made

previously in this study based on lateral variations in thickness of the andesites, and also on the geochemical compositions of individual flow units.

Drilling data from Rotokawa field (e.g. RK16-18) has revealed that the oldest andesitic flows have ponded against a NE-trending greywacke fault located in the western area of the field (Rosenberg et al., 2005). Deposits of andesite and dacite-andesite lavas in the central and northern parts of the Ngatamariki field partially overlies the Rotokawa basaltic andesites and andesites, indicating that they have been erupted from a side vent of the original composite cone or even a satellite cone, which suggests that Ngatamariki and Rotokawa might have been parts of a volcanic complex similar to Tongariro (Fig. 6.6) (Hobden et al., 1996).

At 1.6 Ma, there was an onset of major regional extension and faulting which most likely created a graben-structure running through the fields. This observation is based on confined and lower-lying ignimbrite deposits of the Tahorakuri Formation in well RK17. At the same time, increased extension with subsequent thinning of the crust and a rising asthenosphere had created a high geothermal gradient and thus enough heat for ascending mafic magma to commence partial melting of the lower crust, which started an early phase of volcanism in the TVZ at 1.2 Ma ago (Collins, 2002). Regional uplift and major erosion was responsible for the deposition of sedimentary gravels belonging to the Waikora Formation (e.g. RK25, RK6 and RK8).

Erosion also affected outcrops of Tahorakuri Formation, creating thick (<500 m) overlying units of finely laminated pumice and tuff sediments on top of the ignimbrites. More evolved, dacitic to rhyolitic lavas were erupted at Ngatamariki during this stage, which became interlayered within the Tahorakuri Formation. A quiet period followed with a stable landscape between 1 and 0.3 Ma. This was however disrupted by multiple major eruptions from the Whakamaru Caldera, which was part of the large-scale silicic volcanism taking place in the TVZ at that time.

These eruptions may be responsible for a huge north-westwards step-down of greywacke on a general line from Mt. Tauhara, through Rotokawa and Ohaaki which is probably part of the Whakamaru Caldera northeastern boundary (M. Rosenberg, personal communication, Feb. 2011).

Overall, the basin was infilled with up to 2 km thickness of volcaniclastic material on top of the Ngatamariki and Rotokawa andesites, most of it (> 10,000 km^3) of rhyolitic composition which has erupted within the last 0.6 Ma from the Maroa, Okataina, Kapenga, Whakamaru, Rotorua and Taupo Volcanic Centres (Wright, 1992). A large volume of magma is still trapped at depth, mainly concentrated within the central TVZ, feeding heat, volatiles and chemicals through geothermal fields with an incomparable amount of thermal energy release (Bibby et al., 1995; Hochstein, 1995).

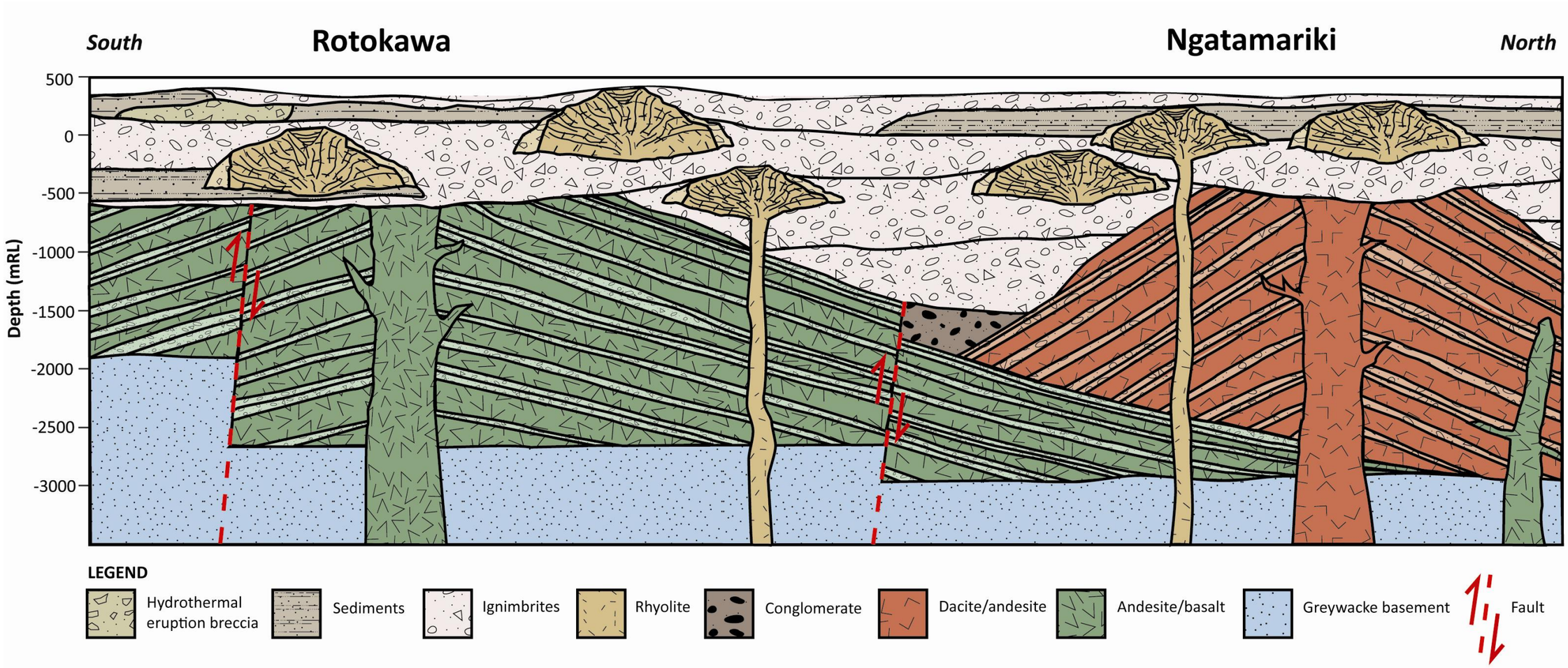

Figure 6.6: Schematic cross-section of the subsurface geology at the Ngatamariki and Rotokawa geothermal fields, with an older basaltic andesite to andesite composite cone at Rotokawa and a younger dacite-andesite cone at Ngatamariki. Increasing felsic volcanism in the TVZ has created rhyolite dome structures and deposited thick sheets of ignimbrites in the overlying stratigraphy.

0 1000

Metres

Chapter 7
Summary and conclusions

Quaternary andesite lavas and breccia has been encountered in several geothermal fields in the TVZ. At Rotokawa, an andesitic unit below ~ 1 km depth is a major production aquifer for the 34 MWe Rotokawa power station and the 140 MWe Nga Awa Purua power station. A similar andesitic unit has been encountered during exploration drilling at the nearby Ngatamariki geothermal field, and the aim of this thesis as outlined in Chapter 1 has been to investigate petrogenetic relationships which may exist within flow units, between wells and also between the Ngatamariki and Rotokawa fields.

Previous work by Browne et al. (1992) on sampled andesites from some of the early wells drilled at Ngatamariki and Rotokawa (RK4, RK5, RK6, RK8, NM2, NM3 and NM4) indicated that Rotokawa had closer chemical affinities with the pyroxene-andesites of TgVC than to Ngatamariki, which appeared different from most other TVZ lavas. In this study, the sampling area was extended both vertically and laterally from more recently drilled wells (RK18, RK21, RK24, RK25, RK27, NM5, NM6 and NM7) in order to gain more knowledge about the andesites. Very few of the samples still had their original mineral assemblage intact, due to extensive hydrothermal alteration. However, by combining petrological and geochemical techniques to see through the effects of alteration, it has been possible to both compare and classify the rock compositions of the two andesites.

Ngatamariki

At Ngatamariki, andesite lava and breccia have been encountered between a maximum depth of 3150 mCHF (NM6) and minimum depth of 777 (NM3) mCHF. Greywacke basement was only encountered in the most southern well (NM6) after

drilling through ~900 m of Ngatamariki Andesite. All other wells end in andesite, or in the case of NM4, diorite. It is therefore not possible to estimate vent location based on lateral variation in thickness at Ngatamariki.

The phenocryst assemblage consists of plagioclase - labradorite with minor bytownite - and clinopyroxene with accessory minerals of quartz, hornblende and Fe-Ti oxides. Sieve-texture in addition to normal or oscillatory zoning suggests disequilibrium during crystallization. The modal abundance of quartz increases at shallow depth (<2200 mCH), which indicates a transgression to a more felsic lava of dacitic composition. Breccia clasts consist of either andesite or a mix of volcanic and sedimentary fragments set in an andesitic matrix. The most widespread alteration style at Ngatamariki is propylitic, with a mineral assemblage of albite, calcite, chlorite, epidote and green amphibole. Less common alteration styles are argillic, advanced argillic and potassic. Vugs and veins are common alteration textures. Alteration intensity commonly increases with depth. Breccia clasts often have abundant, fine grained hematite in the groundmass typical of advanced argillic alteration, compared to the more intense, high temperature propylitic alteration style in the breccia matrix.

Five different rock types were identified at Ngatamariki by TiO_2/Zr ratios obtained by geochemical analysis. Basaltic andesite occurs in the lower units in the southern part of the field (NM6), andesite occurs in the middle units in NM6 and also in the lower levels of NM5 to the north, and dacite-andesite forms a thin layer between the lower boundary of the Tahorakuri Formation and Ngatamariki Andesite across the field (NM6, NM3, NM2). The upper units in the southern and central part of the field (NM6, NM7) are interlayered in the Tahorakuri Formation and have a dacitic composition. Rhyolite is present between the units of dacite-andesite and dacite in the southern part of the field (NM6). The magma affinity determined by Zr/Y ratios varies with depth at Ngatamariki. The volcanic rocks are mainly derived from a calc-

alkaline magma type with the exception of andesites, which are transitional. The microdiorite in NM4 has a composition of basaltic andesite with tholeiitic magma affinity.

Rotokawa

Andesite lava and breccia at Rotokawa occur at a minimum depth of 1250 mCHF (RK28) and a maximum depth of 3050 mCHF (RK16). The greywacke basement has been encountered during drilling in wells RK4, RK16 and RK21. Based on lateral variation in thickness, with thin units of Rotokawa Andesite to the southeast at RK4 and RK21 (850 and 1010 m, respectively) compared to a thick unit at RK16 (2190 m) to the west, the vent is probably located towards the western margin of the field.

The phenocryst assemblage consists of plagioclase - labradorite with minor bytownite - and clino- and orthopyroxene and accessory minerals of biotite and Fe-Ti oxides. Similar to Ngatamariki, disequilibrium is also indicated by sieve-texture and normal or oscillatory zoning. A localised concentration of igneous biotite in RK18 (2221 mRF) indicates temporary deposition of a more hydrous magma from a nearby vent. Rotokawa has the same alteration style as Ngatamariki, although hydrothermal biotite is more common than green amphibole in this field.

Two different rock types have been identified at Rotokawa. There is a widespread basaltic andesite with interlayered andesite in the southern and central part of the field (RK21, RK24, RK25). In the northern part of the field (RK6, RK8), the andesite overlies the basaltic andesite, a trend which continues in the southern end of Ngatamariki (NM6). The magma affinity at Rotokawa is mainly transitional, with a few isolated occurrences of tholeiitic magma type in andesites through the field (RK21, RK24, RK25).

Petrogenesis

The petrogenesis of both Ngatamariki and Rotokawa andesites is complex, as with most subduction-related volcanism. Geochemical modelling and petrographical observations suggests that a combination of magmatic processes have been in operation, either individually or simultaneously, including fractional crystallization, AFC and magma mixing. The spatial separation of andesites and rhyolites in the TVZ also indicate a significant structural control on magmatism, with intermediate magmas occurring where there is greatest dextral transtension and felsic magmas occurring where there is greatest extension. Andesitic volcanism typically precedes rhyolitic volcanism in the TVZ, and based on the results of this study it is likely that the lava flows of basaltic andesite to andesite at Rotokawa represents an old composite cone, compared to a younger dacite-andesite cone at Ngatamariki.

References

Acocella, V., Spinks, K., Cole, J. & Nicol, A. (2003). Oblique back arc rifting of Taupo Volcanic Zone, New Zealand. *Tectonics, 22*, 1-18.

Adams, C. J., Campbell, H. J. & Griffin, W. J. (2008). Age and provenance of basement rocks of the Chatham Islands: An outpost of Zealandia. *New Zealand Journal of Geology & Geophysics, 51*, 245-259.

Allen, R. L. (1988). False pyroclastic textures in altered silicic lavas, with implications for volcanic-associated mineralization. *Economic Geology, 1,* 1424-1446.

Allis, R. G. (1990). Subsidence at Wairakei field. *Geothermal Resources Council Transactions, 14,* 1081-1087.

Allis, R. G., Christenson, B. W., Nairn, I. A., Risk, G. F., Sheppard, D. S. & White, S. P. (1995). *Kawerau geothermal field: Its natural state and response to Development* (Client Report 72436C.10). Institute of Geological and Nuclear Sciences.

Aoki, K. & Fujimaki, H. (1982). Petrology and geochemistry of calc-alkaline andesite of presumed upper mantle origin from Itinome-gata, Japan. *American Mineralogist, 67*, 1-13.

Arculus, R. J. & Powell, R. (1986). Source component mixing in regions of arc magma generation. *Journal of Geophysical Research, 91*, 5913-5926.

Arehart, G. B., Christenson, B. W., Wood, C. P., Foland, K. A. & Browne, P. R. L. (2002). Timing of volcanic, plutonic and geothermal activity at Ngatamariki, New Zealand. *Journal of Volcanology and Geothermal Research, 116*, 201-214.

Arnorsson, S. (1983). Chemical equilibria in Icelandic geothermal systems – implications for chemical geothermometry investigations. *Geothermics, 12*, 119-128.

Arnorsson, S. (1995). Geothermal systems in Iceland: Structure and conceptual models – l. High temperature areas. *Geothermics, 24*, 561-602.

Arnorsson, S., Gunnlaugsson, E. & Hördur, S. (1983). The chemistry of geothermal waters in Iceland ll. Mineral equilibria and independent variables controlling water compositions. *Geochemica et Cosmochimica Acta, 47*, 547-566.

Ayers, J. (1998). Trace element modelling of aqueous fluid-peridotite interaction in the mantle wedge and subduction zones. *Contribution to Mineralogy and Petrology, 132*, 390-404.

Bacon, C. R. & Druitt, T. H. (1988). Compositional evolution of the zoned calcalkaline magma chamber of Mount Mazama, Crater Lake, Oregon. *Contributions to Mineralogy and Petrology, 98*, 224-256.

Bailey, S. W. (1988). Chlorites: Structures and crystal chemistry. *Reviews in Mineralogy, 19,* 347-398.

Ballance, P. F., Ablaev, A. G., Pushchin, I. K, Pletnev, S. P., Birylina, M. G., Itaya, T., Follas, H. A. & Gibson, G. W. (1999). Morphology and history of the Kermadec trench-arc-backarc basin-remnant arc system at 30 to 32°S: Geophysical profile, microfossile and K-Ar data. *Marine Geology, 159*, 35- 62.

Banwell, C. J., Cooper, E. R., Thompson, G. E. K. & McCree, K. J. (1957). Physics of the New Zealand thermal area. *New Zealand Department of Scientific and Industrial Research Bulletin, 123*.

Barbier, E. (2002). Geothermal energy technology and current status: An overview. *Renewable and Sustainable Energy Reviews, 6*, 3-65.

Barrett, T. J., MacLean, W. H. & Årebäck, H. (2005). The Palaeproterozoic Kristineberg VMS deposit, Skellefte district, northern Sweden. Part II: Chemostratigraphy and alteration. *Mineralium Deposita, 40,* 34-38.

Barrick, K. A. (2007). Geyser decline and extinction in New Zealand – Energy development impacts and implications for environmental management. *Environmental Management, 39,* 783-805.

Beck, A. C. & Robertson, E. I. (1955). Geology and Geophysics. In: Geothermal steam for power in New Zealand. *New Zealand Department of Scientific and Industrial Research Bulletin, 117*, 15-19.

Bennie, S. L. (1983). *Geophysical investigations of the Ngatamariki geothermal area* (Report 192). Geophysics Division, Department of Scientific and Industrial Research.

Berry, B. R. (1985). *Ngatamariki geothermal investigations well NM1: Report on completion tests and heating runs: January – March 1985* (report 37/33/1). Ministry of Works and Development.

Beske-Diehl, S. & Li, H. (1993). Magnetic properties of hematite in lava flows from Iceland: Response to hydrothermal alteration. *Journal of Geophysical Research, 98,* 403-417.

Best, M. G. (2003). *Igneous and metamorphic petrology*. Blackwell Science Ltd.

Bibby, H. M., Caldwell, T. G., Davey, F. J. & Webb, T. H. (1995). Geophysical evidence on the structure of the Taupo Volcanic Zone and its hydrothermal circulation. *Journal of Volcanology and Geothermal Research, 68,* 29-58.

Bibby, H. M., Risk, G. F., Caldwell, T. G., Ogawa, Y., Takakura, S. & Uchida, T. (2000). *Deep electrical structure beneath the Taupo Volcanic Zone and the source of geothermal heat* (pp. 81-86). Proceedings of 19th New Zealand Geothermal Workshop.

Bignall, G. (1994). *Thermal evolution and fluid-rock interactions in the Orakeikorako – Te Kopia geothermal system, Taupo Volcanic Zone, New Zealand* (Unpublished PhD thesis). Auckland University, New Zealand.

Bignall, G. (2009). *Ngatamariki geothermal field: Geoscience overview* (Client Report 2009/94). Institute of Geological and Nuclear Sciences.

Bignall, G. & Harvey, C. C. (2005). *Geoscientific Review of the Kawerau Geothermal Field* (Client Report 2005/20). Institute of Geological and Nuclear Sciences.

Bischoff, J. L. & Seyfried, W. E. (1978). Hydrothermal chemistry of seawater from 25° to 350°C. *American Journal of Science, 278,* 838-860.

Bishop, D. G., Bradshaw, J. D. & Landis, C. A. (1985). Provisional terrane map of South Island, New Zealand. In: Howell, D. G. (Ed.), *Tectonostratigraphic Terranes.* Circum-Pacific Council for Energy and Mineral Resources Earth Science Series, vol. 1, Houston, Texas, pp. 515-521.

Bixley, P. F. (1986). *Cooling of the Wairakei reservoir during production (pp. 169-174).* Proceedings of the 11th Reservoir Engineering Workshop, Stanford University, USA.

Bland, K. J., Kamp, P. J. J. & Nelson, C. S. (2008). *Late Miocene – Early Pleistocene paleogeography of the onshore central Hawke's Bay sector of the forearc*

basin, eastern North Island, New Zealand, and some implications for hydrocarbon prospectivity. Proceedings of 2008 New Zealand Petroleum Conference, Auckland, New Zealand.

Blundy, J. D. & Shimizu, N. (1991). Trace element evidence for plagioclase recycling in calc-alkaline magmas. *Earth and Planetary Science Letters, 102,* 178-197.

Bödvarsson, G. S., Björnsson, S., Gunnarsson, A., Gunnlaugsson, E. Sigurdsson, O., Stefansson, V. & Steingrimsson, B. (1990). The Nesjavellir geothermal field, Iceland. Part 1. Field characteristics and development of a threedimensional numerical model. *Geothermal Science and Technology, 2,* 189-228.

Bowen, N. L. (1928). *The evolution of the igneous rocks.* Princeton University Press, Princeton, NJ.

Bromley, C. J., Glover, R., Merrett, M. J. & Fitzgerald, N. (2002). *Rotokawa geothermal field: Resource assessment – first five years* (Client Report 2002/10). Institute of Geological and Nuclear Sciences.

Brotheridge, J.M. (1995). *Surface manifestations past and present of the Ngatamariki geothermal field, Taupo Volcanic Zone, New Zealand* (Unpublished MSc-thesis). University of Auckland, New Zealand.

Brotheridge, J. M. A., Browne, P. R. L. & Hochstein, M. P. (1995). *The Ngatamariki geothermal field, NZ: Surface manifestations – Past and present* (pp. 61-66). Proceedings 17th NZ Geothermal Workshop. Geothermal Institute and Geology Department, University of Auckland.

Brown, G. (1961). *The X-ray identification and crystal structures of clay minerals.* Mineralogical Society, London, UK.

Brown, S. J. A., Wilson, C. J. N. & Wooden, J. (1998). The Whakamaru group ignimbrites, Taupo Volcanic Zone, New Zealand: Evidence for reverse tapping of a zoned silicic magmatic system. *Journal of Volcanology and Geothermal Research, 84,* 1-37.

Browne, P. R. L. (1970). Hydrothermal alteration as an aid in investigating geothermal fields. *Geothermics, 2*, 564-570.

Browne, P. R. L. (1973). *The geology, mineralogy and geothermometry of the Broadlands geothermal field, Taupo Volcanic Zone, New Zealand*. (Unpublished PhD thesis). Victoria University of Wellington, New Zealand.

Browne, P. R. L. (1978). Hydrothermal alteration in active geothermal fields. *Annual Review of Earth and Planetary Sciences, 6,* 229-250.

Browne, P. R. L. (1979). Minimum age of the Kawerau geothermal field, North Island, New Zealand. *Journal of Volcanology and Geothermal Research, 6*, 213-215.

Browne, P. R. L. (1985). *Stratigraphy of RK6: Preliminary report* (Unpublished report). Department of Scientific and Industrial Research.

Browne, P. R. L. (1993). *Application of mineralogical methods to assess the thermal stabilities of geothermal reservoirs.* Proceedings 18th workshop on geothermal reservoir engineering, Stanford University, California.

Browne, P. R. L. & Ellis, A. J. (1970). The Ohaki-Broadlands hydrothermal area, New Zealand: Mineralogy and related geochemistry. *American Journal of Science, 269*, 97-131.

Browne, P. R. L., Graham, I. J., Parker, R. J. & Wood, C. P. (1992). Subsurface andesite lavas and plutonic rocks in the Rotokawa and Ngatamariki geothermal systems, Taupo Volcanic Zone, New Zealand. *Journal of Volcanology and Geothermal Research, 51*, 199-215.

Browne, P. R. L., Graham, I. J., Parker, R. J. & Wood, C. P. (1992). Subsurface andesite lavas and plutonic rocks in the Rotokawa and Ngatamariki geothermal systems, Taupo Volcanic Zone, New Zealand. *Journal of Volcanology and Geothermal Research, 51*, 199-215.

Browne, P. R. L. & Lawless, J. V. (2001). Characteristics of hydrothermal eruptions with examples from New Zealand and elsewhere. *Earth-Science Reviews, 52*, 299-331.

Cathelineau, M., Oliver, R., Izquierdo, G., Garfias, A., Nieva, D. & Izaguirre, O. (1983). *Mineralogy and distribution of hydrothermal mineral zones in Los Azufres (Mexico) geotermal field.* Proceedings 9th Workshop Geothermal Reservoir Engineering, Stanford University, Stanford, California.

Caussiux, M., Proust, D., Siitari – Kauppi, M. Sardini, P. & Leutsch, Y. (2006). Clay minerals formed during propyolitic alteration of granite and their influence on primary porosity: *A multi-scale approach. Clays and Clay Minerals, 54,* 541-554.

Chambefort, I., Dilles, J. H. & Kent, A. J. R. (2008). Anhydrite-bearing andesite and dacite as a source of sulfur in magmatic-hydrothermal mineral deposits. *Geology, 36*, 719-722.

Cody, A. D. (2003). *Geology, history and stratigraphy of hydrothermally altered eruptions in the Rotorua geothermal field* (Unpublished MSc thesis). University of Waikato, Hamilton, New Zealand.

Cody, A.D. (2007). Geodiversity of geothermal fields in the Taupo Volcanic Zone. *DOC Research & Development Series 281*. Department of Conservation, Wellington.

Cole, J. W. (1978). Andesites of the Tongariro Volcanic Centre, North Island, New Zealand. *Journal of Volcanology and Geothermal Research, 3*, 121-153.

Cole, J. W. (1979). Structure, petrology and genesis of Cenozoic volcanism, Taupo Volcanic Zone, New Zealand: A review. *New Zealand Journal of Geology and Geophysics, 22*, 631-657.

Cole, J. W. (1984). Taupo-Rotorua Depression: An ensialic marginal basin of North Island, New Zealand. *Geological Society, London, Special Publication, 16,* 109-120.

Cole, J. W. (1990). Structural control and origin of volcanism in the Taupo Volcanic Zone, New Zealand. *Bulletin of Volcanology, 52*, 445–459.

Cole, J. W. & Lewis, K. B. (1981). Evolution of the Taupo-Hikurangi subduction system. *Tectonophysics, 72*, 1-21.

Cole, J. W., Cashman, K. V. & Rankin, P. C. (1983). Rare-earth element geochemistry and the origin of andesites and basalts of the Taupo Volcanic Zone, New Zealand. *Chemical Geology, 38,* 255-274.

Cole, J. W., Gamble, J. A., Burt, R. M., Carroll, L. D. & Shelley, D. (2001). Mixing and mingling in the evolution of andesite-dacite magmas: Evidence from co-magmatic plutonic enclaves, Taupo Volcanic Zone, New Zealand. *Lithos, 59,* 25-46.

Collar, R. J. & Browne, P. R. L. (1985). *Hydrothermal eruptions at the Rotokawa geothermal field, Taupo Volcanic Zone, New Zealand* (pp. 171-175). Proceedings of 7th NZ Geothermal Workshop.

Collins, J. W. (2002). Hot orogens, tectonic switching and creation of continental crust. *Geological Society of America, 30*, 535-538.

Cooper, R. A. & Tulloch, A. J. (1992). Early Palaeozoic terranes in New Zealand and their relationship to the Lachlan Fold Belt. *Tectonophysics, 214*, 129-144.

Correcher, V., Garcia-Guinea, J. & Delgado, A. (2000). Influence of preheating treatment on the luminescence properties of adularia feldspar ($KAlSi_3O_8$). *Radiation Measurements, 32,* 709-715.

Dalrymple, G. B., Grove, M., Lovera, O. M., Harrison, T. M., Hulen, J. B. & Lanphere, M. A. (1999). Age and thermal history of the Geysers plutonic complex (felsite unit), Geysers geothermal field, California: a $^{40}Ar/^{39}Ar$ and U-Pb study. *Earth and Planetary Science Letters, 173,* 285-298.

Darby, D. J. & Meertens, C. M. (1995). Terrestrial and GPS measurements of deformation across the Taupo back arc and Hikurangi forearc regions in New Zealand. *Journal of Geophysical Research, 100,* 8221-8232.

Davey, F. J. (2010). Crustal seismic reflection measurements across the northern extension of the Taupo Volcanic Zone, North Island, New Zealand. *Journal of Volcanology and Geothermal Research, 190*, 75-81.

Davis, J.C. (1986). *Statistics and data analysis in geology*. New York, USA: John Wiley & Sons Inc.

De Paolo, D.J. (1981). Trace element and isotopic effects of combined wallrock assimilation and fractional crystallization. *Earth and Planetary Science Letters, 53,* 189–202.

Dekov, V. M., Scholten, J., Botz, R., Garbe-Schonberg, M., Thiry, M., Stoffers, P. & Schmidt, M. (2005). Occurrence of kaolinote and mixed-layer kaolinite/smectite in hydrothermal sediments of Grimesy Graben, Tjornes Fracture Zone (north of Iceland). *Marine Geology, 215,* 159-170.

Dieffenbach, E. (1843). *Travels in New Zealand: With contributions to the geography, geology, botany, and natural history of that country, Volume 1*. The University of California, USA: J. Murray.

Donaldson, I. G. (1962). Temperature gradients in the upper layers of the Earth's crust due to convective water flows. *Journal of Geophysical Research, 67* (9), 3449-3459.

Dungan, M. A., Wulff, A. & Thompson, R. (2001). Eruptive stratigraphy of the Tatara-San Pedro Complex, 36 °S, southern volcanic zone, Chilean Andes:

Reconstruction method and implications for magma evolution at long-lived arc volcanic centres. *Journal of Petrology, 42*, 555-626.

Eberhardt, E., Stimpson, B. & Stead, D. (1999). Effects of grain size on initial and propagation thresholds of stress-induced brittle fractures. *Rock Mechanics and Rock Engineering, 32,* 81-99.

Eberhardt, E., Stimpson, B. & Stead, D. (1999). Effects of grain size on initial and propagation thresholds of stress-induced brittle fractures. *Rock Mechanics and Rock Engineering, 32,* 81-99.

Ebinger, C. J. & Casey, M. (2001). Continental break-up in magmatic provinces: An Ethiopian example. *Geology, 29,* 527-530.

Elder, J.W. (1965). Physical processes in geothermal areas. In: Lee, W.H.K. (ed.), *Terrestrial Heat Flow.* American Geophysical Union, Geophysical Monographs, 8, 211- 239.

Elder, J.W. (1966). Heat and mass transfer in the earth, hydrothermal systems. *Department of Scientific and Industrial Research Bulletin, 169.*

Eliasson, T. (1993). *Mineralogy, geochemistry and petrophysics of red coloured granite adjacent to fractures* (SKB-TR-93-06). Swedish Nuclear Fuel and Waste Management Co.

Ellis, A. J. & Mahon, W. A. J. (1967). Natural hydrothermal systems and experimental hot water/rock interactions (Part ll). *Geochimica et Cosmochimica Acta, 31,* 519-538.

Ellis, A. J. & McFadden, I. M. (1972). Partial molal volumes of ions in hydrothermal solutions. *Geochimica et Cosmochimica Acta, 36,* 413-426.

Ellis, A. J. & Mahon, W. A. J. (1977). *Chemistry and geothermal systems*. Academic Press; New York, USA.

Environment Waikato (2005). Reporoa eruption sends plume into Waikato River. *Environment Waikato media release 21/04/2010.*

Ewart, A. & Stipp, J. J. (1968). Petrogenesis of the volcanic rocks of the central North Island, New Zealand, as indicated by a study of Sr^{87}/Sr^{86} ratios, and Sr, Rb, K, U, and Th abundances. *Geochimica et Cosmochimica Acta, 32,* 699–736.

Ewart, A., Brothers, R. N. & Mateen, A. (1977). An outline of the geology and geochemistry and the possible petrogenetic evolution of the volcanic rocks of the Tonga-Kermadec-New Zealand island arc. *Journal of Volcanology and Geothermal Research, 2*, 205-250.

Fenner, C. N. (1931). The residual liquids of crystallizing magmas. *Mineralogical Magazine, 22*, 539-560.

Ferry, J. M. (1979). Reaction mechanisms, physical conditions and mass transfer during hydrothermal alteration of mica and feldspar in granitic rocks from south-central Maine, USA. *Contributions to Mineralogy and Petrology, 68,* 125-139.

Fiebig, J. & Hoefs, J. (2002). Hydrothermal alteration of biotite and plagioclase as inferred from intragranular oxygen isotope- and cation-distribution patterns. European *Journal of Mineralogy, 14*, 49-60.

Fischer, R. V. & Schmincke, H. (1984). *Pyroclastic rocks.* New York, USA: Springer Verlag.

Floyd, P. A. & Winchester, J. A. (1975). Magma type and tectonic setting discrimination using immobile elements. *Earth and Planetary Science Letters, 27*, 211-218.

Fournier, R. O. & Rowe, J. J. (1966). Estimation of underground temperatures from the silica content of water from hot springs and wet-steam wells, *American Journal of Science, 264,* 685-697.

Fournier, R.O. & Pitt, A.M. (1985). *The Yellowstone magmatic-hydrothermal system, U.S.A* (pp. 319-327). Geothermal Resources Council 1985 International Symposium on Geothermal Energy.

Franzson, H., Gudmundsson, A., Fridleifsson, G. O. & Tomasson, J. (1986). *Nesjavellir high-temperature field, SW Iceland – reservoir geology* (pp. 210-213). Proceedings 5th International Symposium on Water-Rock Interaction.

Froggatt, P. C. (1981). Motutere Tephra Formation and redefinition of Hinemaiaia Tephra Formation, Taupo Volcanic Centre, New Zealand. *New Zealand Journal of Geology and Geophysics, 24,* 99-105.

Furlong, K. P. & Kamp, P. J. J. (2009). The lithospheric geodynamics of plate boundary transpression in New Zealand: Initiating and emplacing subduction along the Hikurangi margin, and the tectonic evolution of the Alpine Fault system. *Tectonophysics, 474*, 449-462.

Gamble, J. A., Smith, I. E. M., Graham, I. J., Kokelaar, B. J., Cole, J. W., Houghton, B. F. & Wilson, C. J. N. (1990). The petrology, phase relations and tectonic setting of basalts from the Taupo Volcanic Zone, New Zealand, and the Kermadec Island Arc-Havre Trough, S. W. Pacific. *Journal of Volcanology and Geothermal Research, 43,* 235-270.

Gamble, J. A., Smith, I. E. M., Culloch, M. T., Graham, I. J. & Kokelaar, B. P. (1993). The geochemistry and petrogenesis of basalts from Taupo Volcanic Zone and Kermadec Island Arc, S. W. Pacific*. Journal of Volcanology and Geothermal Research, 54,* 265-290.

Gamble, J. A., Woodhead, J., Wright, I. & Smith, I. E. M. (1996). Basalt and sediment geochemistry and magma petrogenesis in a transect from oceanic island arc to rifted continental margin arc: The Kermadec- Hikurangi Margin, SW Pacific. *Journal of Petrology, 37,* 1523-1546.

Gamble, J. A., Wood, C. P., Price, R. C., Smith, I. E. M., Stewart, R. B. & Waight, T. (1999). A fifty year perspective of magmatic evolution on Ruapehu Volcano, New Zealand: Verification of open system behavior in an arc volcano. *Earth and Planetary Science Letters, 170*, 301-314.

Geophysics Division, DSIR (1985). *Sheet U17 – Wairakei. Electrical Resistivity map of New Zealand 1:50000.* Nominal Schlumberger array spacings 500 m and 1000 m. DSIR, Wellington.

Gifkins, C., Herrmann, W. & Large, R. (2005). *Altered volcanic rocks: A guide to description and interpretation*. Centre for Ore Deposit Research, University of Tasmania.

Giggenbach, W. F. (1980). Geothermal gas equilibria. *Geochimica et Cosmochimica Acta, 44,* 2021-2032.

Giggenbach, W. F. (1981). Geothermal mineral equilibria. *Geochimica et Cosmochimica Acta, 45*, 393-410.

Giggenbach, W. F. (1988). Geothermal solute equilibria: Derivation of Na-K-Mg- Ca geoindicators. *Geochimica et Cosmochimica Acta, 52*, 2749-2765.

Gill, J. B. (1981*). Orogenic andesites and plate tectonics*. Minerals and Rocks, 16. Springer-Verlag, Berlin.

Glover, R. B. & Mroczek, E. K. (2009). Chemical changes in natural features and well discharges in response to production at Wairakei, New Zealand. *Geothermics, 38,* 117-133.

GNS Science Ltd. New Zealand Active Faults Database, *retrieved 19/01/2011 from http://data.gns.cri.nz/af/.*

Grace, J. (1959). *Tuwharetoa: the history of the Maori people of the Taupo District*. Wellington, New Zealand: A. H. & A. W. Reed.

Graham, I. J. & Hackett, W. R. (1987). Petrology of calc-alkaline lavas from Ruapehu volcano and related vents, Taupo Volcanic Zone. *New Zealand Journal of Petrology, 28,* 531-567.

Graham & Mortimer (1992). Terrane characterisation and timing of metamorphism in the Otago Schist, New Zealand, using Rb-Sr and K-Ar geochronology. *New Zealand Journal of Geology and Geophysics, 35,* 391-401.

Graham, I. J., Gulson, B. L., Hedenquist, J. W. & Mizon, K. (1992). Petrogenesis of Late Cenozoic volcanic rocks from the Taupo Volcanic Zone, New Zealand, in the light of new lead isotope data. *Geochimica et Cosmochimica Acta, 56*, 2797-2819.

Graham, I. J., Cole, J. W., Briggs, R. M., Gamble, J. A., Smith, I. E. M. (1995). Petrology and petrogenesis of volcanic rocks from the Taupo Volcanic Zone: A review. *Journal of Volcanology and Geothermal Research, 68*, 59- 87.

Grange, L. I. (1937). *The geology of the Rotoroa-Taupo Subdivision*. NZGS Bulletin, 37.

Gravley, D. M., Wilson, C. J. N., Rosenberg, M. D. & Leonard, G. S. (2006). The nature and age of Ohakuri Formation and Ohakuri Group rocks in surface exposures and geothermal drillhole sequences in the central Taupo Volcanic Zone, New Zealand. *New Zealand Journal of Geology & Geophysics, 49*, 305-308.

Gregg, D. R. & Laing, A. C. M. (1951). *Wairakei geothermal investigation: Hot springs of sheet N94/4, with notes on other springs of N94.* Wellington, New Zealand: Department of Scientific and Industrial Research, New Zealand.

Grindley, G. W. (1959). *Sheet N85 – Waiotapu.* Geological map of New Zealand 1:63 360. Wellington, New Zealand, Department of Scientific and Industrial Research.

Grindley, G. W. (1960). *Sheet 8 - Taupo.* Geological map of New Zealand, 1:250 000. Wellington, New Zealand. Department of Scientific and Industrial Research.

Grindley, G. W. (1961). *Sheet N94 – Taupo.* Geological map of New Zealand 1:63 360. Wellington, New Zealand, Department of Scientific and Industrial Research.

Grindley, G. W. (1965). The geology, structure and exploitation of the Wairakei geothermal field, Taupo, New Zealand. *New Zealand Geological Society Bulletin, 75*.

Grindley, G. W. & Browne P. R. L. (1968). The subsurface geology of the Broadlands geothermal field. *New Zealand Geological Survey Report, 34*, 1-41.

Grindley, G. W., Mumme, T. C. & Kohn, B. (1994). Stratigraphy, paleomagnetism, geochronology and structure of silicid volcanic rocks, Waiotapu/Paeroa Range area, New Zealand. *Geothermics, 23,* pp 476-499.

Grove, T. L. & Kinzler, R. J. (1986). Petrogenesis of andesites*. Annual Reviews of Earth and Planetary Sciences, 14*, 417-454.

Gunderson, R., Cumming, W., Astra, D. & Harvey, C. (2000). *Analysis of smectite clays in geothermal drill cuttings by the methylene blue method: For well site geothermometry and resistivity sounding correlation.* Proceedings of the World Geothermal Congress 2000. Kyushu – Tohoku, Japan.

Hackett, W. R. & Houghton, B. F. (1988). A facies model for a Quaternary andesitic composite volcano, Ruapehu, New Zealand. *Bulletin of Volcanology, 51,* 51-68.

Hallberg, A. (2001). Rock classification, magmatic affinity, and hydrothermal alteration at Boliden, Skellefte district, Sweden – a desktop approach to whole rock geochemistry. In: Weihed, P. (ed.): *Economic geology research, Vol 1, 1999-2000*. Sveriges geologiska undersökning C833, Uppsala, Sverige, pp. 93-131.

Hammons, T. J. (2004). Geothermal power generation worldwide: Global perspective, technology, field experience, and research and development. *Electric Power Components and Systems, 32,* 529-553.

Harker, A. (1909). *The natural history of igneous rocks.* Methuen, London.

Harrison, A. J. & White, R. S. (2006). Lithospheric structure of an active backarc basin: The Taupo Volcanic Zone, New Zealand. *Geophysical Journal International, 167,* 968-990.

Harvey, C. & Browne, P. R. L. (1991). Mixed-layer clay geothermometry in the Wairakei geothermal field, New Zealand. *Clays and Clay Minerals, 39*, 614-621.

Hastie, A. R., Kerr, A. C., Pearce, J. A. & Mitchell, S. F. (2007). Classification of altered volcanic island arc rocks using immobile trace elements: Development of the Th-Co discrimination diagram. *Journal of Petrology, 48*, 2341-2357.

Hatherton, T. Macdonald, W. J. P. & Thompson, G. E. K. (1966). Geophysical methods in geothermal prospecting in New Zealand. *Bulletin Volcanologique, 29*, 485-498.

Hawkesworth, C. J., Norry, M. J., Roddick, J. C., Baker, P. E., Francis, P. W. & Thorpe, R. S. (1979). $^{143}Nd/^{144}Nd$, $^{87}Sr/^{86}Sr$ and incompatible element variations in calc-alkaline andesites and plateau lavas from South America. *Earth and Planetary Science Letters, 42*, 45-57.

Healy, J. (1974). *Ngatamariki geothermal field* (Report NZGS 38, Part D). NZGS Minerals of NZ.

Hedenquist, J. W. (1986). *Geochemistry of the Ngatamariki geothermal field: Preliminary assessment prior to discharge of wells NM1-NM4* (Technical Note 86/4). Chemistry Division, Department of Scientific and Industrial Research.

Hedenquist, J. W. (1986). Geothermal systems in the Taupo Volcanic Zone: Their characteristics and relation to volcanism and mineralization. *The Royal Society of New Zealand Bulletin, 23,* 134-168.

Hedenquist, J. W., Mroczek, E. K. & Giggenbach, W. F. (1988). *Geochemistry of the Rotokawa geothermal system: Summary of data, interpretation and appraisal for energy development* (Technical Note 88/6). Chemistry Division Department of Scientific and Industrial Research.

Hedenquist, J. W., Reyes, A. G., Simmons, S. F. & Taguchi, S. (1992). The thermal and geochemical structure of geothermal and epithermal systems – A framework for interpreting fluid inclusion data. *European Journal of Mineralogy, 4*, 989-1015.

Henley, R. W. & Ellis, A. J. (1983). Geothermal systems ancient and modern: A geochemical review. *Earth-Science Reviews, 19*, 1-50.

Henneberger, R. C. (1982). *Evolution of the Ohakuri geothermal system (pp. 55-60).* Proceedings of the Pacific Geothermal Converence, 1.

Henneberger, R. C. (1983). *The Ohakuri hydrothermal system* (Unpublished MSc-thesis). Auckland University, Auckland.

Henneberger, R. C. (1986). Ohakuri fossil epithermal system. In: Henley, R. W., Hedenquist, J. W. & Roberts, P. J. (eds.) *Guide to the active epithemal (geothermal) systems and precious metal deposits of New Zealand*. Monograph series of mineral deposits, 26. Gebruder Borntraeger, Berlin- Stuttgart, pp. 121-128.

Henneberger, R. C. & Browne, P. R. L. (1988). Hydrothermal alteration and evolution of the Ohakuri hydrothermal system, Taupo Volcanic Zone, New Zealand. *Journal of Volcanology and Geothermal Research, 34*, 211-231.

Herzer, R. H. (1995). Seismic stratigraphy of a buried volcanic arc, Northland, New Zealand, and implications for Neogene subduction. *Marine Petroleum Geology, 12,* 511-531.

Hiess, J., Cole, J. W. & Spinks, K. D. (2007). Influence of the crust and crustal structure on the location and composition of high-alumina basalts of the Taupo Volcanic Zone, New Zealand. *New Zealand Journal of Geology and Geophysics, 50,* 327-342.

Hildreth, W. (1981). Gradients in silicic magma chambers: Implications for lithospheric magmatism. *Journal of Geophysical Research, 86*, 10153-10192.

Hobden, B. J., Houghton, B. F., Lanphere, M. A. & Nairn, I. A. (1996). Growth of the Tongariro volcanic complex: New evidence from K-Ar age determinations. *New Zealand Journal of Geology and Geophysics, 39*, 151-154.

Hochstein, M. P. & Regenauer-Lieb, K. (1989). *Heat transfer in the Taupo Volcanic Zone (NZ): Role of volcanism and heating by plastic deformation.* Proc. 11th New Zealand Geothermal Workshop, 219-223.

Hochstein, M. P. (1995). Crustal heat transfer in the Taupo Volcanic Zone (New Zealand): comparison with other volcanic arcs and explanatory heat

source models. *Journal of Volcanology and Geothermal Research, 68*, 117-151.

Hochstetter, F. von & Petermann, A. (1864). *The geology of New Zealand: In explanation of the geographical and topographical atlas of New Zealand*. Auckland, New Zealand: T. Delattre.

Hogan, J. P. (1993). Monomineralic glomerocrysts: Textural evidence for mineral resorption during crystallization of igneous rocks. *The Journal of Geology, 101,* 531-540.

Hole, J. K., Bromley, C. J., Stevens, N. F. & Wadge, G. (2007). Subsidence in the geothermal fields of the Taupo Volcanic Zone, New Zealand from 1996 to 2005 measured by InSAR. *Journal of Volcanology and Geothermal Resource, 166*, 125-146.

Honda & Muffler (1970). Hydrothermal alteration in core from research drillhole Y-1, Upper Geyser Basin, Yellowstone National Park, Wyoming. *American Mineralogist, 55,* 1635-1644.

Houghton, B. F., Wilson, C. J. N., McWilliams, M. O., Lanphere, M. A., Weaver, S. D., Briggs, R. M. & Pringle, M. S. (1995). Chronology and dynamics of a large scale silicic magmatic system: Central Taupo Volcanic Zone, New Zealand. *Geology, 23*, 13-16.

Hughes, C. J. (1973). Spilites, keratphyres and the igneous spectrum. *Geological Magazine, 109,* 513-527.

Hunt, T. M. (1998). Recent developments in the New Zealand geothermal industry. *Energy Sources, Part A: Recovery, Utilization and Environmental Effects, 20* (8), 777-786.

Hunt, T. M. & Harms, C. (1990). *Gravity survey of the Rotokawa geothermal field* (pp. 91-96). Proceedings of 12th New Zealand Geothermal Workshop.

Irvine, T. N. & Baragar, W. R. A. (1971). A guide to the chemical classification of the common volcanic rocks. *Canadian Journal of Earth Sciences, 8,* 523-548.

Isthmus Group Ltd. (2007). *Rotokawa geothermal power station: Landscape and visual assessment* (2312 C2/ BC).

Jensen, L. S. (1976). A new cation plot for classifying subalkalic volcanic rocks. *Ontario Division of Mines, Miscellaneous Papers, 66.*

Kamp, P. J. J. (1984). Neocene and Quaternary extent and geometry of the subducted Pacific Plate beneath North Island, New Zealand: Implications for Kaikoura tectonics. *Tectonophysics, 108,* 241-266.

Kamp, P. J. J. & Furlong, K. P. (2006). Neogene plate tectonic reconstructions and geodynamics of the North Island sedimentary basins: Implications for the petroleum systems. *2006 New Zealand Petroleum Conference Proceedings 6-10 March*, pp. 16. Retrieved 02 June, 2009, from http://www.crownminerals.govt.nz/cms/pdf-library/petroleum-conferences-1/2006/papers/Poster_papers_23.pdf

Keith, T. E. C. & Muffler, L. J. P. (1978). Minerals produced during cooling and hydrothermal alteration of ash flow tuff from Yellowstone drillhole Y-5. *Journal of Volcanology and Geothermal Research, 3*, 373-402.

Keith, T. E. C., White, D. E., Beeson, M. H. (1978). Hydrothermal alteration and self-sealing in Y-7 and Y-8 drill holes in northern part of Upper Geyser Basin, Yellowstone National Park, Wyoming. *USGS Professional Paper, 1054A.*

Kendall, C. (1976). *Petrology and stable isotope geochemistry of three wells in the Buttes area of the Salton Sea geothermal field, Imperial Valley, California, USA* (Unpublished MSc thesis). University of California, Riverside Rep. Institute of Geophysics and Planetary Physics – 76/17.

Khabar, D., Browne, P. R. L. & Renner, N. (1986). *Note on the composition of river bank springs, Rotokawa geothermal field* (pp. 193-194). Proceedings 8th New Zealand Geothermal Workshop, University of Auckland.

Kilgour, G. N. & Ramirez, E. O. (2008). *Geology of injection well RK22, Rotokawa geothermal field* (Consultancy Report 2008/272). Institute of Geological and Nuclear Sciences.

King, P. R. (2000). Tectonic reconstructions of New Zealand: 40 Ma to the Present. *New Zealand Journal of Geology & Geophysics, 43,* 611-638.

Kissling, W., Ellis, S., Charpentier, F. & Bibby, H. (2009). Convective flows in a TVZ-like setting with a brittle/ductile transition. *Transport in Porous Media, 77*, 335-355.

Kralj, P., Rychagov, S. & Kralj, P. (2010). Zeolites in volcanic-igneous hydrothermal systems: A case study of Pauzhetka geothermal field (Kamchatka) and Oligocene Smrekovec volcanic complex (Slovenia). *Environmental Earth Sciences, 59,* 951-956.

Kristmannsdottir, H. & Tomasson, J. (1978). Zeolite zones in geothermal areas in Iceland. *Natural Zeolites,* Pergamon Press, Oxford and New York, pp. 277-284.

Lawless, J. (2002). *New Zealand's geothermal resources revisited.* Proceedings of the New Zealand Geothermal Association Seminar, Taupo.

Lee, C.-T. A., Leeman, W. P., Canil, D. & Li, Z. X. A. (2005). Similar V/Sc systematic in MORB and arc basalts: Implications for the oxygen fugacities of their mantle source regions. *Journal of Petrology, 46*, 2313-2336.

LeMaitre, R. W., Bateman, P., Dudek, A., Keller, J., Lameyre Le Bas, M. J., Sabine, P. A., Schmid, R., Sorensen, H., Streckeisen, A., Wolley, A. R. & Zanettin, B. (1989). *A classification of igneous rocks and glossary of terms.* Blackwell, Oxford.

Leonard, G. S. (2003). *The evolution of Maroa Volcanic Centre* (Unpublished PhD thesis). University of Canterbury, Christchurch, New Zealand.

Lloyd, E. F. (1972). *Geology and hot springs of Orakeikorako*. New Zealand Geological Survey Bulletin, 85. Wellington, New Zealand: Department of Scientific and Industrial Research.

Luhr, J. F. (2008). Primary igneous anhydrite: Progress since its recognition in the 1982 El Chichón trachyandesite. *Journal of Volcanology and Geothermal Research, 175,* 394-407.

Luyendyk, B. P. (1995). Hypothesis for Cretaceous rifting of east Gondwana caused by subducted slab capture. *Geology, 23,* 73-76.

MacLean, W.H. & Kranidiotis, P. (1987). Immobile elements as monitors of mass transport in hydrothermal alteration: Phelps Dodge massive sulfide deposit, Matagami. *Economic Geology, 82*, 951-962.

MacLean, W. H. & Barrett, T. J. (1993). Lithogeochemical techniques using immobile elements. *Journal of Geochemical Exploration, 48,* 109-133.

Macphearson, C. G., Dreher, S. T. & Thirlwall, M. F. (2006). Adakites without slab melting: High pressure differentiation of island arc magma, Mindanao, the Philippines. *Earth and Planetary Science Letters, 243*, 581-593.

Mahon, W. A. J. (1960). *Open File Report* (No. DL 118/12 – WAJM4). Chemistry Division, Department of Scientific and Industrial Research, Wellington.

Mahon, W. A. J. (1966). Silica in hot water discharged from drillholes at Wairakei, New Zealand. *New Zealand Journal of Science, 9*, 135-144.

Mange, M. A. & Wright, D. T. (2007). *Heavy minerals in use.* Developments in Sedimentology, 58, Elsevier; Amsterdam, Netherlands.

Martin, J. T. & Lowell, R. P. (2000). Precipitation of quartz during high-temperature, fracture-controlled hydrothermal upflow at ocean ridges: Equilibrium versus linear kinetics. *Journal of Geophysical Research, 105*, 869-882.

Martin, R. C. (1961). Stratigraphy and structural outline of the Taupo Volcanic Zone. *New Zealand Journal of Geology and Geophysics, 4,* 449-478.

McCulloch, M. T. & Gamble, J. A. (1991). Geochemical and geodynamical constraints on subduction zone magmatism. *Earth and Planetary Science Letters, 102*, 358-374.

McDonough, W. F., McCulloch, M. T., Sun, S. (1985). Isotopic and geochemical systematic in Tertiary-Recent basalts from southeastern Australia and implications for the evolution of the subcontinental lithosphere. *Geochimica et Cosmochimica Acta, 49*, 2051-2067.

McNabb, A. (1965). *On convection in a porous medium* (pp. C161-C171). Proceedings 2nd Australian Conference on Hydraulics and Fluid Mechanics.

McPhie, J., Doyle, M & Allen, R. (1993). *Volcanic textures: A guide to the interpretation of textures in volcanic rocks.* Centre for Ore Deposit and Exploration Studies, University of Tasmania.

Milicich, S. D. & Hunt, T. (2007). *Thermal features of the Rotokawa Geothermal Field* (Consultancy Report 2007/90). Institute of Geological and Nuclear Sciences.

Milicich, S. D. & Reeves, R. (2009). Thermal features of the Ngatamariki geothermal field (Consultancy Report 2009/97). Institute of Geological and Nuclear Sciences.

Morad, S., El-Ghali, M. A. K., Caja, M. A., Sirat, M., Al-Ramadan, K. & Mansurbeg, H. (2010). Hydrothermal alteration of plagioclase in granitic rocks from Proterozoic basement of SE Sweden. *Geological Journal, 45,* 105-116.

Mortimer, N. (2004). New Zealand's geological foundations. *Gondwana Research, 1*, 262-272.

Mortimer, N., Tulloch, A. J., Gans, P. Calvert, W. N. (1999). Geology and thermochronometry of the east edge of the Median Tectonic Batholith (Median Tectonic Zone): a new perspective on Permian to Cretaceous crustal growth of New Zealand. *Island Arc, 8*, 404-425.

Mortimer, N., Herzer, R. H., Gans, P. B., Laporte-Magoni, C., Calvert, A. T., Bosch, D. (2007). Oligocene-Miocene tectonic evolution of the South Fiji basin and Northland Plateau, SW Pacific Ocean: Evidence from petrology and dating of dredged rocks. *Marine Geology, 237*, 1-24.

Mortimer, N., Raine, J. I. & Cook, R. A. (2009). Correlation of basement rocks from Waka Nui-1 and Awhitu-1 and the Jurassic regional geology of Zealandia. *New Zealand Journal of Geology & Geophysics, 52*, 1-10.

Mysen, B. O. & Boettcher, A. L. (1975). Melting of a hydrous mantle, II. Geochemistry of crystals and liquids formed by anatexis of mantle peridotite at high pressures and high temperatures as a function of controlled activities of water, hydrogen and carbon dioxide. *Journal of Petrology, 16,* 549-593.

Naboko, S. I. (1970). Facies of hydrothermally altered rocks of Kamchatka-Kurile volcanic arc. *Pacific Geology, 2,* 23-27.

Nachit, H., Ibhi, A., Abia, E. H. & Ohoud, M. B. (2005). Discrimination between primary magmatic biotites, reequilibrated biotites and neoformed biotites. *Geomaterials (Mineralogy), 337,* 1415-1420.

Nairn, I. A. (1986). *Rotokawa RK8 stratigraphy* (Unpublished report). Department of Scientific and Industrial Research.

Nairn, I. A., Wood, C. P. & Bailey, R. A. (1994). The Reporoa Caldera, Taupo Volcanic Zone: source of the Kaingaroa Ignimbrites. *Bulletin of Volcanology, 56*, 529-537.

Nelson, C. S. (2008). *Sedimentary geology: ERTH322-08B* [Lecture notes]. Hamilton, New Zealand: University of Waikato, Department of Earth and Ocean Sciences.

Nicholson, K. (1993). Geothermal fluids: *Chemistry and exploration techniques*. Berlin, Germany: Springer-Verlag.

O'Brien, J. M. (2010). *Hydrogeochemical characteristics of the Ngatamariki geothermal field and a comparison with the Orakei Korako thermal area, Taupo Volcanic Zone, New Zealand* (MSc thesis). University of Canterbury.

Parry, W. T. (1998). Fault-fluid composition from fluid-inclusion observations and solubilities of fracture-sealing minerals. *Tectonophysics, 290,* 1-26.

Parry, W. T. & Downey, L. M. (1982). Geochemistry of hydrothermal chlorite replacing igneous biotite. *Clays and Clay Minerals, 30,* 81-90.

Parson, L. M. & Wright, I. C. (1996). The Lau-Havre-Taupo back-arc basin: A southward-propagating, multistage evolution from rifting to spreading. *Tectonophysics, 263,* 1-22.

Peacock, M. A. (1931). Classification of igneous rock series. *Journal of Geology, 39,* 54-67.

Pearce, J. A. & Cann, J. R. (1973). Tectonic setting of basic volcanic rocks determined using trace element analyses. *Earth and Planetary Science Letters, 19*, 290-300.

Pearce, J. A. (1983). Role of the sub-continental lithosphere in magma genesis at active continental margins. In: Hawkesworth, C. J. & Norry, M. J. (eds.), *Continental basalts and mantle xenoliths*. Shiva, Nantwich, pp. 230-249.

Pearce, J. A. (1996). A user's guide to basalt discrimination diagrams. In: Wyman, D. A. (ed.) *Trace Element Geochemistry of Volcanic Rocks: Applications for Massive Sulphide Exploration.* Geological Association of Canada, Short Course Notes 12, 79–113.

Peccerillo, A. & Taylor, S. R. (1976). Geochemistry of Eocene calc-alkaline volcanic rocks from the Kastamonu area, Northern Turkey. *Contributions to Mineralogy and Petrology, 58*, 63-81.

Peccerillo, A. & Wu, T. W. (1992). Evolution of calc-alkaline magmas in continental arc volcanoes: Evidence from Alicudi, Aeolian Arc (Southern Tyrrhenian Sea, Italy). *Journal of Petrology, 33*, 1295-1315.

Pollack, H. N. (1982). The heat flow from the continents. *Annual Review of Earth and Planetary Sciences, 10,* 459-81.

Price, R. C., Mc Culloch, M. T., Smith, I. E. M. & Stewart, R. B. (1992). Pb-Nd-Sr isotopic compositions and trace element characteristics of young volcanic rocks from Egmont Volcano, New Zealand and comparisons with basalts and andesites from the Taupo Volcanic Zone. *Geochimica and Cosmochimica Acta, 56*, 941-953.

Price, R. C., Gamble, J. A., Smith, I. E. M., Stewart, R. B., Eggins, S. & Wright, I. C. (2005). An integrated model for the temporal evolution of andesites and rhyolites and crustal development in New Zealand's North Island. *Journal of Volcanology and Geothermal Research, 140*, 1-24.

Price, R. C., Turner, S., Cook, C., Hobden, B., Smith, I. E. M., Gamble, J. A., Handley, H., Maas, R. & Möbis, A. (2010). Crustal and mantle influences and U-Th-Ra disequilibrium in andesitic lavas of Ngauruhoe volcano, New Zealand. *Chemical Geology, 277*, 355-373.

Putnis, A. & McConnell, J. D. C. (1976). The transformation behavior of meta enriched chalcopyrite. *Contributions to Mineralogy and Petrology, 58,* 127-136.

Rae, A. (2007). *Rotokawa geology and geophysics* (Consultancy Report 2007/83). Institute of Geological and Nuclear Sciences.

Rae, A., Ramirez, L. E. & Bardsley, C. (2009a). *Geology of exploration well NM6, Ngatamariki geothermal field* (Consultancy Report 2009/130). Institute of Geological and Nuclear Sciences.

Rae, A., Ramirez, L. E. & Boseley, C. (2009b). Geology of exploration well NM7, Ngatamariki geothermal field. GNS Science Consultancy Report 2009/289.

Rae, A., McCoy-West, A. J., Ramirez, L. E. (2009c). *Geology of production wells RK26 and RK27, Rotokawa geothermal field* (Consultancy Report 2009/202). Institute of Geological and Nuclear Sciences.

Rae, A., McCoy-West, A. J., Ramirez, L. E., Alcaraz, S. A. (2009d). *Geology of production well RK28, Rotokawa geothermal field* (Consultancy Report 2009/253). Institute of Geological and Nuclear Sciences.

Ramirez, L. E. & Rae, A. (2009a). *Geology of injection well NM5/5A, Ngatamariki geothermal field* (Consultancy Report 2009/253). Institute of Geological and Nuclear Sciences.

Ramirez, L. E. & Rae, A. (2009b). *Geology of injection well RK24/RK24 ST1, Rotokawa geothermal field* (Consultancy Report 2009/90). Institute of Geological and Nuclear Sciences.

Ramirez, L. E., Kilgour, G. N., Rae, A. & Bignall, G. (2008a). *Geology of injection well RK21* (Consultancy Report 2008/90). Institute of Geological and Nuclear Sciences.

Ramirez, L. E., Milicich, S. D., Rae, A. J. & Bignall, G. (2008b). *Geology of injection well RK25* (Consultancy Report 2008/332). Institute of Geological and Nuclear Sciences.

Reed, M. H. (1982). Calculation of multicomponent chemical equilibria and reaction processes in systems involving minerals, gases and aqueous phase. *Geochimica et Cosmochimica Acta, 46,* 513-528.

Reed, M. H. (1997). Hydrothermal alteration and its relationship to ore field composition. In Barnes, H. L. (ed.) *Geochemistry of hydrothermal ore deposits,* John Wiley & Sons, New York, pp. 303-366.

Reed, M. H. (1998). Calculation of simultaneous chemical equilibria in aqueous-mineral-gas systems and its application to modeling hydrothermal processes. In Richards, J. & Larson, P. (eds.) *Techniques in hydrothermal ore deposits geology,* Economic Geology, pp. 109-124.

Reed, M. H. & Spycher, N. F. (1984). Calculation of pH and mineral equilibria in hydrothermal waters with application to geothermometry and studies of boiling and dilution. *Geochimica et Cosmochimica Acta, 48,* 1479-1492.

Reyes, A. G. (2000). *Petrology and mineral alteration in hydrothermal systems: From diagenesis to volcanic catastrophes* (report 18-1998). UNU-GTP.

Reyners, M., Eberhart-Philips, D. & Stuart, G. (2007). The role of fluids in lower-crustal earthquakes near continental arc rifts. *Nature, 446,* 1075-1078.

Rickwood (1989). Boundary lines within petrological diagrams which use oxides of major and minor elements. *Lithos, 22*, 247-263.

Risk, G. (1986). *Electrical Resistivity Survey of the Ngatamariki Geothermal Field* (Contract Report 3). Geophysics Division Department of Scientific and Industrial Research.

Risk, G. F., Caldwell, T. G. & Bibby, H. M. (2003). Tensor time domain electromagnetic resistivity measurements at Ngatamariki geothermal field, New Zealand. *Journal of Volcanology and Geothermal Research, 127*, 33-54.

Robb, L. J. (2005). *Introduction to ore-forming processes.* Blackwell Science: Oxford, UK.

Rollinson, H. R. (1993). *Using geochemical data: Evaluation, presentation, interpretation*. New York, USA: Longman Scientific & Technical. 352 pp.

Rosenberg, M. D., Kilgour, G. N. & Fraser, H. L. (2005). *Geology of RK16, RK17 and RK18* (Consultancy Report 2005/144). Institute of Geological and Nuclear Sciences.

Rotokawa Joint Venture (2007). *Rotokawa geothermal development: Resource consent applications and assessment of environmental effects* (Unpublished report).

Rowland, J. V. & Sibson, R. H. (2004). Structural controls on hydrothermal flow in a segmented rift system, Taupo Volcanic Zone, New Zealand. *Geofluids, 4,* 259-283.

Rowland, J. V. (2010). Spatial and temporal variations in magma-assisted rifting, Taupo Volcanic Zone. *Journal of Volcanology and Geothermal Research, 190*, 89-108.

Sales, R. H. & Meyer, C. (1948). Wall rock interaction at Butte, Montana: *Transactions of the American Institute of Mining and Metallurgic Engineers, 178,* 9-35.

Scott, S. D. (1983). Chemical behavior of sphalerite and arsenopyrite in hydrothermal and metamorphic environments. *Mineralogical Magazine, 47*, 427-35.

Self, S. & Healy, J. (1987). Wairakei Formation, New Zealand: Stratigraphy and correlation. *New Zealand Journal of Geology and Geophysics, 30,* 73-86.

Shannon, R. D. (1976). Revised effective ionic radii and systematic studies of interatomic distances in halides and chalcogenides. *Acta Crystallographica, A32,* 751-767.

Sheppard, D. S. & Lyon, G. L. (1984). Geothermal fluid chemistry of the Orakeikorako field, New Zealand. *Journal of Volcanology and Geothermal Research, 22,* 329-349.

Simmons, S. F. & Christenson, B. W. (1994). Origins of calcite in a boiling geothermal system. *American Journal of Science, 294*, 361-400.

Smith, I. E. M. (1990). *Late Cenozoic volcanic successions in northern New Zealand and their relationship to tectonic setting* (pp. 283-288). Proceedings Pacific Rim Congress, 1990, II.

Soengkono, S., Hochstein, M. P., Smith, I. E. M. & Itaya, T. (1992). Geophysical evidence for widespread reversely magnetised pyroclastics in the western Taupo Volcanic Zone (New Zealand). *New Zealand Journal of Geology and Geophysics, 35*, 47-55.

Spinks, K. D., Acocella, V., Cole, J. W. & Bassett, K. N. (2005). Structural control of volcanism and caldera development in the transtensional Taupo Volcanic Zone, New Zealand. *Journal of Volcanology and Geothermal Research, 144*, 7-22.

Stagpoole, V.M. & Bibby, H.M. (1998a). *Electrical Resistivity map of the Taupo Volcanic Zone, New Zealand: nominal array spacing 1000m, 1:250,000 version 1.0*. Institute of Geological and Nuclear Sciences geophysical map 12. Institute of Geological and Nuclear Sciences Limited, Lower Hutt, New Zealand.

Stagpoole, V.M. & Bibby, H.M. (1998b). *Shallow resistivity of the Taupo Volcanic Zone, New Zealand* (pp. 303-309) In: Simmons, S.F., Morgan, O.E. & Dunstall, M.G. (comp.) Proceedings of the 20th New Zealand Geothermal Workshop 1998. University of Auckland, New Zealand.

Steiner, A. (1953). Hydrothermal rock alteration at Wairakei, New Zealand. *Economic Geology, 48*, 1-13.

Steiner, A. (1963). The rocks penetrated by drillholes in the Waiotapu thermal area, and their hydrothermal alteration (pp. 26-34). In: *Waiotapu Geothermal Field*. DSIR Bulletin 155, Wellington, New Zealand.

Steiner, A. (1968). Clay minerals in hydrothermally altered rocks at Wairakei, New Zealand. *Clays and Clay Minerals, 16,* 193-213.

Stern, A. T. (1987). Asymmetric back-arc spreading, heat flux and structure associated with the central volcanic region of New Zealand. *Earth and Planetary Science Letters, 85*, 365-276.

Stipp, J. J. (1968). *The geochronology and petrogenesis of the Cenozoic volcanics of the North Island, New Zealand* (Unpublished PhD thesis). Australian National University, Canberra, Australia.

Sutherland, R. (1999). Basement geology and tectonic development of the greater New Zealand region: an interpretation from regional magnetic data. *Tectonophysics, 308*, 341-362.

Thorpe, R. S. (1982). *Orogenic andesites and related rocks*. John Wiley & Sons, New York.

Todd, E., Gill, J. B., Wysoczanski, R. J., Handler, M. R., Wright, I. C. & Gamble, J. A. (2010). Sources of constructional cross-chain volcanism in the southern Havre Trough: New insights from HFSE and REE concentration and isotope systematic. *Geochemistry Geophysics Geosystems (G3), 4,* (11), CiteID Q04009.

Turner, S., Hawkesworth, C., Rogers, N., Worthington, T., Hergt, J., Pearce, J., Smith, I. (1997). ^{238}U-^{230}Th disequilibria, magma petrogenesis and flux rates beneath the depleted Tonga-Kermadec island arc. *Geochimica et Cosmochimica Acta, 61*, 4855-4884.

Uruski, C., Stagpole, V. & Baillie, P. (2002). Deepwater Taranaki Basin: Exploring a New Zealand frontier. *Oil & Gas Journal, 100,* (48), 28-33.

Urzua, M. L. A. (2008). *Integration of preliminary one-dimensional MT analysis with geology and geochemistry in a conceptual model of the Ngatamariki geothermal field* (Unpublished MSc thesis). The University of Auckland.

Vance, J. A. (1961). Polysynthetic twinning in plagioclase. *The American Mineralogist, 46,* 1097-1119.

Vance, J. A. (1962). Zoning in igneous plagioclase; normal and oscillatory zoning. *American Journal of Science, 260,* 746-760.

Vance, J. A. (1969). On synneusis. *Contributions to Mineralogy and Petrology, 24*, 7-29.

Vaughan, D. J. & Ixer, R. A. (1980). Studies of the sulphide mineralogy of North Pennine ore and its contribution to genetic models. *Transactions of the Institution of Mining and Metallurgy, B89,* 99-108.

Villamor, P. & Berryman, K. (2001). A late Quaternary extension rate in the Taupo Volcanic Zone, New Zealand, derived from fault slip data. *New Zealand Journal of Geology and Geophysics, 44,* 243-269.

Villamor, P., Van Dissen, R., Alloway, B. V., Palmer, A. S. & Litchfield, N. (2007). The Rangipo Fault, Taupo rift, New Zealand: An example of temporal sliprate and single-event displacement variability in a volcanic environment. *Geological Society of America Bulletin, 119*, 529-547.

Vucetich, C. G. & Pullar, W. A. (1969). Stratigraphy and chnronology of Late Pleistocene volcanic ash beds in Central North Island, New Zealand. In: F. A. Bodley (ed.), *New Zealand Journal of Geology and Geophysics, 12*, pp. 784-837.

Vucetich, C. G. & Howorth, R. (1976). Proposed definition of the Kawakawa Tephra, the c. 20000 years B. P. marker horizon in the New Zealand region. *New Zealand Journal of Geology and Geophysics, 19*, 43-50.

Weaver, C. E. (1967). The significance of clay minerals in sediments. In Nagy, B. & Colombo, V. (eds.), *Fundamental aspects of petroleum geochemistry* (pp. 37-75). New York, USA: Elsevier.

White, N. C. & Hedenquist, J. W. (1995). Epithermal gold deposits: Styles, characteristics and exploration. *SEG Newsletter, 23*, 9-13.

Wilson, C. J. N. (1988). Letter to the editor - Wairakei Formation, New Zealand: Stratigraphy and correlation. *New Zealand Journal of Geology and Geophysics, 31*, 391-396.

Wilson, C. J. N, Rogan, A. M., Smith, I. E. M., Northey, D. J., Nairn, I. A. & Houghton, B. F. (1984). Caldera volcanoes of the Taupo Volcanic Zone, New Zealand. *Journal of Geophysical Research, 89*, 8463-8484.

Wilson, C. J. N., Houghton, B. F., Lloyd, E. F. (1986). Volcanic history and evolution of the Maroa-Taupo area, Central North Island. In: I. E. M. Smith (ed.), Late Cenozoic volcanism in New Zealand. *Royal Society of New Zeland Bulletin, 23*, 194-223.

Wilson, C. J. N., Switsur, V. R. & Ward, A. P. (1988). A new 14C age for the Oruanui (Wairakei) eruption, New Zealand. *Geological Magazine, 125,* 297-300.

Wilson, C.J.N., Houghton, B.F., McWilliams, M.O., Lanphere, M. A., Weaver, S.D. and Briggs, R.M., (1995). Volcanic and structural evolution of the Taupo Volcanic Zone: a review and synthesis. *Journal of Volcanology and Geothermal Research, 68*, l-28.

Wilson, C. J. N., Charlier, B. L. A., Rowland, J. V. & Browne, P.R. L. (2010). U-Pb dating of zircon in subsurface, hydrothermally altered pyroclastic deposits and implications for subsidence in a magmatically active rift: Taupo Volcanic Zone, New Zealand. *Journal of Volcanology and Geothermal Research, 191,* 69-78.

Wilson, M. (1989). *Igneous petrogenesis.* London, UK: Chapman & Hall.

Winchester, J. A. & Floyd, P. A. (1977). Geochemical discrimination of different magma series and their differentiation products using immobile elements. *Chemical Geology, 20,* 325-343.

Winter, J. D. (2001). *An introduction to igneous and metamorphic petrology*. New Jersey, USA: Prentice Hall.

Wood, C. P. (1986a). *Stratigraphy and petrology of NM2: Ngatamariki geothermal field* (Unpublished report). Department of Scientific and Industrial Research.

Wood, C. P. (1986b). *Stratigraphy and petrology of NM3: Ngatamariki geothermal field* (Unpublished report). Department of Scientific and Industrial Research.

Wood, C. P. (1986c). *Stratigraphy and petrology of NM4: Ngatamariki geothermal field* (Unpublished report). Department of Scientific and Industrial Research.

Wooding, R.A. (1963). Convection in a saturated porous medium at large Rayleigh number or Peclet number. *Journal of Fluid Mechanics, 15*, 527-544.

Wooding, R.A. (1964). Mixing-layer flows in a saturated porous medium. *Journal of Fluid Mechanics, 19*, 103-113.

Wright, I. C. (1992). Shallow structure and active tectonism of an offshore continental back-arc spreading system: The Taupo Volcanic Zone, New Zealand. *Marine Geology, 103*, 287-309.

Zacharias, J. (2008). Compositional trends in magmatic and hydrothermal silicates of the petrackova hora intrusive complex, Bohemian Massif – link between the magmatic processes and intrusion-related gold mineralization. *Journal of Geosciences, 53*, 105-117.

Zhang, S. & Veblen, D. R. (2007). *Chemical and structural variations at augite (100) twin boundaries* (abstract #M22A-07). American Geophysical Union, Fall Meeting 2007,

Zimmer, M. M., Plank, T., Hauri, E., Yogodzinski, G. M., Stelling, P., Larsen, J., Singer, B., Jicha, B., Mandeville, C. & Nye, C. J. (2010). *Journal of Petrology, 51,* 2411-2444.

Appendix 1

Microprobe data of primary and secondary minerals

Ngatamariki field NM5A, 2575-2578 mRF

Sample no	Mineral interpretation	SiO_2	TiO_2	Al_2O_3	FeO	MnO	MgO	CaO	Na_2O	K_2O	P_2O_5	SO_3	Cl	Cr_2O_3	NiO	TOTAL
LA4 1	Augite core	51.18	0.58	1.66	10.18	0.12	14.39	19.77	0.25	0.07	0.04	0.00	0.00	0.15	0.06	**98.45**
LA4 1	Augite rim	51.84	0.60	1.67	9.46	0.13	15.11	20.22	0.04	0.05	0.19	0.01	0.00	0.21	0.07	**99.60**
LA4 2	Titanomagnetite	0.21	9.52	2.41	79.39	0.49	0.00	0.00	0.42	0.00	0.00	0.00	0.00	1.10	0.05	**93.59**
LA4 3	Labradorite core	54.05	0.09	27.87	0.53	0.00	0.00	11.56	5.01	0.37	0.12	0.07	0.03	0.02	0.00	**99.72**
LA4 3	Labradorite rim	52.72	0.10	28.75	0.56	0.03	0.00	12.22	4.56	0.37	0.13	0.14	0.07	0.06	0.10	**99.81**
LA4 4	Augite	51.47	0.69	1.67	10.49	0.41	14.05	20.25	0.12	0.14	0.39	0.02	0.04	0.05	0.04	**99.83**
LA4 5	Labradorite core	51.55	0.05	30.09	0.53	0.00	0.03	13.62	3.76	0.23	0.05	0.00	0.00	0.12	0.09	**100.12**
LA4 5	Labradorite rim	52.60	0.11	29.38	0.75	0.00	0.00	12.84	4.19	0.27	0.08	0.00	0.05	0.03	0.00	**100.30**
LA4 6	Augite	51.56	0.61	1.77	9.86	0.30	14.53	19.98	0.09	0.05	0.13	0.00	0.04	0.15	0.10	**99.17**
LA4 7	Chlorite on pyroxene	29.47	0.00	16.32	22.38	0.29	17.74	0.32	0.01	0.14	0.06	0.05	0.00	0.00	0.16	**86.94**
LA4 8	Titanomagnetite	2.16	13.23	0.17	77.53	0.15	0.02	0.25	0.00	0.09	0.00	0.02	0.00	0.55	0.15	**94.32**
LA4 9	Chlorite on pyroxene	30.42	0.12	15.97	21.85	0.31	18.35	0.40	0.14	0.13	0.00	0.02	0.03	0.14	0.00	**87.88**
LA4 10	Labradorite core	53.04	0.14	28.86	0.56	0.02	0.00	12.58	4.28	0.31	0.12	0.02	0.00	0.08	0.16	**100.17**
LA4 11	Titanomagnetite	1.05	13.94	1.84	75.20	0.00	0.00	0.15	0.54	0.08	0.12	0.01	0.09	0.96	0.17	**94.15**
LA4 12	Labradorite core	53.64	0.13	27.84	0.68	0.03	0.00	11.47	4.90	0.38	0.04	0.00	0.03	0.08	0.00	**99.22**
LA4 12	Labradorite rim	53.36	0.02	28.41	0.65	0.00	0.00	11.80	4.62	0.37	0.05	0.02	0.00	0.12	0.08	**99.50**
LA4 13	Chlorite on pyroxene	30.55	0.00	15.86	21.46	0.33	19.04	0.37	0.01	0.09	0.00	0.00	0.00	0.09	0.05	**87.85**
LA4 14	Chlorite on pyroxene	30.09	0.09	14.92	21.43	0.30	18.76	0.31	0.00	0.05	0.00	0.00	0.00	0.05	0.00	**86.00**

Ngatamariki field, NM6 2686-2689 mRF

Sample no	Mineral interpretation	SiO_2	TiO_2	Al_2O_3	FeO	MnO	MgO	CaO	Na_2O	K_2O	P_2O_5	SO_3	Cl	Cr_2O_3	NiO	TOTAL
LA5 1	Augite	51.84	0.51	1.42	11.07	0.32	14.23	19.89	0.25	0.12	0.08	0.00	0.01	0.00	0.00	**99.74**
LA5 1	Augite	51.20	0.60	2.45	11.73	0.41	13.74	19.72	0.34	0.10	0.18	0.16	0.04	0.12	0.00	**100.79**
LA5 2	Chlorite on pyroxene	30.04	0.04	15.95	22.80	0.32	17.31	0.45	0.00	0.06	0.02	0.00	0.03	0.00	0.04	**87.06**
LA5 3	Augite	52.26	0.26	2.70	6.03	0.15	16.84	20.95	0.00	0.15	0.20	0.00	0.06	0.30	0.06	**99.96**
LA5 4	Chlorite on pyroxene	31.04	0.13	13.96	22.02	0.39	17.85	0.34	0.00	0.07	0.00	0.02	0.01	0.00	0.00	**85.83**
LA5 5	Titanomagnetite	1.43	3.66	0.51	87.82	0.12	0.34	0.16	0.00	0.04	0.00	0.01	0.05	0.06	0.27	**94.47**
LA5 6	Chlorite vein	30.58	0.04	17.57	20.95	0.37	16.91	0.60	0.09	0.07	0.10	0.10	0.05	0.00	0.09	**87.52**
LA5 6	Chlorite on pyroxene	30.23	0.00	15.85	21.98	0.24	16.87	0.63	0.00	0.07	0.00	0.00	0.00	0.04	0.00	**85.89**
LA5 7	Bytownite	47.07	0.09	33.08	0.59	0.08	0.00	16.74	1.90	0.19	0.00	0.00	0.00	0.03	0.11	**99.87**
LA5 7	Labradorite rim	52.42	0.09	29.01	0.57	0.06	0.05	12.90	3.94	0.29	0.18	0.00	0.00	0.02	0.00	**99.53**
LA5 8	Chlorite on pyroxene	31.26	0.00	15.23	22.35	0.38	17.60	0.52	0.00	0.11	0.00	0.00	0.09	0.01	0.00	**87.55**
LA5 9	Labradorite core	52.90	0.10	29.11	0.64	0.00	0.10	12.62	4.38	0.25	0.00	0.00	0.00	0.12	0.00	**100.22**
LA5 9	Labradorite rim	51.81	0.00	30.16	0.59	0.00	0.05	13.57	3.89	0.27	0.05	0.00	0.05	0.09	0.18	**100.71**
LA5 10	Labradorite core	50.54	0.13	30.78	0.55	0.00	0.01	14.33	3.40	0.20	0.00	0.02	0.03	0.00	0.07	**100.06**
LA5 11	Labradorite core	51.44	0.02	30.07	0.54	0.08	0.00	14.12	3.54	0.30	0.05	0.00	0.02	0.01	0.00	**100.19**
LA5 12	Titanomagnetite	1.83	12.42	0.45	78.77	0.00	0.33	0.18	0.00	0.13	0.12	0.00	0.00	0.09	0.32	**94.62**

Ngatamariki field, NM6 (cuttings) 2210 mRF

Sample no	Mineral interpretation	SiO_2	TiO_2	Al_2O_3	FeO	MnO	MgO	CaO	Na_2O	K_2O	P_2O_5	SO_3	Cl	Cr_2O_3	NiO	TOTAL
LA15 2	Quartz	96.93	0.00	0.00	0.00	0.00	0.05	0.13	0.00	0.05	0.28	0.01	0.03	0.00	0.04	**97.52**
LA15 4	Albite	67.67	0.00	19.54	0.02	0.06	0.05	0.36	11.65	0.18	0.11	0.08	0.03	0.00	0.03	**99.78**
LA15 4	Rutile	0.20	97.62	0.13	0.51	0.00	0.03	0.12	0.09	0.00	0.00	0.00	0.07	0.03	0.12	**98.92**
LA15 5	Quartz	97.33	0.00	0.00	0.01	0.00	0.00	0.10	0.00	0.06	0.24	0.00	0.07	0.01	0.00	**97.82**

LA15 6	Quartz	97.81	0.00	0.00	0.05	0.00	0.01	0.04	0.00	0.00	0.55	0.00	0.04	0.00	0.00	**98.50**
LA15 8	Albite	67.11	0.00	19.69	0.04	0.00	0.01	0.20	11.77	0.18	0.01	0.00	0.00	0.02	0.05	**99.08**
LA15 9	Albite	68.09	0.15	19.16	0.00	0.00	0.04	0.13	11.66	0.11	0.00	0.00	0.02	0.00	0.00	**99.36**
LA15 11	Albite core	67.39	0.05	19.60	0.05	0.19	0.04	0.54	11.55	0.18	0.08	0.17	0.02	0.00	0.01	**99.87**
LA15 11	Albite rim	67.12	0.00	19.30	0.05	0.01	0.00	0.22	11.60	0.12	0.19	0.00	0.00	0.00	0.00	**98.61**

Rotokawa field, RK21 1876.8 mRF

Sample no	Mineral interpretation	SiO_2	TiO_2	Al_2O_3	FeO	MnO	MgO	CaO	Na_2O	K_2O	P_2O_5	SO_3	Cl	Cr_2O_3	NiO	TOTAL
LA 1 1	Labradorite core	53.59	0.00	28.39	0.52	0.00	0.00	11.90	4.62	0.27	0.00	0.00	0.03	0.07	0.00	**99.39**
LA 1 2	Chlorite on pyroxene	24.96	0.04	17.79	18.91	0.21	15.99	0.18	0.09	0.02	0.00	0.25	0.04	0.01	0.08	**78.57**
LA1 4	Labradorite core	54.27	0.04	28.00	0.46	0.00	0.01	11.41	4.98	0.40	0.00	0.00	0.00	0.15	0.00	**99.72**
LA1 6	Chlorite as vug rim	28.90	0.00	17.82	20.14	0.36	18.12	0.26	0.01	0.12	0.00	0.01	0.05	0.00	0.00	**85.79**
LA1 6	Chlorite as vug core	29.31	0.00	17.42	20.19	0.38	18.52	0.26	0.00	0.05	0.00	0.01	0.00	0.04	0.03	**86.21**
LA1 7	Labradorite core	51.11	0.02	29.86	0.52	0.01	0.05	13.68	3.59	0.23	0.00	0.05	0.00	0.01	0.22	**99.35**
LA1 7	Labradorite rim	51.96	0.17	29.62	0.68	0.00	0.00	13.10	3.89	0.24	0.09	0.02	0.03	0.13	0.07	**100.00**
LA1 8	Chlorite as vug rim	27.17	0.00	18.05	20.10	0.34	17.47	0.20	0.00	0.02	0.00	0.00	0.08	0.01	0.10	**83.54**
LA1 8	Calcite in vug centre	0.00	0.00	0.00	1.57	0.21	0.15	51.33	0.07	0.08	0.04	0.13	0.02	0.00	0.00	**53.60**

Rotokawa field, RK21 1876.2 mRF

Sample no	Mineral interpretation	SiO_2	TiO_2	Al_2O_3	FeO	MnO	MgO	CaO	Na_2O	K_2O	P_2O_5	SO_3	Cl	Cr_2O_3	NiO	TOTAL
LA3 1	Labradorite core	52.90	0.09	28.38	0.57	0.00	0.00	12.02	4.43	0.25	0.01	0.09	0.06	0.07	0.00	**98.87**
LA3 1	Labradorite mid	53.67	0.16	28.64	0.46	0.00	0.00	11.93	4.64	0.26	0.00	0.00	0.03	0.01	0.00	**99.80**
LA3 1	Labradorite rim	51.72	0.00	29.77	0.56	0.03	0.00	13.36	3.89	0.27	0.00	0.00	0.03	0.09	0.02	**99.74**
LA3 2	Titanomagnetite	2.46	12.82	2.95	73.09	0.32	0.09	0.25	0.18	0.10	0.13	0.13	0.00	0.25	0.10	**92.87**

LA3 3	Augite	50.75	0.53	4.55	6.52	0.12	15.60	21.28	0.12	0.09	0.00	0.06	0.00	0.27	0.00	**99.89**
LA3 4	Augite	51.86	0.51	3.03	7.93	0.10	15.65	20.70	0.19	0.06	0.04	0.13	0.04	0.18	0.13	**100.55**
LA3 5	Titanomagnetite	3.70	10.47	1.87	76.91	0.10	0.01	0.32	0.38	0.25	0.01	0.10	0.00	0.12	0.00	**94.24**
LA3 7	Chlorite on orthopyroxene	30.95	0.03	14.28	21.14	0.32	19.31	0.22	0.00	0.22	0.00	0.00	0.02	0.00	0.07	**86.53**
LA3 7	Orthopyroxene	53.75	0.07	0.92	18.33	0.32	24.48	1.85	0.00	0.03	0.09	0.00	0.00	0.15	0.12	**100.11**
LA3 8	Augite core	52.15	0.39	2.10	9.37	0.33	14.70	20.26	0.35	0.08	0.40	0.06	0.04	0.17	0.00	**100.40**
LA3 8	Augite rim	51.46	0.57	2.55	9.58	0.32	14.54	20.37	0.22	0.12	0.00	0.11	0.00	0.20	0.06	**100.10**
LA3 9	Orthopyroxene	52.95	0.29	1.35	20.15	0.35	23.22	1.47	0.00	0.06	0.00	0.18	0.07	0.00	0.00	**100.09**
LA3 10	Bytownite core	47.83	0.09	32.15	0.63	0.06	0.00	16.03	2.43	0.24	0.00	0.19	0.03	0.03	0.00	**99.71**
LA3 10	Labradorite rim	54.81	0.05	27.84	0.55	0.08	0.01	10.61	5.34	0.40	0.00	0.00	0.02	0.05	0.00	**99.76**
LA3 11	Labradorite	52.68	0.00	29.11	0.56	0.00	0.01	12.65	4.23	0.28	0.00	0.00	0.07	0.00	0.04	**99.63**
LA3 12	Orthopyroxene	53.92	0.24	1.01	19.27	0.52	24.31	1.48	0.15	0.06	0.00	0.00	0.01	0.04	0.00	**101.01**
LA3 12	Chlorite on hypersthene	32.45	0.03	14.32	21.16	0.25	18.15	0.43	0.05	0.42	0.00	0.00	0.00	0.13	0.11	**87.50**

Rotokawa field, RK18 2219-2221 mRF

Sample no	**Mineral interpretation**	**SiO_2**	**TiO_2**	**Al_2O_3**	**FeO**	**MnO**	**MgO**	**CaO**	**Na_2O**	**K_2O**	**P_2O_5**	**SO_3**	**Cl**	**Cr_2O_3**	**NiO**	**TOTAL**
LA14 1	Titanomagnetite	0.16	7.30	0.78	84.54	0.49	0.11	0.01	0.23	0.01	0.07	0.11	0.01	0.60	0.06	**94.48**
LA14 3	Labradorite core	52.15	0.07	29.20	0.69	0.15	0.00	12.42	4.34	0.32	0.11	0.00	0.09	0.00	0.02	**99.56**
LA14 2	Orthopyroxene	52.27	0.40	0.98	18.95	0.50	23.51	1.67	0.00	0.06	0.04	0.08	0.02	0.08	0.00	**98.56**
LA14 2	Hydrothermal biotite	42.72	0.05	8.35	17.35	0.28	16.47	1.55	0.07	0.83	0.00	0.17	0.05	0.06	0.03	**87.98**
LA14 4	Augite	52.15	0.41	1.83	8.79	0.36	15.32	20.06	0.28	0.07	0.00	0.00	0.00	0.06	0.00	**99.33**
LA14 5	Augite	52.29	0.24	2.19	7.51	0.12	16.73	19.62	0.00	0.01	0.09	0.06	0.00	0.23	0.00	**99.09**
LA14 6	Augite	49.91	0.75	2.36	10.89	0.34	14.43	19.17	0.11	0.05	0.00	0.00	0.05	0.15	0.23	**98.44**
LA14 7	Titanomagnetite	0.10	25.49	0.99	66.32	1.94	0.11	0.00	0.20	0.00	0.00	0.04	0.01	0.48	0.02	**95.70**
LA14 8	Labradorite core	52.00	0.07	29.36	0.47	0.09	0.15	12.81	4.03	0.36	0.00	0.07	0.03	0.03	0.00	**99.47**
LA14 9	Augite	51.59	0.45	1.87	9.58	0.27	14.38	20.14	0.20	0.06	0.00	0.00	0.04	0.18	0.00	**98.76**

LA14 10	Orthopyroxene	52.76	0.34	1.18	19.36	0.51	22.92	1.71	0.18	0.08	0.08	0.00	0.07	0.00	0.14	**99.33**
LA14 10	Hydrothermal biotite on orthopyroxene	42.01	0.21	8.91	17.98	0.31	16.11	1.19	0.11	1.05	0.00	0.00	0.00	0.01	0.00	**87.89**
LA14 10	Hydrothermal biotite on orthopyroxene	45.83	0.45	10.65	17.64	0.14	17.49	0.84	0.25	4.22	0.04	0.00	0.04	0.00	0.24	**97.83**
LA14 11	Hydrothermal biotite	48.53	0.21	5.37	16.59	0.21	14.65	7.44	0.04	1.60	0.02	0.09	0.09	0.10	0.06	**95.00**
LA14 12	Bytownite core	48.21	0.04	32.07	0.68	0.00	0.00	15.83	2.37	0.24	0.00	0.10	0.00	0.10	0.04	**99.68**
LA14 13	Augite	50.94	0.72	3.09	10.12	0.12	14.84	19.42	0.38	0.15	0.02	0.00	0.07	0.13	0.20	**100.20**
LA14 14	Augite	51.52	0.58	1.86	10.30	0.38	14.60	19.71	0.21	0.09	0.00	0.04	0.00	0.19	0.13	**99.61**
LA14 15	Augite	51.38	0.42	1.39	9.47	0.33	14.90	20.08	0.13	0.08	0.19	0.00	0.05	0.06	0.06	**98.54**

Rotokawa field, RK25 2000 mRF

Sample no	**Mineral interpretation**	**SiO_2**	**TiO_2**	**Al_2O_3**	**FeO**	**MnO**	**MgO**	**CaO**	**Na_2O**	**K_2O**	**P_2O_5**	**SO_3**	**Cl**	**Cr_2O_3**	**NiO**	**TOTAL**
LA48 2	Labradorite	53.55	0.00	29.08	0.43	0.09	0.00	12.53	4.28	0.23	0.10	0.00	0.02	0.00	0.00	**100.31**
LA48 3	Epidote vein	38.09	0.04	23.62	11.24	0.14	0.05	23.12	0.00	0.08	0.16	0.00	0.00	0.12	0.00	**96.66**
LA48 3	Quartz vein	97.72	0.00	0.00	0.00	0.04	0.08	0.10	0.04	0.08	0.27	0.04	0.03	0.16	0.00	**98.56**
LA48 3	Calcite vein	0.00	0.00	0.05	0.15	1.25	0.12	51.94	0.01	0.09	0.00	0.00	0.06	0.00	0.10	**53.77**
LA48 5	Labradorite core	53.72	0.05	29.11	0.62	0.00	0.07	12.13	4.49	0.28	0.00	0.11	0.00	0.00	0.00	**100.58**
LA48 5	Labradorite rim	52.76	0.01	28.89	0.49	0.00	0.08	12.39	4.38	0.23	0.00	0.07	0.03	0.02	0.02	**99.37**
LA48 6	Labradorite core	50.96	0.15	30.31	0.62	0.00	0.05	13.65	3.55	0.20	0.00	0.01	0.03	0.01	0.10	**99.64**
LA48 8	Adularia	64.52	0.00	18.07	0.27	0.00	0.00	0.10	0.45	16.01	0.00	0.00	0.00	0.04	0.00	**99.46**

Rotokawa field, RK27 core #2 2147 mRF

Sample no	**Mineral interpretation**	**SiO_2**	**TiO_2**	**Al_2O_3**	**FeO**	**MnO**	**MgO**	**CaO**	**Na_2O**	**K_2O**	**P_2O_5**	**SO_3**	**Cl**	**Cr_2O_3**	**NiO**	**TOTAL**
LA53 1	Chlorite as vug core	27.10	0.03	16.46	18.06	0.32	18.35	0.22	0.08	0.06	0.00	0.00	0.06	0.00	0.01	**80.75**
LA53 2	Epidote as vug rim	37.76	0.22	24.58	10.37	0.53	0.15	22.72	0.00	0.06	0.00	0.05	0.00	0.04	0.02	**96.50**
LA53 3	Albite core	68.37	0.03	19.39	0.06	0.07	0.00	0.22	11.92	0.15	0.01	0.00	0.00	0.01	0.00	**100.23**

LA53 3	Albite rim	63.72	0.00	21.94	0.29	0.04	0.09	2.75	9.43	0.93	0.13	0.10	0.01	0.02	0.05	**99.50**
LA53 4	Chlorite on pyroxene	24.26	0.00	15.99	16.99	0.44	15.77	0.13	0.05	0.10	0.00	0.00	0.03	0.00	0.00	**73.76**
LA53 5	Chlorite on pyroxene core	29.73	0.04	17.53	18.41	0.37	19.95	0.24	0.04	0.00	0.00	0.04	0.05	0.02	0.00	**86.42**
LA53 5	Epidote as pyroxene rim	37.11	0.00	19.49	15.70	0.04	0.00	22.81	0.00	0.12	0.08	0.00	0.01	0.10	0.00	**95.46**
LA53 6	Epidote vein	37.66	0.16	21.29	13.75	0.25	0.10	23.18	0.00	0.08	0.07	0.02	0.00	0.28	0.00	**96.84**
LA53 6	Adularia	63.17	0.23	18.60	0.26	0.00	0.04	0.00	0.45	15.69	0.21	0.00	0.00	0.12	0.09	**98.83**
LA53 6	Epidote on orthoclase core	37.84	0.00	23.21	11.96	0.14	0.03	23.35	0.00	0.13	0.00	0.03	0.01	0.08	0.00	**96.78**

Rotokawa field, RK27 core #2 2152 mRF

Sample no	**Mineral interpretation**	**SiO_2**	**TiO_2**	**Al_2O_3**	**FeO**	**MnO**	**MgO**	**CaO**	**Na_2O**	**K_2O**	**P_2O_5**	**SO_3**	**Cl**	**Cr_2O_3**	**NiO**	**TOTAL**
LA58 1	Orthopyroxene	52.92	0.22	1.23	19.03	0.36	23.80	1.61	0.00	0.02	0.12	0.00	0.03	0.04	0.07	**99.45**
LA58 1	Chlorite in orthopyroxene cleavage	35.11	0.11	12.26	21.27	0.36	17.25	0.62	0.14	1.14	0.00	0.14	0.03	0.04	0.21	**88.68**
LA58 2	Orthopyroxene	52.92	0.31	1.03	19.02	0.58	23.94	1.64	0.00	0.05	0.05	0.00	0.01	0.00	0.01	**99.56**
LA58 2	Chlorite in orthopyroxene cleavage	38.56	0.22	11.34	19.69	0.20	16.25	0.41	0.60	2.87	0.17	0.05	0.01	0.08	0.00	**90.45**
LA58 2	Hornblende on orthopyroxene	48.89	0.42	6.30	14.52	0.16	15.89	10.43	0.29	1.59	0.00	0.04	0.05	0.13	0.13	**98.84**
LA58 2	Augite core	51.41	0.46	2.31	9.80	0.29	14.57	19.90	0.24	0.21	0.00	0.24	0.00	0.08	0.00	**99.51**
LA58 2	Augite rim	50.59	0.60	2.71	10.31	0.28	14.92	18.76	0.36	0.11	0.00	0.00	0.02	0.19	0.00	**98.85**
LA58 3	Calcite vein core	9.14	0.03	1.75	5.98	1.17	4.34	37.70	0.04	0.28	0.01	0.05	0.00	0.10	0.23	**60.82**
LA58 3	Calcite vein rim	0.67	0.07	0.38	2.51	2.21	0.88	45.96	0.11	0.10	0.00	0.01	0.08	0.01	0.12	**53.11**
LA58 4	Labradorite core	53.36	0.09	28.39	0.68	0.19	0.03	12.01	4.61	0.35	0.04	0.00	0.00	0.11	0.00	**99.86**
LA58 4	Labradorite rim	51.57	0.12	29.29	0.66	0.08	0.05	13.14	3.89	0.30	0.14	0.01	0.07	0.00	0.00	**99.32**
LA58 4	Labradorite spot	54.03	0.08	29.00	1.05	0.05	0.38	11.81	4.65	0.31	0.05	0.04	0.11	0.10	0.08	**101.74**
LA58 5	Augite core	50.09	0.66	4.56	9.02	0.13	14.66	19.81	0.07	0.12	0.00	0.00	0.00	0.42	0.00	**99.54**
LA58 5	Chlorite in augite cleavage	35.68	0.19	12.53	21.17	0.34	16.72	0.70	0.00	1.36	0.01	0.00	0.00	0.03	0.00	**88.73**
LA58 6	Bytownite	50.78	0.08	30.53	0.69	0.03	0.04	14.04	3.43	0.19	0.00	0.00	0.00	0.05	0.00	**99.86**
LA58 8	Orthopyroxene	53.60	0.19	1.10	19.33	0.50	24.19	1.27	0.08	0.03	0.11	0.00	0.01	0.05	0.00	**100.46**

LA58 9	Augite	51.40	0.43	2.36	10.62	0.27	14.98	19.45	0.15	0.09	0.26	0.01	0.00	0.20	0.14	**100.36**
LA58 10	Bytownite core	46.66	0.00	33.09	0.63	0.00	0.00	16.96	1.86	0.18	0.07	0.00	0.03	0.07	0.05	**99.60**
LA58 10	Bytownite mid	48.33	0.08	31.96	0.67	0.00	0.00	15.60	2.45	0.23	0.07	0.01	0.00	0.01	0.00	**99.41**
LA58 10	Labradorite rim	53.27	0.04	29.06	0.91	0.06	0.02	12.44	4.46	0.20	0.04	0.01	0.00	0.05	0.00	**100.56**
LA58 11	Chlorite on augite	40.04	0.23	9.18	18.09	0.18	15.06	0.90	0.38	3.64	0.04	0.00	0.00	0.09	0.11	**87.94**
LA58 11	Augite	51.74	0.38	2.95	6.07	0.12	17.57	19.00	0.38	0.05	0.17	0.00	0.04	0.90	0.07	**99.44**
LA58 12	Labradorite	52.89	0.00	28.87	0.78	0.00	0.11	12.62	4.49	0.24	0.00	0.13	0.04	0.00	0.00	**100.17**
LA58 13	Titanomagnetite	0.34	14.08	2.26	75.59	0.20	0.05	0.06	0.07	0.00	0.06	0.00	0.00	0.90	0.00	**93.61**

Appendix 2

XRD data

This appendix includes graphs of low- and high angle (2 Theta) analysis of six selected samples from RK27 (LA.53 to LA.58). All other XRD-analyses can be found in the enclosed CD-rom. Treatment methods are: AD = air dried at 60°C (red line) and EG = ethylene glycol (green line). Selected samples were heated up in a furnace at 550°C mainly to identify kaolinite, which is destroyed by this treatment (blue line). Y-axis is peak counts, and x-axis is d-spacing in Ångstrom.

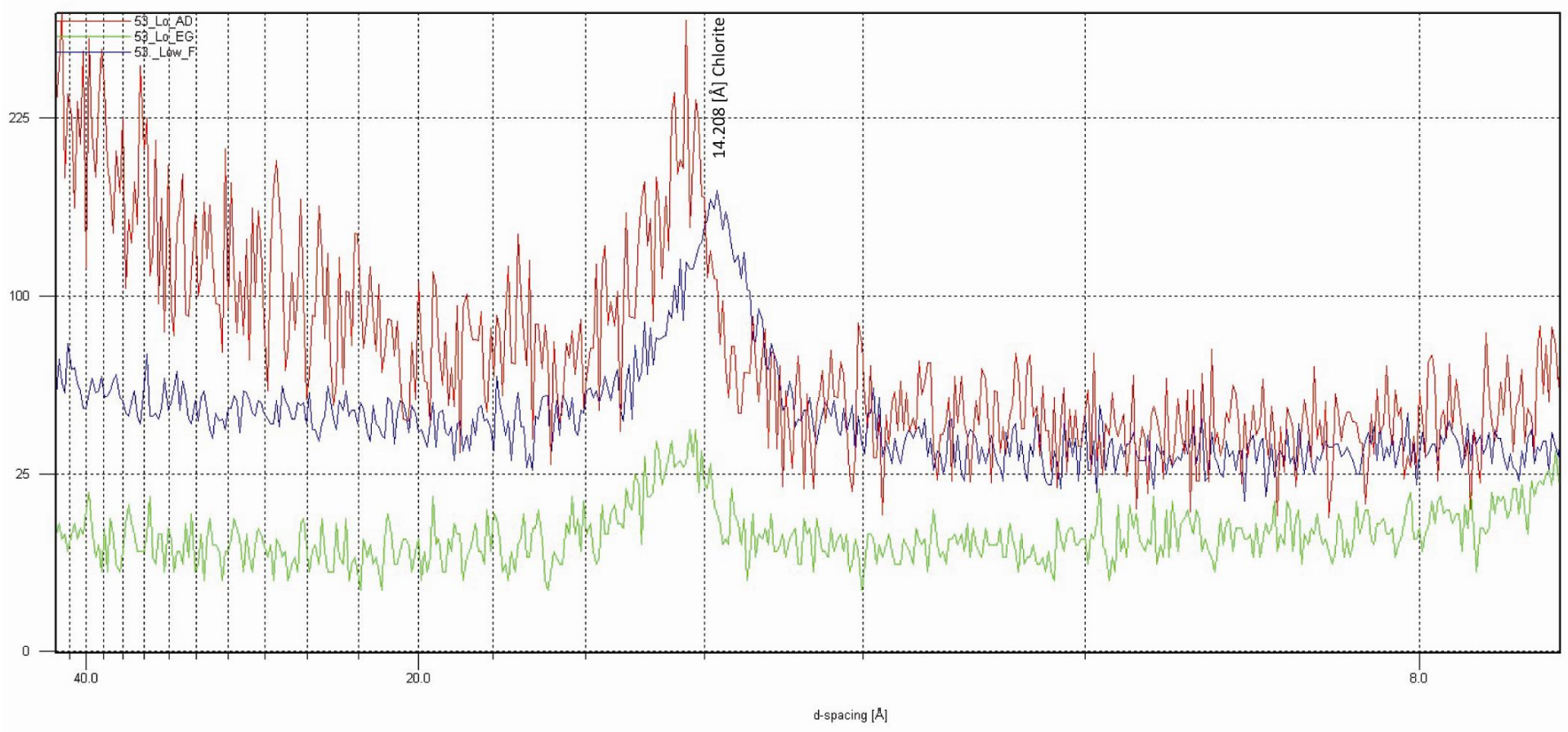
53_Lo_AD
53_Lo_EG
53_Low_F
14.208 [Å] Chlorite
225
100
25
0
40.0
20.0
8.0
d-spacing [Å]

53_Hi_AD
53_Hi_EG
53_Hi_F
1600
900
400
100
0
7.0
6.0
5.0
4.0
3.0
d-spacing [Å]
7.129 [Å]: Chlorite/Kaolinite
4.731 [Å]: Chlorite
4.260 [Å]: Quartz/K-feldspar
4.037 [Å]: Cristobalite
3.758 [Å]: Plagioclase/Albite
3.650 [Å]: Hematite
3.547 [Å]: Chlorite/Anhydrite/
Epidote/Kaolinite
3.343 [Å]: Quartz/K-feldspar/Biotite
3.181 [Å]: Plagioclase/Albite
3.031 [Å]: Calcite
2.935 [Å]: Epidote
2.848 [Å]: Anhydrite
2.655 [Å]: Hematite
2.602 [Å]: Epidote
2.536 [Å]: Hematite
2.458 [Å]: Cristobalite/Biotite
2.386 [Å]: Kaolinite/Anhydrite
2.283 [Å]: Calcite
2.235 [Å]: Anhydrite
2.126 [Å]: Calcite

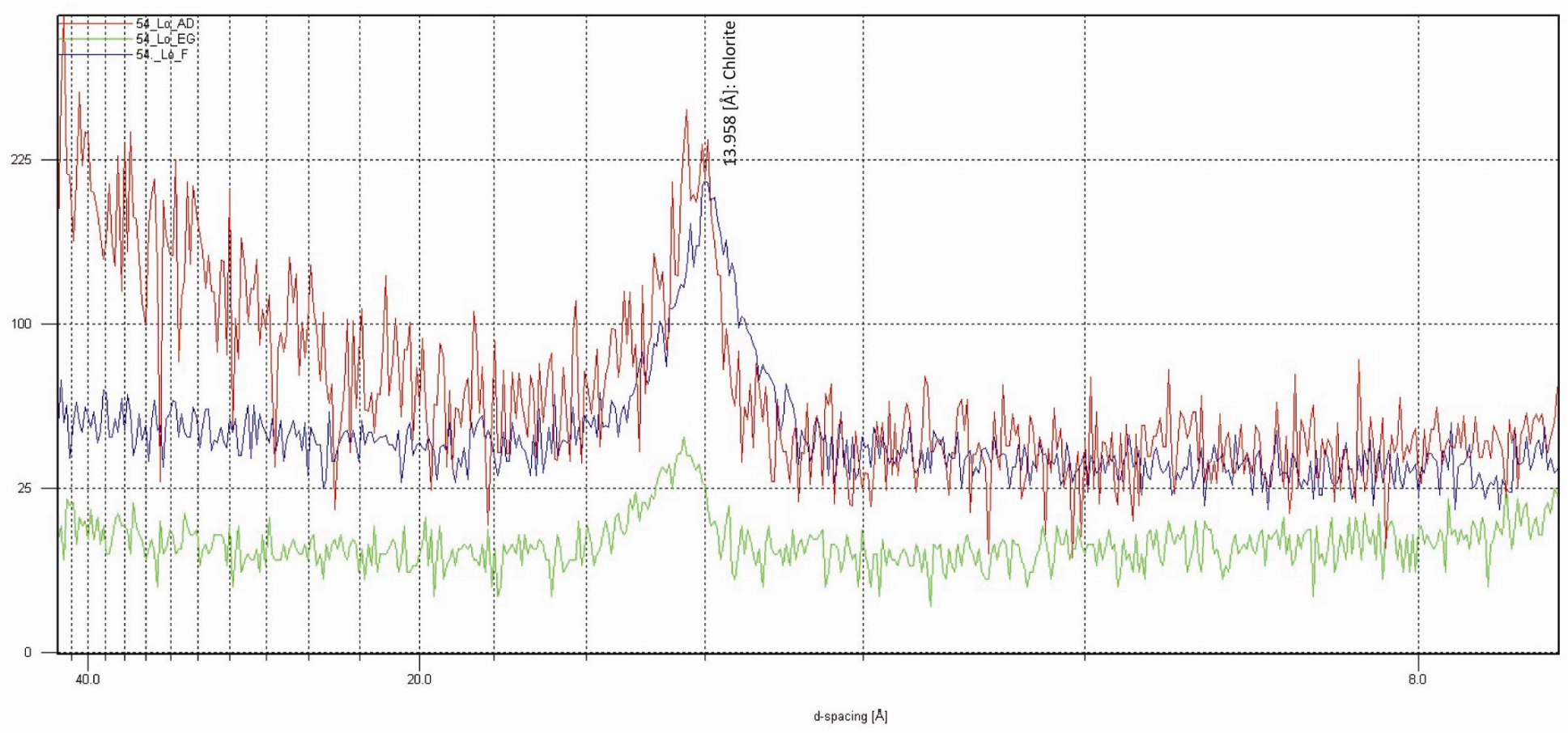
54_Lo_AD
54_Lo_EG
54_Lo_F
13.958 [Å]: Chlorite
225
100
25
0
40.0
20.0
8.0
d-spacing [Å]

54_Hi_AD
54_Hi_EG
54_Hi_F
7.051 [Å]: Chlorite/Kaolinite
6.396 [Å]: Feldspar
4.724 [Å]: Chlorite
4.245 [Å]: Quartz/K-feldspar
4.026 [Å]: Cristobalite
3.765 [Å]: Plagioclase/Albite
3.677 [Å]: Hematite
3.536 [Å]: Chlorite/Anhydrite/ Epidote/Kaolinite
3.340 [Å]: Quartz/K-feldspar/Biotite
3.180 [Å]: Plagioclase/Albite
2.985 [Å]: Calcite
2.931 [Å]: Epidote
2.839 [Å]: Anhydrite
2.699 [Å]: Hematite
2.648 [Å]: Biotite
2.597 [Å]: Epidote
2.532 [Å]: Hematite
2.456 [Å]: Cristobalite/Biotite
2.387 [Å]: Kaolinite/Anhydrite
2.280 [Å]: Calcite
2.235 [Å]: Anhydrite
2.124 [Å]: Calcite
1600
900
400
100
0
7.0
6.0
5.0
4.0
3.0
d-spacing [Å]

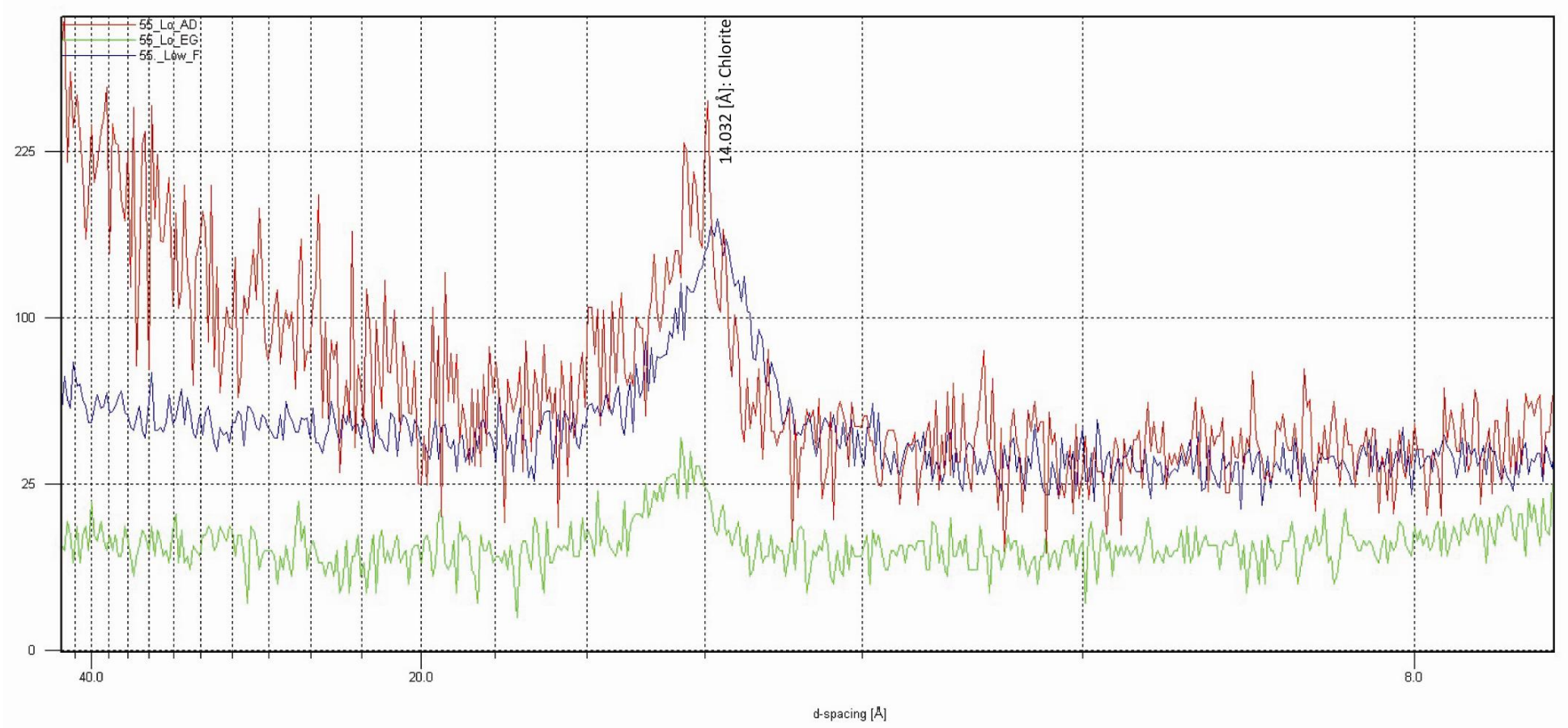
55_Lo_AD
55_Lo_EG
55_Low_F
14.032 [Å]: Chlorite
225
100
25
0
40.0
20.0
8.0
d-spacing [Å]

55_Hi_AD
55_Hi_EG
55_Hi_F
1600
900
400
100
0
7.0
6.0
5.0
4.0
3.0
d-spacing [Å]
7.084 [Å]: Chlorite/Kaolinite
4.698 [Å]: Chlorite
4.243 [Å]: Quartz/K-feldspar
4.034 [Å]: Cristobalite
3.889 [Å]: Feldspar/Calcite
3.749 [Å]: Feldspar/Ilmenite
3.633 [Å]: Feldspar
3.541 [Å]: Chlorite/Anhydrite/ Epidote/Kaolinite
3.339[Å]: Quartz/K-feldspar/Biotite
3.204 [Å]: Plagioclase/Albite
3.177 [Å]: Plagioclase/Albite
3.128 [Å]: Feldspar/Cristobalite
3.028 [Å]: Calcite
2.939 [Å]: Epidote
2.834 [Å]: Anhydrite
2.648 [Å]: Biotite
2.592 [Å]: Epidote/Chlorite
2.517 [Å]: Hematite
2.454 [Å]: Cristobalite/Biotite
2.381 [Å]: Kaolinite/Anhydrite
2.280 [Å]: Calcite
2.231 [Å]: Anhydrite
2.124 [Å]: Calcite
2.091 [Å]: Biotite

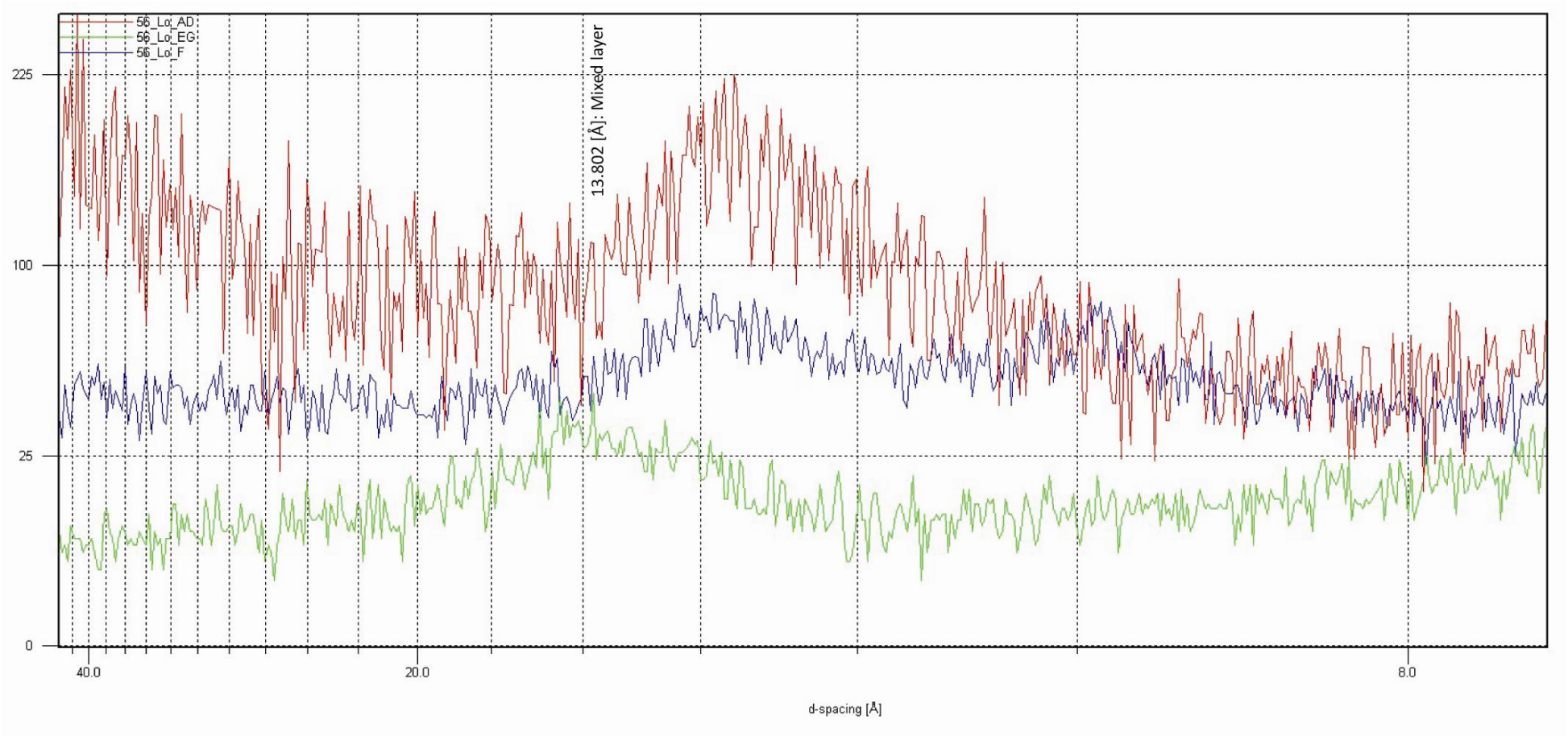
56_Lo_AD
56_Lo_EG
56_Lo_F
13.802 [Å]: Mixed layer
225
100
25
0
40.0
20.0
8.0
d-spacing [Å]

56_Hi_AD
56_Hi_EG
56_Hi_F
7.092 [Å]: Chlorite/Kaolinite
4.239 [Å]: Quartz/K-feldspar
4.026 [Å]: Cristobalite
3.741 [Å]: Plagioclase/Albite
3.627 [Å]: Hematite
3.553 [Å]: Chlorite/Anhydrite/
Epidote/Kaolinite
3.456 [Å]: Feldspar
3.333[Å]: Quartz/K-feldspar/Biotite
3.196 [Å]: Plagioclase/Albite
3.172 [Å]: Plagioclase/Albite
3.124 [Å]: Feldspar/Cristobalite
3.017 [Å]: Calcite
2.942 [Å]: Epidote
2.826 [Å]: Anhydrite
2.647 [Å]: Hematite/Biotite
2.515 [Å]: Hematite
2.446 [Å]: Cristobalite/Biotite
2.279 [Å]: Calcite
2.229 [Å]: Anhydrite
2.120 [Å]: Calcite
900
400
100
0
7.0
6.0
5.0
4.0
3.0
d-spacing [Å]

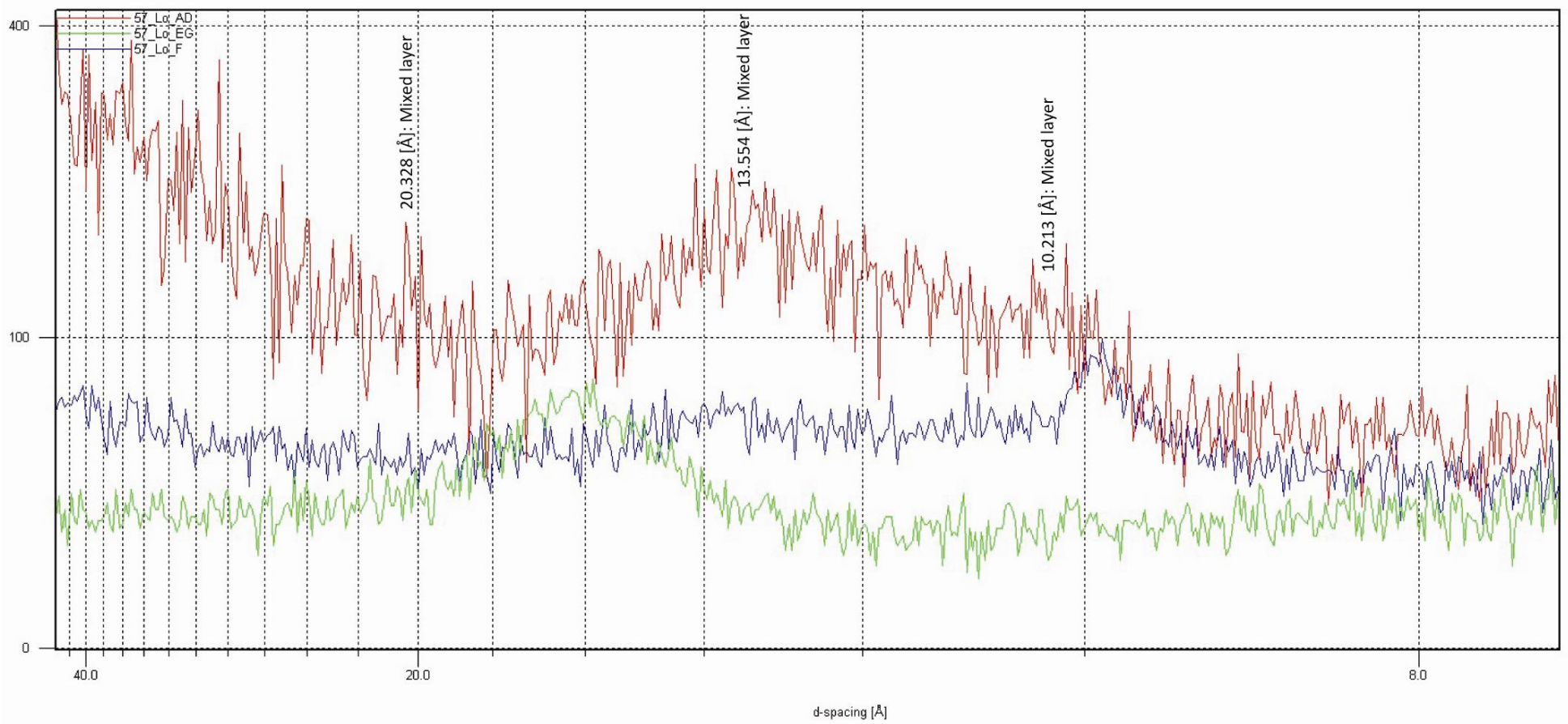
57_Lo_AD
57_Lo_EG
57_Lo_F
20.328 [Å]: Mixed layer
13.554 [Å]: Mixed layer
10.213 [Å]: Mixed layer
400
100
0
40.0
20.0
8.0
d-spacing [Å]

57_Hi_AD
57_Hi_EG
57_Hi_F
7.103 [Å]: Chlorite
4.247 [Å]: Quartz/K-feldspar
4.031 [Å]: Cristobalite
3.880 [Å]: K-feldspar/Calcite
3.749 [Å]: Plagioclase/Albite/Ilmenite
3.629 [Å]: Hematite
3.459 [Å]: Feldspar
3.338[Å]: Quartz/K-feldspar/Biotite
3.203 [Å]: Plagioclase/Albite
3.173 [Å]: Plagioclase/Albite
3.128 [Å]: Feldspar/Cristobalite
3.024 [Å]: Calcite
2.943 [Å]: Epidote
2.833 [Å]: Anhydrite
2.648 [Å]: Hematite/Biotite
2.516 [Å]: Hematite
2.454 [Å]: Cristobalite/Biotite
2.413 [Å]: Chlorite
2.278 [Å]: Calcite
2.230 [Å]: Anhydrite
2.123 [Å]: Calcite
900
400
100
0
7.0
6.0
5.0
4.0
3.0
d-spacing [Å]

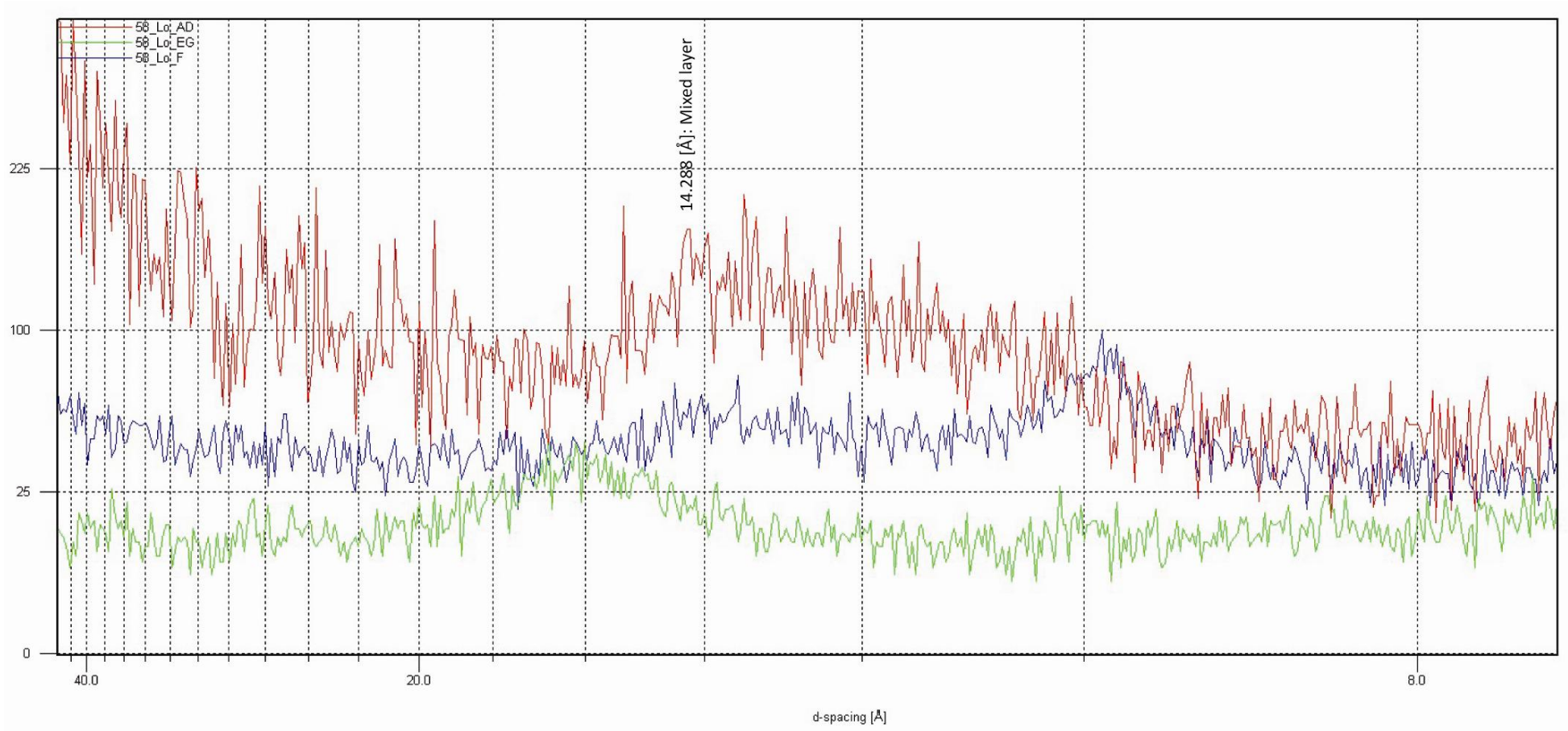
58_Lo_AD
58_Lo_EG
58_Lo_F
14.288 [Å]: Mixed layer
225
100
25
0
40.0
20.0
8.0
d-spacing [Å]

58_Hi_AD
58_Hi_EG
58_Hi_F
900
400
100
0
7.0
6.0
5.0
4.0
3.0
d-spacing [Å]
7.099 [Å]: Chlorite
4.248 [Å]: Quartz/Feldspar
4.038 [Å]: Cristobalite
3.896 [Å]: Feldspar
3.752 [Å]: Plagioclase/Albite/Ilmenite
3.634 [Å]: Hematite
3.343[Å]:Quartz/K-feldspar/Biotite
3.205 [Å]: Plagioclase/Albite
3.180 [Å]: Plagioclase/Albite
3.134 [Å]: Feldspar/Cristobalite
3.019 [Å]: Calcite
2.949 [Å]: Epidote
2.835 [Å]:Chlorite/Feldspar/Cristobalite
2.652 [Å]:Hematite/Smectite/Biotite
2.522 [Å]:Chlorite/Feldspar/Hematite
2.457 [Å]: Cristobalite/Biotite
2.280 [Å]: Calcite
2.124 [Å]: Calcite

Appendix 3

XRF data

Major- and trace element data from Browne et al. (1992) and indicated by *.

Sample	1*	2*	3*	4*	5*	6*	7*	8*
Well	RK6	RK8	RK4	RK5	RK6	RK4	RK5	RK5
Depth (mRF)	2443	2219	1429	2349	2115	1630	1589	2655
Rock type	Basaltic andesite	Basaltic andesite	Basaltic andesite	Basaltic andesite	Basaltic andesite	Basaltic andesite	Basaltic andesite	Basaltic andesite
Alteration intensity	Altered	Low degree of alteration	Low degree of alteration	Low degree of alteration	Altered	Low degree of alteration	Low degree of alteration	Low degree of alteration
Major oxides (wt. %)								
SiO_2	56.15	56.94	57.14	57.26	57.27	57.42	58.22	58.6
TiO_2	0.7	0.75	0.65	0.67	0.7	0.7	0.77	0.72
Al_2O_3	17.09	17.92	17.17	17.6	17.88	17.55	18.46	18.42
Fe_2O_3	8.92	7.79	7.4	7.2	6.76	7.69	5.81	5.81
MnO	0.45	0.14	0.12	0.14	0.21	0.1	0.13	0.14
MgO	5.52	4.26	5.01	4.45	2.46	4.88	2.1	3.33
CaO	6.38	8.86	8.28	8.7	10.7	8.1	8.29	8.74
Na_2O	3.9	2.27	2.86	2.69	2.46	2.49	3.57	2.91
K_2O	0.78	0.95	1.24	1.15	1.41	0.9	0.44	1.18
P_2O_5	0.11	0.12	0.13	0.12	0.15	0.15	0.17	0.15
H_2O	0.1	0.2	0.5	0.2	0.1	0.1	0.1	0.1
LOI	6.2	1.7	1	2.7	5.4	3.1	3.3	3.1
TOTAL	**99.59**	**99.81**	**100.00**	**100.12**	**99.51**	**100.19**	**99.40**	**99.99**
Trace elements (ppm)								
V	255	228	212	221	218	231	214	229
Cr	80	18	70	52	114	68	12	61
Ni	32	10	37	26	30	29	7	22
Cu	82	29	43	35	40	23	27	32
Zn	95	80	75	76	92	76	104	74
Rb	32	24	71	53	39	21	13	29
Sr	367	263	284	299	302	306	360	304
Y	16	19	16	16	19	17	35	19
Zr	77	88	71	77	97	83	106	89
Nb	na	na	na	na	na	na	na	na
Ba	187	307	251	278	358	250	229	325
La	11	13	10	9	11	14	16	12
Ce	na	na	na	na	na	na	na	na
Hf	na	na	na	na	na	na	na	na
W	na	na	na	na	na	na	na	na
Pb	18	12	28	12	16	25	17	14
Th	11	<2	14	<2	7	11	8	7
U	na	na	na	na	na	na	na	na
TiO_2/Zr	55	51	55	52	43	51	44	48
Zr/Y	5	5	4	5	5	5	3	5
$^{87}Sr/^{86}Sr$	0.70532	0.70549	0.70512	0.70515	na	0.70504	0.70517	0.70524
$^{87}Sr/^{86}Sr$ (L)	0.70530	0.70553	0.70509	0.70500	na	0.70499	0.70518	0.70526

Sample	9*	10*	11*	12*	13*	14*	15*	16*
Well	RK6	RK5	RK4	RK4	RK6	NM2	NM3	NM4
Depth (mRF)	2280	2003	1995.5	1830	1861	2000	1991	2460
Rock type	Basaltic andesite	Basaltic andesite	Basaltic andesite	Basaltic andesite	Andesite	Andesite	Andesite-dacite	Basaltic andesite (micro diorite)
Alteration intensity	Low degree of alteration	Low degree of alteration	Altered	Altered	Altered	Low degree of alteration	Low degree of alteration	Altered
Major oxides (wt. %)								
SiO_2	58.65	59.44	60.63	61.28	62.16	56.88	61.80	57.09
TiO_2	0.69	0.71	0.63	0.53	0.46	1.10	0.88	0.88
Al_2O_3	16.74	17.96	17.4	16.2	15.59	18.27	16.38	16.63
Fe_2O_3	6.85	6.83	6.37	6.88	6.23	7.37	6.31	8.63
MnO	0.16	0.13	0.13	0.15	0.08	0.18	0.21	0.17
MgO	5.2	4.31	4.32	4.94	5.02	3.10	3.30	3.35
CaO	7.69	6.72	6.54	6.87	6.17	7.43	6.28	7.00
Na_2O	2.29	2.73	3.58	2.36	2.41	4.51	3.30	5.27
K_2O	1.59	1.05	0.28	0.68	1.76	0.84	1.38	0.71
P_2O_5	0.15	0.13	0.12	0.13	0.12	0.30	0.18	0.27
H_2O	0.6	0.1	0	0.3	0.2	0.10	0.10	0.00
LOI	2.4	4	3.8	5.6	3.8	1.60	1.80	0.40
TOTAL	**99.70**	**100.14**	**100.13**	**99.69**	**100.11**	**99.30**	**99.54**	**99.81**
Trace elements (ppm)								
V	193	244	272	193	158	157	134	185
Cr	99	30	90	158	252	20	45	11
Ni	31	21	47	48	56	7	11	n/a
Cu	41	48	37	28	17	8	26	36
Zn	80	86	77	70	58	95	123	207
Rb	78	33	9	28	54	23	43	15
Sr	294	249	241	274	275	371	295	248
Y	22	20	17	16	14	24	24	42
Zr	94	78	60	71	96	255	210	96
Nb	na	na	na	na	na	na	na	na
Ba	292	504	107	187	373	227	516	300
La	13	10	9	11	16	11	16	20
Ce	na	na	na	na	na	na	na	na
Hf	na	na	na	na	na	na	na	na
W	na	na	na	na	na	na	na	na
Pb	13	13	25	30	16	18	13	84
Th	4	6	8	14	6	4	<2	10
U	na	na	na	na	na	na	na	na
TiO_2/Zr	44	55	63	45	29	26	25	55
Zr/Y	4	4	4	4	7	11	9	2
$^{87}Sr/^{86}Sr$	na	0.70542	0.70491	0.70517	0.70485	na	na	0.70510
$^{87}Sr/^{86}Sr$ (L)	na	0.70522	0.70484	0.70511	0.70481	na	na	0.70507

Major- and trace element data from this study (samples labelled LA.).

Sample	LA.3	LA.4	LA.5	LA.7	LA.9	LA.10	LA.14
Well	RK21	NM5A	NM6	NM6	RK27	RK27	RK18
Depth (mRF)	1876	2575-78	2686-89	3032-35	2153	1853-56	2219-21
Rock type	Basaltic andesite	Andesite	Andesite	Basaltic andesite	Basaltic andesite	Basaltic andesite	Basaltic andesite
Alteration intensity	Subtle	Subtle	Weak	Intense	Moderate	Strong	Weak
Major oxides (wt. %)							
SiO_2	55.97	55.01	56.62	51.03	53.01	49.49	55.14
TiO_2	0.67	0.63	0.64	0.65	0.70	0.85	0.70
Al_2O_3	16.80	16.19	18.06	16.64	17.37	21.42	16.90
Fe_2O_3	7.85	6.13	6.52	6.98	7.47	7.71	8.58
MnO	0.12	0.14	0.10	0.16	0.10	0.12	0.13
MgO	3.92	3.14	2.69	3.52	3.55	4.17	4.65
CaO	7.64	7.93	7.75	7.38	8.93	8.88	7.77
Na_2O	2.65	2.50	2.46	1.73	2.45	3.30	2.74
K_2O	1.32	1.70	1.45	2.12	0.66	0.31	1.46
P_2O_5	0.18	0.18	0.12	0.09	0.17	0.14	0.17
H_2O	na	na	na	na	na	na	na
LOI	1.75	4.55	3.02	8.92	4.52	4.24	1.68
TOTAL	**98.86**	**98.10**	**99.44**	**99.21**	**98.92**	**100.63**	**99.91**
Trace elements (ppm)							
S	145	132	271	8057	199	893	987
V	218	183	191	224	250	235	246
Cr	53	126	10.5	30	79	63	55
Co	39	41	25	27	36	53	33
Ni	23	40	6.2	22	36	37	27
Cu	31	24	31	42	37	52	62
Zn	76	58	75	73	76	110	72
Rb	44	47	36	101	14	9.7	68
Sr	282	273	236	236	315	362	320
Y	20	22	19.6	19	17.3	22	19.3
Zr	88	124	96	78	79	96	80
Nb	4.4	5.7	5.3	3.9	4.3	5.2	4.5
Ba	281	333	257	281	262	197	248
La	5.6	6.8	9.6	< 4.9	8.5	6.8	6.9
Ce	18.3	19	16.9	8.9	14.5	17.9	18.4
Nd	< 10	< 10	< 10	< 10	< 10	9.6	< 10
Hf	3.4	5.5	5.7	3.2	4.8	3.7	2.8
W	300	412	204	74	133	257	209
Pb	6.3	8.4	9.4	5.5	4.6	5.4	5.3
Th	7.7	9.2	7.6	6.1	6.6	7.6	6.8
U	5.9	5.8	5.8	5.6	5.1	5.4	5.7
TiO_2/Zr	45	31	40	50	53	53	52
Zr/Y	4	6	5	4	5	4	4
$^{87}Sr/^{86}Sr$	na	na	na	na	na	na	na
$^{87}Sr/^{86}Sr$ (L)	na	na	na	na	na	na	na

Sample	LA.15	LA.22	LA.23	LA.44	LA.48	LA.51	LA.55	LA.58
Well	NM6	NM6	RK21	RK21	RK25 #1	RK24 ST1	RK27 #2	RK27 #2
Depth (mRF)	2210	2550	1250	2300	2000	1820	2149	2152
Rock type	Dacite	Andesite	Basaltic andesite	Basaltic andesite	Basaltic andesite	Basaltic andesite	Basaltic andesite	Basaltic andesite
Alteration intensity	Weak	Weak	Weak	Strong	Moderate	Moderate	Moderate	Subtle
Major oxides (wt. %)								
SiO_2	61.84	61.13	57.01	57.78	53.09	54.28	51.74	54.72
TiO_2	0.59	0.56	0.70	0.63	0.76	0.69	0.75	0.67
Al_2O_3	13.37	15.07	17.08	16.89	20.10	17.83	18.02	16.69
Fe_2O_3	4.84	5.78	6.62	7.08	7.64	6.55	7.44	8.36
MnO	0.09	0.09	0.09	0.22	0.12	0.05	0.09	0.14
MgO	2.18	2.48	2.17	3.17	3.32	2.14	4.23	4.68
CaO	5.25	5.98	7.28	7.69	8.28	5.46	8.79	8.23
Na_2O	2.99	2.88	2.77	2.06	2.47	2.47	2.89	2.64
K_2O	1.71	1.71	1.19	0.43	0.78	2.35	0.50	1.09
P_2O_5	0.12	0.11	0.15	0.14	0.14	0.33	0.14	0.15
H_2O	na	na	na	na	na	na	na	na
LOI	6.22	3.30	3.02	2.21	2.60	5.60	4.76	1.94
TOTAL	**99.20**	**99.08**	**98.07**	**98.29**	**99.29**	**97.75**	**99.36**	**99.30**
Trace elements (ppm)								
S	1032	1241	1929	2068	918	28280	365	125
V	100	144	193	223	214	311	243	226
Cr	58	91	36	62	35	58	84	65
Co	24	36	39	42	31	49	44	48
Ni	14.1	24	21	21	23	18.3	33	32
Cu	20	28	47	41	135	22	43	63
Zn	58	58	64	445	91	50	77	71
Rb	68	54	33	13.2	28	106	9.5	44
Sr	205	214	310	303	287	312	298	314
Y	23	23	19	18.1	23	25	17.7	19.7
Zr	160	125	76	70	107	87	83	76
Nb	7.4	6.1	4.2	3.7	5.2	4.7	4	3.8
Ba	367	349	290	162	152	473	216	246
La	13.3	8.9	5.3	5.7	7	6.8	7.8	5.4
Ce	30	18.1	14.6	15.1	19.1	17.5	18.6	16.6
Nd	13.2	< 10	< 10	9.9	< 10	< 10	< 10	< 10
Hf	4.7	4.4	3.1	1.8	< 3.3	3.9	3.2	< 2.7
W	184	329	345	281	126	186	215	334
Pb	9.6	8.1	5.5	129	7	17.1	4.3	5.7
Th	9.3	8	6.3	6.6	6.9	6.7	6	5
U	6.1	4.7	4	4.1	4.9	4.7	3.7	4.2
TiO_2/Zr	22	27	55	54	42	48	54	53
Zr/Y	7	6	4	4	5	3	5	4
$^{87}Sr/^{86}Sr$	na	na	na	na	na	na	na	na
$^{87}Sr/^{86}Sr$ (L)	na	na	na	na	na	na	na	na

Sample	Well	Depth (mRF)	S ppm	Ti ppm	V ppm	Cr ppm	Co ppm	Ni ppm	Cu ppm	Zn ppm	Rb ppm	Sr ppm	Y ppm	Zr ppm	Nb ppm	Ba ppm	La ppm	Ce ppm	Nd ppm	Hf ppm	W ppm	Pb ppm	Th ppm	U ppm	TiO_2/Zr ratio	Zr/Y ratio
LA.6	**NM6**	**2686-89**	1362	1973.0	246	< 0.9	25	6.1	15.5	81	30.1	204	19.7	86	5	99	7.7	16.1	< 10	3.5	192	7	5.7	5.5	47	4.4
LA.16	**NM6**	**2250**	4014	2071.9	147	110	37	25	38	60	57	280	21	118	6.5	322	7.6	18.9	< 10	3	230	8.5	8.4	5.2	28	5.6
LA.17	**NM6**	**2300**	530	1910.0	123	71	33	23	28	53	54	239	22	128	6.2	346	10.8	22	10.3	4.3	330	8.5	8.9	5.4	30	5.9
LA.18	**NM6**	**2350**	1003	1988.5	133	86	38	25	33	53	57	233	22	115	5.9	341	12.9	25	9.1	4.1	319	8.5	8.7	6.3	36	5.2
LA.19	**NM6**	**2400**	372	1994.5	156	108	36	35	44	59	42	230	20	101	5.3	328	31.7	48	38	2.3	242	8.6	7.7	5.2	38	4.9
LA.20	**NM6**	**2450**	361	2061.7	152	73	36	19.3	32	48	58	243	23	113	5.7	344	32	50	41.4	5	310	10.2	8.8	5.3	40	4.9
LA.21	**NM6**	**2500**	611	1952.0	137	85	34	22	33	55	54	226	23	119	5.8	333	8	21	11.3	5.2	300	9.2	8.3	4.7	30	5.3
LA.45	**NM7 #1**	**2184**	2130	2348.8	92	29	28	9.4	12	85	29	303	23	223	8.2	563	13.3	29	10.7	6.3	367	14.6	9.7	4.2	18	9.7
LA.46	**NM7 #1**	**2181**	254	2252.3	109	37	26	10.8	9.9	74	47	299	22	199	7.7	417	12.7	30	11.4	4.8	388	10.4	9.3	3.9	20	9.1
LA.47	**NM7 #1**	**2179**	1190	3097.0	158	29	31	8.7	12.5	85	43	339	23	212	7.1	383	9.3	28	< 10	5.1	311	13.4	8.3	4.5	16	9.3
LA.59	**NM5A**	**2905**	1047	2425.0	199	33	30	14.5	28	1335	32	242	22	101	5.4	380	5.7	17.8	9.7	3.4	222	1000	14.2	6.5	34	4.5
LA.66	**NM7**	**1390**	7855	1299.1	9.9	13.6	24	3.90	5.30	66	133	160	26	201	8.4	609	27	46	33	6.8	503	21	12.5	7.0	21	7.8
LA.67	**NM7**	**1400**	7577	1338.1	16.5	3.2	33	5.00	6.90	48	162	150	27	209	8.7	664	20	38	22	7.7	984	16.3	12.3	7.9	17	7.7
LA.68	**NM7**	**1410**	10610	1331.5	16.8	3.7	39	4.20	6.40	84	153	134	29	219	8.9	655	47	73	48	8.0	984	24	12.4	7.3	17	7.5
LA.69	**NM7**	**1420**	8308	1299.1	9.7	3.6	44	3.00	5.90	171	171	121	28	226	8.7	643	20	38	18.1	8.0	1092	147	14.3	8.2	17	8
LA.70	**NM7**	**1430**	10940	1225.4	6.4	< 0.6	42	6.40	9.00	360	169	99	28	224	8.6	545	24	45	26	8.3	1298	173	14.2	8.0	18	8.1
LA.71	**NM7**	**1440**	12070	1231.4	4.2	< 0.6	50	3.50	12.10	701	177	98	29	237	8.9	561	24	43	31	8.8	1315	115	14.4	8.1	18	8.3
LA.72	**NM7**	**1450**	15170	1247.0	< 3.9	6.2	49	4.10	17.90	474	148	145	27	226	8.9	578	27	48	29	8.0	1140	177	14.5	7.7	20	8.4
LA.73	**NM7**	**1460**	7085	1375.9	13.8	11.0	41	7.90	18.20	109	150	293	28	231	9.0	600	22	42	24	8.2	963	48	14.4	7.1	17	8.2
LA.77	**NM6**	**1280**	3968	1763.1	14.6	1	45	4.0	4.6	58	107	149	29	232	8.5	459	27	44	30	7.6	887	10.6	11.6	6.6	19	8
LA.78	**NM6**	**1330**	189	2483.7	27	< 0.7	41	3.8	8.6	72	79	278	29	217	9.2	520	34	56	42	7.4	614	11.9	11.3	5.1	20	7.5
LA.81	**NM6**	**1480**	418	1301.5	4.7	17.1	33	5.9	8.0	57	105	149	31	263	8.9	573	23	43	22	9.2	671	53	14.8	6.1	14	8.4
LA.82	**NM6**	**1530**	359	1148.0	< 3.5	2.4	40	3.8	3.7	56	92	162	29	252	8.0	542	32	52	35	10.1	684	13.6	14.5	6.9	13	8.6

Sample	Well	Depth (mRF)	S ppm	Ti ppm	V ppm	Cr ppm	Co ppm	Ni ppm	Cu ppm	Zn ppm	Rb ppm	Sr ppm	Y ppm	Zr ppm	Nb ppm	Ba ppm	La ppm	Ce ppm	Nd ppm	Hf ppm	W ppm	Pb ppm	Th ppm	U ppm	TiO_2/Zr ratio	Zr/Y ratio
LA.83	**NM6**	**1580**	682	1505.3	6.6	1.9	33	3.8	7.3	59	109	192	31	262	9.9	617	38	63	40	8.3	675	15.8	14.3	5.7	15	8.4
LA.84	**NM6**	**1630**	1363	1309.9	8.3	12.2	38	4.3	3.9	57	102	174	30	257	10.9	588	33	55	42	9.2	694	13.3	13.5	5.8	15	8.6
LA.1	**RK21**	**1876**	188	2464.5	194	60	26	19.5	11.8	80	7.7	316	21	93	4.9	205	7.7	20	< 10	4.7	129	16	8.5	4.7	36	4.4
LA.2	**RK21**	**1876**	125	2374.0	232	59	34	24	18.4	88	18.4	274	20	91	4.6	304	10.9	19.3	< 10	3.2	193	7.3	7.1	5.3	41	4.5
LA.8	**RK27 #2**	**2153**	102	2472.3	234	70	46	33	88	73	44.1	294	18.9	78	4.3	232	7.1	15.2	< 10	3.3	289	5.1	6.3	5.7	48	4.1
LA.11	**RK27**	**1850-53**	4916	2114.4	237	129	31	48	45	70	87	216	19.5	84	4.6	344	5.9	16.2	< 10	3.4	115	5.8	6.1	6.7	47	4.3
LA.12	**RK18**	**2219.1**	3180	2242.7	253	62	37	27	49	74	6.9	407	18	76	4.4	153	7.9	19.5	< 10	< 2.3	220	7.1	7.4	4.8	55	4.2
LA.13	**RK18**	**2221**	2525	2406.4	238	65	33	26	50	78	89	325	19.1	81	4.4	242	4.8	18	< 10	3.2	210	6.4	6.8	5.6	53	4.3
LA.24	**RK21**	**1300**	3022	2146.2	173	60	43	24	53	61	27	285	18.4	66	3.8	261	7	19.8	< 10	2.9	318	7.6	5.4	3.6	49	3.6
LA.25	**RK21**	**1350**	2449	2288.3	171	77	38	30	43	79	26	256	19.3	83	4.3	281	7.8	17.8	< 10	3	186	4.9	5.7	4.8	50	4.3
LA.26	**RK21**	**1400**	1454	2329.7	197	56	33	26	47	63	32	311	17.4	75	4.2	261	4.4	14.7	< 10	2.1	212	6	5.6	4	53	4.3
LA.27	**RK21**	**1450**	395	2371.6	205	57	36	26	49	64	30	306	18	74	3.7	240	5.1	16.2	< 10	2.1	171	5.3	5.3	3.6	54	4.1
LA.28	**RK21**	**1500**	309	2599.4	221	55	38	24	56	66	34	316	18.9	82	4.2	261	6.9	16.5	< 10	3.1	212	5.6	5.2	4.7	49	4.3
LA.29	**RK21**	**1550**	264	2721.7	235	81	47	27	54	65	38	312	19.4	85	4.4	254	6.4	18.2	< 10	2.7	253	5.2	5.5	4	47	4.4
LA.30	**RK21**	**1600**	147	2403.4	214	52	36	20	36	60	32	335	17.9	73	3.9	241	7.2	16.6	< 10	2	162	5.7	5.5	3.6	39	4.1
LA.31	**RK21**	**1650**	285	2357.2	207	54	34	21	53	60	36	338	18.5	71	3.9	267	5.9	17	10.4	< 2.4	168	5.7	5.6	3.8	44	3.8
LA.32	**RK21**	**1700**	980	2552.1	209	63	35	23	56	64	38	313	19.4	75	4.3	266	7.4	18	< 10	< 2.4	136	7.1	5.2	4	41	3.9
LA.33	**RK21**	**1750**	1094	2538.9	224	60	38	21	45	69	30	322	19.3	82	4.3	295	8.4	19.3	< 10	2.8	244	7.1	6.2	3.9	36	4.2
LA.34	**RK21**	**1800**	471	2581.4	251	51	36	21	51	68	40	306	19.7	90	4.2	299	7.1	17.7	< 10	3.5	196	5.8	6.1	4.3	32	4.5
LA.35	**RK21**	**1850**	539	2574.9	305	59	39	22	51	64	41	304	20	86	4.1	283	8.9	19.6	< 10	3.1	213	7	6.3	4.4	32	4.2
LA.36	**RK21**	**1900**	284	2404.6	190	50	44	17.5	39	62	33	301	18.1	79	4.3	322	5.2	17.7	< 10	< 2.1	318	6.5	5.8	3.5	28	4.3
LA.37	**RK21**	**1950**	184	2530.5	210	31	36	11.9	32	61	50	318	19.6	83	4.9	269	9.9	20	11.7	2.3	221	9.8	6.5	3.8	27	4.2

Sample	Well	Depth (mRF)	S ppm	Ti ppm	V ppm	Cr ppm	Co ppm	Ni ppm	Cu ppm	Zn ppm	Rb ppm	Sr ppm	Y ppm	Zr ppm	Nb ppm	Ba ppm	La ppm	Ce ppm	Nd ppm	Hf ppm	W ppm	Pb ppm	Th ppm	U ppm	TiO_2/Zr ratio	Zr/Y ratio
LA.38	**RK21**	**2000**	875	2258.3	195	82	43	24	36	70	38	283	18.6	79	4	266	8.6	17.5	< 10	3.4	247	7.2	6	4.1	28	4.2
LA.39	**RK21**	**2050**	730	1947.8	152	94	42	30	47	53	32	235	17.3	78	3.6	261	6.3	14	< 10	2.3	315	5.5	6.1	4	28	4.5
LA.40	**RK21**	**2100**	1487	2406.4	208	74	41	23	30	62	37	314	18.6	69	4	235	6.7	13.6	< 10	2.1	582	6.2	5.1	3.7	30	3.7
LA.41	**RK21**	**2150**	949	2377.6	207	90	50	22	42	64	20	315	18.1	69	4.7	249	6.5	16.5	< 10	2.5	546	6.8	6.5	4.2	30	3.8
LA.42	**RK21**	**2200**	996	2023.3	198	145	47	35	29	112	10.9	287	17.8	68	4.1	218	7.9	17.4	< 10	2.4	468	27	6.1	4.5	31	3.8
LA.43	**RK21**	**2250**	813	2004.7	206	137	45	38	40	140	10.2	309	19.3	66	4	236	5.9	14.7	9.4	2.8	455	42	6.8	4.4	35	3.4
LA.49	**RK25 #1**	**2001**	543	2376.4	201	147	38	53	37	81	31	202	17.3	84	4	242	7	16.6	< 10	2.1	97	5.3	5.6	4.2	30	4.9
LA.50	**RK25 #1**	**2003**	1881	2496.3	175	153	31	54	7	82	38	179	16.9	81	3.9	217	4.7	14.5	< 10	1.5	119	5.4	4.9	5	36	4.8
LA.52	**RK24 ST1**	**1823**	1002	2247.5	238	51	40	19.2	54	84	8.3	285	20	83	4.5	161	10.2	19.8	< 10	3.3	123	6.5	5.5	3.7	27	4.1
LA.53	**RK27 #2**	**2147**	1036	2357.2	165	71	33	36	64	74	35.3	231	21	78	3.8	499	4.9	13.6	< 10	2.6	95	4.8	5.5	4.5	48	3.8
LA.54	**RK27 #2**	**2148**	397	1932.8	139	63	35	27	95	63	35.8	165	15.1	59	3.3	508	9.2	20	10.5	< 2.8	82	4.8	4.4	4.2	37	3.9
LA.56	**RK27 #2**	**2150**	115	2369.8	225	73	52	33	25	92	37.7	289	18.9	76	3.8	249	7.3	19.1	< 10	2.6	430	5.2	5.4	4.5	33	4
LA.57	**RK27 #2**	**2151**	123	2403.4	232	66	39	31	39	66	40.9	304	19.3	77	3.8	257	7.7	16.4	< 10	< 2.3	218	4.8	5	4.8	29	4
LA.86	**RK24 ST1**	**1505**	182	2443.6	179	77	51	32	57	74	25	234	18.6	78	4.1	197	5.6	16.1	9.9	4.9	277	5.5	5.6	4.5	53	4.2
LA.87	**RK24 ST1**	**1555**	362	2261.9	190	81	36	32	43	65	33	293	18.0	77	4.1	249	8.0	16.1	< 10	3.4	215	5.3	6.1	4.5	49	4.3
LA.88	**RK24 ST1**	**1605**	131	2347.6	207	72	37	26	56	63	27	303	17.8	72	3.8	211	7.6	15.2	< 10	4.7	198	5.2	6.0	4.3	55	4
LA.89	**RK24 ST1**	**1655**	231	2370.4	217	94	37	28	49	64	25	305	17.8	70	4.1	233	4.9	15.2	9.4	4.0	134	4.7	5.8	4.5	57	3.9
LA.90	**RK24 ST1**	**1705**	365	2489.7	217	69	42	25	67	67	32	295	19.0	84	4.2	310	6.5	17.5	10.1	3.7	156	5.7	6.8	5.1	50	4.4
LA.91	**RK24 ST1**	**1755**	358	2581.4	235	73	40	26	47	66	39	301	19.4	86	4.3	275	6.8	16.1	15.3	3.5	236	5.8	6.3	4.8	50	4.4
LA.92	**RK24 ST1**	**1805**	1991	2206.8	237	36	33	16.1	44	78	33	275	19.3	90	4.4	258	7.1	17.9	10.2	3.1	212	5.4	7.2	4.4	41	4.6
LA.93	**RK24 ST1**	**1855**	1925	2015.5	161	18.4	30	8.0	31	73	37	316	20	96	5.0	246	10.4	26	13.0	4.7	225	13.9	8.7	4.6	35	4.8
LA.94	**RK24 ST1**	**1905**	2525	1860.2	152	18.3	28	9.0	31	71	52	314	18.9	97	4.4	343	10.3	21	< 10	3.7	335	9.9	8.6	4.1	32	5.1

Sample	Well	Depth (mRF)	S ppm	Ti ppm	V ppm	Cr ppm	Co ppm	Ni ppm	Cu ppm	Zn ppm	Rb ppm	Sr ppm	Y ppm	Zr ppm	Nb ppm	Ba ppm	La ppm	Ce ppm	Nd ppm	Hf ppm	W ppm	Pb ppm	Th ppm	U ppm	TiO2/Zr ratio	Zr/Y ratio
LA.95	**RK24 ST1**	**1955**	5239	1819.5	137	16.3	32	9.5	28	102	45	313	19.4	95	4.6	369	10.2	24	11.4	5.0	382	9.2	8.3	4.5	32	4.9
LA.96	**RK24 ST1**	**2005**	2767	2329.7	206	70	33	19.8	35	67	29	296	18.1	80	4.3	228	6.6	17.4	< 10	4.2	259	4.2	5.9	4.6	49	4.4
LA.97	**RK24 ST1**	**2055**	5065	2044.3	185	72	31	24	34	61	34	236	17.1	76	4.0	205	6.2	14.8	10.3	4.6	235	5.9	6.5	4.3	45	4.5
LA.98	**RK24 ST1**	**2105**	5790	1947.8	170	33	29	12.8	26	56	41	239	18.1	92	4.2	249	7.2	14.8	< 10	4.2	247	5.5	6.8	4.2	35	5.1
LA.99	**RK24 ST1**	**2155**	9549	1905.2	200	90	40	24	31	86	26	239	16.4	74	3.3	177	5.1	13.8	10.4	4.3	385	5.8	6.3	4.7	43	4.5
LA.105	**RK25**	**1835**	3948	2299.7	149	27	33	12.6	24	58	67	232	23	125	6.8	356	13.4	30	17.9	7.8	447	9.0	10.9	7.3	31	5.5
LA.106	**RK25**	**1885**	18090	2730.1	156	35	49	15.8	32	52	67	237	24	114	6.6	357	14.7	30	17.9	6.7	469	6.8	10.6	7.8	40	4.8
LA.107	**RK25**	**1935**	7237	2484.9	168	34	43	13.9	33	61	66	191	22	119	6.8	364	16.5	31	16.4	6.5	389	9.1	10.0	7.8	35	5.3
LA.108	**RK25**	**1985**	6076	2669.0	173	28	53	14.2	32	60	57	225	23	120	6.8	275	14.0	27	15.8	5.4	415	8.0	10.4	6.9	37	5.2
LA.109	**RK25**	**2035**	3864	2441.2	202	28	43	18.9	35	67	36	205	23	90	5.3	195	7.7	18.0	< 10	6.3	269	7.7	8.0	6.5	45	3.9
LA.110	**RK25**	**2085**	3180	2387.8	191	47	45	18.3	37	67	37	266	22	99	5.5	251	8.8	19.8	10.5	4.7	350	6.7	8.8	6.6	40	4.5
LA.111	**RK25**	**2135**	1752	2472.9	200	53	44	23	56	84	58	224	23	95	5.3	262	8.1	18.4	< 10	6.4	319	9.1	8.5	6.8	44	4.1
LA.112	**RK25**	**2185**	2419	2315.9	216	64	35	26	44	83	34	261	22	88	4.9	191	5.6	17.1	< 10	6.8	257	7.8	8.2	6.7	44	4
LA.113	**RK25**	**2235**	3320	2356.6	197	77	38	26	41	71	54	249	22	100	5.9	360	10.3	21	13.6	6.3	263	8.3	9.2	7.0	39	4.5
LA.114	**RK25**	**2285**	1882	2256.5	179	47	43	17.6	35	71	42	258	20	93	5.6	296	8.2	17.7	< 10	6.4	282	8.5	8.1	6.4	40	4.6
LA.115	**RK25**	**2335**	2979	2285.3	172	34	36	19.2	21	65	43	272	21	95	5.9	285	8.4	21	< 10	6.5	285	7.9	8.9	6.2	40	4.6
LA.116	**RK25**	**2385**	2594	2247.5	176	33	34	15.6	25	65	39	282	21	96	6.2	257	10.5	20	12.4	5.7	326	8.7	8.6	6.1	39	4.6
LA.117	**RK25**	**2435**	3234	2386.6	197	55	44	29	41	72	37	285	19.2	90	5.8	266	7.0	16.6	< 10	11.1	378	7.7	7.7	5.6	44	4.7
LA.118	**RK25**	**2485**	1592	2372.8	212	68	41	25	44	65	42	284	20	91	6.0	249	7.5	20	12.3	8.5	280	7.4	7.2	5.6	44	4.4
LA.119	**RK25**	**2535**	1529	2307.5	164	38	32	18.1	29	62	41	278	21	104	6.0	414	9.1	22	12.0	7.2	387	7.8	9.0	6.2	37	5.1
LA.120	**RK25**	**2585**	1888	2376.4	183	48	35	19.1	33	62	42	302	21	98	6.5	339	8.8	22	12.2	6.5	317	9.0	8.7	6.4	40	4.6
LA.121	**RK25**	**2635**	1776	2387.2	205	62	39	25	42	62	36	304	19.9	95	6.0	298	8.1	20	10.3	9.9	273	9.5	7.2	5.0	42	4.8
LA.122	**RK25**	**2685**	4447	2586.2	237	53	43	17.4	32	55	44	292	22	90	5.6	321	13.5	23	< 10	5.9	246	8.7	8.0	6.4	48	4.2
LA.123	**RK25**	**2705**	4361	2367.4	193	56	32	17.9	52	60	47	277	21	108	7.0	383	12.0	24	16.6	6.9	292	9.9	9.7	6.6	36	5.1

Appendix 4

Mass change calculations – results

Altered samples:	LA.7	14*	16*	LA.9	LA.10	LA.44	LA.48	LA.51
Well	NM6	NM2	NM4	RK27	RK27	RK21	RK25 #1	RK24 ST1
Depth (mRF)	3032-35	2000	2460	2153	1853-56	2300	2000	1820
Alteration intensity	Intense	Low degree of alteration	Altered	Moderate	Strong	Strong	Moderate	Strong
TiO_2/Zr ratio	50	26	55	53	53	54	42	48
Major elements (wt. %)								
SiO_2	5.4	3.3	0.4	4.0	7.5	-0.5	2.9	1.9
TiO_2	0.0	-0.4	-0.2	0.0	-0.2	0.1	-0.1	0.0
Al_2O_3	1.1	-3.0	0.6	0.1	-4.0	0.4	-2.3	0.0
Fe_2O_3	0.5	-1.6	-1.1	0.1	-0.2	0.5	-0.4	0.9
MnO	0.0	0.0	0.0	0.0	0.0	-0.1	0.0	0.1
MgO	0.6	-0.4	1.0	0.7	0.1	1.2	0.4	1.9
CaO	0.9	-1.1	0.8	-0.9	-0.8	0.3	0.1	2.9
Na_2O	0.8	-1.6	-2.6	0.2	-0.7	0.6	0.0	0.0
K_2O	-0.9	0.8	0.4	0.5	0.8	0.7	0.6	-1.1
P_2O_5	0.1	-0.2	-0.1	0.0	0.0	0.0	0.0	-0.2
H_2O	0.0	0.0	0.0	0.0	0.0	0.0	0.0	0.0
LOI	-6.4	2.4	2.2	-2.0	-1.7	0.4	-0.1	-3.1
TOTAL	**2.0**	**-1.9**	**1.4**	**2.7**	**0.9**	**3.4**	**1.2**	**3.2**
Trace elements (ppm)								
V	-1.9	20.0	-36.2	26.1	10.8	0.4	-4.1	85.5
Cr	-21.1	-50.8	-35.1	30.3	14.6	15.3	-23.4	4.5
Ni	-1.8	-12.0	-25.9	10.7	11.7	-4.4	1.6	-4.7
Cu	3.3	-15.9	-11.3	-6.7	8.5	-4.8	106.0	-13.4
Zn	-1.4	19.8	131.9	1.2	35.0	370.3	16.7	-24.2
Rb	61.5	-30.1	-32.1	-29.7	-33.7	-32.4	-6.0	68.9
Sr	-53.7	129.0	-46.5	22.5	69.7	9.2	8.5	25.5
Y	0.5	1.0	24.0	-0.9	3.3	0.0	3.0	6.0
Zr	-2.9	99.1	18.5	0.8	17.5	-7.7	12.7	2.6
Nb	-0.4	na	na	0.1	1.0	-0.5	0.5	0.3
Ba	-5.3	-160.3	-15.5	-39.9	-104.2	-147.1	-122.5	195.2
La	-8.9	-0.7	10.6	-0.7	-2.3	-3.6	-1.9	-2.0
Ce	-7.2	na	na	-2.2	1.3	-1.8	3.0	1.6
Hf	-0.4	na	na	1.8	0.6	-1.0	-4.6	-0.1
W	-224.2	na	na	-160.5	-36.6	-10.5	-176.6	-114.2
Pb	-6.5	8.2	69.8	-8.7	-7.8	115.5	-2.8	5.9
Th	-1.7	-4.8	1.9	-1.3	-0.3	-1.4	-0.8	-1.0
U	0.5	na	na	0.4	0.6	-0.5	-0.8	-0.6
TOTAL	**-271.6**	**2.6**	**54.2**	**-156.7**	**-10.5**	**295.0**	**-191.5**	**235.8**

Altered samples:	LA.55	1*	5*	7*	9*	11*	12*	13*
Well	RK27 #2	RK6	RK6	RK5	RK6	RK4	RK4	RK6
Depth (mRF)	2149	2443	2115	1589	2280	1995.5	1830	1861
Alteration intensity	Moderate	Altered	Altered	Low degree of alteration	Low degree of alteration	Altered	Altered	Altered
TiO_2/Zr ratio	54	55	43	44	44	63	45	29
Major elements (wt. %)								
SiO_2	5.6	1.3	-1.3	-2.2	-2.7	0.0	-5.3	-3.2
TiO_2	-0.1	0.0	0.0	-0.1	0.0	0.1	0.2	0.2
Al_2O_3	-0.7	0.2	0.0	-0.6	1.1	-1.7	1.7	0.4
Fe_2O_3	0.1	-1.4	0.5	1.5	0.5	1.0	0.5	-0.1
MnO	0.0	-0.3	-0.1	0.0	0.0	0.0	0.0	0.0
MgO	0.1	-1.2	1.3	1.7	-1.4	0.4	-1.1	-2.1
CaO	-0.9	1.5	-2.3	0.2	0.8	0.0	1.6	0.7
Na_2O	-0.2	-1.3	0.0	-1.1	0.2	-0.5	0.1	0.4
K_2O	0.6	0.3	-0.1	0.9	-0.3	0.6	0.6	-0.2
P_2O_5	0.0	0.0	0.0	0.0	0.0	0.0	0.0	0.0
H_2O	0.0	0.2	-0.1	-0.1	-0.6	0.0	-0.3	-0.2
LOI	-2.2	-3.6	-2.9	-0.8	0.1	-0.6	-3.1	-0.2
TOTAL	**2.4**	**-4.2**	**-5.0**	**-0.8**	**-2.4**	**-0.7**	**-5.2**	**-4.2**
Trace elements (ppm)								
V	20.8	33.1	-2.3	-6.8	-28.6	75.7	-29.8	0.5
Cr	37.3	33.4	56.2	-45.5	41.9	53.2	101.6	183.0
Ni	7.5	6.3	8.4	-14.7	9.2	17.0	26.0	36.9
Cu	-3.0	35.6	10.3	-3.0	10.5	-28.7	-3.3	-6.2
Zn	1.7	20.0	18.2	30.2	6.2	0.0	-3.8	-16.7
Rb	-36.5	-14.3	4.5	-21.6	43.3	-58.3	-7.0	7.1
Sr	3.8	72.9	22.5	80.1	13.3	-59.1	-7.9	25.6
Y	-0.3	-2.0	-0.5	15.5	2.6	-0.3	-3.3	-8.3
Zr	5.5	-0.6	4.6	14.3	3.3	-20.2	-18.2	-46.0
Nb	-0.2	na	na	na	na	na	na	na
Ba	-94.9	-125.1	84.6	-44.3	18.8	-292.3	-86.5	19.0
La	-1.5	1.7	2.1	7.1	4.2	-1.8	2.2	5.0
Ce	1.6	na	na	na	na	na	na	na
Hf	0.4	na	na	na	na	na	na	na
W	-76.0	na	na	na	na	na	na	na
Pb	-9.6	4.0	6.0	7.0	2.9	6.0	19.7	6.7
Th	-2.0	3.0	-0.7	0.3	-3.7	-0.8	6.3	-2.4
U	-0.9	na	na	na	na	na	na	na
TOTAL	**-146.2**	**67.9**	**214.1**	**18.6**	**123.7**	**-309.7**	**-4.1**	**204.1**

Appendix 5

Normalising values

Normalising values of primordial mantle which are used in the calculation of spider diagrams, they are listed in their plotted order (McDonough et al., 1985).

Element	Value (ppm)
Rb	0.69
Ba	6.81
Th	0.088
K	240
Nb	0.75
La	0.71
Ce	1.85
Sr	23.7
P	92
Zr	11.1
Ti	1300
Y	4.6

Appendix 6

Other data

Other data which are available on the enclosed CD-rom:

- list where sample numbers in this study are converted to the sample number series used by the Waikato University;
- petrographic data sheets;
- additional XRD-graphs;
- complete XRF data; and
- transcripts from well reports.